CANADIAN THESES ON MICROFICHE

THESES CANADIENNES SUR MICROFICHE

NOTICE

The quality of this microfiche is heavily dependent upon the quality of the original thesis submitted for microfilming. Every effort has been made to ensure the highest quality of reproduction possible.

If pages are missing, contact the university which granted the degree.

Some pages may have indistinct print especially if the original pages were typed with a poor typewriter ribbon or if the university sent us a poor photocopy.

Previously copyrighted materials (journal articles, published tests, etc.) are not filmed.

AVIS

La qualité de cette microfiche dépend grandement de la qualité de la thèse soumise au microfilmage. Nous avons tout fait pour assurer une qualité supérieure de reproduction.

S'il manque des pages, veuillez communiquer avec l'université qui a conféré le grade.

La qualité d'impression de certaines pages peut laisser à désirer, surtout si les pages originales ont été dactylographiées à l'aide d'un ruban usé ou si l'université nous a fait parvenir une photocopie de mauvaise qualité.

Les documents qui font déjà l'objet d'un droit d'auteur (articles de revue, examens publiés, etc.) ne sont pas microfilmés.

THIS DISSERTATION HAS BEEN MICROFILMED EXACTLY AS RECEIVED

LA THÈSE A ÉTÉ MICROFILMÉE TELLE QUE NOUS L'AVONS REÇUE

Canada

0-3- -06194-3

PERMISSION TO MICROFILM — AUTORISATION DE MICROFILMER

• Please print or type — Écrire en lettres moulées ou dactylographier

Full Name of Author — Nom complet de l'auteur

KEVIN BRYAN STERNE

Date of Birth — Date de naissance	Country of Birth — Lieu de naissance
2nd July, 1950	SOUTH AFRICA

Permanent Address — Résidence fixe

3190 SHAKESPEARE STREET
VICTORIA, BRITISH COLUMBIA
V8T 3A4

Title of Thesis — Titre de la thèse

Horizon Cylinder Testing of Oil Sands

University — Université

ALBERTA

Degree for which thesis was presented — Grade pour lequel cette thèse fut présentée

M. Sc.

Year this degree conferred — Année d'obtention de ce grade	Name of Supervisor — Nom du directeur de thèse
198	Dr. E. EISENSTEIN

Date	Signature
23rd April 198	

NL-91 (4/77)

THE UNIVERSITY OF ALBERTA

HOLLOW CYLINDER TESTING OF OIL SANDS

by

(C) KEVIN BRYAN STERNE

A THESIS

SUBMITTED TO THE FACULTY OF GRADUATE STUDIES AND RESEARCH

IN PARTIAL FULFILMENT OF THE REQUIREMENTS FOR THE DEGREE

OF MASTER OF SCIENCE

IN

CIVIL ENGINEERING

DEPARTMENT OF CIVIL ENGINEERING

EDMONTON, ALBERTA

SPRING, 1981

22 July 1982

Faculty of Graduate Studies and Research
University of Alberta
Edmonton, Alberta
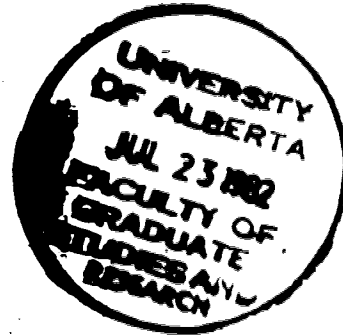
Dear Madam/Sir

A former student of mine has informed me that you require permission to microfilm his thesis as it has a copy of a paper of mine as an Appendix.

The student's name and thesis is:

Mr Kevin B Sterne
Hollow Cylinder Testing of Oil Sands
Master of Science (1981)
Department of Civil Engineering, U of A
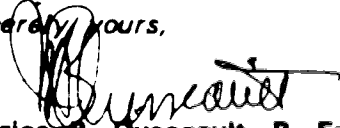
The name of the paper is:

A versatile hollow cylinder triaxial device
by Maurice B. Dusseault

Mr Sterne and the Faculty of Graduate Studies and Research have my permission to microfilm and copy the thesis, including the paper, for scientific and educational purposes.

Thank you for your consideration in these matters, I remain,

Sincerely yours,

Maurice B. Dusseault, P. Eng.
(After September 1st)
Professor of Earth Sciences
University of Waterloo
Waterloo, Ontario, CANADA, N2L 3G1

THE UNIVERSITY OF ALBERTA

RELEASE FORM

NAME OF AUTHOR   KEVIN BRYAN STERNE

TITLE OF THESIS   HOLLOW CYLINDER TESTING OF OIL SANDS

DEGREE FOR WHICH THESIS WAS PRESENTED   MASTER OF SCIENCE

YEAR THIS DEGREE GRANTED   SPRING, 1981

     Permission is hereby granted to THE UNIVERSITY OF
ALBERTA LIBRARY to reproduce single copies of this
thesis and to lend or sell such copies for private,
scholarly or scientific research purposes only.

    The author reserves other publication rights, and
neither the thesis nor extensive extracts from it may
be printed or otherwise reproduced without the author's
written permission.

(SIGNED) ....

PERMANENT ADDRESS:
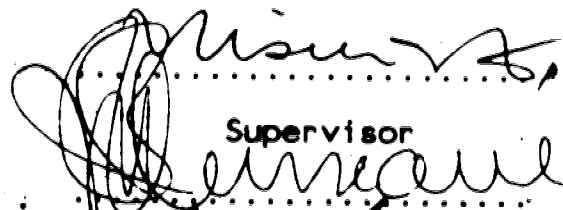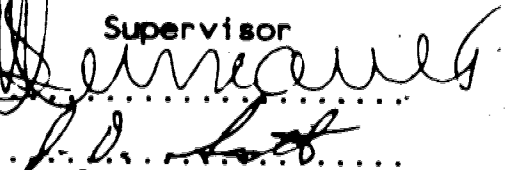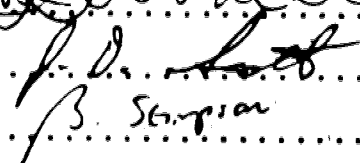
    .3190. Shakespeare Street.........

    .Victoria, British. Columbia......

    ....

DATED .April. 20..........1981

THE UNIVERSITY OF ALBERTA
FACULTY OF GRADUATE STUDIES AND RESEARCH

The undersigned certify that they have read, and
recommend to the Faculty of Graduate Studies and Research,
for acceptance, a thesis entitled HOLLOW CYLINDER TESTING
OIL SANDS submitted by KEVIN BRYAN STERNE in partial
fulfilment of the requirements for the degree of MASTER ⁻ᴵ
SCIENCE in CIVIL ENGINEERING.

....
Supervisor
....

....

B. Simpson

Date.... April 20, 1981 ....

Abstract

The deformations that occur around shafts and tunnels depend, in part, on the elastic deformation moduli. These moduli are usually stress-path dependent and it is therefore important to follow the correct stress path in the laboratory when determining deformation moduli.

The stress-path dependency of Athabasca oil sand has been investigated. Three series of drained triaxial tests were conducted on 'undisturbed' samples of oil sand along different stress paths. Two of the series were conducted in a high pressure triaxial cell, and the other series was conducted on hollow cylinder samples under plane-strain conditions. The laboratory results have shown that the deformation of oil sand is path dependent. Of even greater significance is the fact that sample preparation techniques have a dominant role in the sample disturbance that occurs.

A numerical model was developed to predict the deformations that occur in the hollow cylinder tests. The predicted deformations are good, provided that the Young's modulus is correctly specified and that the model accounts for the variation of this modulus with confining pressure.

Acknowledgements

discussion.

The writer would like to thank all those people who helped make his stay at the University so enjoyable.

Finally, the writer wishes to express his sincere appreciation for the patience and support provided by his wife Fran.

Table of Contents

List of Tables

List of Figures

List of Plates

xvi

List of Symbols

A_i : area of the internal membrane

A_s : area of the sample

a : internal radius or a curve-fitting parameter

b : external radius or a curve-fitting parameter

b_1, b_2 : parameters describing the variation of Young's
   modulus with radial stress

C_s : soil compressibility coefficient

c : effective cohesion intercept

$d\epsilon$: strain increment

$d\sigma$: stress increment

E : Young's modulus

Ea, E_b : parameters describing the variation of Young's
   modulus with radial stress

E_{eff} : effective tangent modulus

E_i : initial tangent modulus

F_r : total radial force across the sample

L_0 : initial length of a sample

N : shear strength parameter

n_c : porosity after consolidation

n_i : porosity after sample preparation

P : axial load on a sample

p_e : external pressure

p_i : internal pressure

$(p_e/p_i)_f$: effective pressure ratio at collapse

R : radius of the plastic zone

r : radius to any element in a hollow cylinder

u_a : displacement at the internal wall

u_r : radial displacement

V_i : volume of the internal membrane

V_s : volume of the sample pore fluid

v : volumetric strain

w_{bit} : bitumen content

w_f : final fluid content at the end of a test

w_i : initial fluid content

α : dilation parameter

γ_b : bulk density

ϵ_f : strain at failure or collapse

ϵ_v : volumetric strain

ϵ_a : axial strain

ϵ_r : radial strain

ϵ_θ : tangential strain

ϵ^e : elastic component of the strain

ϵ^p : plastic component of the strain

ν : Poisson's ratio

σ_c' : effective consolidation pressure

σ_d : deviator stress

σ_n : effective normal stress on the failure plane

σ_p : radial stress at the elastic-plastic boundary

σ_r : radial stress

$(\sigma_r)_{ave}$: average radial stress in a hollow cylinder

σ_r^c : radial stress at which the slope of the $E-(\sigma_r)_{ave}$ line changes magnitude

σ_z : axial stress

σ_θ : tangential stress

$(\sigma_\theta)_{ave}$: average tangential stress in a hollow cylinder

σ^e: denotes stresses in the elastic zone

σ^p: denotes stresses in the plastic zone

$\sigma_{\theta R}$: tangential stress at the elastic-plastic boundary

σ_0 : sum of the radial and tangential stresses

σ_1' : maximum effective stress

σ_3' : minimum effective stress

$\triangle r$: nodal spacing of the finite difference mesh

$\triangle v_i$: change in volume of the internal membrane

$\triangle v_s$: change in volume of the sample pore fluid

$\triangle \epsilon$: strain increment

$\triangle \sigma$: stress increment

τ_{max} : maximum shear stress on an element of soil

$\tau_{r\theta}$: shear stress on a soil element in the r-θ plane

ϕ': effective angle of shearing resistance

ϕ_s': effective secant angle of shearing resistance

Definitions :

Collapse : a large volume change of the internal
membrane with a small change in internal pressure

Failure : the maximum deviator stress that a triaxial
sample can sustain

Yield Point : stress at which the first plastic
deformation occurs

<u>Yielding</u> : when the yield point at the internal wall is
exceeded

CHAPTER 1

INTRODUCTION

1.1 General

The oil sands of the Athabasca deposit in Alberta are currently recovered by open pit mining techniques. There are now two such mines operating near Fort McMurray ; Syncrude Canada Ltd. and Suncor Inc. Two further operations are scheduled to begin construction in the near future ; Alsands near Fort MacKay (open pit mining) and the Cold Lake Project in Eastern Alberta (·*in situ* recovery).

Open pit mining is only feasible for deposits that do not lie deeper than approximately 70 m. Much of the rich oil sands in Alberta occur in the middle McMurray Formation which in most places far exceeds the practical limits for open pit mining. As the world price of petroleum continues to escalate, it is now becoming economical to proceed to *in situ* recovery processes which involve shafting and tunnelling.

Three *in situ* recovery processes involving tunnelling are possible (Devenney and Raisbeck,1980). The first involves sinking a shaft through the overlying formation into the limestone which lies beneath the oil sands, and then tunnelling into the limestone. Injection wells would be drilled from the tunnel into the oil sand above. Another possibility is that used in the USSR at Yarega (Devenney and Raisbeck,1980). The shaft is sunk to a depth just above the

1

reservoir and a tunnel driven horizontally. Injection wells are drilled down into the reservoir. The third arrangement is similar to the first, the tunnel being driven in the oil sand deposit. Figure 1.1 shows these three possible recovery procedures.

Irrespective of which procedure is used, it is important to determine how the oil sand will behave during excavation. Shafting and tunnelling in either the overburden or the limestone bedrock pose convention problems only as the behaviour of these materials is well understood. The oil sands pose special problems as its behaviour upon excavation is not well understood so far. The problem is further complicated by the lack of any previous experience of deep excavations in this material.

There are only two case histories available to be studied and neither of these involved deep excavations. The GCOS test shaft (Hardy and Scott,1978) was sunk to only 23.5 metres when instability of the walls caused severe slabbing and thus the abandonment of the shaft. The Saline Creek Tunnel (Smith et al.,1978) showed the oil sands at that location to behave competently, but the overburden at this site was only 27.5 meters.

It is thus imperative that more geotechnical knowledge be obtained and used with all the available theory of oil sand behaviour to enable a better understanding of how this material will behave when excavated to depths exceeding 300 metres.
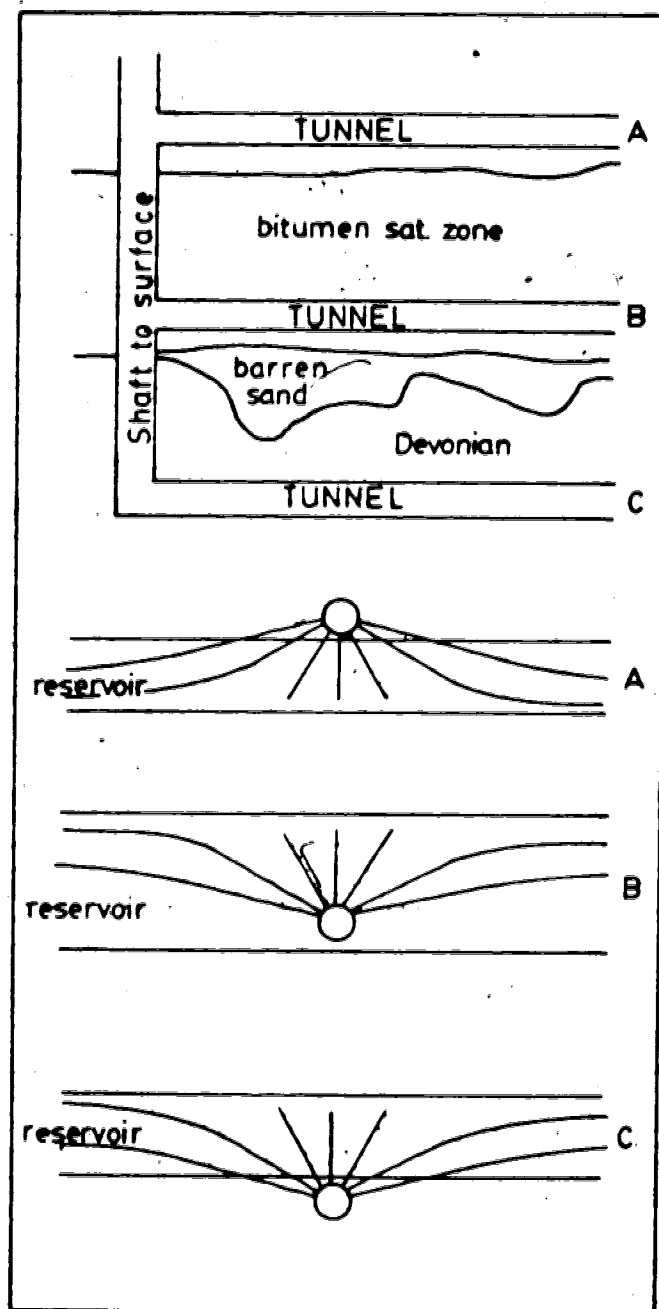
Figure 1.1 Possible in situ recovery methods for oil sands
(after Devenney and Raisbeck,1980)

The oil sands *in situ* are a very dense, uncemented sandstone. Their shear strengths are much higher than those of normal granular deposits due to the interlocking nature of the sand grains which results in a material that has a very high dilatancy (Dusseault,1977). There is no chemical cementing present in the oil sands and this results in a Mohr-Coulomb peak envelope which passes through the origin (Dusseault and Morgenstern,1978), and hence the oil sands may be classified as a cohesionless material. At higher stress levels, dilatancy will be suppressed and this results in a curvature of the Mohr envelope.

A tangent drawn to the envelope (at high stress levels) will give a cohesion intercept which has been defined as the fabric cohesion (Dusseault,1977).

The pores of the oil sands are filled with water, bitumen and gas, which is present either as free gas or dissolved gas (Dusseault and Morgenstern,1978). The bitumen does not contribute to the strength of the material at normal temperatures, but has a marked effect on the permeability of water through the material. The oil sands are thus low permeability materials and behave in an undrained manner when subjected to a fast stress or temperature change (Dusseault,1979).

These phenomena of oil sands are obviously factors which would contribute to the behaviour of the material upon excavation. When the material is unloaded (or the temperature increased) the gas comes out of solution and,

because of its low permeability, there is an expansion of the material. This expansion results in a disruption of the fabric, and hence a decrease in the shear strength (Harris and Sobkowicz,1977).

The exsolution of gas continues as the unloading progresses. The gas bubbles eventually form a connected drainage system and bleed off of the gases occurs (Scott,1978). At this stage, the material begins to behave in a drained manner. One of the major problems yet to be solved is the question of how long a time interval is required before drainage occurs. This problem is of significance in the design of shaft and tunnel linings and, until solved, the behaviour of oil sands upon excavation can only be estimated as lying between its two modes of behaviour; undrained and drained.

1.2 Aim of the Thesis

The aim of this thesis is to examine the stress-strain behaviour typical for, and applicable to, ground response around tunnels and shafts. The presence of gas will have a major influence on the undrained behaviour of oil sands and it is thus necessary to obtain samples for laboratory testing that still have gas in the material. This may be accomplished if in situ freezing techniques are used, and the problems of obtaining undisturbed samples by this technique have been discussed by Dusseault (1980). The gas has no effect on the results of drained tests provided the

samples have not been disturbed.

The research undertaken by the author was restricted to examining the drained behaviour of the oil sands at depths exceeding 300 metres. The tests were conducted on relatively undisturbed samples in order to examine the stress-deformation behaviour of the *in situ* material. The data obtained from such tests allows for an evaluation to be made as to whether the material in its undisturbed state is competent enough to withstand the stresses imposed upon it during shafting or tunnelling. This in itself is only one of the 'bounds' that need to be examined to fully understand the behaviour of oil sands, the undrained behaviour being the other bound.

The laboratory program consisted of performing a series of drained hollow cylinder triaxial tests as it is believed that the stress path followed in this test more closely resembles that which occurs in the field. The influence of stress path on the deformation behaviour was examined by conducting two other series of triaxial tests on solid samples of 37.5 mm diameter. The test results from all tests can then be compared.

The analysis of the hollow cylinder triaxial data depends upon the assumptions made regarding the stress distribution within the cylinder. A numerical model was developed to interpret the test results and thus enable some conclusions to be drawn concerning the validity of these assumptions.

1.3 Outline of the Thesis

The sample collection techniques and the unique method of sample preparation for both the hollow cylinder and triaxial tests are discussed in Chapter 2. Laboratory techniques and equipment are also presented in this chapter.

Chapter 3 deals with the theoretical stress distribution within the hollow cylinder, and the method of calculating strains from the volume changes measured during the test. In Chapter 4, the development and theoretical aspects of the numerical model are presented. A sensitivity analysis of the influence of the various parameters on the solution is given.

The laboratory results are given in Chapter 5 along with a discussion of these results. The hollow cylinder triaxial results are analysed in more detail in Chapter 6 which compares the actual test results with those predicted by the numerical model. A detailed discussion of these comparisons is given.

The conclusions reached from this research are summarized in Chapter 7.

CHAPTER 2

LABORATORY EQUIPMENT SAMPLES AND PROCEDURES

2.1 Introduction

The stress-deformation behaviour of oil sands is being investigated to determine the behaviour of this material when deep excavations such as shafts and tunnels are constructed. It was decided to use a hollow cylinder triaxial device (HCTD) for the testing program as this device is more versatile than a conventional triaxial cell and allows several stress paths to be followed in loading of the sample. A stress path resembling that which occurs in the field can also be modelled in this apparatus by maintaining a constant cell pressure and decreasing the internal pressure.

The HCTD used in this research program was designed and built at the University of Alberta (Dusseault,1979), and has the capability of sustaining cell pressures of up to 20 MPa. These high cell pressures are of the same order as the *in situ* stresses that will be encountered in deep excavations. Discussion of this apparatus and the problems encountered will be dealt with in a later section.

2.2 Literature review of previous HCTD usage

Hollow cylinder tests in the laboratory have been conducted as far back as 1957. The author has undertaken a literature review to determine the various capabilities of

the different HCTD's and the purposes for which they were employed. This review has been limited mainly to the testing of soils since the uncemented nature of the oil sand makes this material similar to a dense sand, rather than a rock.

The majority of the researchers have used the HCTD to investigate the shape of the yield surface for their particular material. The HCTD is well suited for this type of investigation as control of all three principal stresses is possible. Thus the shape of the failure surface in 3-D stress space between the two conventional points (triaxial compression and extension) may be obtained by following various stress paths during the testing program. Kirkpatrick(1957) used a medium to fine-grained sand and allowed full drainage during shear. He conducted an extensive testing program as did Wu *et al*.(1963) to determine the applicability of the various failure criteria. Wu *et al*.(1963) conducted their experiments on both a remoulded plastic clay and a uniform Ottawa sand. No drainage was allowed during shear, but pore-pressure measurements were recorded.

Haythornthwaite(1960) investigated the yield and flow criteria of a remoulded silt and his apparatus allowed the application of both a vertical stress and torque. Frydman *et al*.(1973) used glass microspheres as their material and ran drained tests in their program.

The only investigators to have used 'undisturbed'

samples in an experimental program were Suklje and Drnovsek(1965). They used a Tertiary clay and ran a series of plane-strain and plane-stress tests to determine the tensile deformability of this material. Their apparatus did not have the capability of allowing drainage nor to measure pore-pressure. Details of their sample preparation for the undisturbed clay were not given. Whitman and Luscher(1962) ran a series of experiments to investigate the soil-structure interaction problem of a buried pipe. The tests were conducted on dry Ottawa sand under plane-strain conditions.

Broms and Jamal(1965) used the HCTD to analyse the results of conventional triaxial tests. They ran undrained tests on a rounded beach sand, and used the hollow cylinder data to explain why the angle of friction measured in triaxial compression and extension differed. Their results show that the difference is due to a non-uniform stress distribution in the sample. In another paper by Broms and Casbarian(1965), the hollow cylinder data was used to examine the effects of rotation of the principle stress axes on shear strength. Procter(1967) used the hollow cylinder to investigate the stress-dilatancy behaviour of a dense sand.

The capabilities of these various devices are very similar. All authors had independent control of the cell pressure, bore pressure and axial stress. Volume changes in the bore could also be measured, while the volume change of

the pore fluid was only measured by Kirkpatrick(1957) and Frydman et al.(1973). The other authors, except Suklje and Drnovsek(1965), had the capability of measuring pore pressures. Axial strains and stresses were measured by various devices.

The cell pressure used by these authors all varied, but in no instance did it exceed 400 kPa. This pressure is far less than the proposed pressures to be used in this testing program. However, the use of these lower pressures enabled the researchers to use a modified triaxial cell whereas this research requires the use of a completely new piece of equipment.

The stress distributions within the hollow cylinder specimen were calculated in various ways. Suklje and Drnovsek(1965) based their solution on the theory of elasticity. They realized that these solutions were only valid in a limited stress range. Broms and Jamal(1965) conducted triaxial compression tests on their cylinders and thus had a uniform stress distribution within the cylinder.

The research carried out by Frydman et al. (1973), Whitman and Luscher(1962) and Kirkpatrick(1957) was only concerned with the stresses at failure, and an average tangential stress was calculated from equilibrium requirements of a half section of the cylinder, the average radial stress being found either from the failure criterion used or by assuming a linear distribution of the radial stresses within the cylinder. Wu et al.(1963) determined

the actual stress distribution at failure from a limiting equilibrium analysis.

Procter(1967) discussed the means available for calculating the stress distribution. He decided, on defining a radial stress distribution (linear) as he did not think that elaborate elasto-plastic analysis was valid for particulate media. His analysis was based on average stresses since the calculated strains in the cylinder were average strains.

Stress distributions can also be found in text books such as Jaeger and Cook(1976) and Timoshenko and Goodier(1970) for hollow cylinders. Jaeger and Cook(1976) give solutions based on elasticity and plasticity while Timoshenko and Goodier(1970) only deal with elasticity.

The literature review revealed valuable insight into the problems associated with hollow cylinder testing. However, no information was found that would assist in the sample preparation of undisturbed material, and the low pressure range in which these hollow cylinder devices were operated did not provide much insight into the problems that would be encountered when testing at high pressure.

2.3 The University of Alberta HCTD

This apparatus is described in detail in a paper published by Dusseault(1981), a copy of which is included in Appendix C. The basic features described in this paper have not been changed, but a few minor modifications were

necessary.

The top cap was modified such that the porous stone can be attached to it and be flush with the bottom of the cap. This eliminated the possibility of puncturing the external membrane against the porous stone when applying high cell pressures. A problem still existed with the internal membrane as it tended to pinch between the stone and cap. This problem was finally solved by inserting a ring of Neoprene rubber around such joints.

It was desireable to have the capability of deairing the system after it was assembled. Two additional ports were drilled through the top cap such that they opened onto the porous stone. Deairing is thus possible by applying a back pressure to the pore pressure line and opening the line at the top of the cap.

The major modifications made were to the membranes. Several leaks in the internal membrane occurred during testing and it was thus necessary to increase the thickness of the membrane to 0.7 mm. The external membrane was bonded onto a specially designed membrane clamping ring. This eliminated one source of leaks, namely through the O-rings clamped onto the membrane at this location. The thickness of this membrane is less than that reported in Dusseault's paper. This membrane is approximately 2 mm thick.

A detailed description of sample assembly and test procedures is given in a later section of this chapter. Details of the assembled cell and measuring systems are

·shown on Plate 2.1.

2.4 Advantages and Disadvantages of the HCTD

The hollow cylinder test has been selected for this research as it enables control of all three principal stresses. However, this is also possible by utilizing a true triaxial cell. Frydman(1973) has discussed the problems associated with this apparatus: end effects and strain measurements. The end effects are the major·drawback of the true triaxial apparatus. These end effects are not encountered in the HCTD, and the measurement of strain is accomplished by measuring the volume changes occurring within the cell, bore and sample.

The HCTD has additional advantages as discussed by Suklje and Drnovsek(1965):

1. The stress state is better defined without uncontrolled stress concentrations.

2. Tests can be conducted at various stress states.

3. Deformation anisotropy can be taken into account.

4. Long-term and drained tests can be more easily conducted.

Despite these advantages, there still exist several drawbacks to the apparatus:

1. A non-homogeneous stress state exists in the sample which complicates the interpretation of the test results. Assumptions have to be made regarding the stress distribution within the sample. This can be done
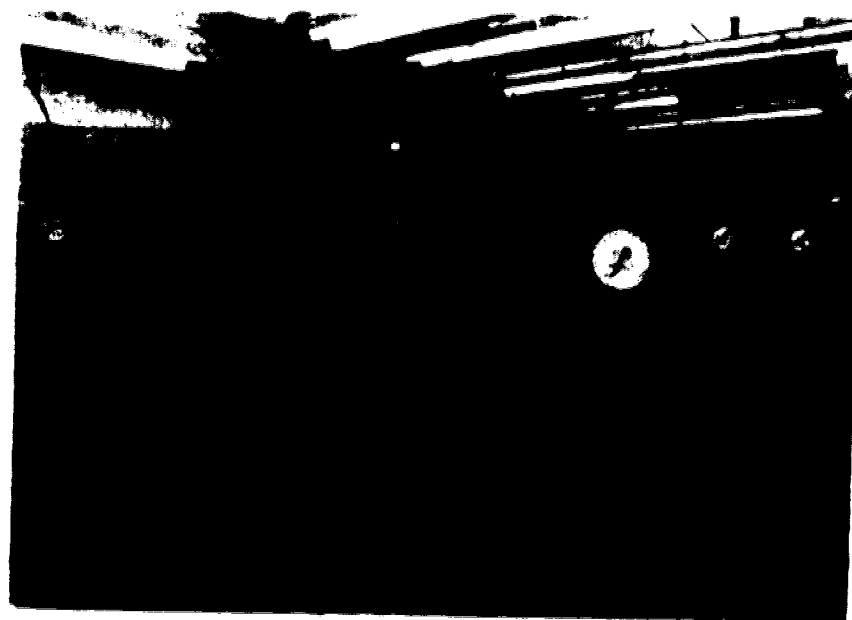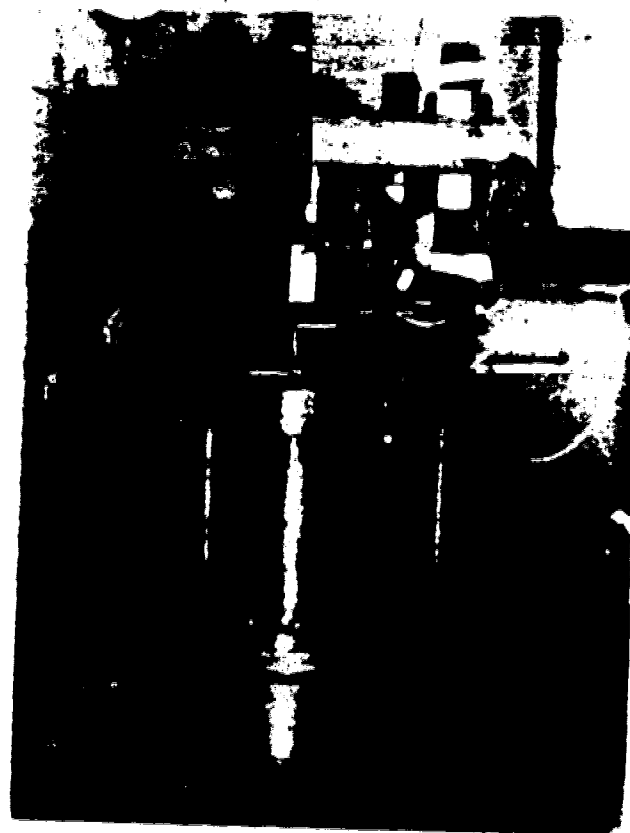
Plate 2.1 Instrumented Cell and Measuring System

by using elastic theory or by specifying a failure criterion to calculate the stresses in the plastic zone.

2. Special rubber membranes are required to resist high cell pressures without rupturing or leaking.

3. Problems are encountered in the preparation of the samples (discussed in more detail later).

These drawbacks still do not detract from the versatility of the apparatus. It is possible to conduct plane-strain tests along different stress paths in a relatively simple manner, and with accurate control of pressures and volume changes. Tests may be run either in an undrained mode with pore-pressure measurements, or with full drainage. A single test yields much valuable data:

1. Stress-strain curves based on average stresses within the sample.

2. Volume change behaviour due to dilatancy

3. Pore-pressure response(for undrained tests).

4. Closure of the bore with change in pressure.

5. Peak strength and hence strength parameters.

6. Determination of both elastic parameters (E and ν).

The factor which contributed largely to the use of this apparatus in the testing program is the fact that the stress path to failure in a shaft, and to a great extent in a tunnel, can be more easily and closely modelled than in any other piece of laboratory equipment.

2.5 Outline of laboratory program

It was initially intended to investigate the stress path dependency of oil sands by conducting three different series of drained tests in the HCTD. The laboratory program was modified when problems with the HCTD were encountered (see Appendix F). One series of tests were conducted in the HCTD (Series A) and two other series in a high pressure triaxial cell (Series B and C). The stress path followed in each of the three series of tests is shown in Figure 2.1 and discussed below.

2.5.1 Hollow Cylinder Triaxial Tests (Series A)

This series consisted of two plane-strain drained tests consolidated to 7 Mpa and 10 MPa respectively. The samples were sheared by maintaining a constant external pressure and decreasing the internal pressure incrementally until collapse of the sample occurred. The volume changes of the internal membrane and the pore fluid were monitored throughout the test.

2.5.2 Triaxial Compression Tests (Series B)

Two samples were consolidated to 7 MPa and 10 MPa respectively and sheared at a constant strain rate with full drainage by increasing the axial stress while maintaining a constant cell pressure. Volume changes of the pore fluid were continuously monitored against a constant back pressure.
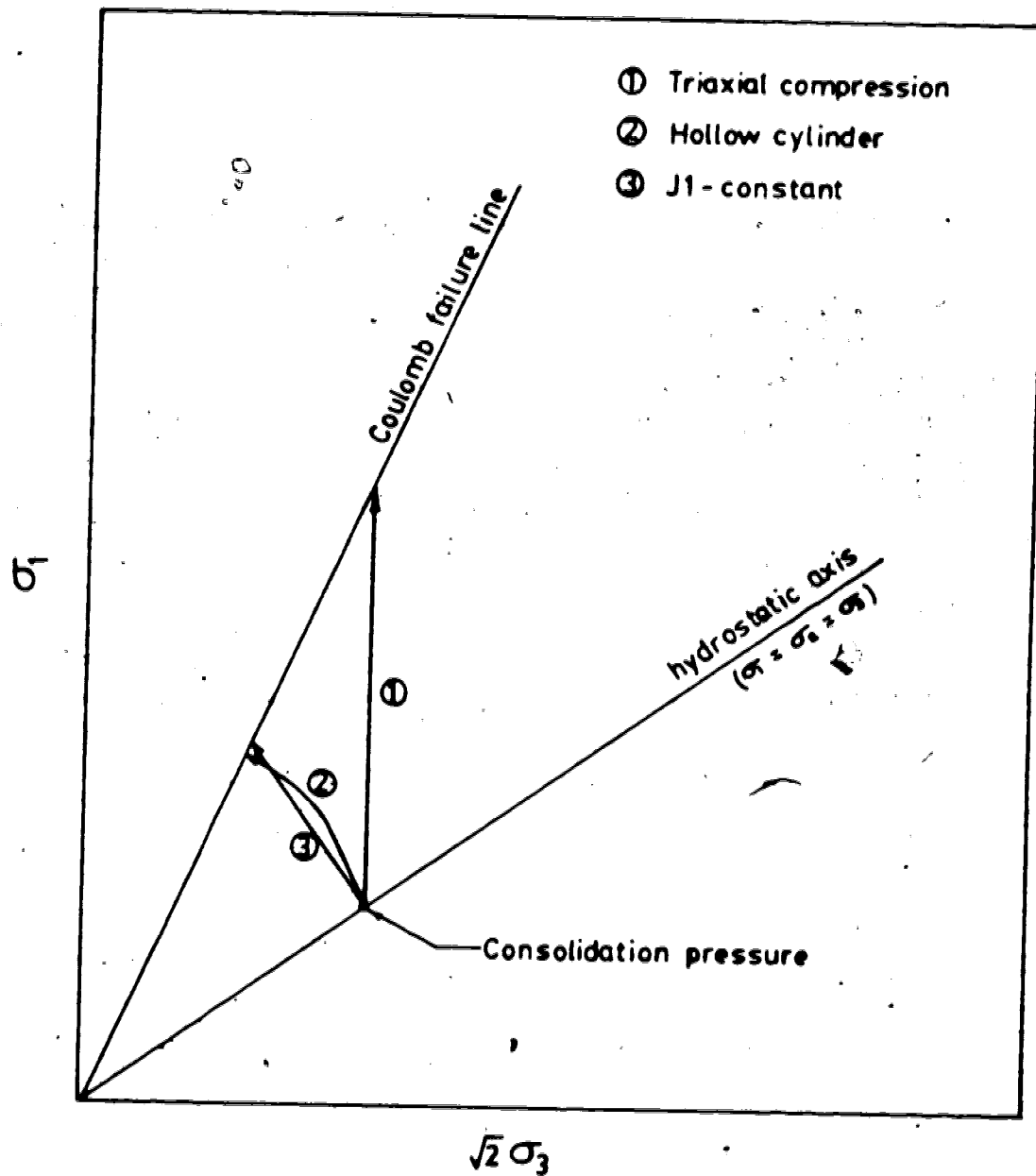
Figure 2.1 Stress paths followed in the laboratory tests

2.5.3 Constant Mean Principle Stress Tests (Series C)

In these tests, two samples were consolidated to 5 MPa and 7 MPa respectively. The samples were sheared at a constant strain rate under drained conditions with constant mean principal stress ($J1 = (\sigma_1 + \sigma_2 + \sigma_3)/3 = $ constant) by increasing the axial stress and decreasing the cell pressure. Volume changes were again monitored throughout the test against a constant back pressure.

Details of the sample assembly and test procedures are given in a later section. An oedometer test was used to determine the compressibility of oil sands at high pressure.

2.5.4 Selection of strain rate

The strain rate selected for Series B and C tests was based initially on the method proposed by Bishop and Henkel(1957,pp125-127) where the time to failure depends upon both the drainage conditions and the coefficient of consolidation.

Negligible volume changes are occurring in the sample after 10 minutes for each application of cell pressure. The theoretical t_{100} value is less than 10 minutes, and the calculated time to failure is only 1 hour.

The coefficient of consolidation, C_V, is a function of both the coefficient of compressibility and the permeability. The coefficient of compressibility is stress dependent, and the permeability of water through the oil sand sample will increase as the sample dilates.

The value selected for the coefficient of consolidation was obtained from the isotropic consolidation test, and the calculated time to failure should be conservative. However, due to the variability of these parameters and the presence of the bitumen, the time to failure in these tests was taken as 4 hours.

2.6 Sampling and Sample Preparation

2.6.1 Sampling

Sampling of oil sands is difficult as sample disturbance results from the expansion caused by gas coming out of solution when the confining pressure is reduced. Dusseault(1980) has discussed this phenomena in detail and has shown that conventional geotechnical methods of obtaining samples are inadequate for use in the oil sands. The best methods for obtaining relatively high quality samples is by pressure coring and *in situ* freezing procedures, or within natural slopes where the gas has been depleted.

In situ freezing techniques are very costly, hence it was decided to obtain block samples from an open pit mine where the gas has slowly escaped and thus disturbance is minimized. Preliminary determination of sample densities gave a bulk density of 2.0 g/cc (porosity of 35%) which compares favourably with the results reported by Dusseault(1980).

The material used was obtained from the GCOS (Great
Canadian Oil Sands Ltd., now Suncor Inc.) open-pit mining
operation north of Fort McMurray. The samples were
collected from the middle McMurray Formation and are
bitumen-rich oil sands. The sampling procedure used was to
cut a block from the large blocks of material that have
fallen off the face of the excavated walls along exfoliation
fractures. Immediately after a block had been cut, it was
wrapped in a plastic bag and well bound with
fibre-reinforced tape. The sample was then transported
carefully down the slope and stored on a thick foam mattress
in the back of the vehicle. Extreme care was taken in the
handling of the samples in order to minimize disturbance and
possible breakage of the larger blocks.

On arrival at the laboratory, the blocks were wrapped
in cheese-cloth and waxed to prevent any further moisture
loss and deterioration. The waxed samples were then stored
in a moist room until they were required for testing.

2.6.2 Sample Preparation

2.6.2.1 Oedometer and Triaxial Samples

All triaxial samples were obtained from a single block
of rich oil sand, while the oedometer sample was obtained
from a block of lean oil sand. The block was removed from
the moist room and allowed to freeze in a cold room at -18°
C. The block was cut into smaller pieces approximately 10
cm square by 15 cm long with a diamond saw. These blocks

were wrapped in plastic bags, taped, then stored in the cold room in a container of dry ice.

When a sample was required for testing, the block was unwrapped and placed in a lathe (installed in the cold room). The sample was trimmed using tungsten-carbide bits. It is important that the sample does not heat up during this operation as this will result in some expansion. To minimize this effect, the sample was returned several times to the dry ice container to keep it well frozen. The entire length of the sample is never trimmed as some end bearing surface is needed to clamp the sample in the lathe.

The ends of the trimmed sample are cut with the diamond saw to approximately the required length and the sample is then refrozen in the dry ice. The final stage of the preparation consisted of grinding the ends of the sample on a belt sander to the correct length. A metal guide was mounted on the sander to ensure that the ends of the samples were square and parallel. Extreme care was taken to ensure that the ends did not heat up.

2.6.2.2 Hollow Cylinder Samples

The preparation of these samples required some experimentation. The method described below is that which was finally used in the preparation of the actual test specimens.

A block sample was left to freeze in the cold room and then cut into a cube of approximately 20 cm square by 25 cm.

This cube was frozen into a wooden box containing saturated sand. At least 5 cm of sand was placed beneath the sample and about 5 cm around the perimeter of the sample. The wooden box was clamped onto a milling machine table (in the cold room) and dry ice packed around the sample to its full height.

The block was left to freeze for at least two hours after the dry ice was placed. A diamond core barrel, 51.4 mm external diameter, was used to core the centre hole. Coring was done dry, pressured nitrogen being used to blow up the cuttings. The coring was done slowly and no more than 5 cm cored at any one time before letting any built-up heat dissipate. Dry ice was placed in a bag and inserted in the cored hole to assist in the cooling operation. The core barrel had to be constantly cleaned to remove the broken core. Inspection of the bore immediately after each coring operation revealed no signs of heating on this inside wall of the sample.

A similar procedure was used to obtain a sample of 15 cm external diameter. A 15 cm diameter core barrel was used which had a larger clearance than most core barrels on the inside wall. This facilitated the collection and removal of cuttings. The barrel was centred over the first hole and coring carried out in a similar manner. The trimming of this oversize sample was done on the lathe. An aluminum shaft was frozen into the bore and filled with dry ice before mounting it in the lathe. Trimming was carried out

as described earlier with regular refreezing periods. The
ends of the sample could be finished on the lathe due to the
mounting procedure used. This ensured that the ends were
flush and parallel.

The sample preparation techniques described above are
illustrated in part on Plates 2.2 and 2.3.

2.7 Sample Assembly and Test Procedures

The triaxial samples are assembled as for a normal
triaxial test on any other material. Once the sample has
been placed in the membrane, the membrane is filled with
water to displace the air. The sample is allowed to thaw
against a cell pressure of 350 kPa and a back pressure of
200 kPa prior to the commencement of the consolidation test.
The consolidation is conducted against a back pressure of
1050 kPa, each increment of cell pressure being maintained
until no noticeable volume change of the pore fluid is
occurring (usually 10 min.). The final consolidation
pressure is applied for at least 30 min. before starting the
shear test, which is carried out at a constant strain rate.
For the $\sigma1$-constant tests, a programmable calculator was
used to determine the cell pressure required at any
particular axial stress. The cell pressure was determined
by allowing for an area correction for the axial stress
following Bishop and Henkel(1962). Throughout the test the
cell pressure was calculated at 1 to 2 minute intervals and
the pressure reduced as required. This procedure worked
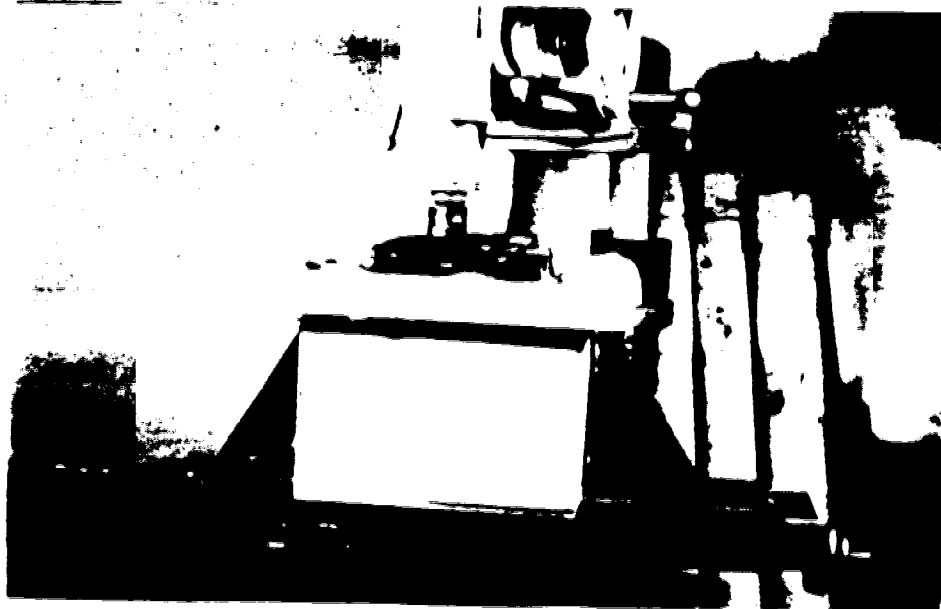
Plate 2.2 Sample preparation techniques
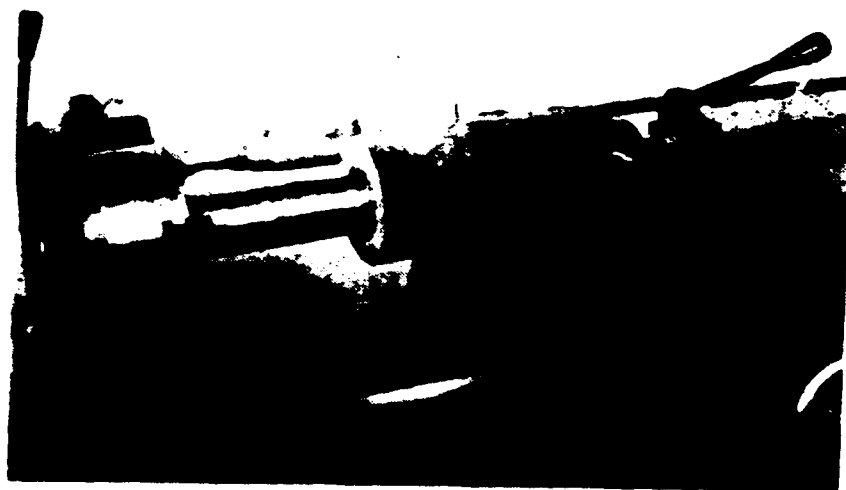
Plate 2.3 Sample preparation techniques

well as the maximum variation in J1 was less than 2%.

The hollow cylinder samples were mounted onto the base plate in the cold room. The external membrane clamp is fastened to the base plate and the sample inserted. The internal membrane is inserted and the ram placed on top of the load cap. The external membrane is sealed against the load cap and the ram by means of O-rings and hose clamps. The base plate is removed from the cold room and the cell placed onto it.

The cell is filled with water and an initial pressure of 55 kPa applied to both membranes prior to installing the cell in the plane-strain frame. The cell pressure is raised slightly while the system is flushed with a pressure of 70 kPa to 100 kPa. This operation removes air from the porous stones and between the sample and membranes. After flushing, the cell and bore pressures are increased to 350 kPa while the back pressure is increased to 200 kPa. Under these conditions the sample is left to thaw overnight. The consolidation test is conducted against a back pressure of 1050 kPa. The shear test is stress controlled. The cell pressure is kept constant and the internal pressure decreased in 500 kPa increments. Each increment is maintained for at least 5 min. or until no further volume changes occur. The increments are reduced to about 140 kPa in the final stages of the test.

2.8 Sample Saturation

The method of testing for sample saturation as outlined in Bishop and Henkel(1962) is not applicable when testing oil sand. The low compressibility of the material results in a B-value less than unity at saturation. The samples tested had an initial degree of saturation of only 80%, hence a large back pressure was required to saturate them.

Full saturation can be accomplished by use of a back pressure, but it is also a function of time (Black and Lee,1973). The samples had an applied back pressure of 1050 kPa (150 psi) and this pressure should be sufficient to fully saturate them. After application of the back pressure, the pore volume change was monitored and no noticeable volume changes were occurring prior to the start of the consolidation test. However, the sensitivity of the burettes may not have been sufficient for this purpose. The time interval from the application of the back pressure to the start of the shear test was usually 1.5 hours, and this should also assist in saturating the samples.

Full saturation is critical when conducting undrained tests and a satisfactory laboratory procedure to test for saturation will be required. Undrained tests on oil sand will be attempted by another researcher soon, and two methods of testing for saturation are outlined below.

The first method is based on the fact that the B-value is independent of back pressure (Wissa,1969). The back pressure is increased for each B-test while keeping the

effective consolidation pressure constant. Full saturation results when the calculated B-value remains constant. In order to maintain a constant effective consolidation pressure, each increment of back pressure and cell pressure must be exactly equal before measuring B. Another method proposed by Wissa(1969) is to apply several large increments of cell pressure without allowing drainage. The B-values are measured and will be the same (or slightly smaller) for each increment of cell pressure at saturation.

Other methods may be devised, but the method chosen should be relatively simple and quick. This procedure may well be the critical part of any undrained tests that are performed, and serious attention must be directed towards this problem.

2.9 Measurements and Measuring Systems

All data collected during the test were recorded by electronic measuring systems except for the volume changes. Axial loads are measured on a 89 kN load cell and axial strain with a linearly variable displacement transducer (LVDT). The cell pressures and back pressures are measured with 13.8 MPa pressure transducers. Measurements of volume changes are made on reversible burette type volume change indicators. For the hollow cylinder tests these indicators have an accuracy of 0.1 cc. The triaxial samples require a more sensitive burette due to the smaller volume of these samples, and burettes with an accuracy of 0.01 cc were used.

The pressure systems used in the laboratory are discussed in Appendix F, which also deals with the problems encountered in the laboratory during this research program.

CHAPTER 3

CALCULATION OF STRESSES AND STRAINS IN THE HOLLOW CYLINDER

3.1 Introduction

The stress distribution within the hollow cylinder depends upon both the stress state and the type of test being analysed. If the state of stress is such that no yielding occurs at any point within the cylinder, then the stress distribution can be determined from the theory of elasticity. When yielding occurs, plasticity solutions are required to determine the distributions.

The series of tests conducted on the hollow cylinder samples were performed under plane-strain conditions. For this case, the axial stress is the intermediate principal stress and the sample deforms axisymmetrically, the slip lines occurring in the r-θ plane. The distribution of stresses can be determined from limiting equilibrium conditions by specifying a failure criterion for the material. The solution for the case where the axial stress is the major principal stress requires that a stress-strain law be specified to solve for the stress distribution (Wu et al.,1963).

In this series of tests, the external pressure is kept constant and the internal pressure decreased until the sample collapses. The tangential stress is the major principal stress and the radial stress the minor one. The stress state is such that yielding first occurs at the

31

internal wall of the sample.

The solutions for the distribution of radial and tangential stresses within the hollow cylinder are given in the following sections for both the case of no yielding and for the case when yielding has occured.

3.2 Elastic Solution for the Stress Distribution

The axisymmetric problem may be solved in terms of the equilibrium equations, Hooke's Law, the compatibility requirements and the Airy stress function. By applying the appropiate boundary conditions, the solution for the radial and tangential stress distributions age determined :

$$\sigma_r = \frac{A}{r^2} + 2C \qquad \qquad \ldots 3.1(a)$$

$$\sigma_\theta = -\frac{A}{r^2} + 2C \qquad \qquad \ldots 3.1(b)$$

$$\mathcal{T}_{r\theta} = 0 \qquad \qquad \ldots 3.1(c)$$

where:

$$A = \frac{-a^2 b^2 (p_e - p_i)}{b^2 - a^2} \quad ; \qquad 2C = \frac{-p_i a^2 + p_e b^2}{b^2 - a^2}$$

The symbols used in the above equations are illustrated in Figure 3.1.
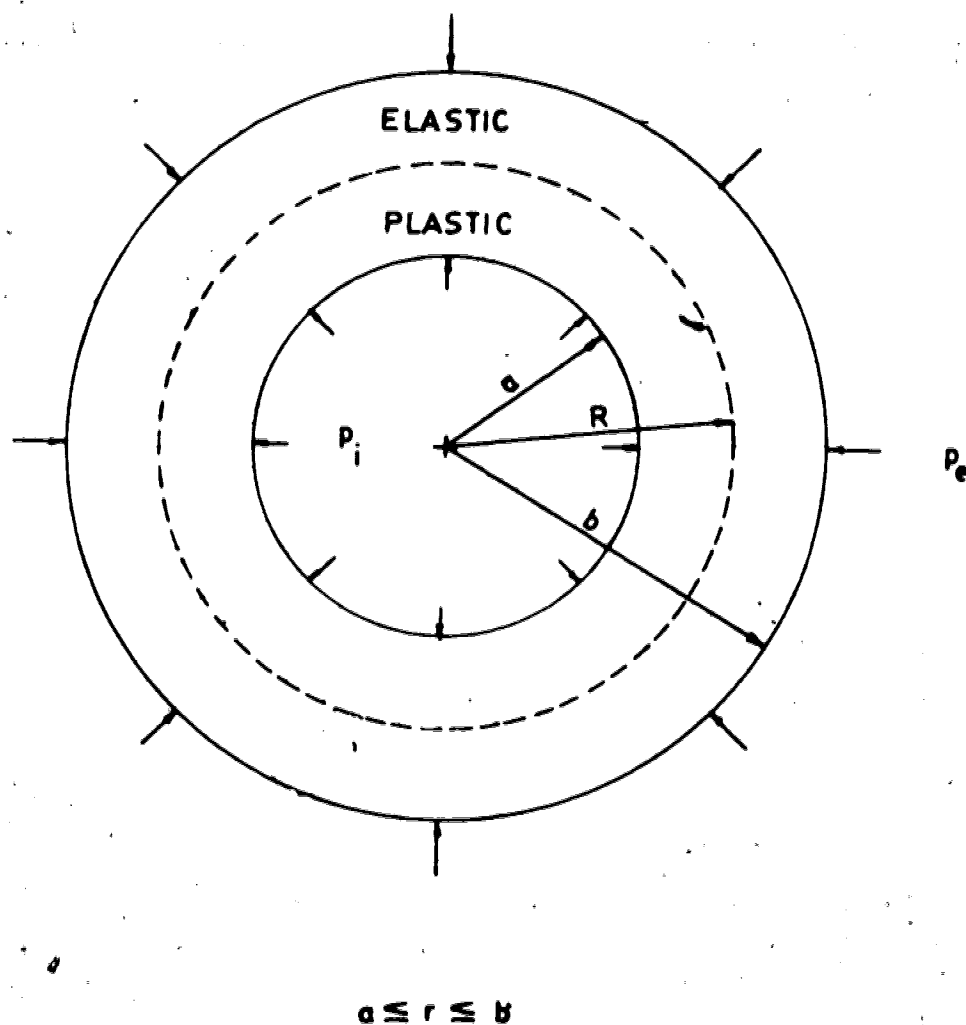
Figure 3.1 Definition of the terms used in the Stress
Analysis

The derivation of these equations is given in Appendix A. The average stresses in the sample are found by integrating the above stress distributions across the width of the cylinder and dividing by the wall thickness. The results are given below :

$$(\sigma_r)_{ave} = 2C + \frac{A}{ab}$$ 3.2

$$(\sigma_\theta)_{ave} = 2C - \frac{A}{ab}$$ 3.3

3.3 Stress Distribution after Yielding

As discussed before, yielding commences at the internal wall of the sample. A plastic zone develops axisymmetrically around the inner surface, while the remainder of the sample is still behaving elastically. This plastic zone is shown diagramatically in Figure 3.1. The stresses in the elastic zone cannot be calculated from the equations given previously as the boundary conditions have changed. The solution for the stresses in the elastic zone requires that the extent of the plastic zone be known.

3.3.1 Stresses in the Plastic Zone

The Mohr-Coulomb failure criterion is assumed to be valid for this material. The validity of this assumption is discussed in Chapter 4. By combining the equilibrium equations with the failure criterion, the stress

distribution is obtained :

$$\sigma_r = \frac{1}{N-1}\left[A r^{N-1} - 2c N^{1/2} \right] \qquad \dots 3.4$$

$$\sigma_\theta = \frac{N}{N-1}\left[A r^{N-1} \right] + \frac{2c N^{1/2}}{N-1} \qquad \dots 3.5$$

where A is solved from the boundary conditions :

$$A = \frac{P_i(N-1) + 2c N^{1/2}}{a^{N-1}}$$

$$N = \frac{1 + \sin\phi}{1 - \sin\phi}$$

The derivation of these equations is given in Appendix B.

3.3.2 Stresses in the Elastic Zone

The solution for these stresses can be obtained from Equations 3.1 provided that the boundaries of the elastic zone are modified. The elastic zone is now defined by an internal radius (R) and an external radius (b). The pressures on the internal and external walls are σ_p and p_e respectively.

Substitution of these values into Equation 3.1 gives :

$$\sigma_r^e = \frac{P_e b^2 - \sigma_p R^2}{b^2 - R^2} - \frac{R^2 b^2 (P_e - \sigma_p)}{r^2 (b^2 - R^2)} \qquad \dots 3.6(a)$$

$$\sigma_\theta^e = \frac{P_e b^2 - \sigma_p R^2}{b^2 - R^2} + \frac{R^2 b^2 (P_e - \sigma_p)}{r^2 (b^2 - R^2)} \qquad \ldots\ldots 3.6(b)$$

$$\tau_{r\theta} = 0 \qquad \ldots\ldots 3.6(c)$$

It is necessary to calculate the radius of the plastic zone and the radial stress at the elastic-plastic boundary before the stress distributions can be determined.

3.3.2.1 Radius of the Plastic Zone

The radius is determined by assuming that the radial stress at the boundary is continuous. Before yielding occurs, the sum of the elastic radial and tangential stresses (σ_0) is a constant value at any point within the cylinder (for each set of applied boundary pressures). After yielding has occurred, the sum of the elastic stresses in the elastic zone is also a constant value, but this constant is a function of the radius of the plastic zone. The solution for the radius of the plastic zone is simplified if it is assumed that this constant is of the same magnitude as would be calculated if no yielding had occurred. In Chapter 6, the validity of this assumption is discussed.

The radius of the plastic zone, based on the assumptions outlined above, is determined by equating the values of the radial stress at the boundary calculated from the elastic and plastic solutions. The solution is given

below and the derivation shown in Appendix B.

$$R = a \left\{ \frac{2}{N+1} \left[\frac{\sigma_0(N-1) + 2cN^{1/2}}{P_i(N-1) + 2cN^{1/2}} \right] \right\}^{\frac{1}{N-1}} \qquad \ldots .3.7$$

The radial stress at the elastic-plastic boundary is found from Equation 3.4 :

$$\sigma_p = \left[P_i + \frac{2cN^{1/2}}{N-1} \right] \left[\frac{R}{a} \right]^{N-1} - \frac{2cN^{1/2}}{N-1} \qquad \ldots .3.8$$

3.4 Average Stresses within the Hollow Cylinder

3.4.1 Average Tangential Stress

The average tangential stress can be found by integrating the stress distribution across the width of the wall and dividing by the wall thickness. However, the average stress can also be found by considering the static equilibrium of a half-section of the cylinder. Figure 3.2 shows this section and the calculation. This approach is simpler and the solution is independent of the extent of the plastic zone. The average tangential stress is :

$$(\sigma_\theta)_{ave} = \frac{P_o b - P_i a}{b - a} \qquad \ldots .3.9$$

3.4.2 Average Radial Stress

The average radial stress can be determined in two ways. A linear distribution of the stresses may be assumed (or any other shape) and the average stress calculated from
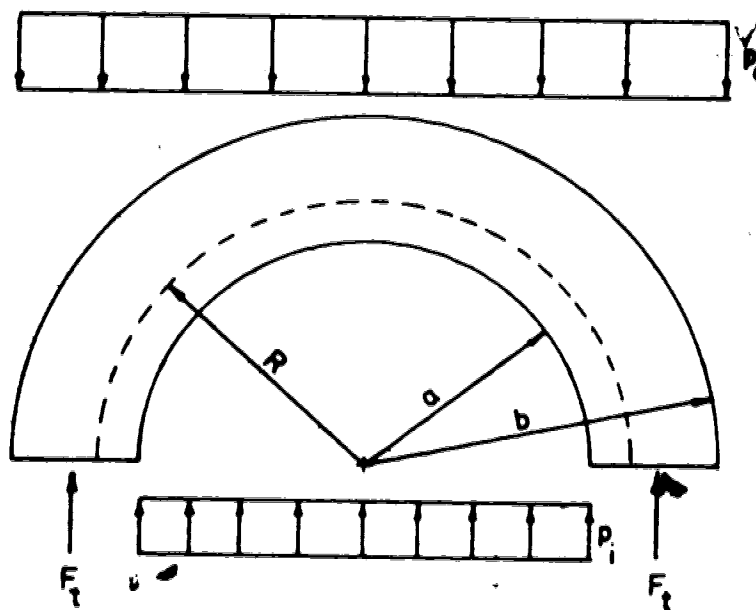
For equilibrium :

$$2F_t + p_i(2a) - p_e(2b) = 0$$

$$\therefore F_t = p_e b - p_i a$$

$$(\sigma_e)_{ave} = \frac{F_t}{b-a}$$

$$= \frac{p_e b - p_i a}{b-a}$$

Figure 3.2 Static Equilibrium conditions for the half Cylinder

distribution, or the stress distribution given in Equations 3.4 and 3.6(a) may be integrated across the width of the cylinder and divided by the wall thickness.

The average radial stress based on a linear distribution is :

$$(\sigma_r)_{ave} = \frac{P_e + P_i}{2} \qquad \qquad ....3.10$$

The average stress found by integration is derived in Appendix B and given for a cohesionless material by :

$$(\sigma_r)_{ave} = \frac{F_r}{b-a} \qquad \qquad ....3.11$$

where:

$$F_r = P_i \left[\frac{R^N}{Na^{N-1}} - \frac{a}{N} + \frac{(b-R)}{(b+R)} \frac{R^N}{a^{N-1}} \right] + P_e b \frac{(b-R)}{(b+R)}$$

Both of these solutions have been used in the analysis of the hollow cylinder test data. Their effect on the stress-strain curves and strength parameters are discussed in Chapter 6.

3.4.3 Average Axial Stress

The load applied at the top of the sample is measured throughout the test and thus the average axial stress can be determined directly :

$$(\sigma_z)_{ave} = \frac{P - P_i A_i}{A_s} \qquad \qquad ....3.12$$

The meaning of the symbols are as defined in the nomenclature.

3.5 Determination of the Strength Parameters

The strength of a cohesionless material at high confining pressures may be defined by a secant value of the friction angle, ϕ_s. This angle is determined from the effective principal stresses at failure (for a Mohr-Coulomb material):

$$\sin \phi_s' = \frac{\sigma_1' - \sigma_3'}{\sigma_1' + \sigma_3'} \qquad \qquad ....3.13$$

The value of ϕ_s determined by this method will be dependent on the magnitude of the average radial stress, and the calculation of this stress will have a large influence on the friction angle. An alternate method of determining the peak friction angle is found from the elasto-plastic analysis. At collapse of the sample, the radius of the plastic zone becomes equal to the external radius (b) and the radial stress will thus be equal to the external pressure (P_e) in Equation 3.8. Rearrangement of this equation under these conditions give :

$$\left[\frac{p_s}{p_i}\right]_f = \left[\frac{b}{a}\right]^{N-1} \qquad \qquad \dots 3.14$$

The pressure ratio and ratio of the radii at collapse are known from the test results, and the strength parameter (N) can be calculated.

Comparison of the friction angles determined by these methods are given in Chapter 6.

3.6 Calculation of the Average Strains in the Cylinder

The calculation of the strains are based on average strain increments rather than total strains. Strain increments have been used as the test is performed by reducing the internal pressure incrementally. Total strains are calculated by adding the strain increments.

The principal strain axes are assumed to coincide with the principal stress axes, and compressive strains are considered as being positive. The small strains theory is used, i.e :

$$dv = d\epsilon_z + d\epsilon_r + d\epsilon_\theta \qquad \qquad \dots 3.15$$
$$= d\epsilon_r + d\epsilon_\theta \quad \text{for plane-strain}$$

The calculation of strains by this method has been dealt with by Procter(1967). His derivations are presented in a form that can be readily programmed. A copy of these derivations is given in Appendix D.

3.6.1 Average Radial Strain

The average strain increment is defined as :

$$d\epsilon_r = \frac{\text{mean change in specimen wall thickness}}{\text{mean wall thickness}}$$

The wall thickness at any increment is calculated from the measured volume changes of the bore and sample :

$$a_i = \sqrt{a_0^2 - \frac{(\Delta v_b)_i}{\pi L_0}}$$

$$b_i = \sqrt{b_0^2 - \frac{(\Delta v_s + \Delta v_b)_i}{\pi L_0}}$$

The average radial strain increment is :

$$d\epsilon_r = \left[\frac{(b_i-b_j)-(a_i\ a_j)}{(b_i+b_j)-(a_i+a_j)}\right] \times 2 \qquad \ldots 3.16$$

The jth increment is the current increment and the ith increment the previous one. The total radial strain is found by summation of the strain increments :

$$(\epsilon_r)_j = \sum_1^j d\epsilon_r \qquad \ldots 3.17$$

3.6.2 Average Volumetric Strain

The average volumetric strain increment is given by :

$$dv = \left[\frac{(\Delta v_s)_j - (\Delta v_s)_i}{2(v_s)_0 - (\Delta v_s)_j - (Dv_s)_i} \right] \times 2 \qquad \ldots 3.18$$

The total volumetric strain is :

$$(v)_j = \sum_1^j dv \qquad \ldots 3.19$$

3.6.3 Average Tangential Strain

When the average radial and volumetric strain increments have been calculated, the average tangential strain increment is determined from Equation 3.15 :

$$d\epsilon_\theta = dv - d\epsilon_r \qquad \ldots 3.20$$

The total tangential strain is :

$$(\epsilon_\theta)_j = \sum_1^j d\epsilon_\theta \qquad \ldots 3.21$$

3.7 Determination of the Elastic Deformation Moduli

Young's Modulus (E) is obtained from the linear elastic constitutive equations :

$$\Delta \epsilon_r = \frac{1}{E}\left[\Delta \sigma_r - \nu (\Delta \sigma_\theta + \Delta \sigma_z) \right] \qquad \ldots 3.22(a)$$

$$\Delta \epsilon_\bullet = \frac{1}{E}\left[\Delta \sigma_\bullet - \nu(\Delta \sigma_r + \Delta \sigma_z)\right] \qquad \ldots 3.22(b)$$

$$\Delta \epsilon_z = \frac{1}{E}\left[\Delta \sigma_z - \nu(\Delta \sigma_r + \Delta \sigma_\bullet)\right] \qquad \ldots 3.22(c)$$

For plane-strain conditions, Equation 3.22(c) is set equal to zero and the following relationship is obtained :

$$\Delta \sigma_z = \nu(\Delta \sigma_r + \Delta \sigma_\bullet) \qquad \ldots 3.23$$

Poisson's ratio is determined from Equation 3.23 :

$$\nu = \frac{\Delta \sigma_z}{\Delta \sigma_r + \Delta \sigma_\bullet} \qquad \ldots 3.24$$

Young's Modulus is calculated by substituting Equation 3.23 into Equation 3.22(b) :

$$E_{ps} = \frac{E}{1-\nu^2} = \frac{\Delta \sigma_\bullet - (\frac{\nu}{1-\nu})\Delta \sigma_r}{\Delta \epsilon_\bullet} \qquad \ldots 3.25(a)$$

$$= \frac{\Delta \sigma_d}{\Delta \epsilon_\bullet} \qquad \ldots 3.25(b)$$

In the hollow cylinder test, yielding occurs at the inside wall at a pressure ratio ($\frac{P_e}{P_i}$) of only 2 to 3. The elastic modulus is thus defined for only a small portion of the average stress-strain curve. The use of a psuedo-elastic modulus (defined as the slope of the average stress-strain curve at any stress level) is dealt with in Chapter 4.

3.8 Summary

The calculation of stresses and strains within the hollow cylinder has been presented. An incremental approach has been used for the calculations of strains due to the manner in which this series of tests have been conducted. Several assumptions have been made in the analysis of the stress distributions. Some of these assumptions are those typically made for soils, the others for simplicity of the solution alone. In either case, the validity or influence of the assumptions on the analysis of the test data will be discussed in the following chapters.

CHAPTER 4

DEVELOPMENT OF THE NUMERICAL MODEL

4.1 Introduction

The interpretation of data from a hollow cylinder triaxial test is a problem that has as yet not been properly examined. Assumptions have to be made regarding the stress distribution within the cylinder. These assumptions have been discussed in Chapter 3.

Once a stress distribution has been determined, the problem of how to interpret the elastic deformation moduli remains. Linear elastic formulations enable the Young's modulus to be defined in terms of deviatoric stress and tangential strain as presented in Chapter 3. It still remains to be shown that the moduli determined in such a manner from the hollow cylinder data do in fact represent the true moduli for the material.

The writer has approached this problem by determining the elastic constants (assuming a linear radial stress distribution) from the average stress-strain curve for the test. These moduli are then used as input in an idealized model in an attempt to predict the deformation of the cylinder that are measured during a test. The analytical model developed for this problem is dealt with in the following sections. The stress and strain determinations from the hollow cylinder test have been described in the previous chapter.

4.2 Formulation of the Problem

Oil sands, as well as other materials, exhibit curvilinear failure envelopes. This initiated the development of an axi-symmetric solution that could incorporate this type of failure envelope. Curvilinear failure envelopes have not been used in any of the elasto-plastic closed form solutions available in the literature.

The strain-weakening behaviour of oil sands (Dusseault,1977) was another design factor to be considered. The solution should be able to model such behaviour as closely as possible. It has been shown that strain-weakening behaviour can be modelled with an elastic-perfectly plastic model (Korbin,1976).

The effect of confinement on the Young's modulus is evident from the test results which show a marked non-linear stress-strain curve (see Chapter 5). This non-linear stress-strain curve is the result of the influence of reduced confinement of the sample as well as the non-linear behaviour of the material. It is thus necessary to incorporate the strain-softening effect of the deformation modulus into the model.

4.3 Theoretical Aspects of the Model

The use of a linear or non-linear elastic model will not be satisfactory in the prediction of deformations. These models work well at small strains, but in a hollow

cylinder, the strains are large, especially once yielding has occurred.

Elastic models have further limitations (Hoeg,1978). They do not model typical soil behaviour such as dilation (for dense sands), stress history, stress path dependency and strain-weakening. These effects can be modelled by using elasto-plastic models.

The theory of plasticity was originally developed for metals and has been adapted and extended to model soil behaviour. The deformations are determined by defining a flow rule and a work-hardening law, which are relationships between the plastic strain increment and the stress increment vectors.

The undrained behaviour of soils can still be modelled on the basis of classical plasticity, but the volume changes that occur during drained behaviour need to be incorporated into the theory. The Mohr-Coulomb strength relationship can be considered to be a yield criterion and a flow rule must be postulated which will predict the plastic volume changes accurately.

The use of an associated flow rule with the Mohr-Coulomb yield criterion has been found to give unrealistically large plastic volume changes (Hoeg,1978 ; Morgenstern,1975) and this led to the introduction of a non-associated flow rule: i.e., the yield criterion and the plastic potential function are not identical. The non-associated flow rule can account for volume changes that

occur between two limits, that of no volume change and that
of maximum volume change (associated flow rule). The model
developed below has the capability of incorporating a
dilation parameter (which is constant within the plastic
zone) that has some value between these two limits.

4.3.1 Failure Criterion

The Mohr-Coulomb failure criterion has been shown to be
applicable for drained tests on dense sand (Kirkpatrick,
1957). The non-linearity of the Mohr envelope is modelled
by using an empirical criterion postulated by
Dusseault(1977) for cohesionless materials :

$$T = a \, \sigma_n^{b}$$

.....4.1

where σ_n is the normal stress on the failure plane

and a, b are curve fitting parameters

For simplicity, it is assumed that this equation
describes the failure criterion which passes through the top
of the Mohr circles, i.e. that failure occurs along planes
of maximum shear stress (Figure 4.1). The normal stress is
then given by :

$$\sigma_n = \frac{\sigma_\theta + \sigma_r}{2}$$

.....4.2
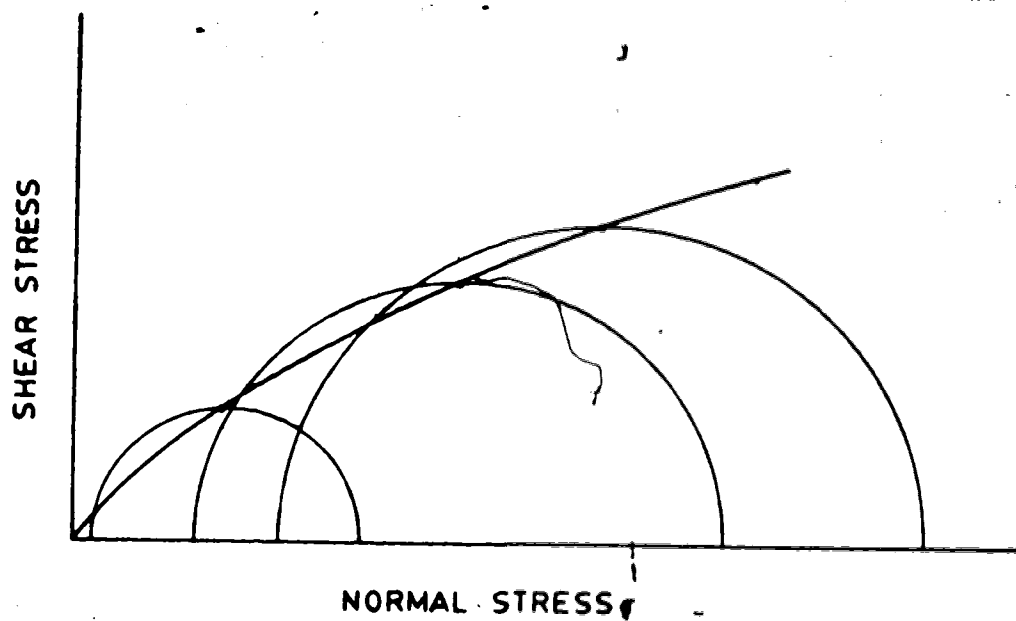
Figure 4.1 Failure criterion adopted in the model
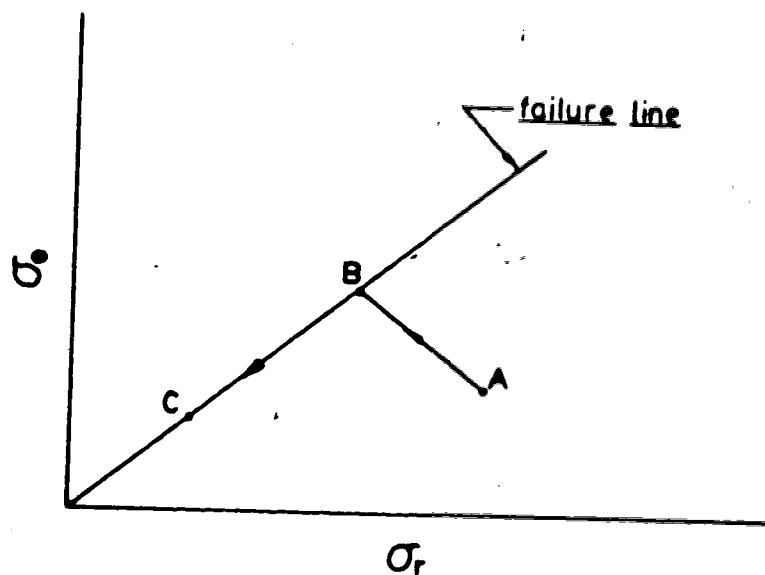
Figure 4.2 Stress path followed by a typical soil element in the model

In the hollow cylinder test, plane strain is maintained in the vertical direction (in this series of tests). The author believes that, as a result of this constraint, failure planes are unlikely to be the same as for the conventional triaxial test, and that failure along planes of maximum shear stress is most probable. However, as mentioned, it is simple to incorporate any other analytic criterion into the model. The Mohr-Coulomb equation could be modified to give the following criterion :

$$\sigma_\bullet = a\, \sigma_r^b$$

The maximum shear stress is given by :

$$\tau_{max} = \frac{\sigma_\bullet - \sigma_r}{2}$$

and the failure criterion may be rewritten as :

$$\frac{\sigma_\bullet - \sigma_r}{2} = a\left(\frac{\sigma_\bullet + \sigma_r}{2}\right)^b \qquad \ldots 4.3$$

4.3.2 Determination of Stresses in the Cylinder

In order that the failure criterion is not violated, the stress path followed by an element in the cylinder is as illustrated in Figure 4.2. The stress path AB represents the stress increments while the cylinder is behaving elastically, and Point B represents the stress state at yielding of the element.

When the element has yielded, the stresses are defined by the failure criterion and hence decrease with decreasing

internal pressure (path BC). The calculation of the stresses is dealt with in the following section.

4.3.2.1 Pre-Yield Condition

The stresses in the cylinder are calculated from the linear elastic equations derived for a hollow cylinder (see Chapter 3). The stress distributions are given by Equations 3.1(a) to 3.1(c).

4.3.2.2 Post-Yield Condition

The stresses in the plastic zone are calculated by considering the equilibrium equation and failure criterion in the plastic zone (Equations B.2 and 4.3). The solution of these equations is complex and makes a closed form solution unsuitable. A finite-difference technique is used to solve the equations.

For the axi-symmetric case, $\sigma_r = \text{fct}(r)$, and the Taylor series for this function can be expanded as follows :

$$(\sigma_r)_{i+1} = (\sigma_r)_i + \Delta r \left(\frac{d\sigma_r}{dr}\right)_i + \frac{(\Delta r)^2}{2!}\left(\frac{d^2\sigma_r}{dr^2}\right) + \cdots\cdots$$

Ignoring second order and higher terms yield :

$$\left(\frac{d\sigma_r}{dr}\right)_i = \frac{(\sigma_r)_{i+1} - (\sigma_r)_i}{\Delta r} = \frac{\Delta\sigma_r}{\Delta r}$$

From Eqn. B.2 : $\dfrac{d\sigma_r}{dr} = \dfrac{\sigma_\theta - \sigma_r}{r}$

$$\therefore \Delta \sigma_r = \frac{\Delta r}{r_i}(\sigma_\bullet - \sigma_r)_i \qquad \ldots \ldots 4.4$$

$$(\sigma_r)_{i+1} = (\sigma_r)_i + \Delta \sigma_r \qquad \ldots \ldots 4.5$$

The radius of the plastic zone is calculated by assuming continuity of the radial stresses at the elastic-plastic boundary. At the boundary, $\sigma_r = \sigma_p$ and the failure criterion can also be applied.

From Equations 3.6(a) and 3.6(b) we get :

$$\sigma_\bullet^e + \sigma_r^e = 2\left[\frac{P_\bullet b^2 - \sigma_p R^2}{b^2 - R^2}\right] \qquad \ldots \ldots 4.6(a)$$

$$= 2\sigma_0$$

$$\therefore \sigma_\bullet^e = 2\sigma_0 - \sigma_r^e \qquad \ldots \ldots 4.6(b)$$

Substituting Equation 4.6(b) into the failure criterion gives :

$$\frac{(2\sigma_0 - \sigma_r^e) - \sigma_r}{2} = a\left(\frac{2\sigma_0 - \sigma_r^e + \sigma_r}{2}\right)^b$$

$$\therefore \sigma_0 - \sigma_r^e = a\sigma_0^b$$

and :

$$\sigma_r^e = \sigma_0 - a\sigma_0^b \qquad \ldots \ldots 4.7$$

Equations 4.5 and 4.7 are solved iteratively. The cylinder is divided into a number of discrete nodes. The elastic stresses on the inside wall are calculated for each load increment until the failure criterion must be invoked. At this stage, the tangential stresses are related to the radial stresses by the failure criterion. These stresses on the wall form the first set of values to be used in the iterative process. $\triangle\sigma_r$ is calculated for the increment $\triangle r$, and thus the value of $(\sigma_r)_{i+1}$ is determined. $(\sigma_\bullet)_{i+1}$ is found from Equation 4.3.

The value of $(\sigma_r)_{i+1}$ and $(r)_{i+1}$ are substituted into Equation 4.7 and the value of σ_r^e is compared to σ_p. The procedure continues until either the difference

$$\left|(\sigma_p - \sigma_r^e)\right|$$

is within the specified tolerance or the difference $(\sigma_p - \sigma_r^e)$ changes sign from one iteration to the next. At this point, σ_r and r correspond to the radial stress at the plastic boundary and the radius of the plastic boundary respectively.

The stresses in the elastic zone are then calculated from Equations 3.6(a) and 3.6(b).

4.3.3 Strain Distribution

4.3.3.1 Elastic Strains

Before yielding occurs, the strains are determined from Hooke's law and the elastic stress distribution (see Equations 3.22(a) to 3.22(c)).

Strains are dealt with in an incremental manner. At

the completion of each load increment, the model boundaries
are modified by the amount of radial displacement at each
wall. Integration of the strain-displacement equations
yield :

$$\epsilon_\theta = \oint \frac{u_r}{r}$$

$$\therefore u_r = r\epsilon_\theta$$

$$i.e. \quad \Delta u_r = r \Delta \epsilon_\theta \qquad \qquad \ldots .4.8$$

This incremental strain procedure was instituted in the
model since the loading is applied incrementally, and the
stress distribution is sensitive to the values of the
boundary radii.

4.3.3.2 Strains in the Plastic Zone

The strains in the plastic zone are assumed to consist
of an elastic and plastic portion, thus :

$$\epsilon_\theta = \epsilon_\theta^e + \epsilon_\theta^p \qquad \qquad \ldots .4.9(a)$$

$$\epsilon_r = \epsilon_r^e + \epsilon_r^p \qquad \qquad \ldots .4.9(b)$$

The elastic portion of the strain is assumed to obey
Hooke's law while the plastic strains are defined by a flow
rule. Both the radial and tangential elastic strains

$\left(\epsilon_{\bullet}^{e}, \epsilon_{r}^{e}\right)$ are taken as being constant in the plastic zone and equal in magnitude to the strains at the elastic-plastic boundary, which simplifies the solution. The elastic strains in the plastic zone can thus be defined by :

$$\Delta \epsilon_{\bullet}^{e} = \frac{1-\nu^{2}}{E}\left[\Delta \sigma_{\bullet R} - \left(\frac{\nu}{1-\nu}\right)\Delta \sigma_{p}\right] \qquad \ldots.4.10(a)$$

$$\Delta \epsilon_{r}^{e} = \frac{1-\nu^{2}}{E}\left[\Delta \sigma_{p} - \left(\frac{\nu}{1-\nu}\right)\Delta \sigma_{\bullet R}\right] \qquad \ldots.4.10(b)$$

The strain compatibility equation may be written :

$$r\frac{d\epsilon_{\bullet}^{p}}{dr} + \epsilon_{\bullet}^{p} - \epsilon_{r}^{p} = \epsilon_{r}^{e} - \epsilon_{\bullet}^{e} - r\frac{d\epsilon_{\bullet}^{e}}{dr} \qquad \ldots.4.11(a)$$

Since $\epsilon_{\bullet}^{e}$ is constant in the plastic zone, $\frac{d\epsilon_{\bullet}^{e}}{dr} = 0$, and :

$$r\frac{d\epsilon_{\bullet}^{p}}{dr} + \epsilon_{\bullet}^{p} - \epsilon_{r}^{p} = \epsilon_{r}^{e} - \epsilon_{\bullet}^{e} \qquad \ldots.4.11(b)$$

The flow rule adopted is a modified form of the associated flow rule (Guenot, 1978) and is given as :

$$\epsilon_{r}^{p} + \alpha \epsilon_{\bullet}^{p} = 0 \qquad \ldots.4.12$$

where α = dilation parameter. When α =1, the condition of no volume change is modelled. The associated flow rule is obtained when α = N, the shear strength parameter. This represents the case of maximum volume change.

The compatibility equation is rewritten as :

$$\frac{d\epsilon_\theta^p}{dr} = \left[\frac{\epsilon_r^e - \epsilon_\theta^e - \epsilon_\theta^p(1+\alpha)}{r} \right] \qquad \ldots 4.13$$

This equation can also be solved by a finite-difference technique, similar to that given previously for the stress distribution :

$$\frac{\Delta\epsilon_\theta^p}{\Delta r} = \frac{(\epsilon_\theta^p)_{i+1} - (\epsilon_\theta^p)_i}{\Delta r}$$

$$\therefore \Delta\epsilon_\theta^p = \frac{\Delta r}{r_i} \left[(\epsilon_r^e - \epsilon_\theta^e)_i - (\epsilon_\theta^p)_i (1+\alpha) \right] \qquad \ldots 4.14$$

The solution is obtained by selecting an arbitrary value for $(\epsilon_\theta^p)_i$ at the inside wall. The iteration is carried out until r = R . At this point, the plastic strain must be zero. The value of $(\epsilon_\theta^p)_i$ is changed until the solution satisfies the tolerance specified.

The total strains are the sum of the elastic and plastic strains. The plastic strains calculated to satisfy the compatibility equation represent the total plastic strain at any stage of the test. These values are then

transformed into plastic strain increments by subtracting the total plastic strain at the previous load increment. The change in radial displacement is calculated from the strain-displacement equation and the model boundaries are adjusted as described earlier.

4.3.4 Strain-Softening Effect

The incremental procedure used in the analysis is well suited for incorporating a deformation modulus that is stress-dependent. It remains to be ascertained which particular function best describes this softening effect.

An average stress-strain curve from a hollow cylinder test on Ottawa sand is shown in Figure 4.3, based on the assumption of a linear radial stress distribution. It can be seen from this curve that the behaviour of the material is non-linear, and thus the tangent Young's modulus (E) will decrease with increasing deviatoric stress. In other words, the modulus will decrease with a decrease in the average radial stress.

A suitable function has to be defined which can best describe the variation of the deformation modulus within the elastic region of the cylinder. Three alternate functions were examined :

1. A variation of the modulus with average radial stress
2. A variation of the modulus with average deviatoric stress
3. A variation of the modulus with the radial stress at the
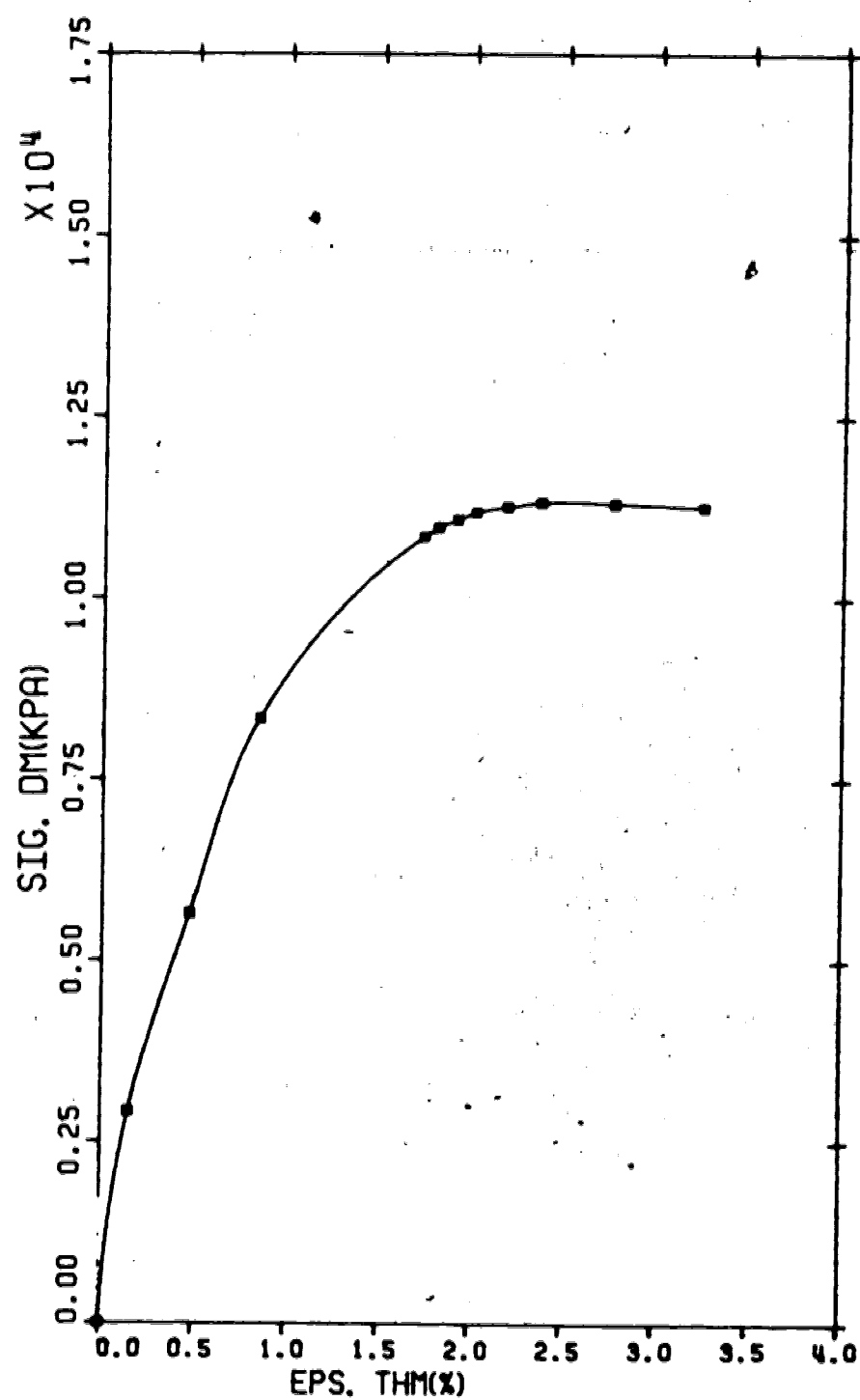
Figure 4.3 Average stress-strain curve for the Ottawa sand test

elastic-plastic boundary

The plots of these functions for the Ottawa sand test are shown in Figure 4.4. The values of E are calculated from the slope of the stress-strain curve (Figure 4.3) at different stress levels. The wall closures are compared with the actual closures in Figure 4.5.

The function that yields the best result is the first one (E varies with average radial stress). This function can be described by a bi-linear distribution of the following form :

$$\text{For } (\sigma_r)_{ave} > \sigma_r^c , \quad E = E_a - \lambda\left[P_e - (\sigma_r)_{ave} \right] \qquad \ldots\ldots 4.15(a)$$

$$\text{For } (\sigma_r)_{ave} < \sigma_r^c , \quad E = E_b - \lambda\left[P_e - (\sigma_r)_{ave} \right] \qquad \ldots\ldots 4.15(b)$$

where σ_r^c = average radial stress at the intersection of the above lines.

The average radial stress used in Equations 4.15 depends on whether yielding has occurred or not. Prior to yielding, the average radial stress is defined as :

$$(\sigma_r)_{ave} = \frac{P_e + P_i}{2} \qquad \ldots\ldots 4.16$$
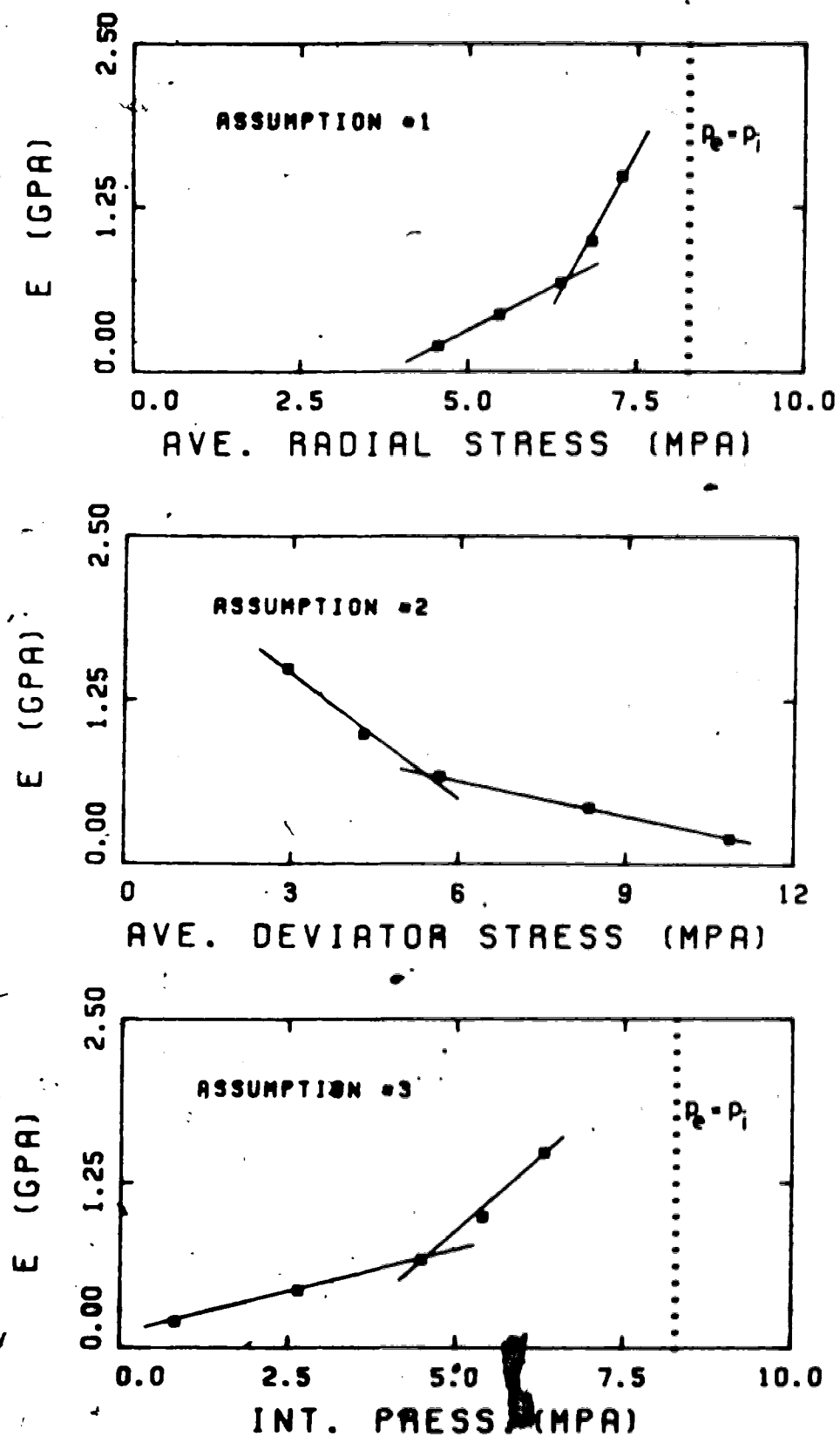
Figure 4.4 Possible functions for defining E in the elastic zone
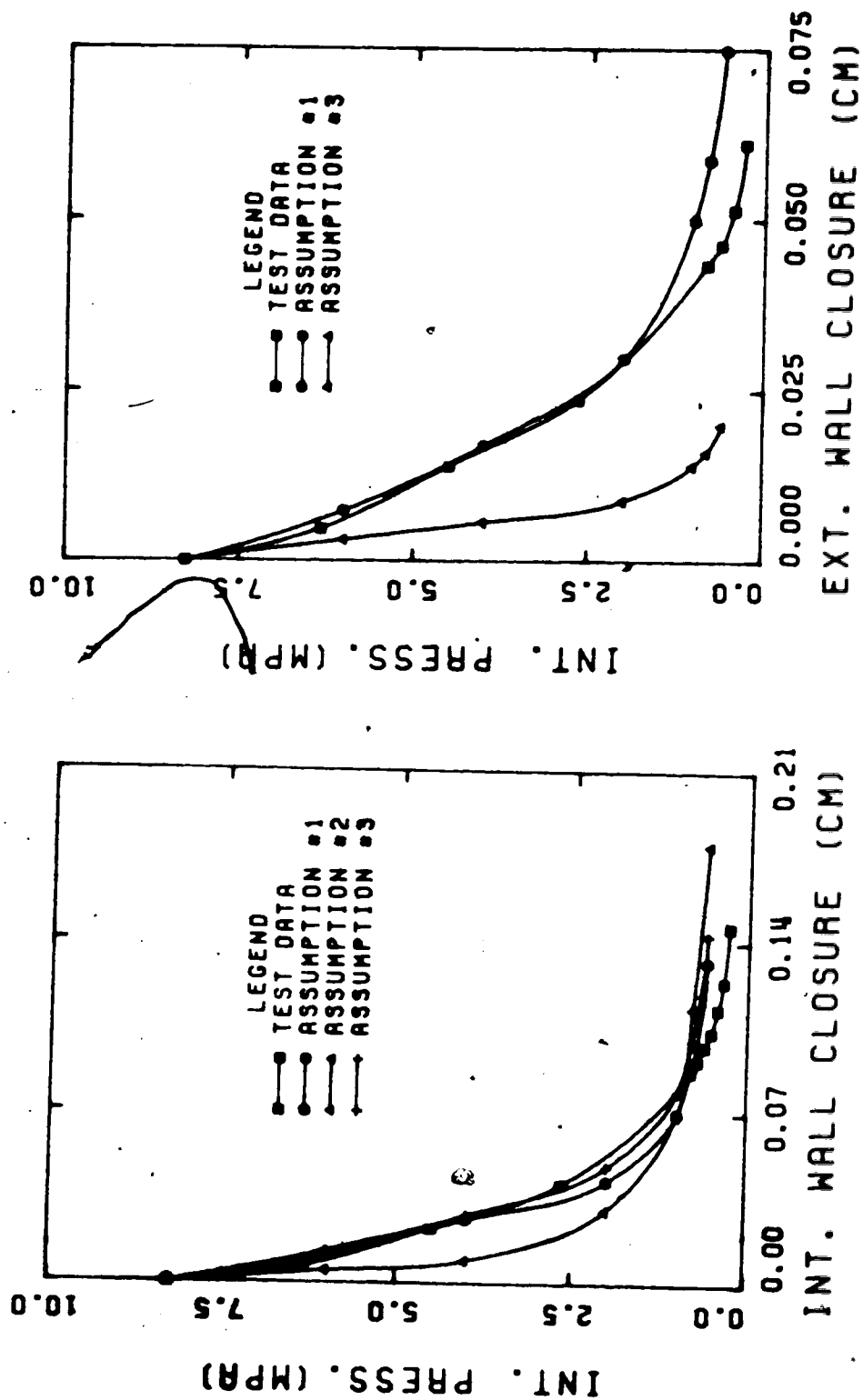
Figure 4.5 Influence of the E-function on the wall closure

Once yielding has occurred, the average radial stress
is given by :

$$(\sigma_r)_{ave} = \frac{\sigma_p + p_e}{2} \qquad \qquad \ldots 4.17$$

This value is used as the elastic strains in the
plastic zone are determined from the stresses at the
elastic-plastic boundary. The modulus used reflects the
average confinement in the elastic zone.

4.4 Output from the Program

The model calculates and outputs the following data :

- initial input parameters

- radial and tangential stress at each node

- value of the radius at each node

- elastic and plastic strain increments at the internal
wall

- internal pressure and wall closures (internal and
external)

- radial stress at the boundary from both the elastic
and plastic solutions

- radius of the plastic zone

Typical radial and tangential stress distributions
within the cylinder are shown in Figure 4.6.
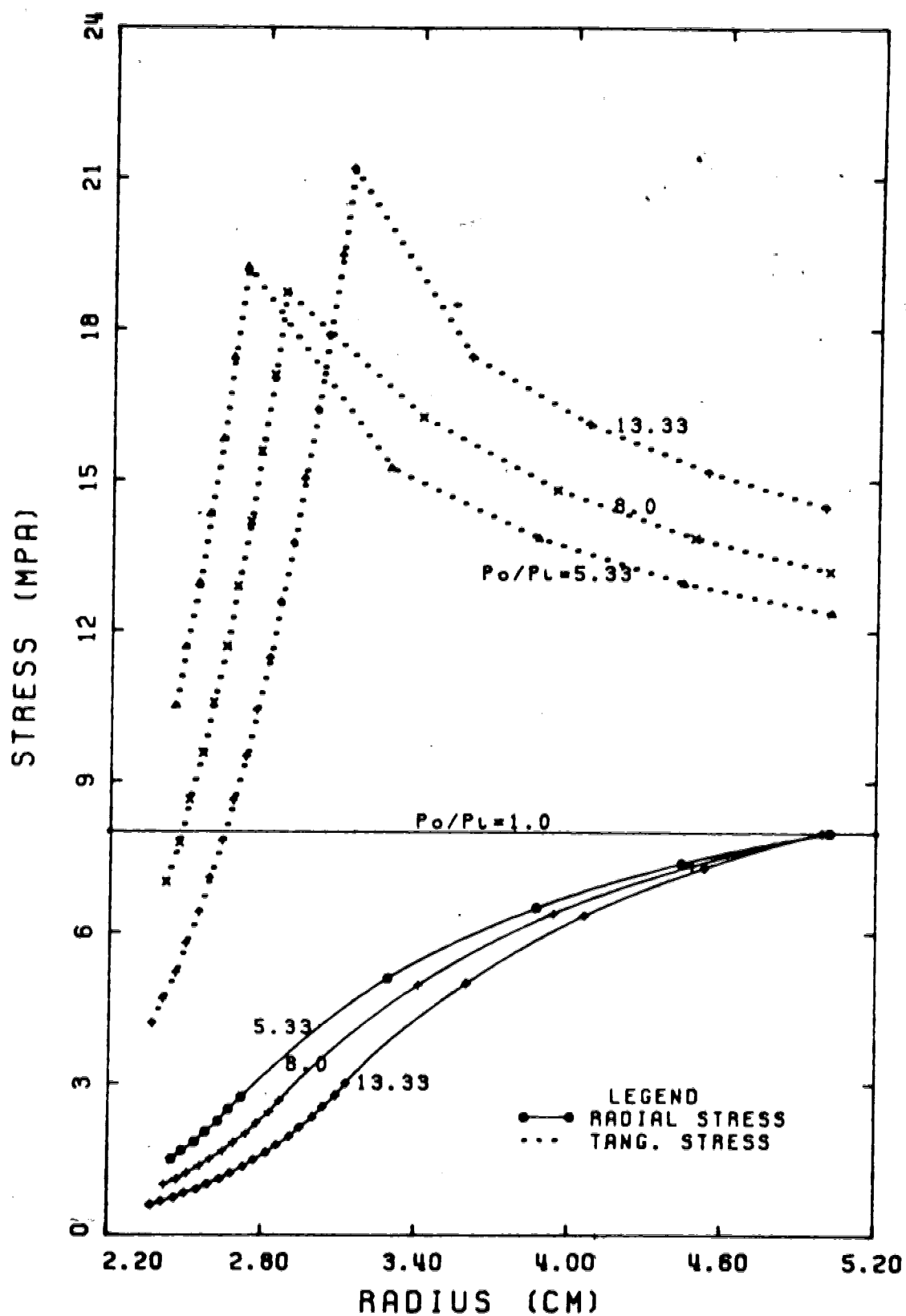
Figure 4.6 Radial and Tangential stress distributions
within a hollow cylinder

4.5 Sensitivity Analysis

The model was used to check the sensitivity of the solution to the various input parameters and the size of the iteration grid ($\triangle r$). The strength parameters (a,b) and dilation factor (α) all influence the solution. The closures determined from the analyses have been normalized to the elastic closures. This normalization procedure eliminates the influence of the elastic deformation parameters on the solution.

The results of the analyses are presented in Figures 4.7 to 4.11.

4.6 Discussion

The size of the iteration grid ($\triangle r$) only has a large influence on the closure when the dilation parameter is large. This case is close to that of the associated flow rule and, as has been discussed before, is not applicable to drained behaviour of sands. It can thus be concluded that the size of the iteration grid does not have a significant influence on the closure.

The spacing of the nodes should be selected with some judgement since the value of the plastic radius calculated will lie between two values which differ by an amount $\triangle r$. Accuracy of the solution will depend on whether the nodes are finely or coarsely spaced. Actual variation of $\triangle r$ in a finely spaced nodal system will not have much influence on the closure.
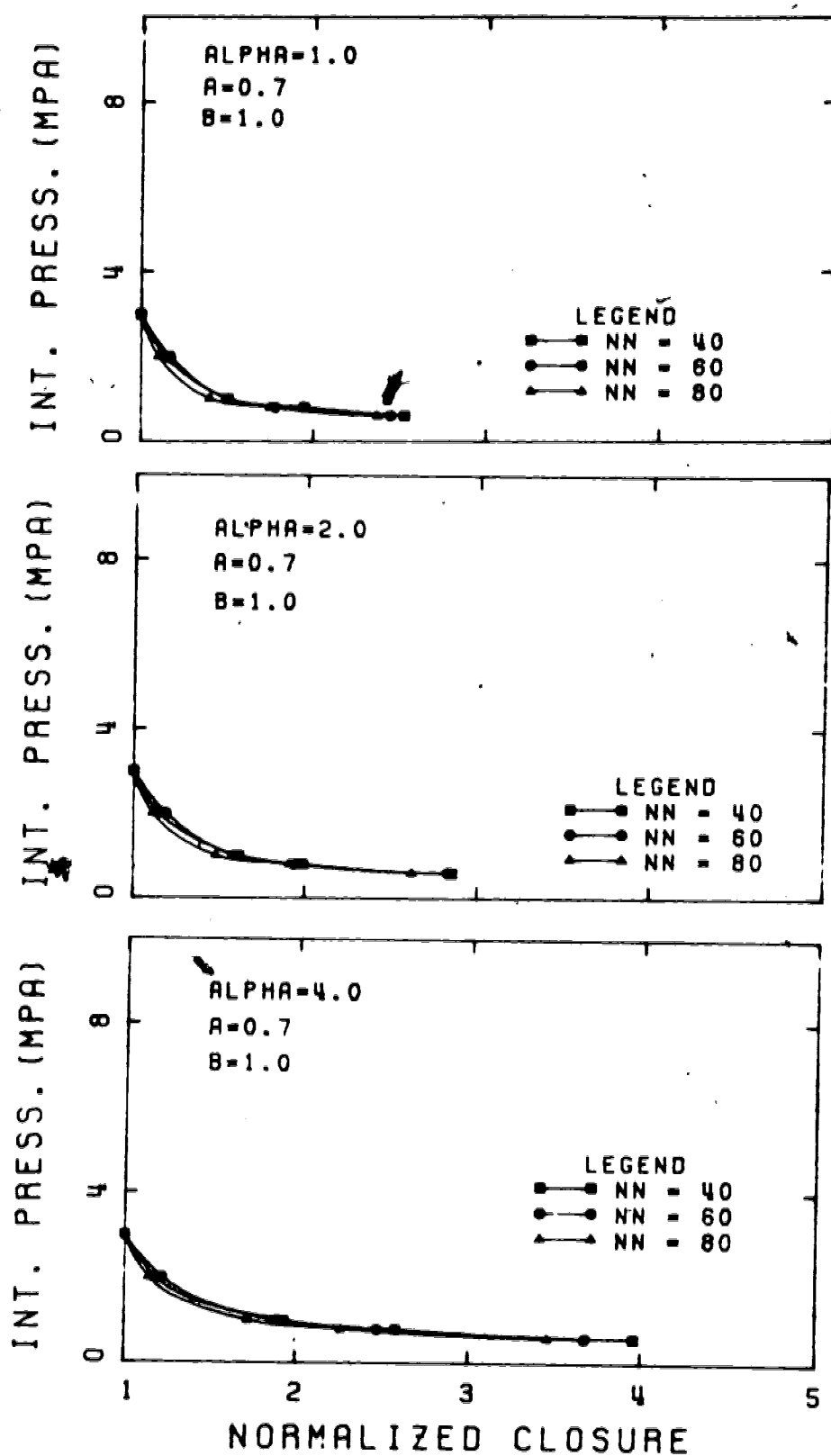
Figure 4.7 Sensitivity of the number of nodes on the solution
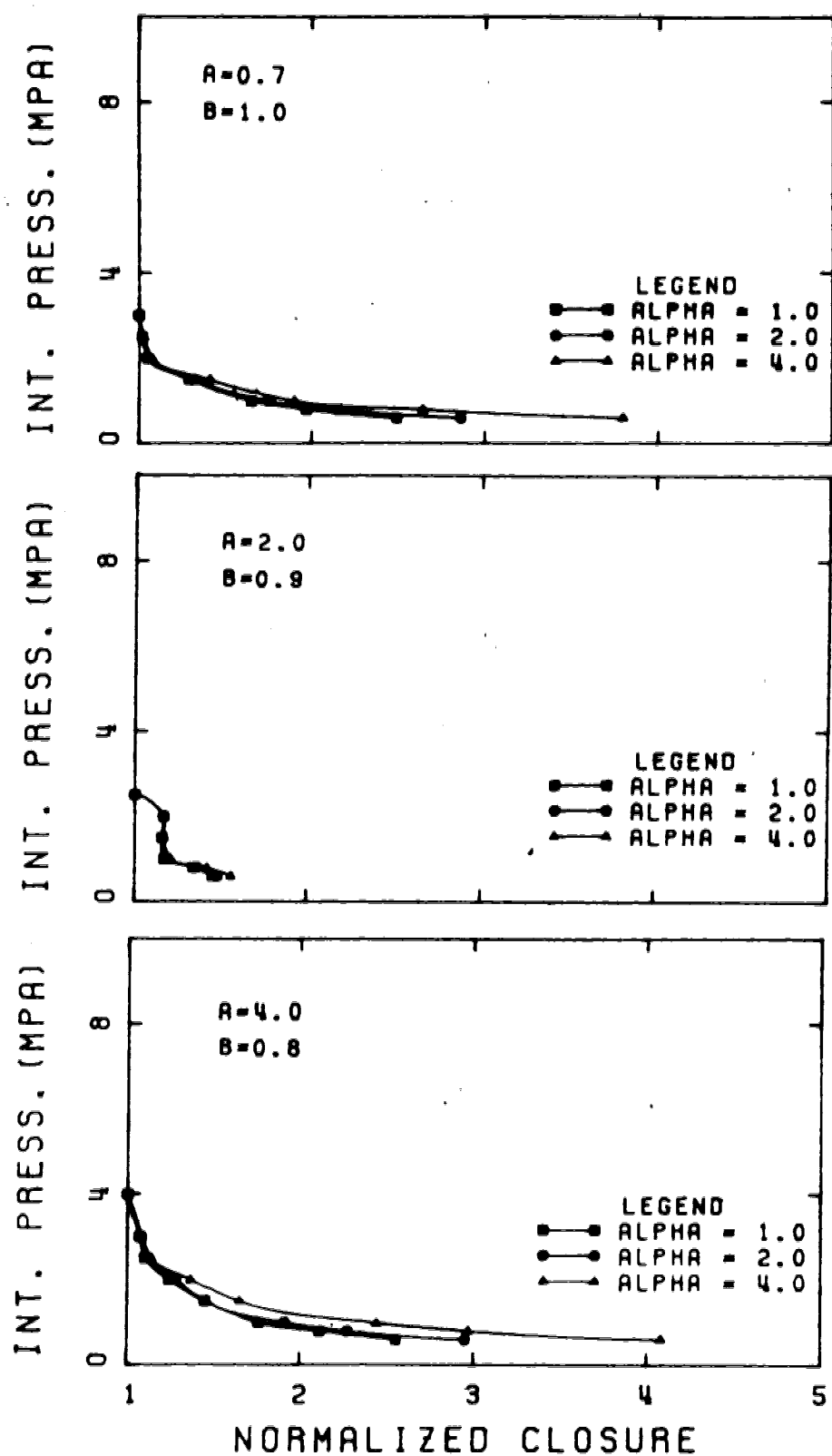
Figure 4.8 Sensitivity of the Alpha-parameter on the solution
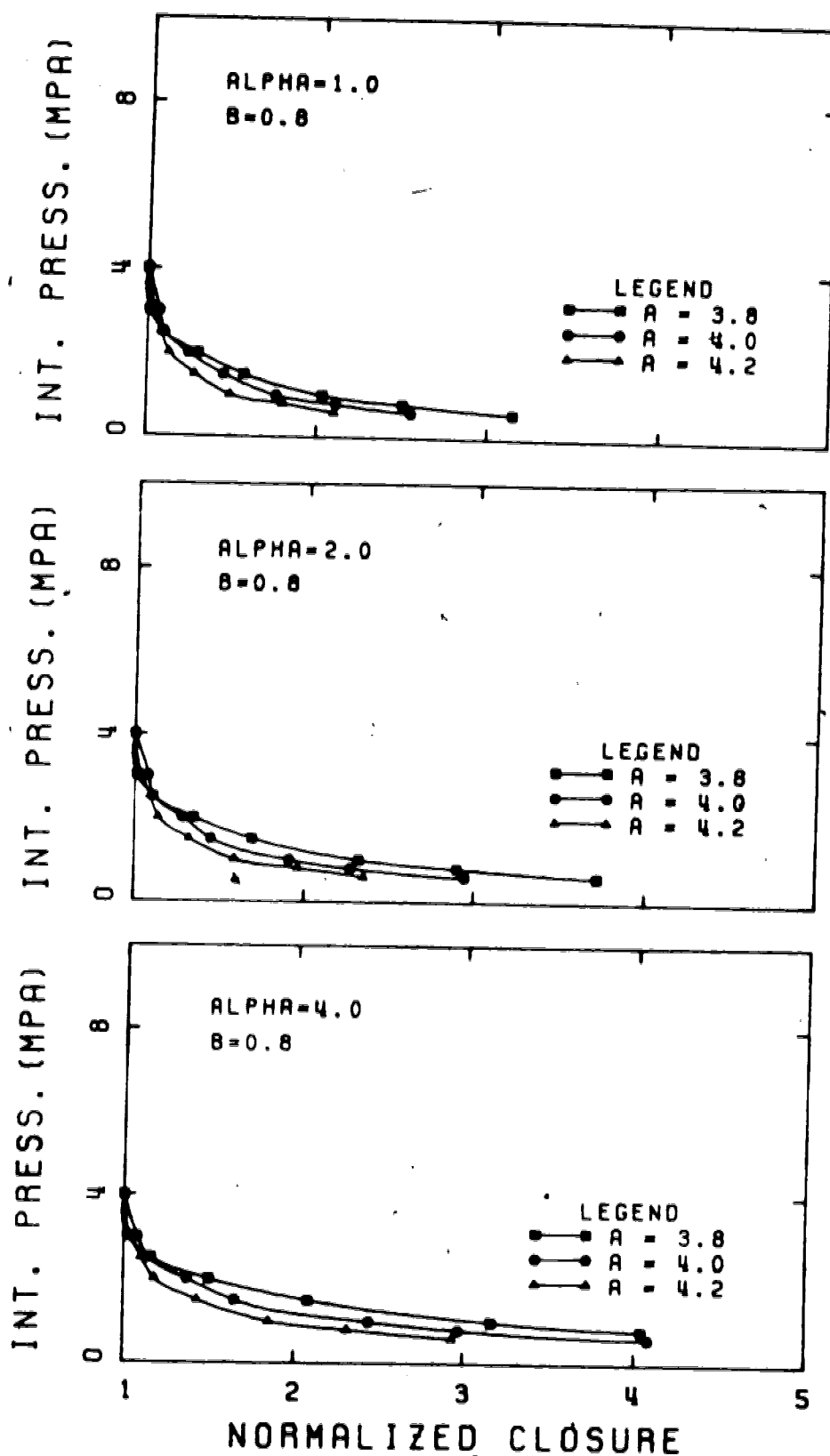
Figure 4.9 Sensitivity of the a-parameter on the solution (b=0.8)
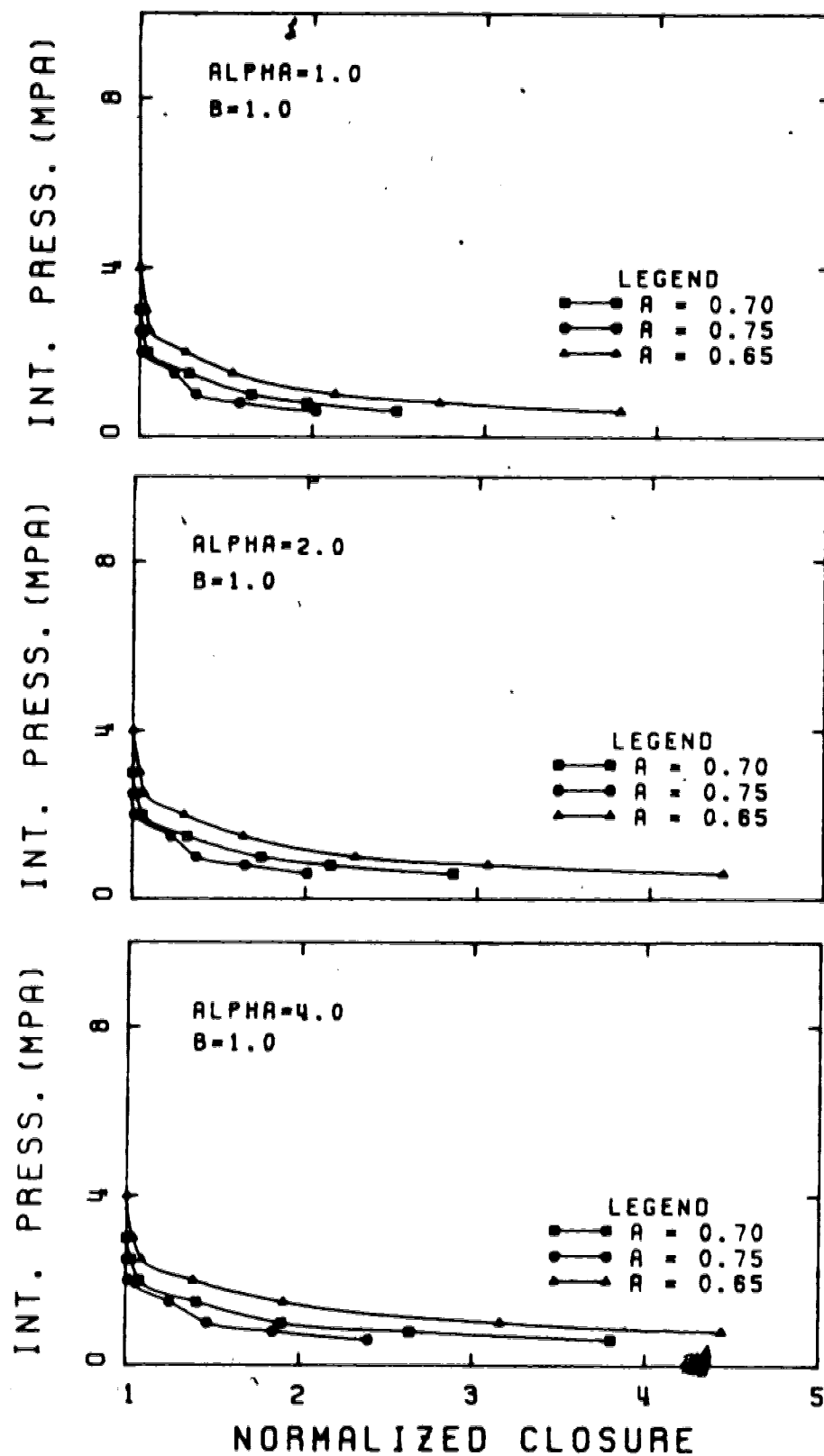
Figure 4.10 Sensitivity of the a-parameter on the solution
(b=1.0)
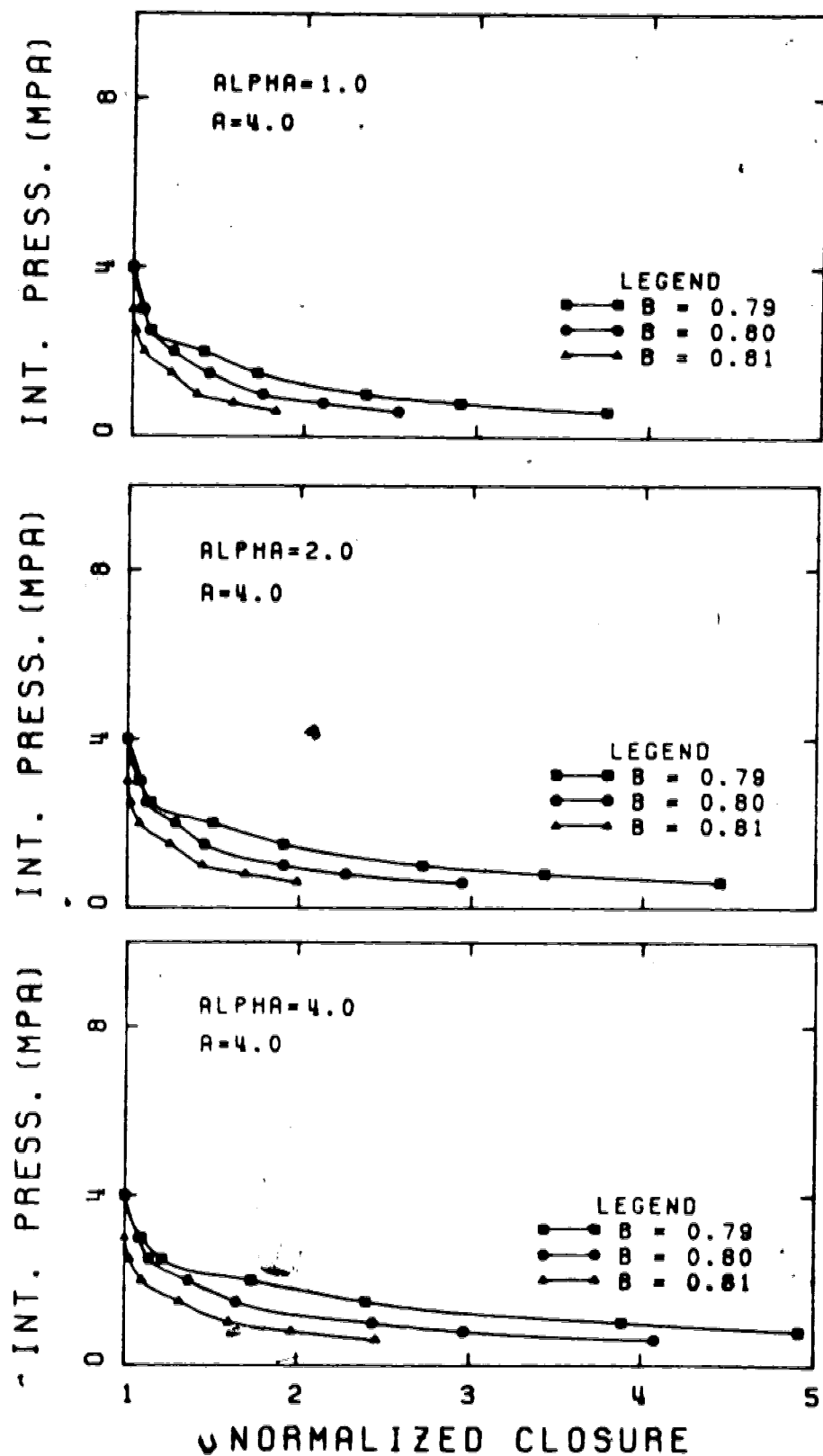
Figure 4.11 Sensitivity of the b-parameter on the solution
(a=0.7)

.The dilation parameter (α) has a significant influence on the solution, especially when it has a value approaching that required to represent the associated flow rule. The value of α cannot be determined from laboratory tests and must be selected intuitively.

The associated flow rule is probably only valid for drained behaviour near peak strength, and behaviour of the material after peak will best be represented by a non-associated flow rule. The larger the plastic strains, the lower will the α-value be. The plastic strains in the hollow cylinder test are large, and a value of $\alpha = 1$ (i.e. no volume change) will probably be the best value to use in the analysis. This value of α was used in the analysis of the Ottawa sand sample (see Figure 4.5) when comparing predicted closures with the measured ones.

The strength parameters (a,b) have two influences on the results. The higher the value of either of these parameters, the higher is the yield point (the stress at which yielding first occurs). The yield point does not seem to be significantly affected by a small change in the a-value when b is less than unity.

The closures are also affected by the strength parameters. The higher the value of a or b, the smaller are the closures. This is to be expected since the comparisons are made at equal internal pressures. In a stronger material, less plastic flow has occured at the same pressure ratio.

In Figure 4.8, the results shown in the centre diagram are completely different to the other two diagrams. These results have been rechecked, and no error was found. A slight variation in the a or b values resulted in a set of curves similar to the other two. It must be concluded that the analytical procedure is unstable for this particular set of data. The effects of grid size and size of the stress increments may influence this instability.

The variation of E in the elastic region of the cylinder must be correctly specified. A constant E value will result in a large under-prediction of the deformations. The value of E is a function of the degree of confinement within the elastic region as well as the stress level.. The variation of E within the elastic region can be modelled by a bi-linear variation of the modulus with the average radial stress, as determined from the hollow cylinder test.

The results of the sensitivity analysis have shown the importance of careful selection of the input parameters. The values of the strength parameters, dilation parameter and the nodal spacing can have a large influence on the predicted deformations. While the magnitude of Young's modulus will affect the closures, a more detrimental effect will result if the variation of modulus with the degree of confinement is not considered.

The model has been developed for the purpose of predicting the deformations that occur in the hollow cylinder test. Although this has been the main objective,

the model can also be used to analyse the deformations that occur in deep tunnels or around shafts (i.e. the stress field must be isotropic).

The plane-strain solution is applicable for tunnel analysis, but the gravitational effects must still be considered. A shaft analysis is a plane-stress problem, but it has been suggested by McCreath(1981) that the problem can be analysed with sufficient accuracy by the plane-strain solution. Gravitational effects do not influence the solution for the deformations that occur around a shaft.

The model has been shown to predict the closures in a hollow cylinder test with sufficient accuracy (see also Chapter 6). The finite boundaries of the cylinder make the use of determining the elastic modulus from the average radial stress in the elastic region (Assumption #1) viable. In the case of a shaft or tunnel, the external boundary will not be subjected to any significant movements and hence the use of Assumption #3 to determine the elastic modulus will probably yield a better solution. It was shown in Figure 4.5 that this assumption actually gave a better prediction of the internal wall movement, but did not give a good prediction of the external wall movement.

The model may be modified to suit any particular requirement. The determination of the elastic modulus may be found by any method with relatively few changes required in the program. The failure criterion may also be specified differently if required. The criterion used can incorporate

a strength loss (strain-weakening) with relative ease. This feature has not been included in the model since the deformations of the cylinder can be predicted reasonably well without it. The parameters that describe the strength loss cannot be measured in the test and this results in another variable that has to be experimented with during the analysis.

A non-linear elastic-perfectly plastic model has thus been developed which can predict the deformations that occur in the hollow cylinder test with reasonable accuracy. This model is an analytical tool that will assist in the data interpretation of these tests. It also has the possibility of being used in the analysis of the deformations that occur around shafts and tunnels at fairly deep locations.

CHAPTER 5

EXPERIMENTAL RESULTS

5.1 Introduction

The influence of stress path on the deformation behavior of oil sands is examined. A laboratory program was conducted in which oil sands were tested under three different stress paths. The triaxial testing of the samples was conducted in a hollow cylinder triaxial device and in a high pressure triaxial cell.

An oedometer test was conducted to determine the compressibility of the soil skeleton, and to compare this result with those determined from the triaxial tests. Index properties of the samples were determined.

The material tested was an oil rich, dense sand with cross-bedding. Sample collection and preparation techniques have been presented in Chapter 2. All samples were taken perpendicular to the cross-bedding.

5.2 Laboratory Procedures

5.2.1 Index Tests

Index tests were conducted to determine grain size distribution, density, porosity and fluid content (bitumen and water). Grain size distributions were conducted on both the original samples and the samples after completion of the tests. The samples were washed on a number 200 U.S. sieve (0.074 mm) and the analysis conducted according to ASTM

75

standards. The material passing the #200 sieve has been designated as the percentage fines of the sample.

The densities were determined from the prepared samples, whose dimensions and weight were recorded prior to testing. Fluid contents were obtained by conducting extraction tests on the samples after the test. Original fluid contents were estimated from representative material taken from the block samples.

5.2.2 Oedometer Test

The testing apparatus used was designed and built at the University of Alberta. The frame had the capability of applying normal stresses of up to 16 MPa to the sample by means of dead weights loaded onto a lever arm. The applied loads were measured on a 44 kN load cell and the vertical displacements on a linear variable differential transducer. The compressibility of the soil skeleton was determined from the slope of the volumetric strain-effective stress curve.

5.2.3 Triaxial Tests

The test procedures and sample preparation for the hollow cylinders and triaxial samples have been decribed in detail in Chapter 2.

5.3 Laboratory Results

5.3.1 Index Tests

5.3.1.1 Grain Size Distribution

The grain size distribution for all samples are given in Appendix E for both the original samples and for those after completion of the tests. A typical grain size curve of the oil sands tested is given in Figure 5.1. It can be seen that the material is a uniform, fine-grained, micaceous sand with a small percentage of fines.

An increase in the amount of fines after completion of the oedometer and triaxial tests indicates that grain crushing occurs under high pressures. Table 5.1 shows the results of the grain size analyses.

5.3.1.2 Density and Fluid Contents

The results of these tests are presented in Table 5.2. The bulk density of the samples range from 1.93-1.99 g/cc. This density is higher than would be expected for a dense sand and is indicative of the interlocking nature of the sand.

The initial fluid content (bitumen + water) of 17%-19% is equivalent to a degree of saturation of approximately 80%. This value is low and due, to some degree, to the drying of the blocks. However, the low saturation is also due to expansion of the sample. The initial porosity of the blocks were approximately 35%, which is higher than that expected in situ.

Table 5.1 Results of the grain size analyses

Sample #	Press. (MPa)	% Fines Passing No. 200 sieve	
		Before	After
Oedometer	16.0	20.4	23.4
A-1	7.3	2.6	6.4
A-2	10.0	2.6	4.9
B-1	7.4	6.7	8.1
B-2	10.1	6.7	12.1
C-1	7.0	6.7	10.1
C-2	4.3	6.7	5.4

Table 5.2 Results of the Index tests

Sample #	γ_b g/cm³	n_i† %	w_{bi}†† %	w_i†† %	w_f†† %
Oedometer	2.00	34.3	1.3 (1.1)	15.2	14.7
A-1	1.99	36.0	17.5 (14.7)	17.1	19.4
A-2	1.98	36.8	17.5 (14.7)	18.1	19.2
B-1	1.96	37.6	16.2 (13.7)	18.6	21.4
B-2	1.94	38.2	16.0 (13.2)	18.6	21.0
C-1	1.93	38.5	15.9 (13.0)	18.6	22.1
C-2	1.95	38.0	17.4 (14.3)	18.6	22.0

† Porosity before consolidation

†† Based on dry weight of soil

Figures in brackets based on sample volume
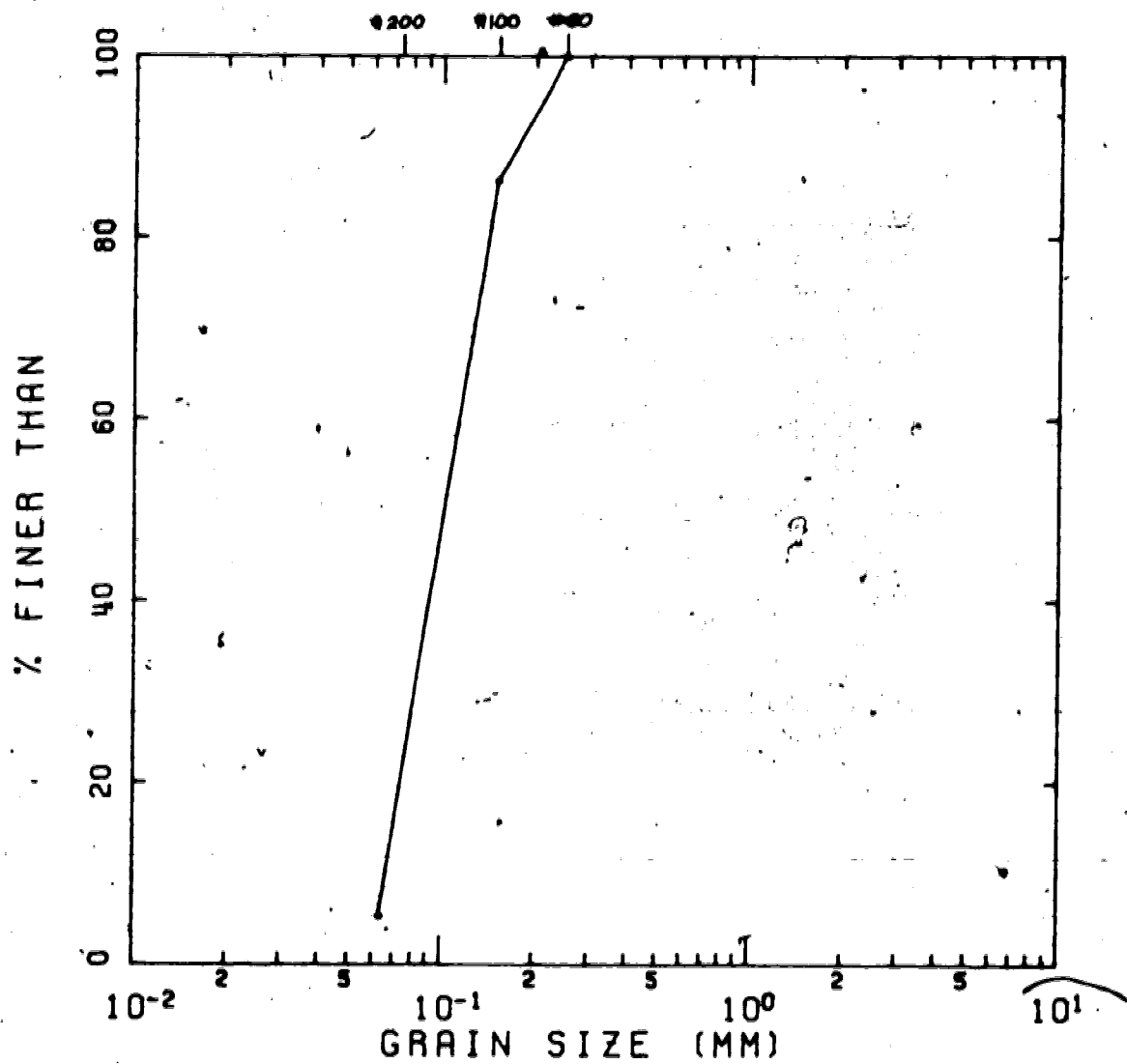
Figure 5.1 Typical grain size distribution for oil sand samples

5.3.1.3 Oedometer Results

The compressibility of oil sands is stress dependent, as can be seen from Figure 5.2. The compressibility remains relatively constant after one load-unload cycle, and it is not necessary to conduct cyclic compressibility tests on the triaxial samples prior to shearing. The results of the test are shown in Table 5.3(a). The compressibility of the oil sands tested is higher than that reported by Barnes (1980) and similar to those reported by Dusseault (1980). These higher compressibilities indicate that some sample disturbance has occurred. The reported compressibilities are given in Table 5.3(b) and (c).

5.3.2 Triaxial Tests

5.3.2.1 Strength Results

The results of the compressibility test, prior to shearing, of the samples are given in Appendix H, and the data shown in Table 5.3. The stress-strain curves obtained from the three series of tests are shown in Figures 5.3 to 5.5 along with the volumetric strain-effective stress curves. It should be noted that the stress-strain curves for Series A (hollow cylinder tests) are based on the assumption of a linear radial stress distribution within the sample.

The axial stress vs. radial+tangential stress results for Series A are shown in Figures 5.6(a) and 5.6(b). These curves are used to determine Poisson's ratio for the

Table 5.3 Compressibility data

(a) Test results

Sample #	Compressibility, C_S (kPa^{-1}) $\times 10^{-6}$		
	4 MPa	7 MPa	10 MPa
Oedometer 1st Loading Unloading Reloading 2nd Unloading	3.46 —→ —— ——	2.60 0.90 0.65 0.22	2.60 0.61 0.65 0.22
A-1 A-2	1.46 1.61	1.06 0.96	—— 0.55
B-1 B-2	3.35 4.12	2.56 2.82	—— 2.07
C-1 C-2	3.60 3.46	2.64 ——	—— ——

(b) After Barnes (1980)

Material	Modulus of Compressibility, a_v ($kPa^{-1} \times 10^{-6}$)			
	Load	Unload	Reload	Unload
Fine-grained Mc Murray Formation (oil-free)	0.80	0.33	0.35	0.28

Note: $C_S = \dfrac{a_v}{1 + e_o} \doteq \dfrac{a_v}{1.5}$ (for $n = 32\%$)

(c) After Dusseault (1980)

Material	Compressibility (kPa^{-1}) $\times 10^{-6}$
Highly disturbed samples	10^{-3} to 10^{-5}
High_quality core	5×10^{-6}
Probable in situ value	10^{-6} to 10^{-7}
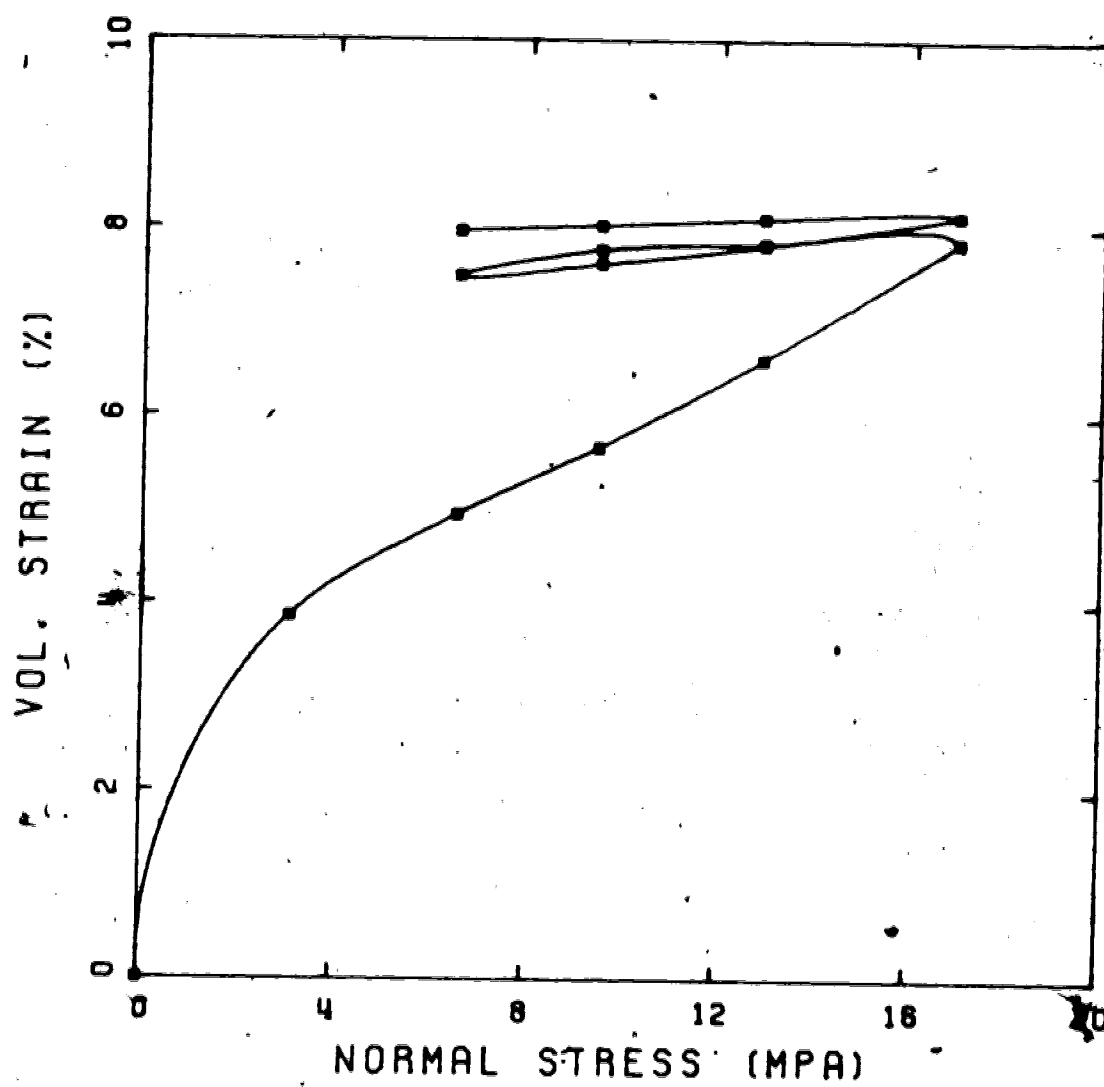
Figure 5.2 Oedometer compressibility test
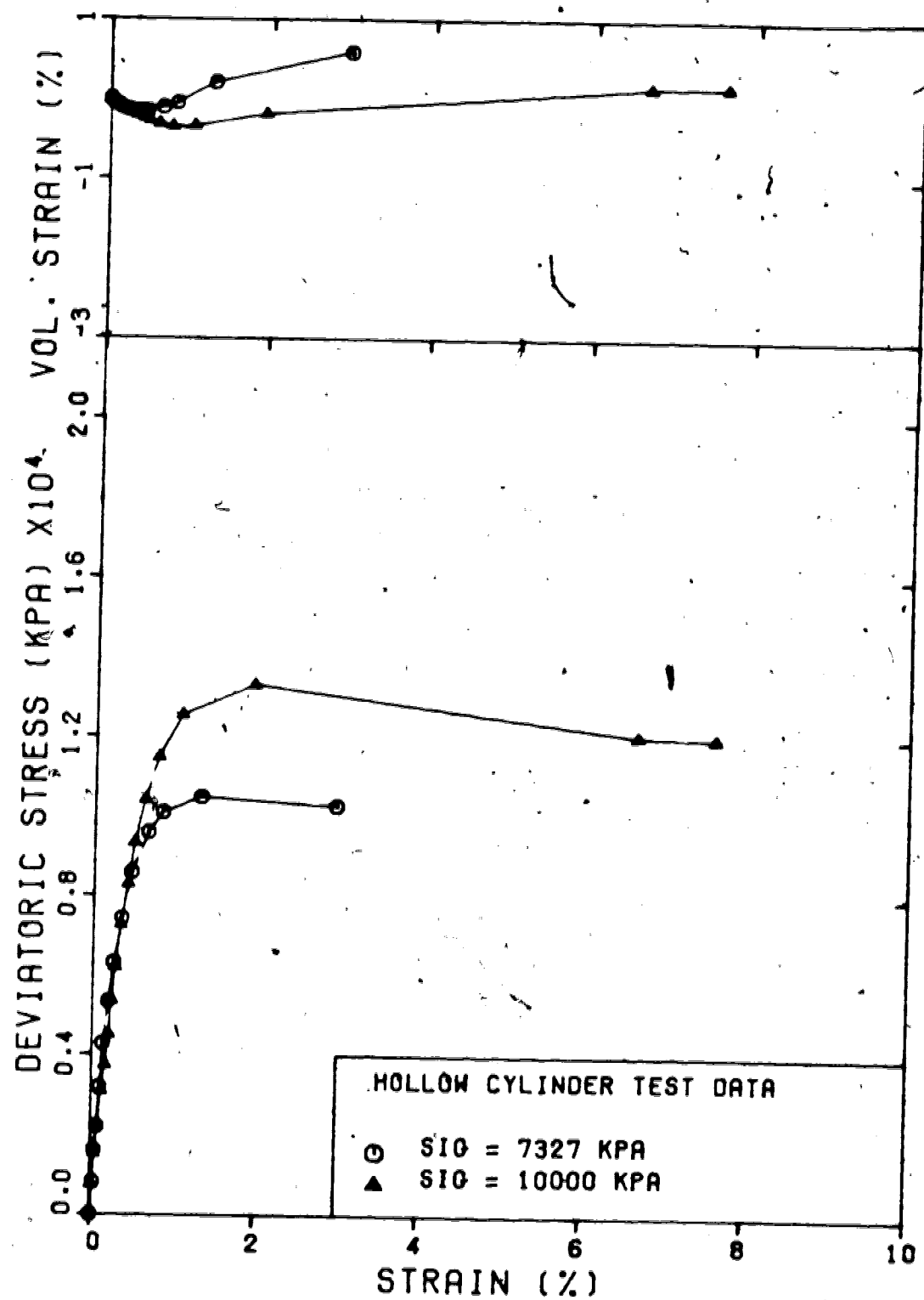
Figure 5.3 Stress-strain curves for Series A
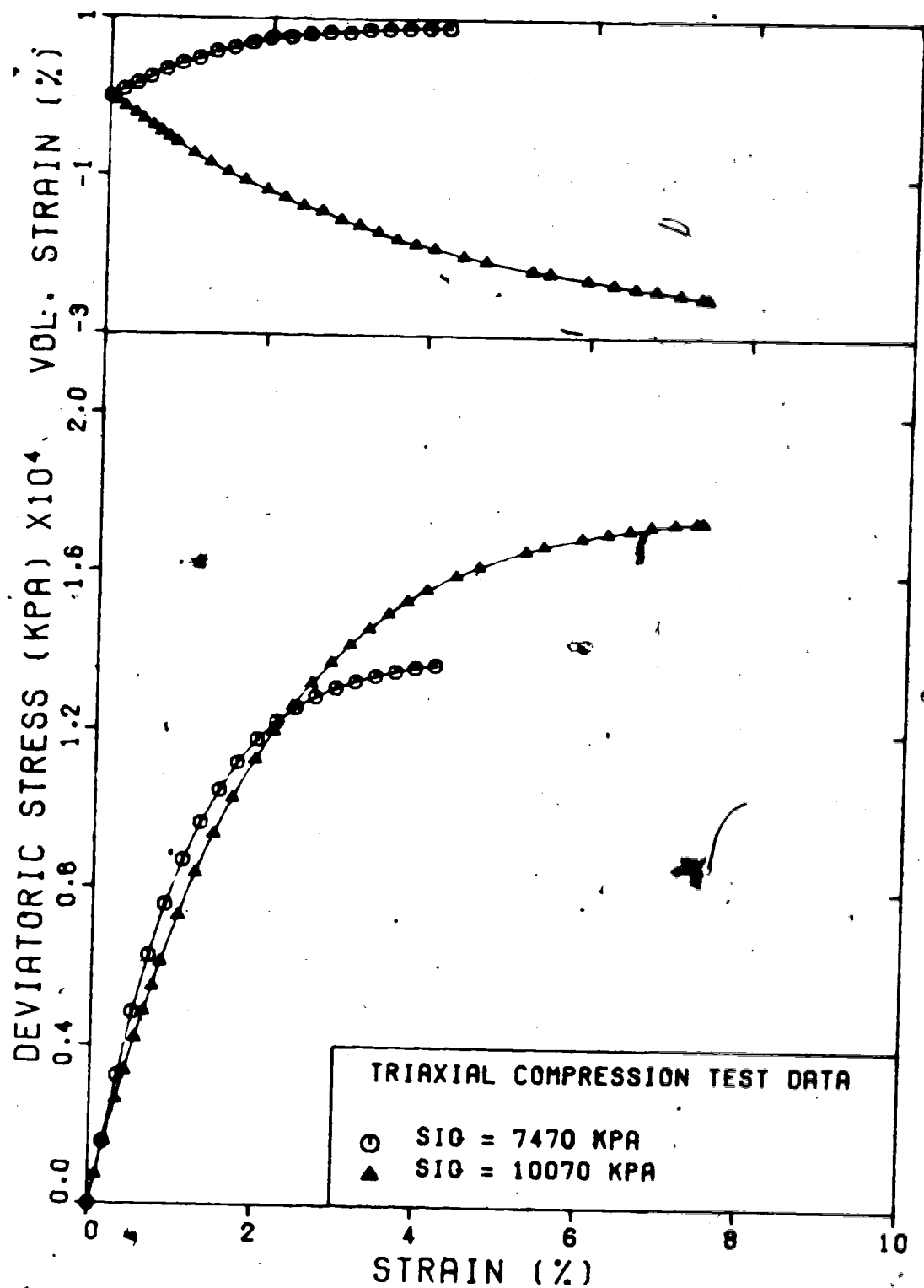
Figure 5.4 Stress-strain curves for Series B
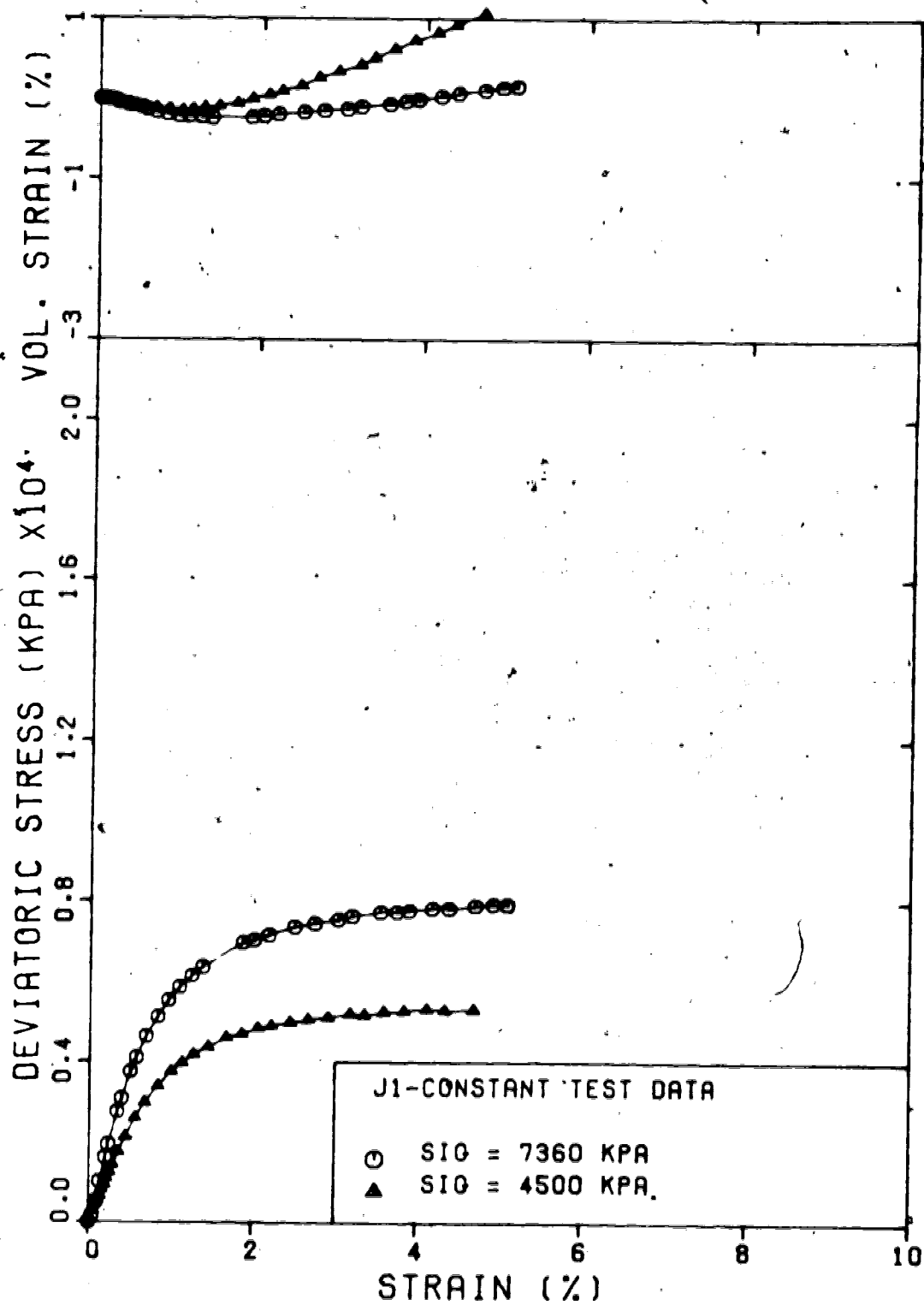
Figure 5.5 Stress-strain curves for Series C
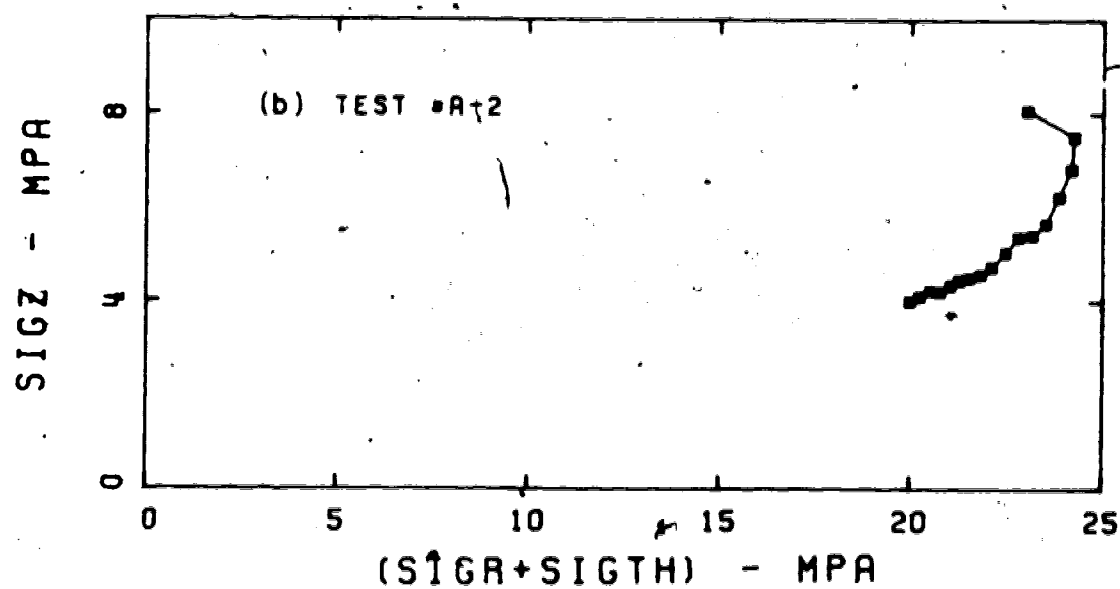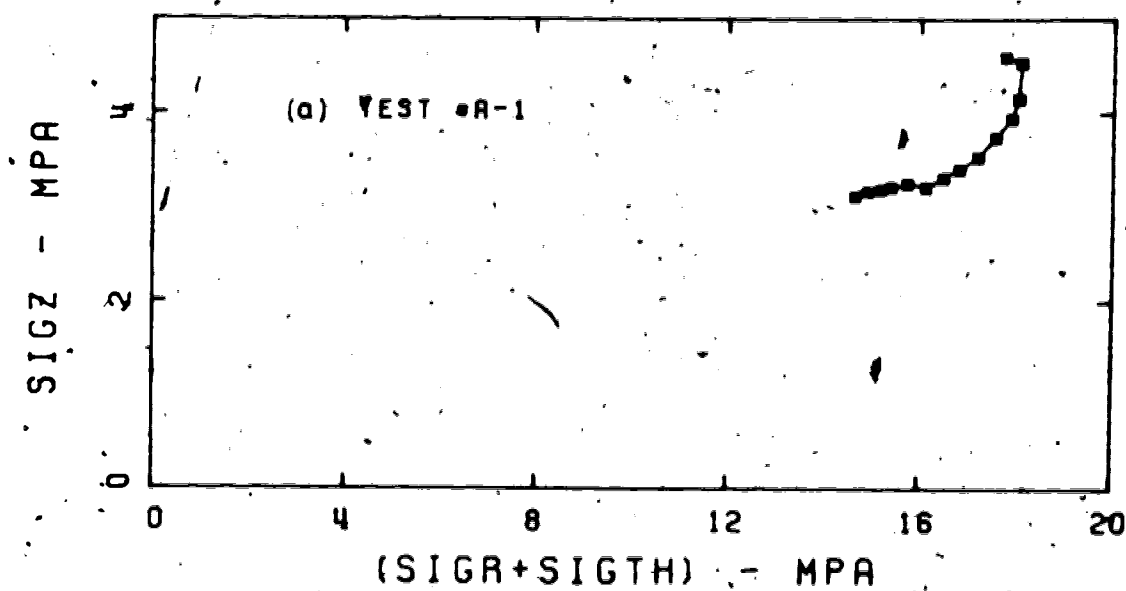
Figure 5.6 Axial stress vs. radial+tangential stress
(Series A)

plane-strain condition of these tests. The effective stress
paths for all tests are shown in Figure 5.7, and the results
of the tests are summarized in Table 5.4. The effective
friction angle (ϕ_s') is defined as the secant angle of
friction:

$$\sin \phi_s' = \frac{(\sigma_1 - \sigma_3)_f}{(\sigma_1' + \sigma_3')_f}$$

The angle of friction is calculated from the stresses
at failure. For the triaxial tests (Series B and C),
failure is defined as the maximum deviator stress. The
stresses at failure for the hollow cylinder tests (Series A)
are defined as the stress state just prior to collapse of
the sample.

The failure envelope for Series B and C tests is shown
in Figure 5.8. It can be seen that the envelope is
approximately linear in the stress range considered, but
does not pass through the origin. This indicates that
curvature of the envelope would occur in the lower stress
range, since the oil sands have no shear strength at zero
effective stress (Dusseault,1978).

The results of Series B and C tests have been compared
with similar tests conducted by Dusseault (1978,1981) on
both Ottawa sand and oil sand. The comparison is shown in
Figure 5.9. This comparison is useful in analysing the
results. Dusseault's results are obtained from both lean

Table 5.1 Summary of test results

Sample #	Porosity† %	σ'_c MPa	$\left(\dfrac{\sigma_1-\sigma_3}{2}\right)_f$ MPa	$\left(\dfrac{\sigma'_1+\sigma'_3}{2}\right)_f$ MPa	$\left(\dfrac{\sigma'_1}{\sigma'_3}\right)_f$	$(\varepsilon_a)_f$ %	$(\varepsilon_v)_f$ %	ϕ'_s
A-1	35.2	7.3	5.2	9.1	3.8	1.3	-0.21	35.4°
A-2	35.8	10.0	6.7	12.1	3.4	1.9	0.19	33.2°
B-1	36.2	7.4	6.8	14.2	2.9	4.2	-0.89	28.8°
B-2	35.8	10.1	8.7	18.7	2.7	7.4	2.50	27.5°
C-1	36.7	7.0	4.0	8.4	2.8	4.9	-0.14	28.3°
C-2	36.2	4.3	2.7	5.1	3.2	4.1	-0.82	31.5°

† Calculated at the end of consolidation

Note: ϕ'_s for Series A based on the assumption of a linear radial stress distribution in the cylinder

89
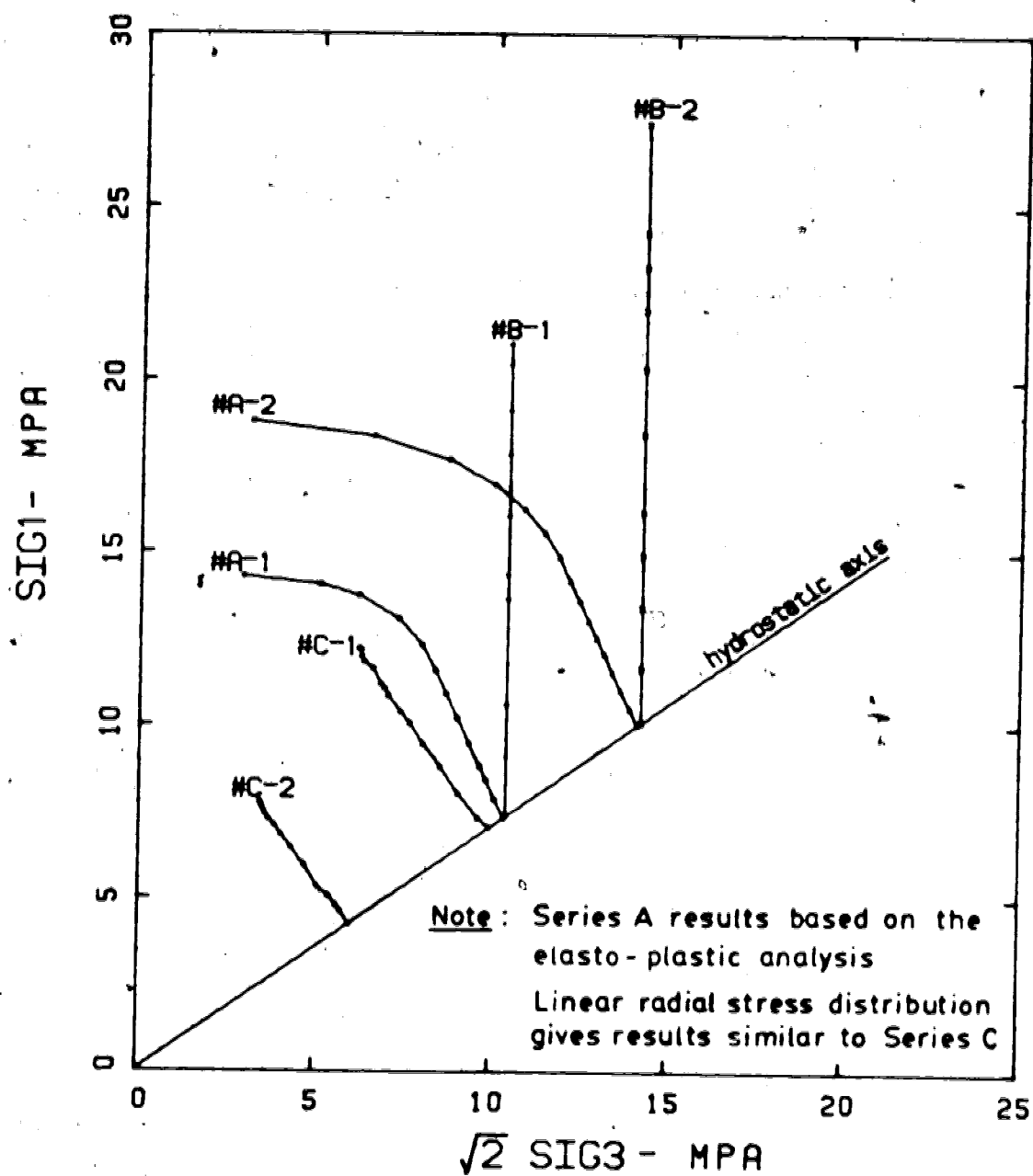
Figure 5.7 Effective stress paths for all tests
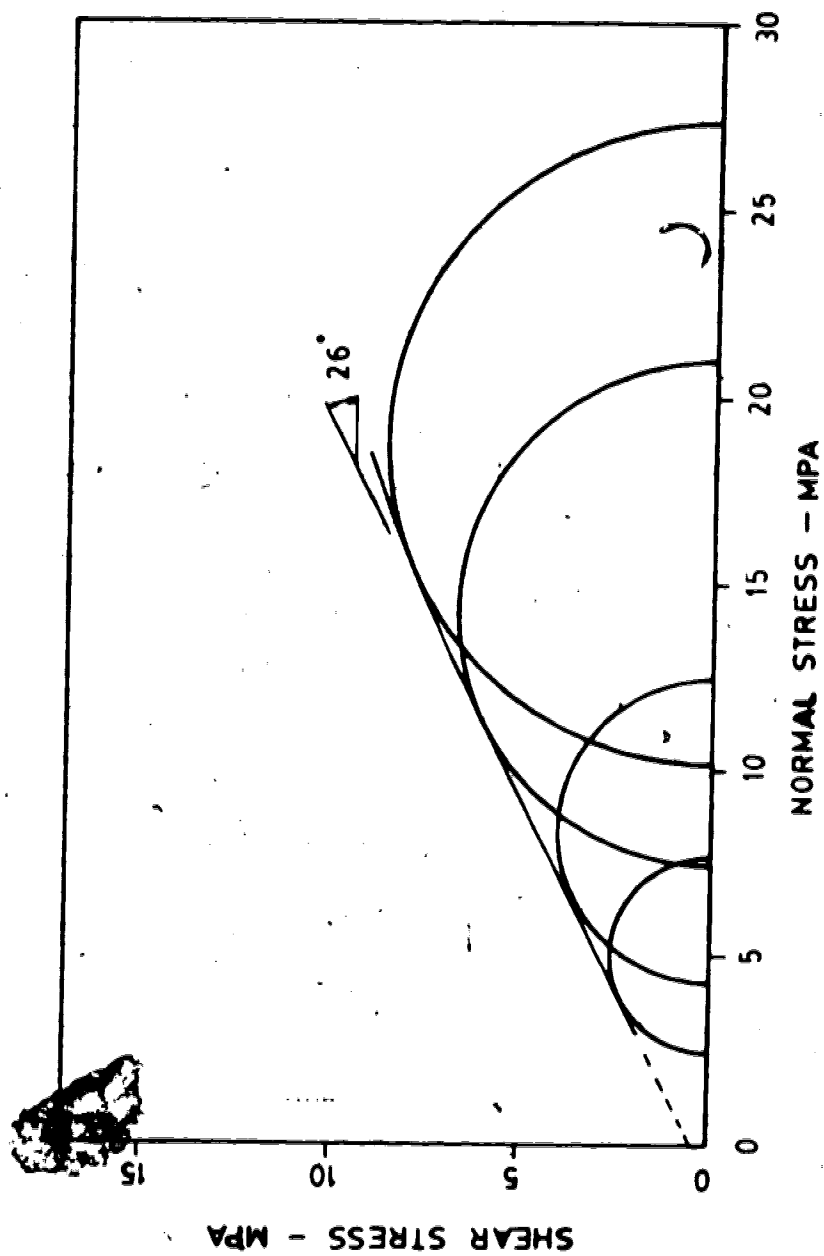
Figure 5.8 Strength envelope for Series B and C tests

91
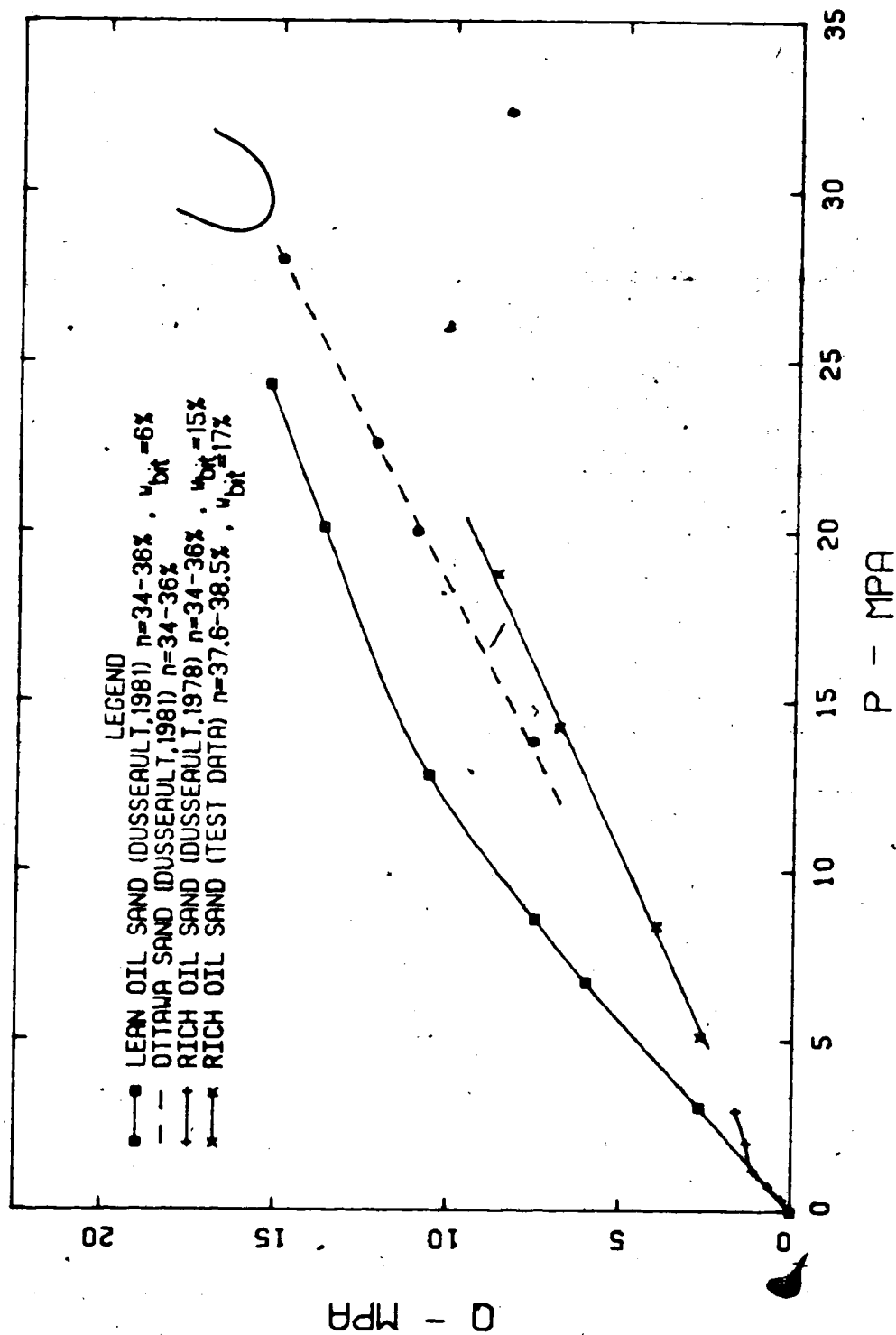
Figure 5.9 Comparison of test results with published data

and rich oil sand samples of different diameters. The results indicate that the strength of the oil sand as measured in this laboratory program are much lower than the reported strengths

Discussion of these results is given in a later section.

5.3.2.2 Deformation Results

The influence of stress path on the elastic deformation moduli can be examined in three ways. The variation of the Young's modulus with consolidation pressure for each series of tests can be compared (Figure 5.10(a)), the volumetric strain at failure can be compared at different consolidation pressures for the three stress paths (Figure 5.10(b)), or the Poisson's ratio can be compared (Figure 5.10(c)). When comparison of the Young's moduli are made, it is convenient to define the modulus as the slope of the stress-strain curve between two particular stress levels. Two moduli are defined in this manner as given below:

$$E_i = \frac{\sigma_{25}}{\epsilon_{25}}$$

$$E_{eff} = \frac{\sigma_{50} - \sigma_{25}}{\epsilon_{50} - \epsilon_{25}}$$

where σ_{25}, σ_{50} are stresses at 25% and 50% of the maximum deviator stress.

$\epsilon_{25}, \epsilon_{50}$ are strains corresponding to σ_{25} and σ_{50}
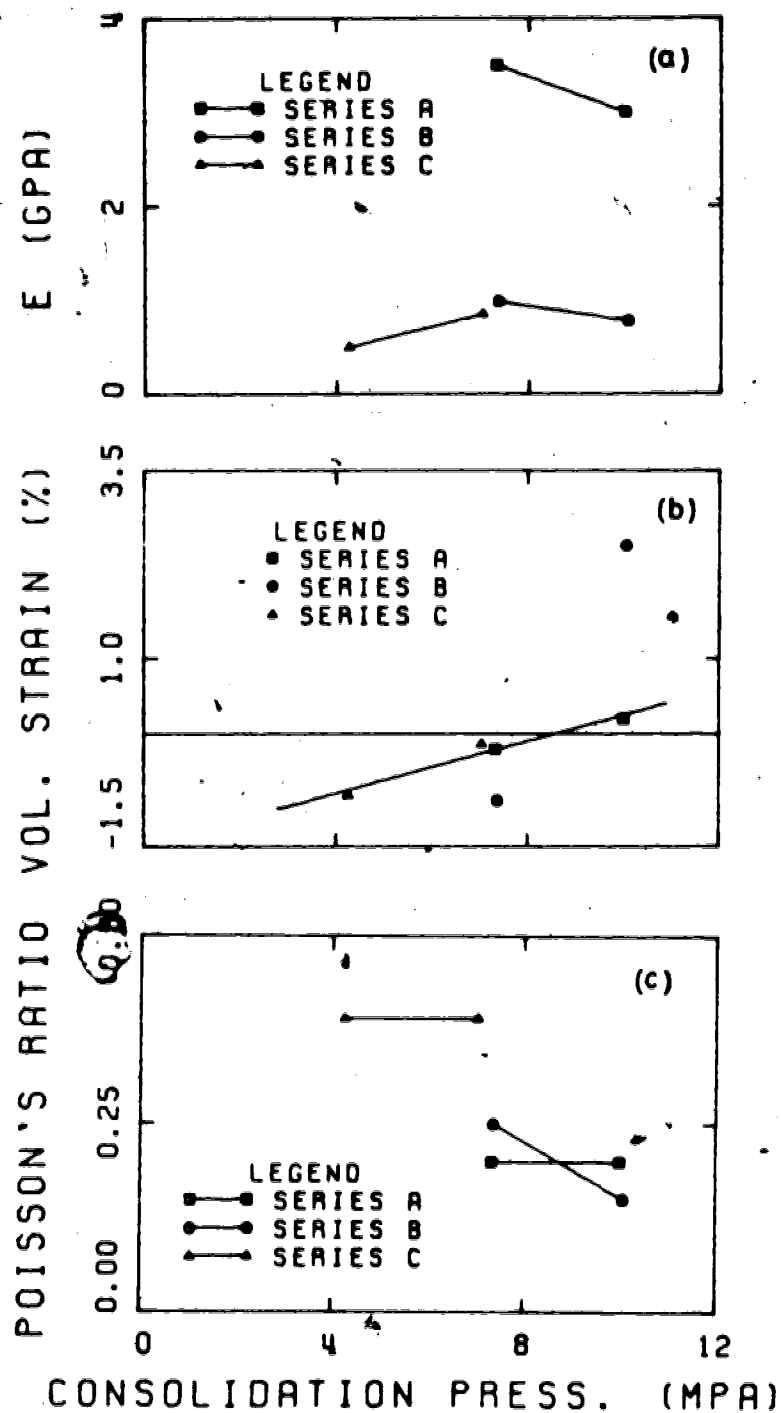
Figure 5.10 Influence of the stress path on the deformation behaviour

While this approach may not give the actual modulus at any particular stress level, it makes comparisons simpler. The deformation moduli are summarized in Table 5.5.

Comparison of these plots show that the deformation moduli are dependent on the stress path followed in the test. These results are discussed in more detail later.

5.4 Failure Modes of Triaxial Samples

5.4.1 Hollow Cylinder Tests (Series A)

The samples were carefully disassembled after testing. The hollow cylinders still had an approximately circular cross-section and were self-supporting. They were then frozen in a cold room, sectioned, and photographed.

Plate 5.1 shows the condition of Samples #A-1 and #A-2 immediately after testing. The failure surface is clearly visible for Test #A-2 as the membrane is distorted in the vicinity of the shear plane.

The half-sections of the frozen samples are shown in Plates 5.2 and 5.3 for Tests #A-1 and #A-2 respectively. The failure surface for Test #A-1 is not distinctive but a trace of the surface can be seen on the inside and outside walls of the cylinder. This failure surface is only found in one location i.e. there is no shearing across the entire sample. The failure mode is typical for the hollow cylinder test when sheared under such conditions. Sample #A-2 failed in an identical manner, but the failure surface is much more distinct.

Table 5.5 Summary of the deformation moduli

Sample #	Initial Tangent Modulus (GPa)	Eff. Tangent Modulus (GPa)	Poisson's Ratio
A-1	3.50	3.00	0.20-0.21
A-2	3.00	2.00	0.20-0.21
B-1	0.982	0.872	0.24-0.26
B-2	0.776	0.593	0.13-0.17
C-1	0.848	0.714	0.37-0.42
C-2	0.496	0.419	0.37-0.42

A-2

A-1
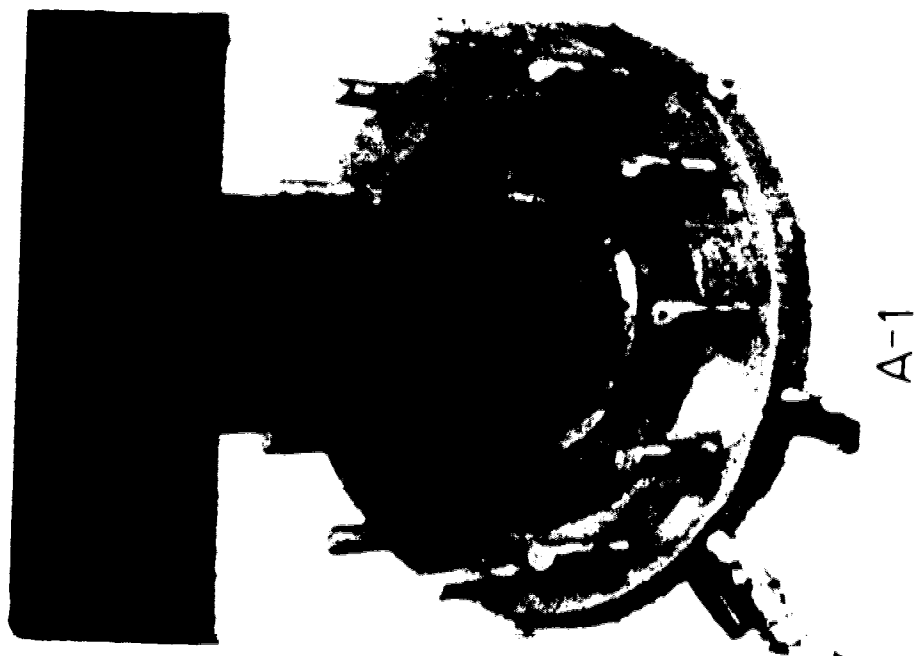
Plate 5.1 Condition of samples A-1 and A-2 immediately after the tests
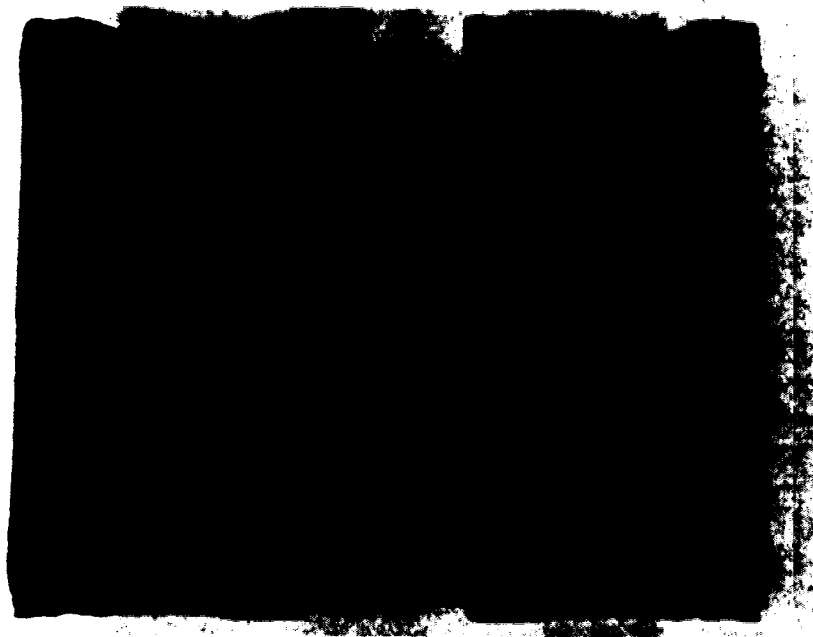
Plate 5.2 Half-sections of sample A 1 after the test
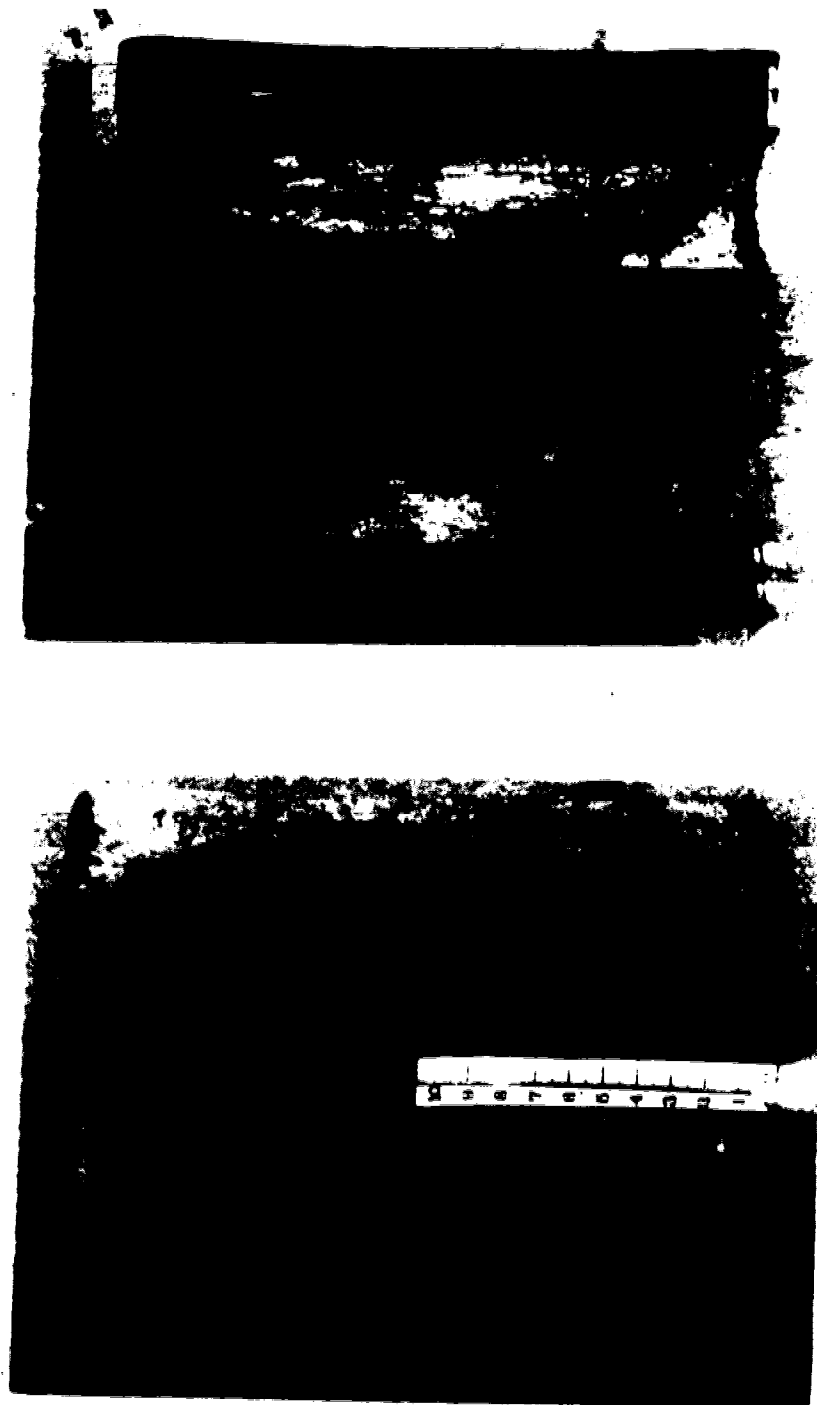
Plate 5.3 Half-sections of sample A-2 after the test

The actual shape of the failure surface through the wall of the sample cannot be examined due to the bitumen in the material. However, from the trace of the surfaces on both inside and outside walls, it is likely that the failure surface is spiral in plan view. Failure occurs along the most kinematically possible surface.

The trace of this surface is inclined at approximately 70 degrees to the horizontal in the middle third of the sample height. This surface then changes direction at the top of the sample due to the end effect of the loading cap. The end effect of the bottom of the sample is not as pronounced.

Examination of the half-section of the cylinder showed the bore to have deformed in a uniform manner. No deviation from uniform movement could be seen, even near the ends of the sample. This uniform deformation supports the use of an axi-symmetric analysis of the sample, as well as the use of volume change measurements to determine the strains that occur in the sample (which are assumed to be uniform along the height of the cylinder).

5.4.2 Triaxial Tests (Series B and C)

At the completion of the test, the samples were removed from the membrane and examined. No distinct' shear planes were visible and the overall deformation of the sample was uniform. No bulging of the sample occurred.

The end restraint of the load cap resulted in a minor

distortion at the top of the sample.

5.5 Discussion of Results

The strength of the hollow cylinder tests depend on the analysis used, and hence have not been included in Figure 5.9. A detailed analysis of this series of tests is presented in Chapter 6.

The strength envelopes shown in Figure 5.9 reflect the influence of bitumen content on the strength of oil sand. The data from lean oil sands tested by Dusseault (1978) provide an upper bound to the shear strength while the strengths determined from this testing program provide a lower bound. The bitumen *per se* does not contribute to the strength of oil sands (Dusseault,1978) but has a dominant role in the amount of sample disturbance that will occur.

For the rich oil sand, the exsolution of gas that occurs when unloading the material (during sampling) results in an expansion of the material and a disruption of the fabric. This results in a significant drop in the shear strength.

The original porosity of the samples (35%) is higher than the *in situ* porosity but still reflects a porosity lower than for most dense sands. A comparison of the porosities immediately after preparation of the samples shows an increase. This increase is larger for the triaxial samples (n=37.6%-38.5%) than for the hollow cylinder ones (n=36%). These porosity changes are summarized in Table

5.6.

The increase in porosity after sample preparation is due to sample disturbance, and is reflected more in a smaller sample than in a larger one. The dissipation of the heat generated when trimming a sample will depend on the volume of the sample. The small triaxial samples (37.5mm) have a smaller volume and therefore heat up more. This results in more expansion as is evident from the porosity measurements. During trimming of the hollow cylinder samples, the bore was kept cold by using dry ice in the shaft. This helped in dissipating the heat generated by trimming.

The tests on rich oil sands conducted by Dusseault (1978) were carried out at lower stress levels on larger diameter samples (75 mm). These results show a large curvature of the envelope and tend to correspond with the test results of this program. One data point from those tests coincides with the envelope obtained for lean oil sands. This indicates that the oil sand has a higher strength than the majority of the tests would indicate. The reduction in strength is due again to disturbance of the material during sampling and possibly during preparation of the samples.

The rich oil sand samples tested yield lower strengths than obtained for Ottawa sand. The oil sand is a fine-grained, sub-angular sand and should thus have a higher strength than the coarser-grained, rounded Ottawa sand.

Table 5.6 Influence of sample disturbance on porosity and density

MATERIAL	w_{bit} [tt] (%)	Before Preparation		After Preparation	
		γ_b (g/cc)	n (%)	γ_b (g/cc)	n (%)
Block used for Oedometer sample	2.0 (1.7)	2.01	35.2	2.00	35.5
Block used for Series B & C	16.6 (14.1)	2.01	35.5	1.93 -1.96	34.6 -38.5
Block used for Series A	16.2 (13.7)	2.01	35.2	1.98 -1.99	36.0 -36.8

tt Figures in brackets based on sample volume

However, the initial porosity of the Ottawa sand is approximately 34%, while that of the oil sand, after consolidation, is only 35% to 36%. This difference in porosity will have a significant effect on the frictional resistance of the material. Variations in grain size and shape will also have some influence on the shear strength, but it is the difference in porosities that will have the largest effect.

The results show that once an oil sand sample is disturbed, its original fabric is destroyed and will not be recovered by subsequent reconsolidation. Consolidation of a sub-angular sand, even to pressures of 12 MPa, will not result in a porosity that can be obtained by vibrating a rounded sand. It is thus extremely important to minimize sample disturbance of oil sands.

The drained strength of rich oil sand has not been determined with any degree of confidence. A lower bound value from the test results may be used, but this will result in conservative design analysis. It has been shown that the careful and elaborate procedures used to prepare samples of low gas saturation has not been sufficient to prevent sample disturbance. This will pose a more serious problem when trying to prepare gas saturated samples obtained at depth.

The laboratory preparation techniques will have to be improved. Coring of hollow cylinder samples can be improved by using a drilling fluid that has been cooled, but such a

fluid must not penetrate the walls of the sample. Trimming
techniques provide the most pr█████s, and a system for
reducing the heat generatio████ to be examined.

The strains at failure of the tests also indicate the
effect of sample disturbance. In Series A, the strain to
failure (1.3%-2%) is typical for a brittle material while
those for Series B and C (4%-7%) are more typical of a dense
sand at high pressures (ductile). Same of this difference
may be due to the plane-strain condition for the hollow
cylinder tests.

The influence of stress path on the deformation moduli
have been shown in Figures 5.10(a) to 5.10(c). The data are
not sufficient to make direct conclusions, but the trends
shown do indicate that deformation moduli are path
dependent. Young's modulus for all three series of tests
show different behavior. The hollow cylinder tests yield
higher moduli but this could be due to the relative amounts
of sample disturbance. However, the trend of Series B and C
are different even though the sample preparation and initial
porosities are the same.

The Poisson's ratio is dependent on the failure mode of
the material. Series A and C show no dependency on the
consolidation pressure. In Series B, the modulus decreases
with consolidation pressure. This behaviour is a result of
the different failure modes that occur in this series of
tests (dilation and contraction). The influence of stress
path can be best examined from Figure 5.10(b). The stress

path followed in Series A and C (see Chapter 2) are similar, and their volume change behaviour is also similar. The volume change behaviour of Series B is completely different. At a higher consolidation pressure (10MPa), dilatancy is suppressed while at a pressure of 7 MPa the volumetric strain is more negative (dilatant) than for the other two series.

The results shown in Figure 5.10 show the dependency of the deformation behaviour on stress path. However, the material has been disturbed and these trends may be completly different for the intact material. The difference between Series B and C should still be the same. For an undisturbed sample, suppression of dilatancy will probably occur at a higher confining pressure while the J1-constant test at this consolidation pressure still requires a reduction of cell pressure during the test, and hence will not suppress dilation.

5.6 Conclusions

The influence of stress path on the deformation behaviour of oil sands must be considered in any analysis. The stress path associated with deformation around tunnels or shafts can be approximated in a hollow cylinder triaxial test or in a J1-constant triaxial test. A triaxial compression test is not relevant to such analyses and will provide incorrect deformation properties.

The results of the laboratory tests show the influence of the sample preparation techniques and sample collection on the disturbance of rich oil sands. These procedures need to be perfected before reliable strength and deformation properties can be determined.

CHAPTER 6

PREDICTION OF THE HOLLOW CYLINDER RESULTS FROM THE NUMERICAL MODEL

6.1 Introduction

The deformation behaviour of the oil sands as determined from the hollow cylinder tests was given in the previous chapter. Those results were based on the assumption of a linear radial stress distribution within the cylinder. In this Chapter, the deformation behaviour is examined by comparing stress-strain curves for the tests based on different assumptions.

The closures measured in the tests are compared with those predicted by the numerical model developed in Chapter 4. The model is also used to determine the strength of the cylinders and the values are compared with the actual test data. The influence of the assumptions made (regarding stress distribution) when determining the cylinder strength from the test data is examined.

6.2 Analytical Procedure

The procedure adopted in the analysis is shown in the flow chart in Figure 6.1. The test data is used to estimate the strength parameters and to determine the relationship between Young's modulus and average radial stress. Values for the dilation parameter (α) and Poisson's ratio (ν) are selected.
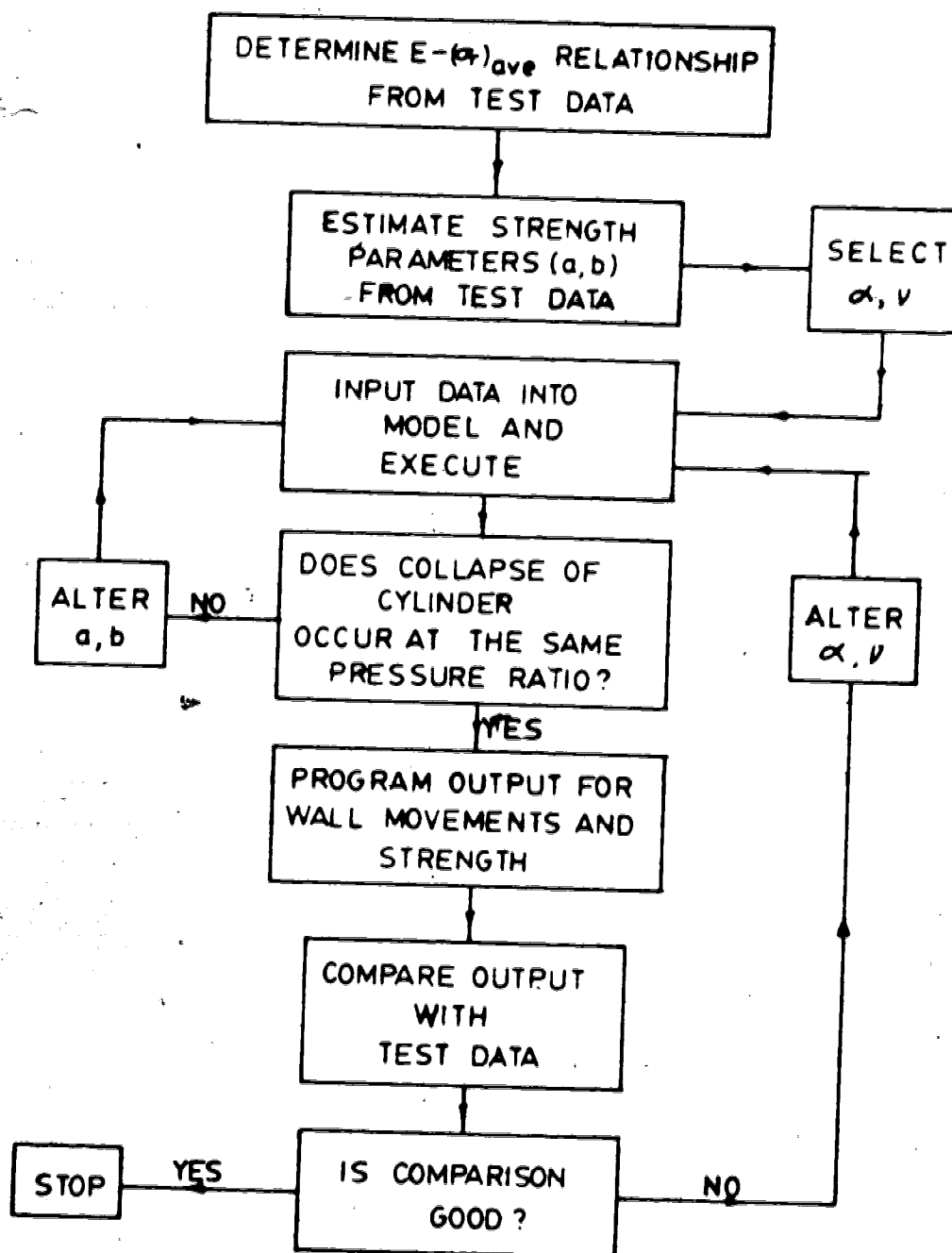
Figure 6.1 Flow chart showing the analytical procedure

These values are used as the initial input parameters.
The strength parameters are adjusted until the cylinder
collapses at the same pressure ratio as occurs in the actual
test. The predicted closures are compared with the actual
closures and the input parameters can be adjusted until the
best comparison is achieved.

The strength parameters (a, b) required to achieve
equivalent collapse of the cylinder are compared with those
determined from the test data. These parameters are used to
assess the validity of the different assumptions made
regarding the stress distribution within the cylinder.

6.3 Analysis of the Hollow Cylinder test

Two assumptions were made when determining the average
radial stress in the cylinder. The first was that the
stress varied linearly throughout the cylinder, while the
second assumption was based on plasticity theory to
determine the stress distribution. The theory was
simplified by assuming that the value of σ_0 (see Chapter 3)
after yielding occurs is the same as the value of σ_0 with
no yielding.

The two hollow cylinder tests conducted on oil sand
samples as well as one conducted on an Ottawa sand sample
are examined in the following sections.

6.3.1 Sample #A-1

The stress-strain curves for both assumptions are shown in Figure 6.2, and the measured closures are given in Figure 6.3 for both the internal and external walls. The $E-(\sigma_r)_{ave}$ relationship determined from the stress-strain curve is shown in Figure 6.4.

The failure criterion was based on a linear Mohr-Coulomb envelope (i.e b=1.0) since the secant angle of friction is determined from actual test data on this basis.

The comparison of the predicted closures with the measured ones is shown in Figure 6.5. The predicted closures are based on an assumed α-value of 1.0 (no plastic volume change occurring) and a Poisson's ratio of 0.25.

The strength parameter (a) determined from the analysis corresponds to a secant angle of friction which passes through the top of the Mohr circle. This value is then converted to a secant friction angle which is tangent to the Mohr-circle. This allows for comparisons to be made with the measured values and the theoretical value as determined from Equation 3.14 (after Wu et al., 1963). The comparison of the strength parameter is given in Table 6.1 along with the other two tests.

6.3.2 Sample #A-2

The stress-strain curves and measured closures from the test are given in Figures 6.6 and 6.7. The variation of E with average radial stress is shown in Figure 6.8. The

Table 6.1 Strength parameters determined from the different
assumptions

Sample #	ϕ'_s			
	from model	after Wu et al.	from el.-pl. assumption	from linear assumption
Ottawa sand	45.2°	45.3°	50.1°	34.6°
A-1	46.9°	46.7°	48.4°	35.4°
A-2	38.6°	38.4°	51.9°	33.2°
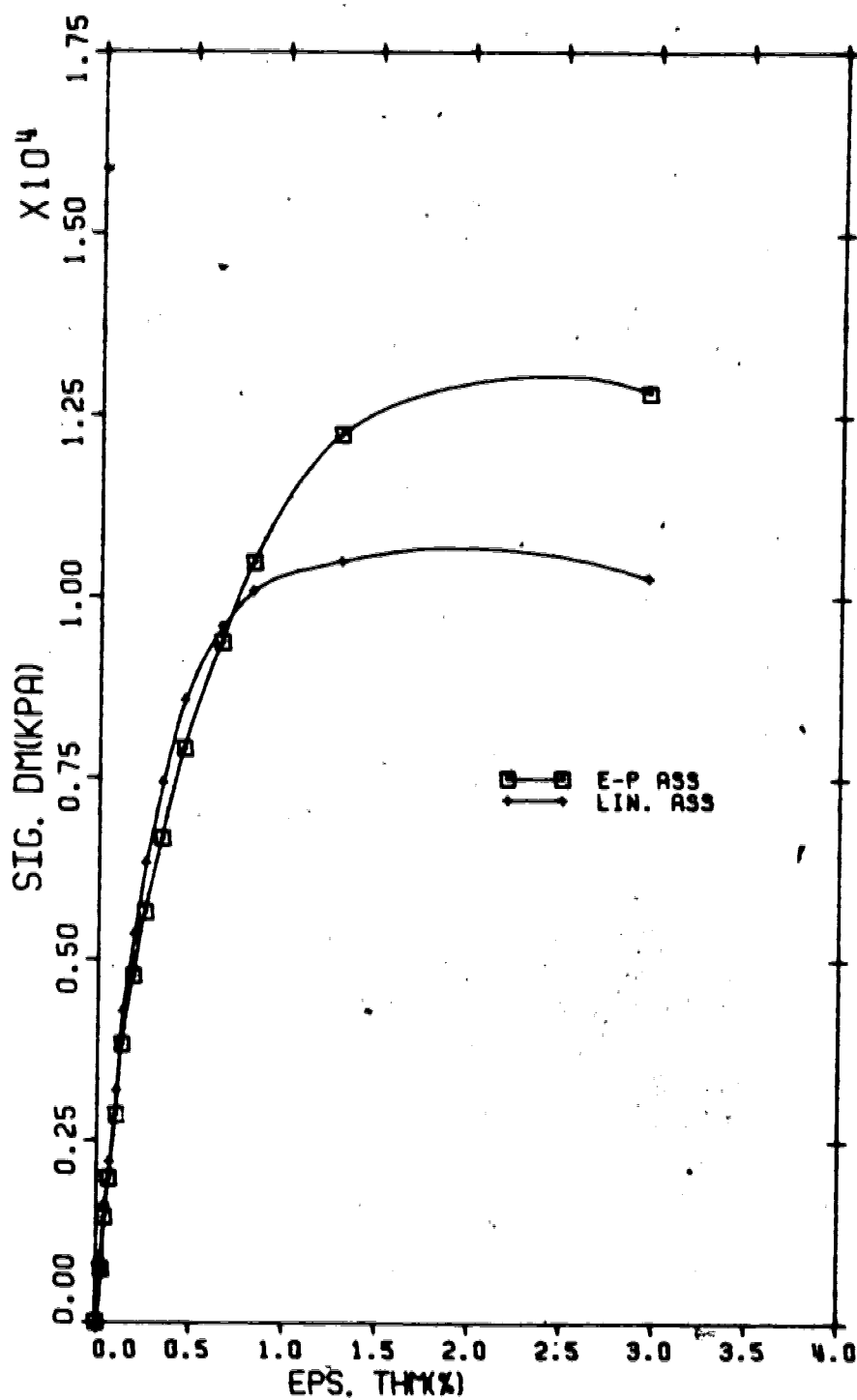
Figure 6.2 Stress-strain curves : Test #A-1
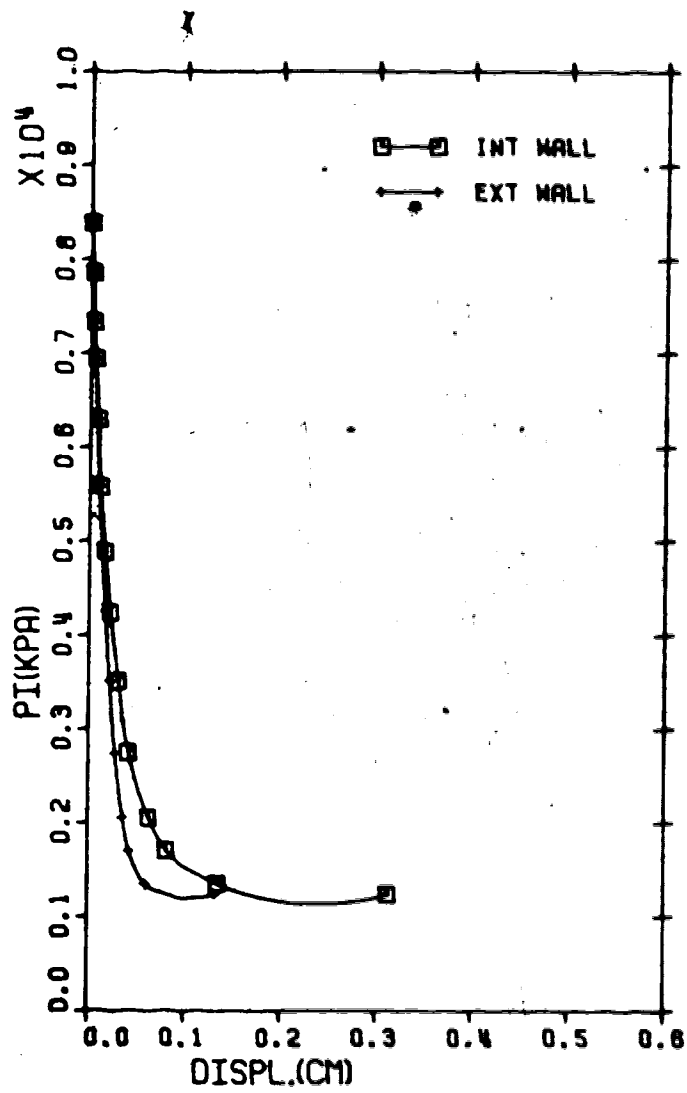
Figure 6.3 Measured wall movements : Test #A-1
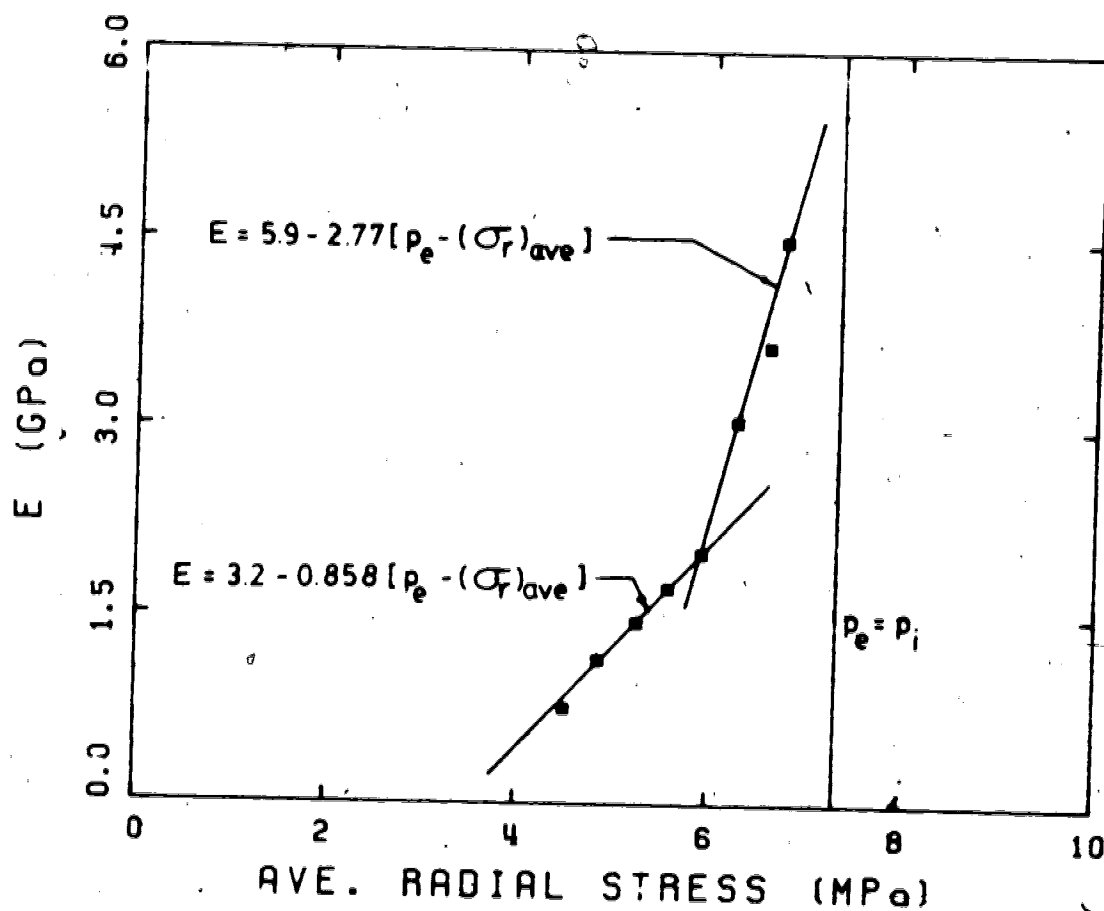
Figure 6.4 Variation of E with average radial stress : Test
#A-1
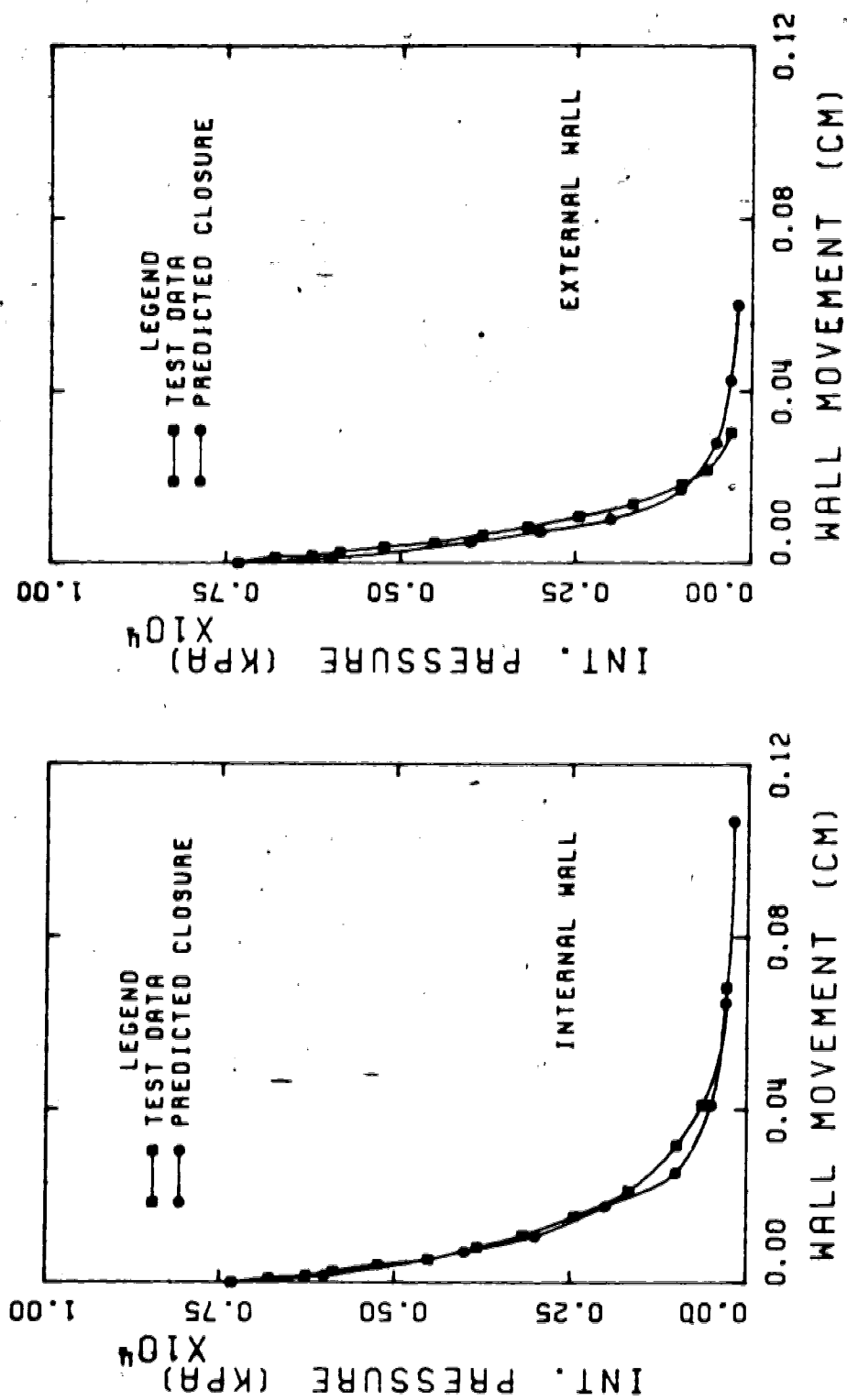
Figure 6.5 Comparison of predicted closure with actual
closure : Test #A-1
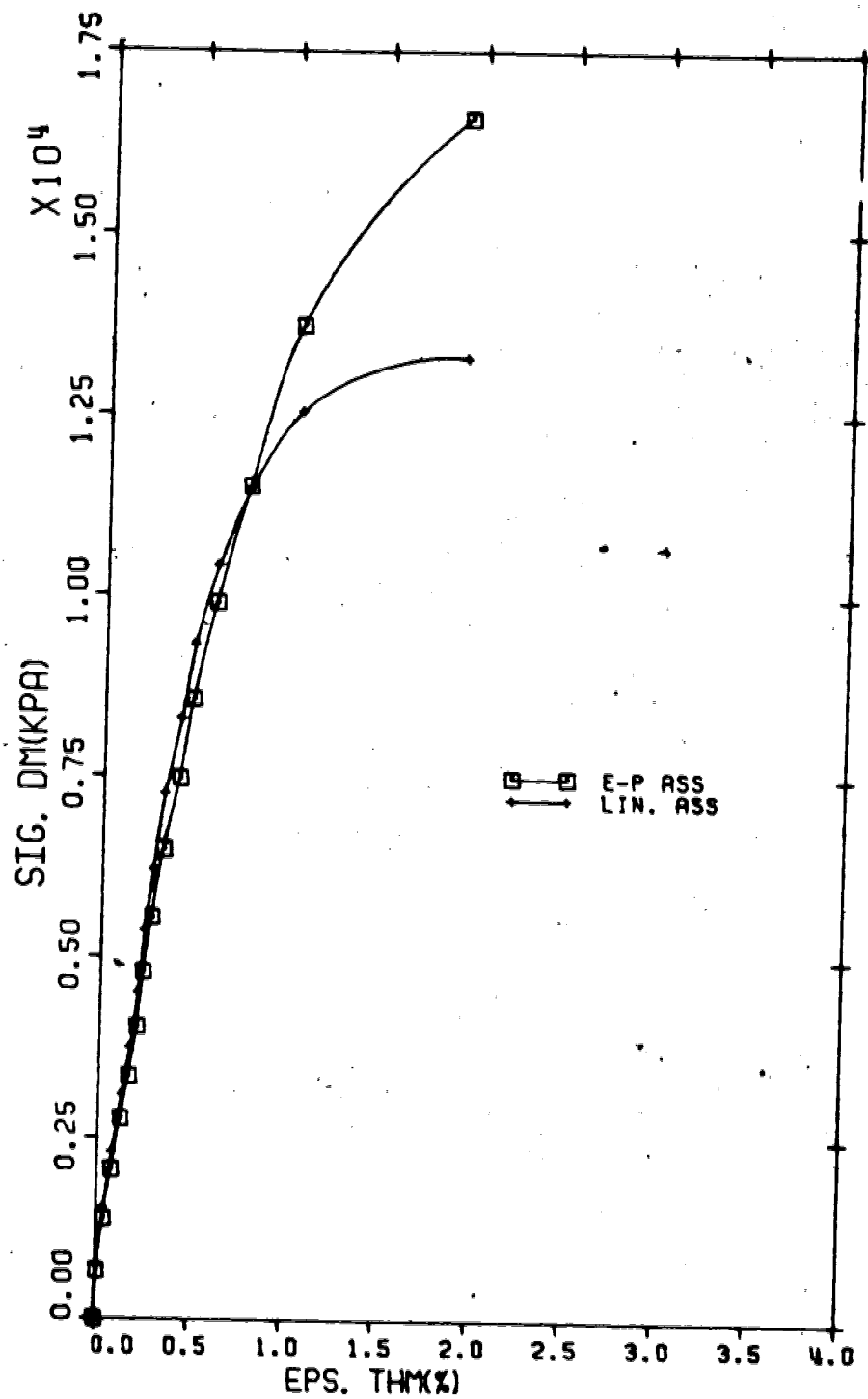
Figure 6.6 Stress-strain curves : Test #A-2
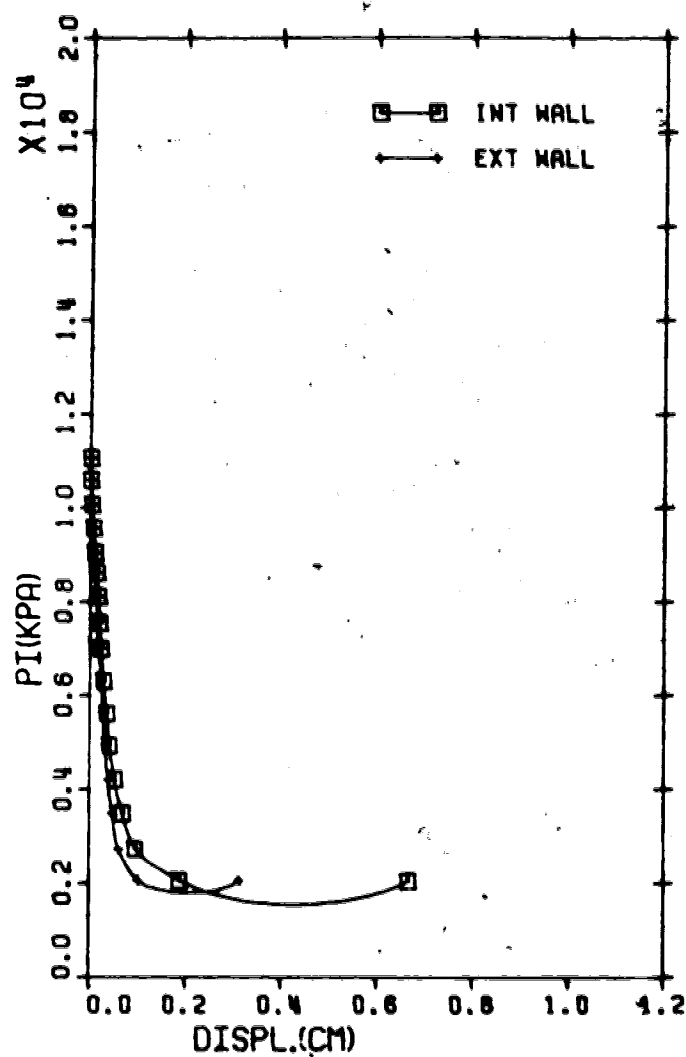
Figure 6.7 Measured wall movements : Test #A-2
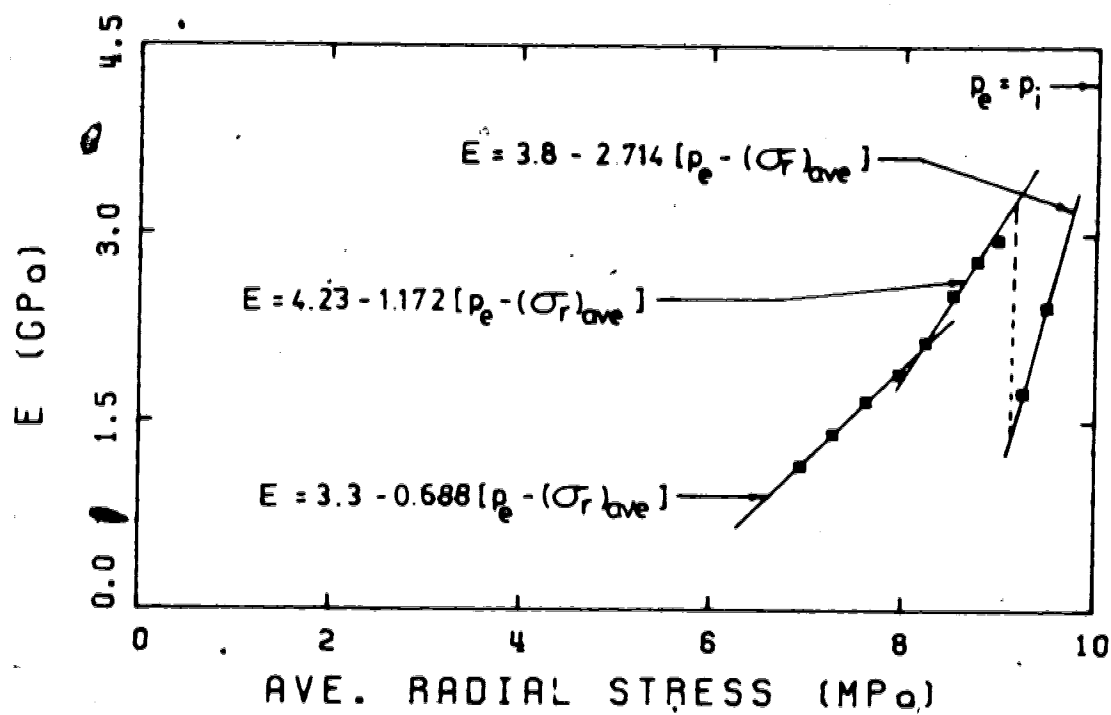
Figure 6.8 Variation of E with average radial stress : Test #A-2

predicted closures are compared with the actual closures in
Figure 6.9, and the strength parameters are shown in Table
6.1. The Young's moduli used have also been altered to
include the variation of E in the very low stress range (see
Figure 6.6). These results are shown in Figure 6.10.

6.3.3 Ottawa Sand Sample

This test has been included to compare with the
closures that occur in oil sand samples. The porosity of
the sample was 33% and the bulk density 1.77 g/cc. The
grain size distribution for the sand is shown in Figure
6.11.

The stress-strain curves are shown in Figure 6.12 and
the closure curves in Figure 6.13. The E- $(\sigma_r)_{ave}$
relationship is shown in Figure 6.14, and the predicted
closures are compared with the actual ones in Figure 6.15.
The strength parameters are shown in Table 6.1.

6.4 Discussion of Results

6.4.1 Shear strength of the cylinders

The initial elastic portion of the stress-strain curves
for all three tests are not significantly influenced by the
assumption made for the stress distribution. However, once
yielding has occured, and especially when the plastic radius
is large, the stress-strain behaviour of the cylinder is
strongly influenced by the assumption made.
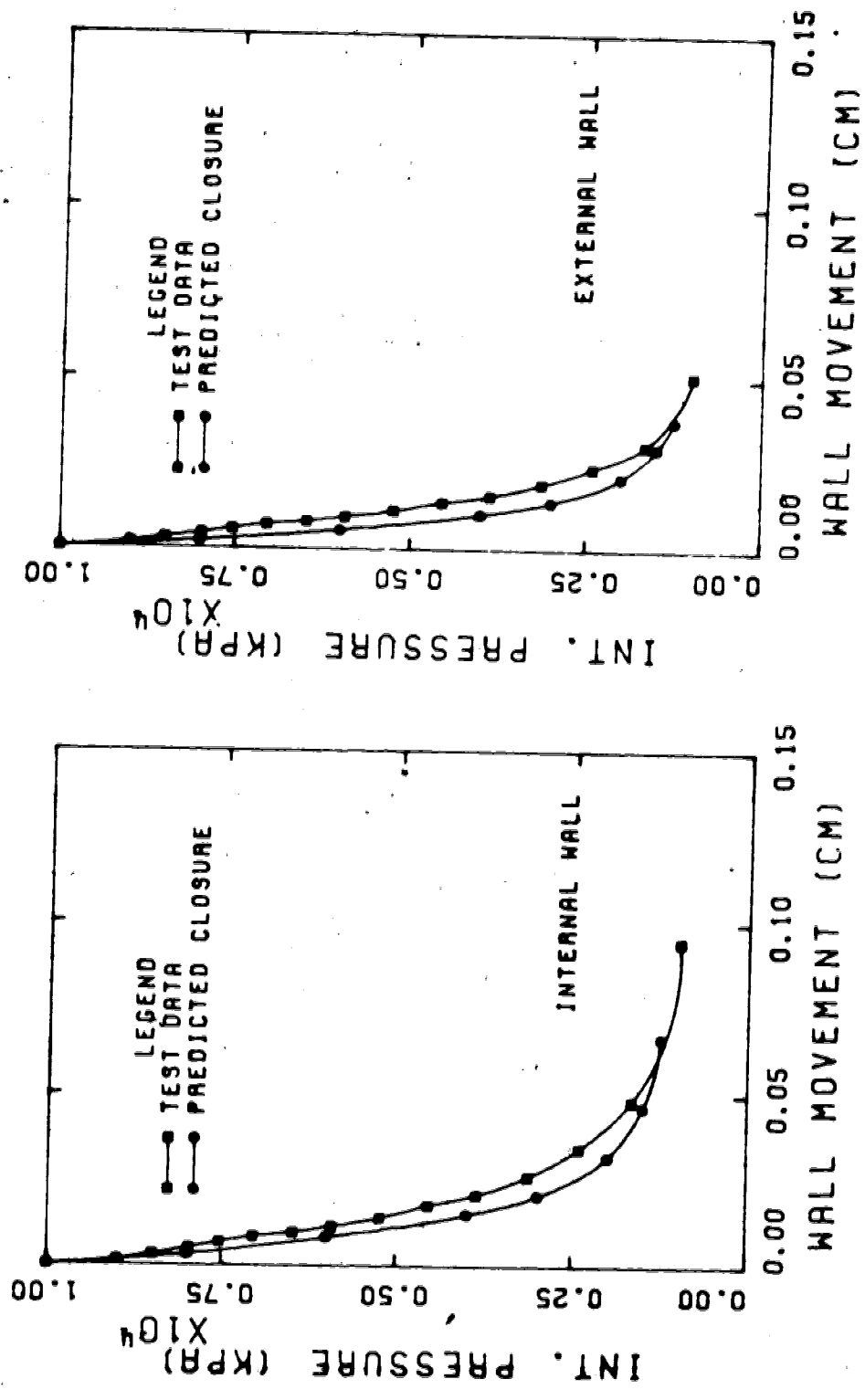
Figure 6.9 Comparison of predicted closure and actual
closure : Test #A-2
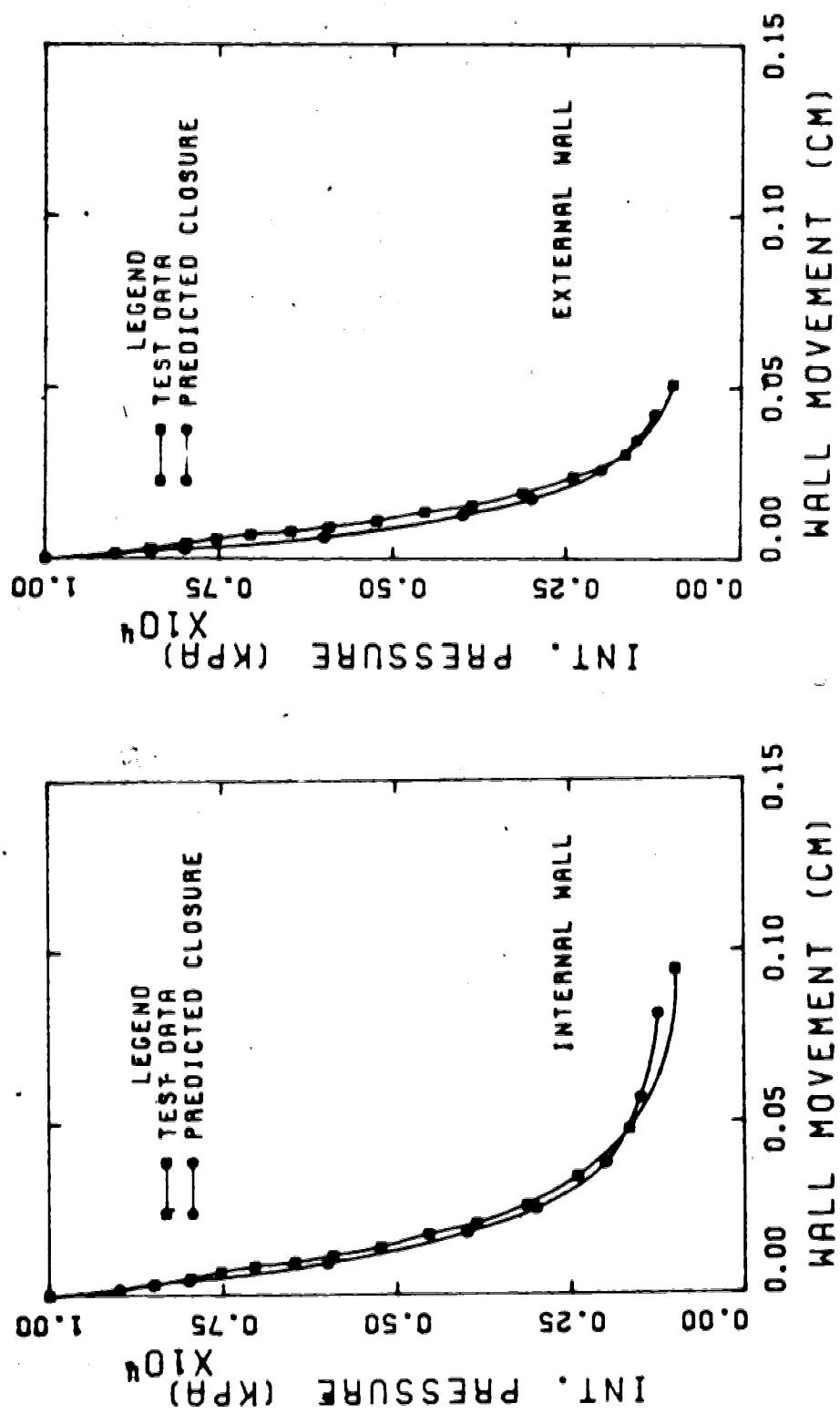
Figure 6.10 Comparison of predicted closure and actual
closure : Test #A-2 (adjusted moduli)
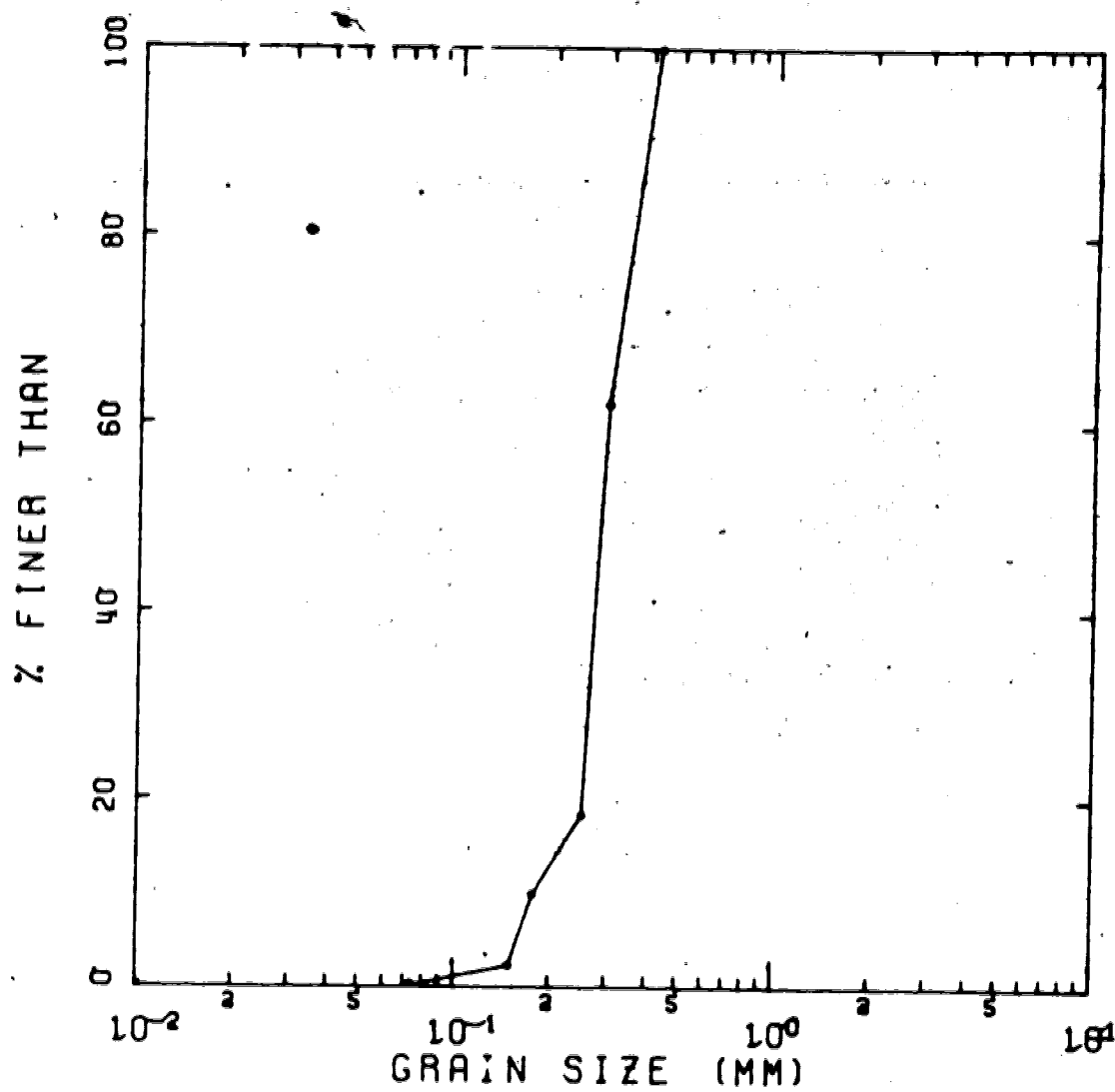
Figure 6.11 Grain size distribution for Ottawa sand
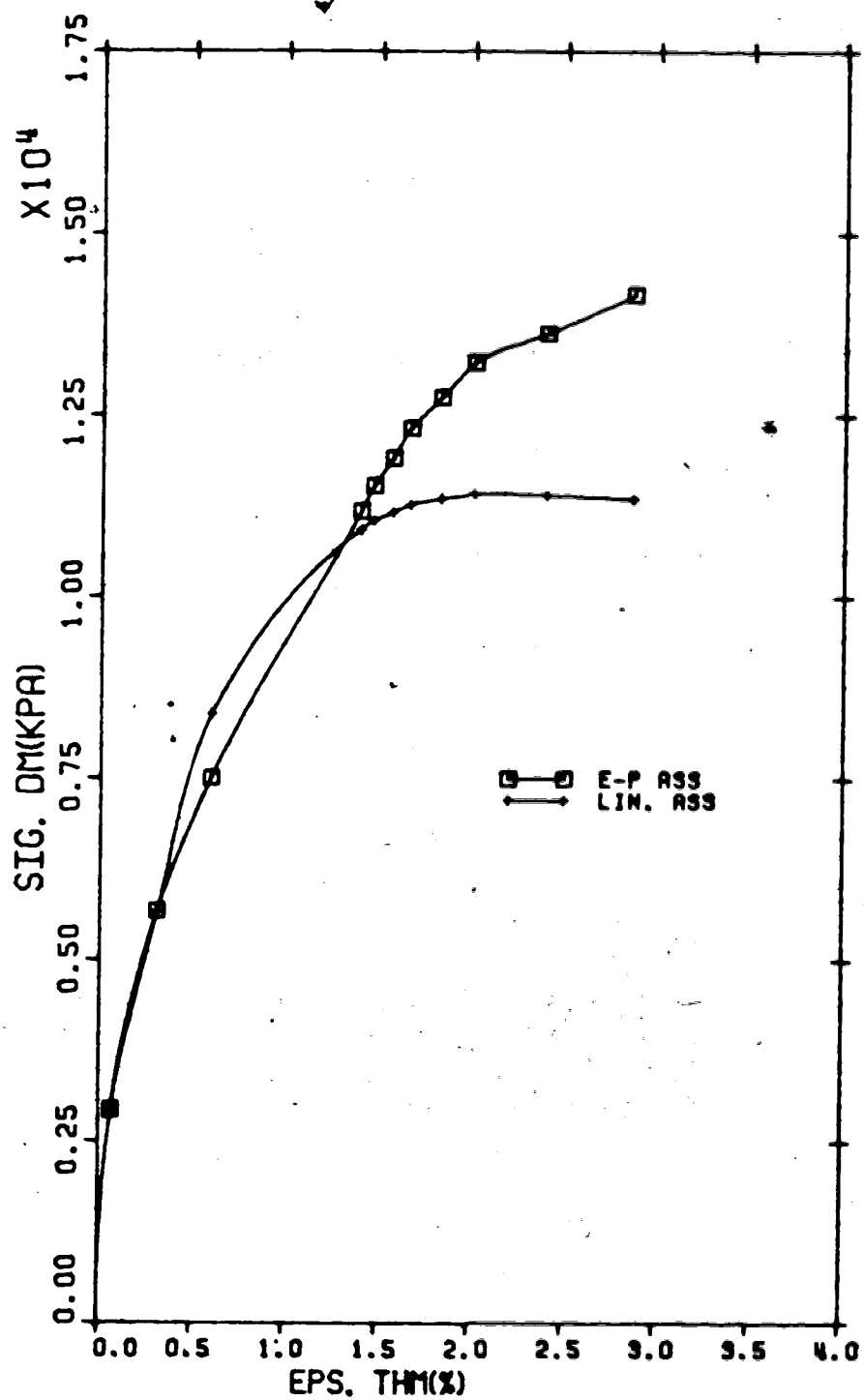
Figure 6.12 Stress-strain curves : Ottawa sand sample
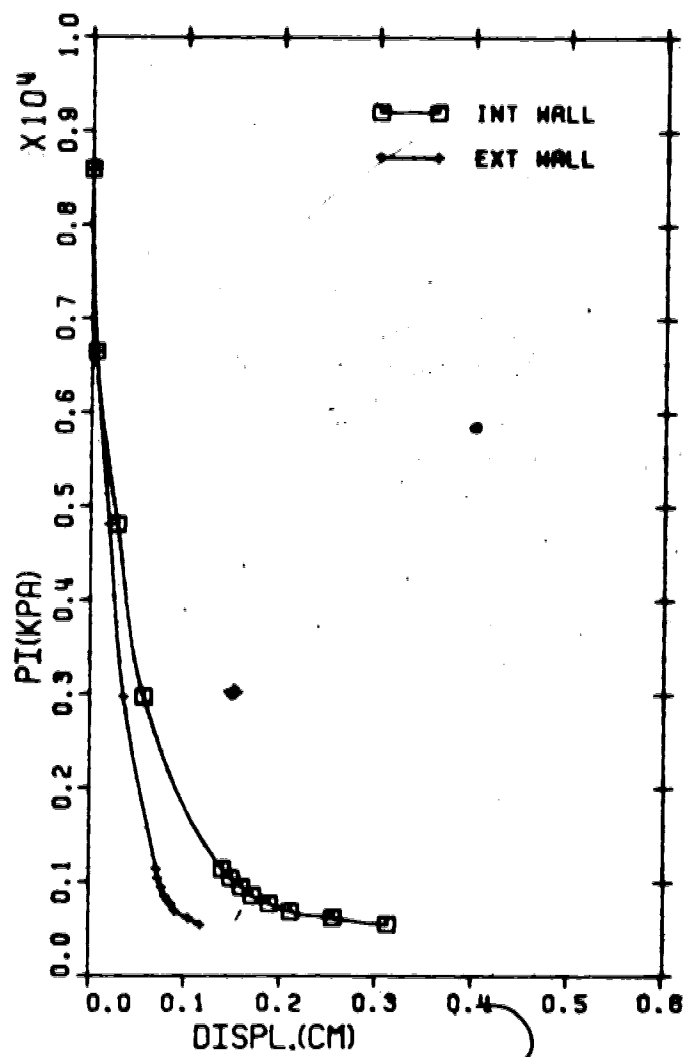
Figure 6.13 Measured wall movements : Ottawa sand sample
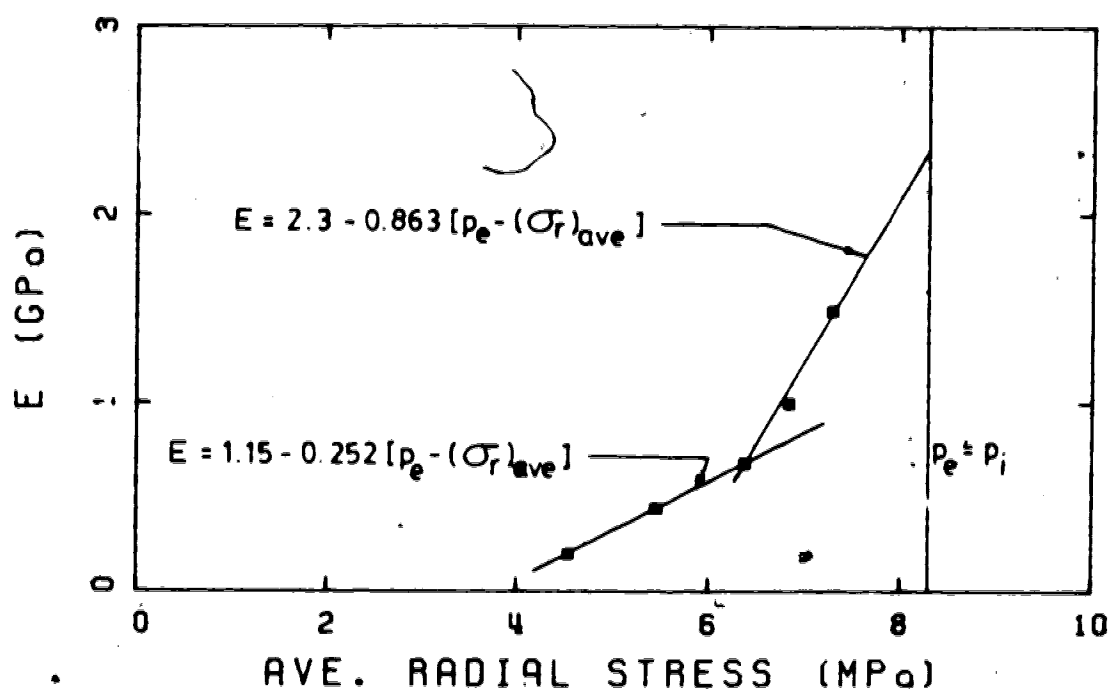
Figure 6.14 Variation of E with average radial stress :
Ottawa sand sample
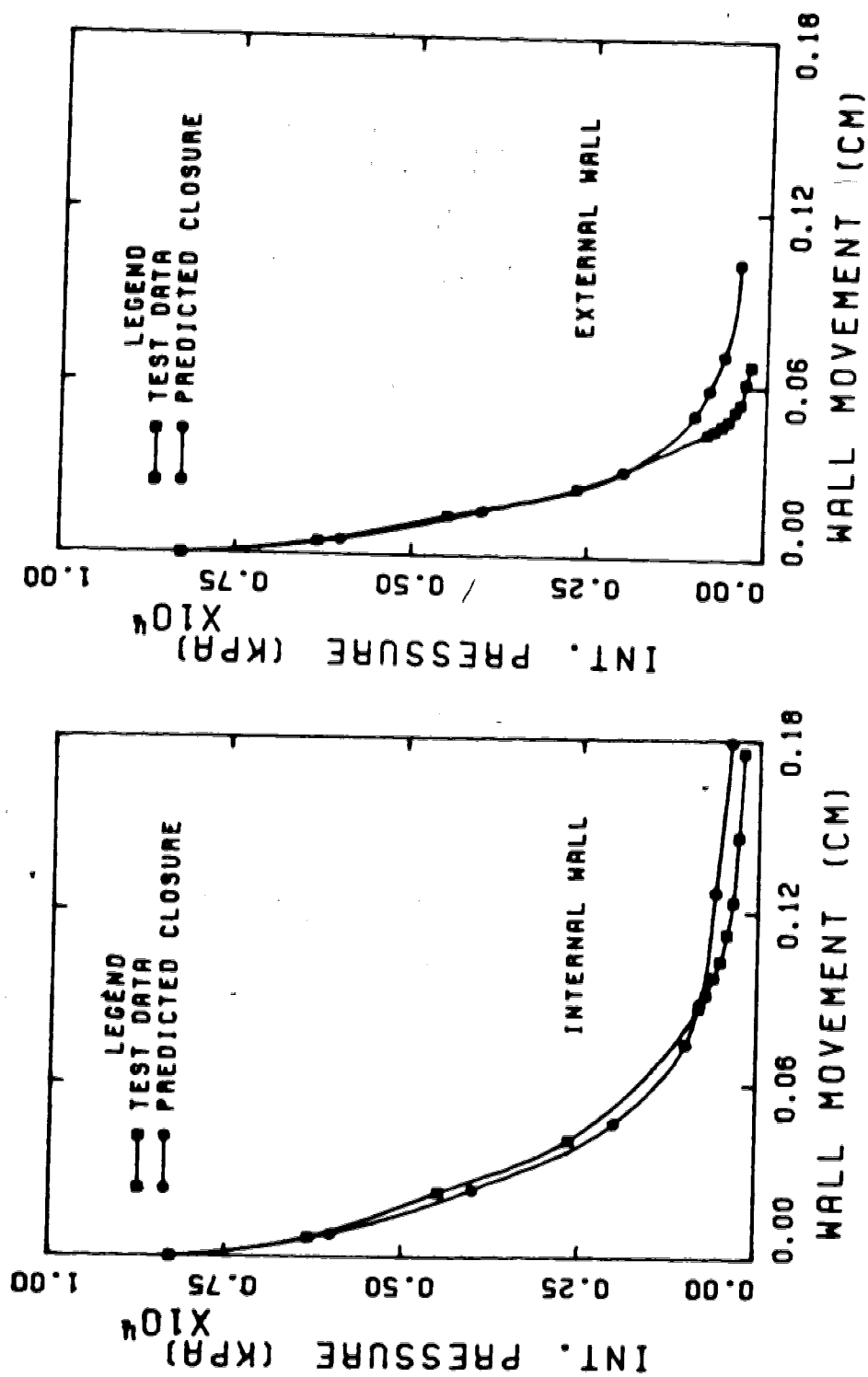
Figure 6.15 Comparison of predicted closure and actual closure : Ottawa sand sample

The $E-(\sigma_r)_{ave}$ relationship used was determined from the stress-strain curve based on the linear radial stress assumption. As has been shown, this curve is similar to the the second one in the elastic range, and it is this portion of the curve that is used to determine the $E-(\sigma_r)_{ave}$ relationship.

The use of this simplified stress-strain curve is then valid when analysing elastic deformation behaviour. The maximum deviator stress is underestimated and hence lower strength properties are determined.

The second assumption made may also be used in determining elastic deformation behaviour. However, the assumption largely overpredicts the maximum deviator stress and hence the strength parameters.

The strength parameters as determined by Wu *et al*.(1963) are identical to those determined from the numerical model. This gives confidence in the analytical capabilities of the model.

These friction angles are larger than those determined from the 37.5 mm diameter triaxial samples by up to 18 degrees. Plane-strain tests usually have a friction angle of about 4 degrees higher than conventional triaxial tests. This large difference is due to the amount of sample disturbance that has occurred prior to testing, as has been discussed in a previous section.

These results indicate that the hollow cylinder triaxial samples are still relatively undisturbed and have

some interlocking of the grains that account for the higher strength.

The tangential stress at failure is known and, with the friction angle determined, the radial stress at failure may be calculated. It is thus possible to plot these results on a p-q diagram. The results of Figure 5.4 are reproduced in Figure 6.16 with the hollow cylinder data included. It can be seen from this plot that the hollow cylinder oil sand strengths lie much closer to the results for a lean oil sand than do the triaxial test data for Series B and C.

6.4.2 Wall Movements

The predicted wall movements result in a good comparison with the measured movements. The predicted internal movements are lower than the actual movements soon after the commencement of yielding. This is due to the assumption made regarding the average radial stress in the elastic zone. Once yielding occurs and the plastic zone begins to develop, the average radial stress in the elastic zone increases rapidly and thus results in an increase in Young's modulus. This subsequently results in less elastic straining in the plastic zone.

The predicted movements are larger than the actual movements when the cylinder approaches the collapse state. this is due to the problem of modelling post-failure strains as well as to the influence of the overprediction of the external wall movements.
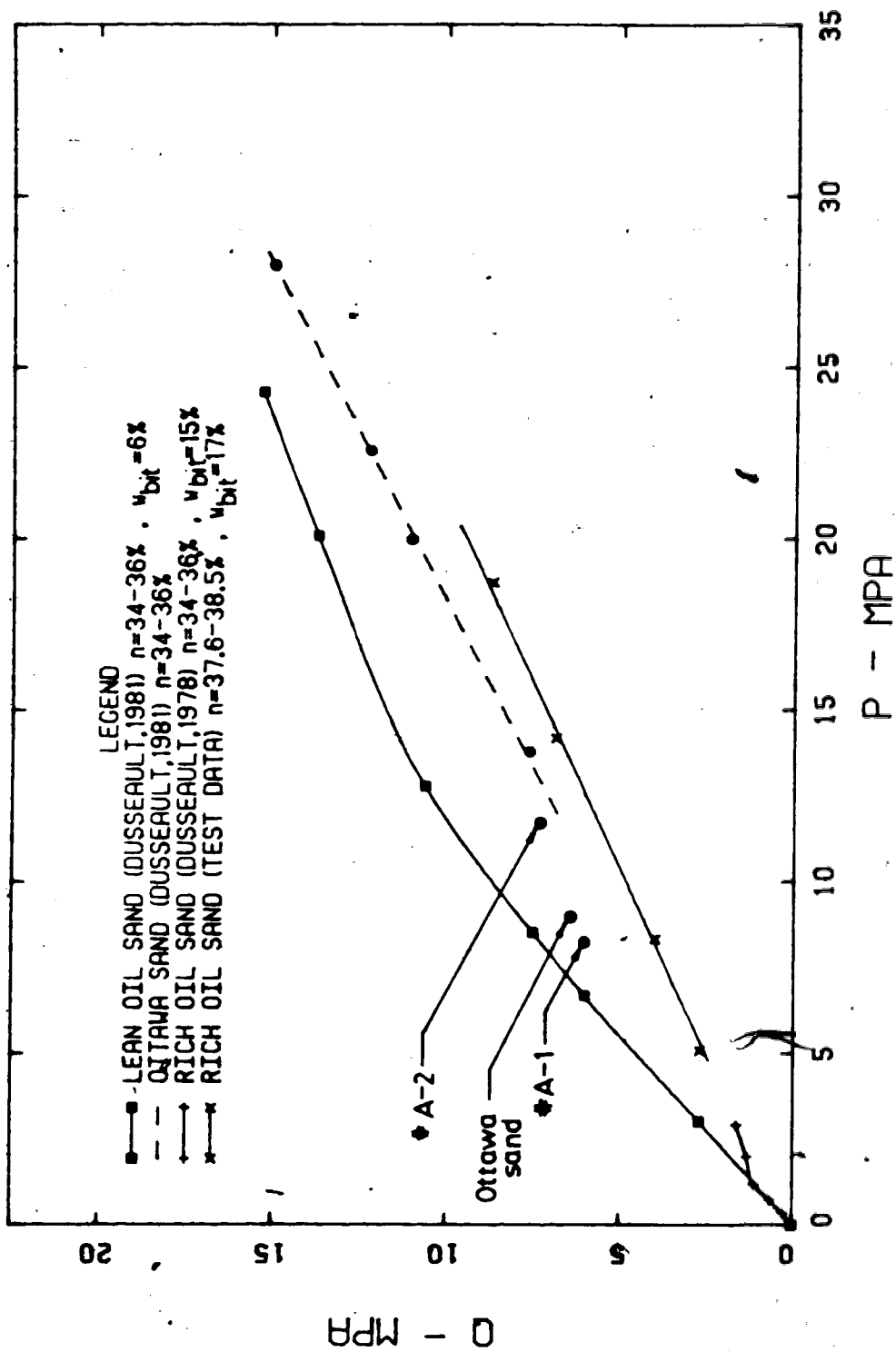
Figure 6.16 Comparison of test data with published data

The external wall movements are slightly underpredicted by the model in the elastic range and overpredicted as the sample nears the collapse state. This is a result of the determination of E in the elastic zone and to the rapidly increasing stresses at the external wall as the plastic radius approaches the value of the external radius.

The overprediction of the external wall movements will result in an error in the determination of the internal wall movements. The sample radii are modified after each stress increment and the stress calculations are based on these modified radii. Thus, as the sample nears collapse, the stress distribution will be affected by the error in the external boundary dimension. The stresses will be higher than actually exist, and the internal wall movements will be overpredicted.

The importance of the non-linearity of the stress-strain curve is demonstrated in the results of Test #A-2. In Figure 6.9, the predicted closures are far less than the measured ones, even in the elastic range of the material. When the elastic moduli are adjusted to account for variation in E at the low stress level, the predicted closures are much better (Figure 6.10). The plastic strain increments are a function of the total elastic strains in the plastic zone, and hence it is important to correctly predict the elastic strains.

The incongruity of the stress-strain curve for Test #A-2 in the low stress range is difficult to account for.

The loading cap should be well seated after the consolidation test, thus it does not seem feasible that this incongruity is a result of seating. The measured closures also respond in a similar manner, as can be seen from Figure 6.9.

The difference in closure curves between the oil sand samples and Ottawa sand sample should be noted. The Ottawa sand responds in a more ductile manner than the oil sand. The closure curve for Ottawa sand shows a more non-linear behaviour and substantial "flow" occurs prior to collapse. In the oil sand samples, the closure is more linear and collapse occurs suddenly. This difference in behaviour is due to the difference in the shape of the grains as well as the interlocking of the oil sand grains.

The failure mode of the hollow cylinder samples has been discussed in the previous chapter. However, the post-collapse mechanism of Test #A-2 has not been discussed. Collapse of a cylinder is defined as a very large volume change of the bore with a small decrease in internal pressure. In this test, the volume changes were allowed to continue without shutting down the pressure systems (as is the usual practise). After a short time, the volume changes stopped and further reduction of the internal pressure did not result in any substantial volume changes of the bore or the pore fluid.

The internal pressure was continually decreased until the effective radial stress at the inside surface was zero.

Even under this condition, volume changes did not occur.
The sample thus stabilized (probably by arching) under zero
effective internal pressure and an external pressure of 10
MPa.

Physical examination of the sample after the test
showed a distinct failure surface typical for this type of
test. The internal diameter was uniform except in the zone
of the failure surface.

This arching phenomenon needs to be examined
experimentally in further detail before any conclusions may
be drawn. The arching may be a function of the wall
thickness and is probably not to be expected in the
deformation around a shaft or tunnel in cohesionless
material. It should be noted that the shape of the bore of
the Ottawa sand sample after the test was not
distinguishable as the sample had collapsed completely.
Hence this arching phenomenon is probably greatly influenced
by the shape of the grains and the soil structure.

6.5 Conclusions

The numerical model developed during this research has
the capability of predicting the deformations that occur in
a hollow cylinder test with reasonable accuracy. The
dilation parameter selected for the analysis was unity, the
case of no plastic volume change. Any other values of this
parameter will result in larger overpredictions of the
deformations as the cylinder nears the collapse state.

The use of a simplified analysis to determine the stresses in the sample is valid only when studying the elastic deformation of the hollow cylinders. Two different assumptions were used in the analyses and both gave similar results in the elastic range.

These simplified analyses are not valid when determining the shear strength of the hollow cylinders. The shear strength as determined from Wu et al.(1963) corresponds with that determined from the numerical model. The model can thus be used as an analytical tool in the reduction of the hollow cylinder test data.

The arching phenomenon observed in Test #A-2 needs to be examined in further detail. This phenomenon was not evident in the Ottawa sand sample and is probably a function of the grain shape and soil structure. The influence of wall thickness has a large effect on the arching mechanism.

CHAPTER 7

CONCLUSIONS

The research herein has examined the deformation behaviour of oil sands. An experimental program was conducted on intact specimens of oil sand. The problems associated with sample preparation and disturbance have been discussed and a detailed analysis of the interpretation of hollow cylinder test data has been made.

The research has resulted in a better understanding of the problems associated with the testing of oil sands, as well as the deformational behaviour of this material. The following sections summarize the major findings of this research.

7.1 Sample Preparation and Laboratory Equipment

The influence of sample preparation techniques on the amount of sample disturbance that occurs has been shown. It is necessary to improve these techniques if reliable data is to be obtained from laboratory testing.

The disturbance that can occur in the preparation of samples is due to the heat generated by the coring and trimming procedures. The effects of disturbance can be reduced by using larger size samples to dissipate the heat. However, it is necessary to improve these techniques so as to minimize the heat generation.

Many of the problems encountered in conducting high

pressure tests have been described. The hollow cylinder triaxial device has been used with limited success and many more successful tests are required before the equipment may be called operational. The problem of leaks developing in the internal membrane may be minimized by using flexible Neoprene rubber rings at all interfaces between the sample and the equipment (loading cap, porous stones).

The high pressure triaxial cell for 37.5 mm diameter samples operated without any problems. This will be an extremely valuable piece of equipment once the sample disturbance problem for small samples is solved.

7.2 Material Behaviour

The laboratory results have shown that the deformation behaviour of oil sand is path dependent. This path dependency needs to be examined more thoroughly. The influence of sample disturbance will be reflected in the test results and may not be indicative of the *in situ* behaviour of the material.

The oil sands deform in a non-linear manner. This non-linearity is the result of irreversible strains that occur in particulate media and is a function of the amount of slip that occurs between particles. In the case of the hollow cylinder tests, the reduction in the confinement of the sample will also result in a non-linear response.

The oil sands dilate when sheared. This dilatancy is a function of the confining pressure and can be suppressed at

high pressures. This change in mode of failure has been shown to be path dependent.

Crushing of the sand grains occurs at these high pressures as indicated by the increase in the amount of fines after testing. Some crushing also occurs during the consolidation of the samples, but these two phenomena have not been examined separately.

An arching phenomenon has been observed in a hollow cylinder sample. Insufficient test data have made it impossible to analyse this phenomenon in detail, but it is dependent on the shape of the sand grains as well as the interlocking nature of these materials.

7.3 Hollow Cylinder Test Data

The hollow cylinder test is ideal for examining the deformations that occur around shafts and tunnels. The stress path followed in this test is similar to actual field behaviour, and the influence of reduced confinement on the deformation moduli can be readily examined.

A numerical model has been used to show how this influence of confinement may be incorporated. This approach is simpler than the more conventional ones used in non-linear analyses. This approach makes the hollow cylinder test a powerful tool for obtaining design parameters.

The interpretation of data from a hollow cylinder test has been examined. The assumption of axi-symmetric

deformation is valid as is evident from the examination of the cylinders after the test. End restraints have no significant influence on the deformed shape of the cylinders, though the shape of the failure surface is influenced by these restraints. The uniform deformation can thus be reliably measured on a volume change indicator.

The radial stress distribution within a hollow cylinder may be approximated as varying linearly. The stress-strain curve will give reliable deformation moduli within the elastic portion of the curve. The shear strength of the sample must be determined from an analytical solution such as that given by Wu *et al.* (1963) or from the model developed in Chapter 4. The assumptions made regarding the radial stress distribution will result in an incorrect determination of the shear strength.

7.4 Concluding Remarks

The results of this laboratory program have revealed several traits of oil sand behaviour which should assist in a better understanding of this material. The detrimental effect of sample disturbance must be overcome before reliable data can be obtained.

Many other areas of research must still be addressed. The most important of these, as far as *in situ* recovery procedures are concerned, are an examination of the undrained behaviour of oil sand and the influence of high temperatures on the mechanical properties.

Bibliography

Bishop, A.W. 1973. The influence of an undrained change in stress on the pore pressure in porous media of low compressibility. Geotechnique, 23(3), pp.435-442.

Bishop, A.W., and Henkel,D.J. 1957. The measurement of soil properties in the triaxial test. Edward Arnold (Publishers) Ltd., London, England.

Bishop, A.W., and Hight, D.W. 1977. The value of Poisson's ratio in saturated soils and rocks under undrained conditions. Geotechnique, 27(3), pp.369-384.

Bishop, A.W., Webb, D.L., and Skinner, A.E. 1965. Triaxial tests on soils at elevated cell pressures. Proceedings of the 6th International Conference on Soil Mechanics and Foundation Engineering, Vol. 1, pp.170-174.

Black, D K., and Lee, K.L. 1973. Saturating laboratory samples by back pressure. Proceedings of the ASCE Journal of the Soil Mechanics and Foundations Division, 99(SM1), pp.75-93.

Broms, B.B., and Casbarian, A.D. 1965. Effects of rotation of the principle stress axes and of the intermediate principal stress on the shear strength. Proceedings of the 6th International Conference on Soil Mechanics and Foundation Engineering, Vol.1, pp.179-183.

Broms, B.B., and Jamal, A.K. 1965. Analysis of the triaxial test - cohesionless materials. Proceedings of the 6th International Conference on Soil Mechanics and Foundation Engineering, Vol.1, pp.184-188.

Cornforth, M.S.1964. Some experiments on the influence of
strain conditions on the strength of sand.
Geotechnique, 14(2), pp.172-178.

Devenney, D.W., and Raisbeck, J.M. 1980. Rock mechanics
considerations for in situ development of oil sands.
Underground Rock Engineering, CIM Special Volume 22,
Canadian Institute of Mining and Metallurgy, pp.90-96.

Dusseault, M.B. 1977. The geotechnical characteristics of
the Athabasca oil sands. Ph.D thesis, University of
Alberta, Edmonton, Alberta.

———— 1980. Sample disturbance in Athabasca oil sands.
Canadian Petroleum Technology, 18(2), pp.85-92.

———— 1981. A versatile hollow cylinder triaxial device.
In print.

———— 1981. Unpublished data.

Dusseault, M.B., and Morgenstern, N.R. 1978. Shear strength
of Athabasca oil sands. Canadian Geotechnical Journal,
15(2), pp.216-238.

———— 1979. Locked sands. Quarterly Journal of Engineering
Geology, 12, pp.117-131.

Finn, W.D., Wade, N.H., and Lee, K.L. 1967. Volume changes
in the triaxial and plane-strain tests. Proceedings of
the ASCE Journal of the Soil Mechanics and Foundations
Division, 93(SM6), pp.297-308

Florence, A.L., and Schwer, L.E. 1978. Axisymmetric
compression of a Mohr-Coulomb material around a circular
hole. International Journal for Numerical and

Analytical Methods in Geomechanics, Vol.2, pp.367-379.

Fradis, F., and Frydman, S. 1977. Stress-strain behavior of sand under generalized stress conditions. Proceedings of Speciality Session 9, 9th International Conference on Soil Mechanics and Foundation Engineering, pp.

Frydman, S. 1968. The effects of stress history on the stress-deformation properties of sand. M.Sc. thesis, Technion, Israeli Institute of Technology, Haifa, Israel.

—— 1974. Yielding of sand in plane-strain. Proceedings of the ASCE Journal of the Soil Mechanics and Foundations Division, 100(GT5), pp.491-501.

—— 1976. The strain-hardening behaviour of particulate media. Canadian Geotechnical Journal, 13, pp.

Frydman, S., and Zeitlen, J.G. 1969. Some pseudo-elastic properties of granular media. Proceedings of the 7th International Conference on Soil Mechanics and Foundation Engineering, Vol.1, pp.135-141.

Frydman, S., Zeitlen, J.G., and Alpan, I. 1973. The yielding behaviour of particulate media. Canadian Geotechnical Journal, 10, pp.341-361.

Guenot, A. 1979. Investigation of tunnel stability by model tests. M.Sc thesis, University of Alberta, Edmonton, Alberta.

Hamza, M., and Davachi, M. 1979. Solution schemes for shear and average effective stress unloading stress paths. Proceedings of the 3rd International Conference on

Numerical Methods in Geomechanics, Aachen, pp.331-338.

Hardy, R.M., and Scott, J.D. 1978. The 1963 GCOS Test Shaft. Post Conference Contribution, AOSTRA Seminar on Underground Excavation in Oil Sands, Edmonton, Alberta, Paper #13.

Harris, M.C., and Sobkowicz, J.C. 1977. Engineering behaviourof oil sands. Proceedings of the Canada-Venezuela Oil Sands Symposium, Edmonton, Alberta, pp.270-281.

———— 1978. Feasibility study on underground excavation in oil sands. Proceedings of the Seminar on Underground Excavations in Oil Sands, Edmonton, Alberta, Paper #5.

Haythornthwaite, R.M. 1960. Stress and Strain in Soils. Plasticity, Proceedings of the 2nd Symposium on Naval Structural Mechanics, pp.185-193.

Hoeg, K. 1978. Deformation computations in Geotechnical engineering. Norwegian Geotechnical Institute,Publication No.123, pp.1-19.

Jaeger, J.C., and Cook, N.G.W. 1976. Fundamentals of Rock Mechanics. John Wiley and Sons, Inc., New York, NY.

Kirkpatrick, W.M. 1957. The condition of failure for sands. Proceedings of the 4th International Conference on Soil Mechanics and Foundation Engineering, Vol.1, pp.172-178.

———— 1965. Effect of grain size and grading on the shearing behavior of granular materials. Proceedings of the 6th International Conference on Soil Mechanics and Foundation Engineering, Vol.1, pp.273-277.

Korbin, G.E. 1976. Simple procedure for the analysis of
deep tunnels in problematic ground. 17th U.S. Symposium
on Rock Mechanics, Site Characterization, pp.1A3-1 to
1A3-7.

Lee, K.L., and Black, D.K. 1972. Time to dissolve air
bubbles in drain lines. Proceedings of the ASCE Journal
of the Soil Mechanics and Foundations Division, 98(SM2),
pp.181-194.

Lee, K.L., Morrison, R.A., and Haley, S.C. 1969. A note on
the pore pressure parameter B. Proceedings of the 7th
International Conference on Soil Mechanics and
Foundation Engineering, Vol.1, pp.231-239.

Lee, K.L., and Seed, H.B. 1967. Drained strength
characteristics of sands. Proceedings of the ASCE
Journal of the Soil Mechanics and Foundations Division,
93(SM6), pp.117-141.

McCreath, D. 1981. Analysis of formation pressures on
tunnel and shaft linings. M.Eng. Project, University of
Alberta, Edmonton, Alberta.

Poulos, S.J. 1964. Control of leakage in the triaxial test.
Harvard Soil Mechanics Series, No. 71.

Procter, D.C. 1967. The stress-dilatency behaviour of dense
sand in the hollow cylinder test. M.Sc. thesis,
University of Manchester, England.

Roesner, E.K., and Poppen, S.A. 1978. Shaft sinking in the
oil sands of Alberta. Proceedings of the Seminar on
Underground Excavation in oil sands, Edmonton, Alberta,

Paper #11.

Rowe, P.W. 1969. The relation between the shear strength of sands in triaxial compression, plane-strain and direct shear. Geotechnique, 19(1), pp.75-86.

Scott, J.D. 1978. General Report. AOSTRA Seminar on Underground Excavation in oil sands, Edmonton, Alberta.

Smith, L.B., Chatterji, P.K., Insley, A.E., and Sharma, L. 1978. Construction of Saline Creek Tunnel in Athabasca oil sand. AOSTRA Seminar on Underground Excavation in oil sands, Edmonton, Alberta, Paper #7.

Suklje, L., and Drnovsek, J. 1965. Investigation of the tensile deformability of soils using hollow cylinders. Proceedings of the 6th International Conference on Soil Mechanics and Foundation Engineering, Vol.1, pp.368-372.

Timoshenko, S.P., and Goodier, J.N. 1970. Theory of Elasticity. McGraw-Hill, Inc., New York, NY.

Vesic, A.S., and Clough, G.W. 1968. Proceedings of the ASCE Journal of the Soil Mechanics and Foundations Division, 94(SM3), pp.661-688.

Whitman, R.V., and Luscher, V. 1962. Basic experiment into soil-structure interaction. Proceedings of the ASCE Journal of the Soil Mechanics and Foundations Division, 88(SM6), pp.135-167.

Wissa, A.E. 1969. Pore pressure measurements in saturated, stiff soils. Proceedings of the ASCE Journal of the Soil Mechanics and Foundations Division, 95(SM4), pp.1063-1073.

Wu, T.H., Loh, A.K., and Malvern, L.E. 1963. Study of
    failure envelopes of soils. Proceedings of the ASCE
    Journal of the Soil Mechanics and Foundations Division,
    89(SM1), pp.145-181.

APPENDIX A

Elastic solution for the plane-strain problem

The continuum mechanics relationships for the plane-strain problem can be found in several elasticity text books, and are summarized below in terms of polar co-ordinates :

Equilibrium Equations:

$$\frac{\partial \sigma_r}{\partial r} + \frac{1}{r}\frac{\partial \mathcal{T}_{r\theta}}{\partial \theta} - \frac{\sigma_\theta - \sigma_r}{r} + F_r = 0$$

$$\frac{1}{r}\frac{\partial \sigma_\theta}{\partial \theta} + \frac{\partial \mathcal{T}_{r\theta}}{\partial r} + 2\frac{\mathcal{T}_{r\theta}}{r} + F_\theta = 0$$

$$\qquad\qquad\dots A.1$$

Hookes Law:

$$\epsilon_r = \frac{1-\nu^2}{E}\left[\sigma_r - \left(\frac{\nu}{1-\nu}\right)\sigma_\theta\right]$$

$$\epsilon_\theta = \frac{1-\nu^2}{E}\left[\sigma_\theta - \left(\frac{\nu}{1-\nu}\right)\sigma_r\right] \qquad\dots A.2$$

$$\gamma_{r\theta} = \frac{1}{G}\mathcal{T}_{r\theta}$$

Strain-Displacement Equations:

$$\epsilon_r = \frac{\partial u_r}{\partial r}$$

$$\qquad\qquad\dots A.3$$

$$\epsilon_\theta = \frac{u_r}{r} + \frac{1}{r}\frac{\partial u_\theta}{\partial \theta}$$

$$\gamma_{r\theta} = \frac{1}{r}\frac{\partial u_r}{\partial \theta} + \frac{\partial u_\theta}{\partial r} - \frac{u_\theta}{r}$$

Stress components in terms of the Airy stress function:

$$\sigma_r = \frac{1}{r}\frac{\partial \phi}{\partial r} + \frac{1}{r^2}\frac{\partial^2 \phi}{\partial \theta^2}$$

$$\sigma_\theta = \frac{\partial^2 \phi}{\partial r^2}$$

....A.4

$$\tau_{r\theta} = \frac{1}{r^2}\frac{\partial \phi}{\partial \theta} - \frac{1}{r}\frac{\partial^2 \phi}{\partial r \partial \theta} = -\frac{\partial}{\partial r}\left(\frac{1}{r}\frac{\partial \phi}{\partial \theta}\right)$$

The bi-harmonic equation is derived by considering the equilibrium equations, Airy stress function, compatibility requirements and Hookes Law :

$$\nabla^4 \phi = 0$$

....A.5

For the axi-symmetric solution, $\frac{\partial}{\partial \theta} = 0$. The general solution of the bi-harmonic equation for this case gives the Airy stress function and hence the stress components :

$$\sigma_r = A(1 + 2\ln r) + 2B + \frac{C}{r^2}$$

$$\sigma_\theta = A(2\ln r + 3) + 2B - \frac{C}{r^2}$$

....A.6

$$\tau_{r\theta} = 0$$

In the hollow cylinder, the region occupied by the cylinder is not simply connected and hence the compatibility equations are not sufficient to guarantee single valued displacements. It is therefore necessary to consider the strain-displacement equations as well. Integration of these equations give radial displacements which must be equivalent. For this condition to be satisfied, the

constant A in Eqn.A.6 must be zero. Thus the stress distribution in the hollow cylinder is given by :

$$\sigma_r = 2B + \frac{C}{r^2}$$

$$\sigma_\theta = 2B - \frac{C}{r^2} \qquad\qquad \text{....A.7}$$

$$\tau_{r\theta} = 0$$

The constants B and C are solved from the boundary conditions.

Boundary Conditions

The sign convention used in the derivation is that compressive strains and stresses are positive.

The boundary conditions for the hollow cylinder test are :

$$\text{At } r = a, \quad \sigma_r = P_i$$

$$\text{At } r = b, \quad \sigma_r = P_e$$

$$\therefore P_i = 2B + \frac{C}{a^2} \qquad\qquad \text{....A.8}$$

$$P_e = 2B + \frac{C}{b^2}$$

Elimination of 2B from these equations solves for C :

$$C = \frac{-a^2 b^2 (P_e - P_i)}{b^2 - a^2} \qquad\qquad \text{....A.9}$$

Elimination of C from eqn.A.8 solves for 2B :

$$2B = \frac{-p_i a^2 + p_e b^2}{b^2 - a^2}$$

....A.10

Substitution of eqns.A.9 and A.10 into eqn.A.7 gives the solution for the stress distribution in the hollow cylinder :

$$\sigma_r = \frac{p_e b^2 - p_i a^2}{b^2 - a^2} - \frac{a^2 b^2 (p_e - p_i)}{r^2 (b^2 - a^2)}$$

....A.11

$$\sigma_\theta = \frac{p_e b^2 - p_i a^2}{b^2 - a^2} + \frac{a^2 b^2 (p_e - p_i)}{r^2 (b^2 - a^2)}$$

$$\tau_{r\theta} = 0$$

APPENDIX B

Elasto-plastic solution for the stress distribution in the hollow cylinder test

The derivations which follow are based on the following assumptions :

1. Linear Mohr-Coulomb failure criterion

2. Elastic-perfectly plastic behaviour

Stress Distribution in the Plastic Zone

The Mohr-Coulomb failure criterion relates the maximum and minimum principle stresses at failure as follows :

$$\sigma_\theta = N\sigma_r + 2cN^{1/2} \qquad \dots B.1$$

The equilibrium equation for the axi-symmetric case is :

$$\frac{d\sigma_r}{dr} = \frac{1}{r}(\sigma_\theta - \sigma_r) \qquad \dots B.2$$

Substituting Eqn.B.1 into Eqn.B.2 yields :

$$\frac{d\sigma_r}{dr} = \frac{1}{r}[\sigma_r(N-1) + 2cN^{1/2}] \qquad \dots B.3$$

Integration of the above equation determines the radial stress distribution in the hollow cylinder :

$$\sigma_r = \frac{1}{N-1}\left[Ar^{N+1} + 2cN^{1/2}\right] \qquad \dots B.4$$

Boundary Conditions

The boundary conditions after the initiation of failure are given by :

$$\text{At } r = a, \quad \sigma_r = P_i$$

$$\text{At } r = b, \quad \sigma_r = P_e \qquad \dots B.5$$

$$\text{At } r = R, \quad \sigma_r = \sigma_p$$

Substitution of the applicable boundary condition into Eqn.B.4 solves for the constant A :

$$A = \frac{P_i(N-1) + 2cN^{1/2}}{a^{N-1}} \qquad \ldots\ldots B.6$$

The radial stress distribution in the plastic zone is thus :

$$\sigma_r^P = \frac{1}{N-1}[P_i(N-1) + 2cN^{1/2}][\frac{r}{a}]^{N-1} - \frac{1}{N-1}[2cN^{1/2}] \qquad \ldots\ldots B.7$$

The tangential stress distribution is calculated from from the failure criterion (Eqn.B.1) :

$$\sigma_\theta^P = N\sigma_r^P + 2cN^{1/2}$$

$$\therefore \sigma_\theta^P = \left[P_i N + \frac{2cN^{3/2}}{N-1}\right]\left[\frac{r}{a}\right]^{N-1} - \frac{2cN^{1/2}}{N-1} \qquad \ldots\ldots B.8$$

The radial stress at the elastic-plastic boundary is calculated from Eqn.B.7 and the boundary condition $(\sigma_r = \sigma_p$ at r=R) :

$$\sigma_p = \left[P_i + \frac{2cN^{1/2}}{N-1}\right]\left[\frac{R}{a}\right]^{N-1} - \frac{2cN^{1/2}}{N-1} \qquad \ldots\ldots B.9$$

Stress Distribution in the Elastic Zone

The solution is similar to that derived in Appendix A (Eqn.A.11). However, the boundary conditions are modified as follows :

$$\text{At } r=R , \quad \sigma_r = \sigma_p$$

$$\text{At } r=b , \quad \sigma_r = P_e$$

Thus in Eqn.A.11, if 'a' is replaced by 'R' and 'p_i' by 'σ_p', the solution is given by :

$$\sigma_r^e = \frac{P_e b^2 - \sigma_p R^2}{b^2 - R^2} - \frac{R^2 b^2 (P_e - \sigma_p)}{r^2 (b^2 - R^2)}$$

$$\sigma_\theta^e = \frac{P_e b^2 - \sigma_p R^2}{b^2 - R^2} + \frac{R^2 b^2 (P_e - \sigma_p)}{r^2 (b^2 - R^2)} \qquad \ldots\ldots B.10$$

$$\tau_{r\theta}^e = 0$$

The stresses in the elastic zone cannot be determined until the radius of the plastic zone is found.

Radius of the Plastic Zone

It is assumed that the radial stresses are continuous at the elastic-plastic boundary. From the elastic solution it can be shown that :

$$\sigma_\theta^e + \sigma_r^e = 2\left(\frac{P_e b^2 - p_i a^2}{b^2 - a^2}\right) = 2\sigma_0 \qquad \ldots\ldots B.11$$

This equation is valid for all values of the radius in the elastic zone. Thus :

$$(\sigma_r)_{r=R} = \sigma_p = 2\sigma_0 - \sigma_\theta^\bullet \qquad \ldots B.12$$

At the plastic boundary, failure has just been reached and hence the failure criterion can be applied :

$$(\sigma_\theta)_{r=R} = \sigma_{\theta R} = N\sigma_p + 2cN^{1/2}$$

$$\therefore \sigma_p = \frac{\sigma_{\theta R} - 2cN^{1/2}}{N} \qquad \ldots B.13$$

Elimination of $\sigma_{\theta R}$ from eqns. B.12 and B.13 :

$$\sigma_p = \frac{2\sigma_0 - 2cN^{1/2}}{N+1} \qquad \ldots B.14$$

The radial stress at the boundary from the plastic solution is :

$$\sigma_p = \left[P_i + \frac{2cN^{1/2}}{N-1} \right]\left[\frac{R}{a}\right]^{N-1} - \frac{2cN^{1/2}}{N-1} \qquad \ldots B.15$$

Equating Eqns. B.14 and B.15 solves for the radius of the plastic zone :

$$R = a\left\{ \frac{2}{N+1}\left[\frac{\sigma_0(N-1) + 2cN^{1/2}}{P_i(N-1) + 2cN^{1/2}} \right] \right\}^{\frac{1}{N-1}} \qquad \ldots B.16$$

Average Radial Stress in the Cylinder

The total radial force in the cylinder is given by :

$$F_r = \int_a^b \sigma_r \, dr = \int_a^R \sigma_r^p \, dr + \int_R^b \sigma_r^e \, dr \qquad \ldots \text{B.17}$$

Now,

$$\int_a^R \sigma_r^p \, dr = \int_a^R \left[P_i \left(\frac{r}{a} \right)^{N-1} \right] dr \qquad \text{for a cohesionless material}$$

$$= P_i \left[\frac{R^N - a^N}{N a^{N-1}} \right]$$

$$\int_R^b \sigma_r^e \, dr = \int_R^b \left[\frac{P_e b^2 - \sigma_p R^2}{b^2 - R^2} \right] dr - \int_R^b \left[\frac{b^2 R^2 (P_e - \sigma_p)}{r^2 (b^2 - R^2)} \right] dr$$

$$= \frac{P_e b (b-R) - \sigma_p R (R-b)}{b + R}$$

Substituting for σ_p (Eqn.B.9) and rearranging :

$$F_r = P_i \left[\frac{R^N}{N a^{N-1}} - \frac{a}{N} + \frac{(b-R)}{(b+R)} \cdot \frac{R^N}{a^{N-1}} \right] + P_e b \frac{(b-R)}{(b+R)} \qquad \ldots \text{B.18}$$

The average radial stress in the cylinder is then defined as :

$$(\sigma_r)_{ave} = \frac{F_r}{b - a} \qquad \ldots \text{B.19}$$

APPENDIX C

A Versatile Hollow Cylinder Triaxial Device (a copy of a
paper by M.B. Dusseault, 1981)

A VERSATILE HOLLOW CYLINDER

TRIAXIAL DEVICE

by

Maurice B. Dusseault, B.Sc., Ph.D., P.Eng.
Associate Professor of Mineral Engineering
AOSTRA Chair
University of Alberta
Edmonton, Alberta
T6G 2G6

ABSTRACT

A high-pressure, thick-walled hollow cylinder test device has been perfected to explore the consequences of stress paths which are typical of pressuremeter configurations, tunnelling, or shafting in soils materials. Several features have been incorporated to facilitate data gathering, and the device is readily adaptable to K_o or standard compression and extension triaxial tests.

The device has been used on tests in artificial dense sand specimens constructed by a freezing technique, and will be used in an extensive study of the behavior of oil sands. Typical results of tests on dense Ottawa Sand (C-109) are presented.

INTRODUCTION

Greater design demands and the increasing capabilities of numerical modelling techniques in geomechanics have limited the usefulness of the more simplistic constitutive laws of soil behavior. There is a need for laboratory testing techniques which can follow stress paths similar to those which soils undergo in nature. The popularity of tests such as the direct shear and triaxial compression tests lies in their simplicity and the widespread need for strength data for limit equilibrium analysis; however, these tests do not provide data adequate for all deformation behavior analyses.

The hollow cylinder triaxial device (HCTD) has been designed and built to provide data from tests with careful stress path control. The HCTD can also serve as a model of shafting in a uniform horizontal stress field, to explore material behavior under various radial stress gradients, and (with minor modifications) for a variety of standard tests.

THE UNIVERSITY OF ALBERTA HIGH PRESSURE HOLLOW CYLINDER TRIAXIAL DEVICE

The device was designed in response to the needs of oil sands research and development. Mine-assisted in situ projects will require shafts and tunnels to gain access to deep deposits (Dusseault, 1978), and massive surface injection/production in situ projects require knowledge of complex material behavior (Imperial Oil Limited, 1978) such as fracture toughness.

The initial step in the development of the HCTD was to build a special top cap for a standard triaxial device (Figure 1). The top-hat

internal membrane is formed by molding and curing latex on an aluminum mold, and the Teflon membrane seat prevents internal membrane rupture. This low-pressure device (1.7 MPa) does not permit axial stress control or true plane strain, therefore a true HCTD was constructed. The first HCTD (which is very similar to the second described more fully below) has a maximum confining pressure (p_o) of 6.3 MPa, and has a top cap design (Figure 2) which permits axial fluid flow but provides poor sealing capability at pressures greater than 5.5 MPa. This first device has proven very useful in the evaluation of the behavior of dense sands and is still in use; however, because the oil sand displays high strengths and a curvilinear Mohr-Coulomb failure envelope (Dusseault and Morgenstern, 1979), higher outside pressures are required to carry a hollow-cylinder test to the state of plane strain cylinder collapse.

The second HCTD (Figures 3 and 4) is a high-pressure thick-walled cylinder testing apparatus with the following capabilities:

(1) high pressure range (p_o = 20 MPa with FS of about 1.5);

(2) sample size of 101.6 mm outside diameter, 50.8 mm inside diameter, 200 to 240 mm in length (depending on membranes available);

(3) independent pressure control and volume change measurements on inside, outside and pore liquids; and

(4) a 101.6 mm ram with a low-friction seal and Teflon ram guide to allow plane axial strain with passive stress measurement, independent axial stress control (K_o control), or specified strain rate with stress measurement.

To increase the versatility of the HCTD the following features were included in the design:

(1) the apparatus is built of standard available corrosionless material and O-ring seals;

(2) the cell base, body, and top can be used directly for other sample inside and outside diameters which require only minor redesign (cap and pedestal, ram guide, ram, or membranes);

(3) a ram guide and ram for easy conversion to conventional triaxial compression tests is available; and

(4) sufficient interior clearance has been provided for heating and cooling coils, or for mounting of diametral strain measurement devices.

This HCTD is equipped with 17.5 MPa working pressure no-volume-change valves and 3.175 mm brass tubing; a 44.5 kN axial load cell ($\overline{\sigma}_z$); a 14 MPa fluid pressure transducer; two high-pressure (14 MPa) systems with two in-line 14 MPa volume change indicators allowing pressure control of p_o, p_i, or monitoring of ΔV_o, ΔV_i; and two low-pressure regulator-controlled pressure systems with individual volume change indicators for the pore fluid or for lower pressures (< 1.4 MPa) on p_i or p_o. For testing, the HCTD is mounted in an extremely stiff plane strain test frame, or in a 90 kN capacity infinitely variable strain rate test frame. The cell has been tested to 17 MPa and has been used in tests on dense sands to confining stresses (p_o) of 12.6 MPa. Tests with p_o less than about 6 MPa use latex exterior membranes (1.5 mm thick) molded in our laboratory; higher pressures require Neoprene exterior membranes (3 mm thick). High-pressure membranes require

special molds and high-pressure and high-temperature injection of the Neoprene. The molds have been made in the University of Alberta and Neoprene injection is performed commercially.

The fully assembled fluid-filled HCTD is heavy and requires a small crane for handling. Individual components can be lifted by one person, but assembly is simplified if a second person is available for about 15 minutes.

SAMPLE ASSEMBLY AND MOUNTING

Specimens of significant cohesive strength can be prepared and mounted directly in the HCTD, but fabricated specimens of dense sand or oil sand specimens require special preparation techniques.

Ordinary specimens are trimmed to 101.6 mm external diameter, placed in a split retaining cylinder and cored with a 50.8 mm diamond coring device. Oil sand specimens must be trimmed to diameter in a lathe by use of tungsten-carbide tipped bits (Dusseault and Morgenstern, 1978) in a cold room at temperatures of -25°C to prevent sample deterioration. The core drilling must be carried out with the oil sand at very low temperatures and heat from the coring process must not be allowed to build up.

Because of the top hat design of the inner and outer membranes, a special jig (Figure 5) has been built to allow thick-walled sand cylinders to be assembled under water directly on a vibratory (60 Hz) table. Shock loading, static top loads, and rodding during assembly are aids to densification. A porous stone is placed on the top of the. specimen, and a perforated lucite top disc is placed on the stone. The

bottom of the jig is placed in a cold bath (-18°C) in a cold room (-2°C) and a static load of 250 N is placed on the Lucite top disc. One-dimensional freezing takes place with excess fluid expelled through the top. When frozen, the jig is disassembled (special techniques are required) and the sample is mounted in the HCTD in the cold room. Special methods (e.g. back-pressures and pore suction) are necessary during initial flooding of the cell and the internal membrane to prevent collapse of the dense sand cylinder.

Many small steps have been omitted from this description. A comprehensive paper on sample and test techniques is being prepared.

CAPABILITIES OF THE UNIVERSITY OF ALBERTA HCTD

A variety of test types can be pursued using the HCTD. The major stress paths and the ones of greatest interest deserve particular mention.

Radial Strain Tests

For plane strain cylinder collapse (PSCC), three basic configurations are possible; p_i, p_0 or u may be monotonically changed until failure occurs.

(1) p_0 increasing; p_i, u constant. A sample is stabilized at the stress conditions $p_0 = p_i > u$, then p_0 is increased to failure; ΔV_i, ΔV_u, ϵ_z, $\bar{\sigma}_z$ are measured.

(2) p_i decreasing; p_0, u constant. A sample is stabilized at the stress conditions $p_0 = p_i \gg u$, then p_i is decreased to failure; ΔV_0, ΔV_u, ϵ_z, $\bar{\sigma}_z$ are measured.

(3) u increasing; p_o, p_i constant. A sample is stabilized at the
stress conditions p_o > p_i > u, then p_o and p_i are held
constant while u is increased to failure; ΔV_o, ΔV_i, ϵ_z, $\bar{\sigma}_z$ are
measured.

These three test configurations are statically determinate
(Timoshenko and Goodier, 1951), and therefore stresses may be calculated
directly by specifying a failure criterion only (Wu et al., 1963).

For plane strain cylinder burst (PSCB) conditions, statically
determinate tests may be performed in the HCTD which are directly
analagous to the PSCC tests. Note that u can at no time be greater than
p_o or p_i, but that p_i is greater than p_o during PSCB conditions.
Because failure is catastrophic in PSCC and PSCB tests, constant vigi-
lance is required near failure to shut down pressure lines. All tests
can be performed in an undrained mode with measurement of pore pressure
rather than pore volume change.

Axial Strain-Controlled and Stress-Controlled Tests

Test configurations where failure is approached by straining
in an axial direction are in general not statically determinate (Wu et
al., 1963). Since p_o, p_i, and u may be kept constant, complete volume
change data may be collected during testing. Normal stress gradients
(p_o > p_i) or reverse gradients (p_i > p_o) may be used across the radius
of the specimen. Because the ram is the same diameter as the specimen,
compression or extension tests may be performed.

The introduction of a servo-mechanism or a constant-stress
load device along the specimen axis will permit stress control or creep

testing of thick-walled hollow cylinders. A stress-control feature is necessary if the device is to be used as a shaft-modelling apparatus.

Compressibility Tests

Because the ram is the same diameter as the cylindrical specimen, a no-axial-strain compressibility test can be performed. The basic triaxial cell yields an all-round compressibility ($\Delta\sigma_1 = \Delta\sigma_2 = \Delta\sigma_3$); the oedometer provides the condition $\Delta\sigma_z = \Delta\sigma_1 > (\Delta\sigma_2 = \Delta\sigma_3)$ during loading; and the HCTD provides the condition $(\Delta\sigma_1 = \Delta\sigma_2) > (\Delta\sigma_3 = \Delta\sigma_z)$ during loading with no axial yield providing that $p_i = p_0 > u$ for all stress increments. For the plane axial strain HCTD compressibility test, ΔV_u, ε_z and $\overline{\sigma}_z$ are measured after each stress step. Compressibility tests may also be performed at a constant radial stress ratio; i.e. $(p_0 - u)/(p_i - u)$ as a positive constant less than the failure ratio. More complex stress paths are readily envisioned.

TYPICAL TEST DATA

Cyclic plane axial strain compressibility tests were performed on a dense Ottawa Sand. To confirm the assumption of plane strain, axial displacement was measured as well as axial load. A constant pore pressure permitted accurate determination of pore fluid volume changes, and p_0 was identical to p_i for all stress increments. The data (Figure 6) indicate small axial strains (some compliance must exist because of the load cell and confinement frame); therefore, plane strain con-

ditions are approached. The coefficients of volume compressibility are presented in Table 1.

Two types of cylinder collapse tests on dense Ottawa Sand have been performed: PSCC-Type 1 and PSCC-Type 2. Figures 7 and 8 show data generated during typical tests. Volume changes of pore fluid are expressed as percentages of pore volume and may be converted directly to total volume change by multiplying by the porosity. These two tests correspond to increasing J1 or decreasing J1, and the volume change behavior of the specimens is therefore quite different. To ensure that the specimens were very similar, cyclic consolidation (compressibility tests) to 12.7 MPa was performed on both specimens until elastic (recoverable) response was approximated. Further comments and interpretation of the test data are reserved for a future publication on the strength and volume change behavior of oil sand and very dense Ottawa Sand.

CONCLUDING REMARKS

The hollow cylinder triaxial concept is not original (Kirkpatrick, 1957; Haythornthwaite, 1960; Wu et al., 1963; Handin et al., 1967; Jaeger and Cook, 1969); however, the University of Alberta high-pressure HCTD incorporates a number of new features permitting a great variety of test configurations including a simple conversion to standard triaxial testing. The HCTD was designed primarily for plane strain ($\epsilon_z = 0$), high-pressure, thick-walled cylinder tests of the collapse or burst type, and for cyclic compressibility tests. Other test configuations with different materials are being planned.

ACKNOWLEDGEMENTS

LIST OF SYMBOLS AND ABBREVIATIONS

Δ	change (in volume, pressure or stress)
P_o, P_i	outside and inside pressures
u	pore pressure
$\bar{\sigma}_z$, σ_1, σ_2, σ_3	mean axial stress, major, intermediate, and minor principal stresses
$J1$	$\dfrac{\sigma_1 + \sigma_2 + \sigma_3}{3}$ - first stress invariant
K_o	principal stress ratio
V_u, V_o, V_i	pore, outside, and inside volumes
ϵ_z	axial strain
HCTD	hollow cylinder triaxial device
PSCC; PSCB	plane-strain cylinder collapse; cylinder burst

REFERENCES

Dusseault, M.B. (Editor), 1978. AOSTRA Seminar on Underground Excavation in Oil Sands. University of Alberta, Edmonton, Collection of 14 papers (Available through Alberta Oil Sands Information Centre, Edmonton, Alberta).

Dusseault, M.B. and Morgenstern, N.R., 1978. Sampling and testing of Athabasca Oil Sands for stability studies. In The Oil Sands

of Canada-Venezuela, 1977. Editors D.A. Redford and
A.G. Winestock, CIM Special Volume 17, pp. 260-269.

Dusseault, M.B. and Morgenstern, N.R., 1979. Locked sands. Quarterly
Journal of Engineering Geology, V. 12, pp. 117-131.

Handin, J., Heard, H.C. and Magouirk, J.N., 1967. Effects of the
intermediate principal stress on the failure of limestone,
dolomite, and glass at different temperatures and strain rates.
Journal of Geophysical Research, V. 72, pp. 611-640.

Haythornthwaite, R.M., 1960. Stress and strain in soils; In Plasticity.
Proceedings of the Second Symposium on Naval Structural
Mechanics, Rhode Island; Pergamon Press, pp. 185-193.

Imperial Oil Limited, 1978. The Cold Lake Project. A report to the
Energy Resources Conservation Board, Calgary, Alberta.

Jaeger, J.C. and Cook, N.G.W., 1969. Fundamentals of Rock Mechanics.
Chapman and Hall Ltd. and Science Paperbacks, London, 515 pp.

Kirkpatrick, W.M., 1957. The condition of failure for sands. Pro-
ceedings of the 4th International Conference on Soils Mechanics,
Volume 1, pp. 172-178.

Timoshenko, S. and Goodier, N., 1951. Theory of Elasticity, McGraw-
Hill, New York.

Wu, T.H., Loh, A.K. and Malvern, L.E., 1963. Study of failure envelope
of soils. Journal of the Soil Mechanics and Foundations
Division, ASCE, SM1, pp. 145-181.

TABLE 1

DRAINED HOLLOW CYLINDER COMPRESSIBILITY
TEST DATA $(\Delta p_i = \Delta p_o)$

$p_o (p_i)$ kPa	$\Delta \sigma_z$ kPa	$\Delta \epsilon_z$ $\times 10^{-3}$	$\dfrac{\Delta V_u}{V}$ $\times 10^{-3}$	$m_v (= \Delta p \dfrac{\Delta V_u}{V})$ $kPa^{-1} \times 10^{-6}$
696 → 1390	+268	-0.69	-3.38	4.87
1390 → 2774	+584	-0.37	-3.22	2.33
2774 → 4143	+596	+0.61	-2.09	1.53
4143 → 5650	+673	+0.95	-1.85	1.23
5650 → 6926	+513	+1.01	-1.61	1.26
6926 → 8316	+563	+1.01	-1.20	0.86
8316 → 6929	-494	-0.89	+0.72	0.52
6929 → 4150	-663	-2.31	+2.09	0.75
4150 → 1396	-1240	-0.62	+4.82	1.75
1396 → 4139	+939	+0.41	-3.86	1.41
4139 → 6926	+881	+2.26	-2.81	1.01
6926 → 8319	+543	+1.20	-1.21	0.87
8319 → 6920	-431	-0.89	+0.64	0.52
6920 → 4144	-620	-2.34	+2.09	0.75
4144 → 1392	-1228	-0.69	+4.90	1.78
1392 → 4149	+945	+0.53	-3.94	1.43
4149 → 6922	+865	+2.17	-2.81	1.01
6922 → 8328	+477	+1.31	-1.13	0.81

Note: Since all strains are known, and assuming elastic isotropic behavior

$$\frac{\Delta V}{V} = \epsilon_1 + \epsilon_2 + \epsilon_3, \quad \text{and} \quad \epsilon_2 = \epsilon_3$$

$$E = \text{Young's Modulus} = \frac{2\Delta p^2 - \Delta p \Delta \sigma_z - \Delta \sigma_z^2}{\Delta p \dfrac{\Delta V}{V} - \Delta \epsilon_z (\Delta \sigma_z + 2\Delta p)}$$

$$\text{and } \nu = \text{Poisson's Ratio} = \frac{\Delta \sigma_z \dfrac{\Delta V}{V} - \Delta \epsilon_z (\Delta \sigma_z + 2\Delta p)}{2\Delta p \dfrac{\Delta V}{V} - 2\Delta \epsilon_z (\Delta \sigma_z + 2\Delta p)}$$
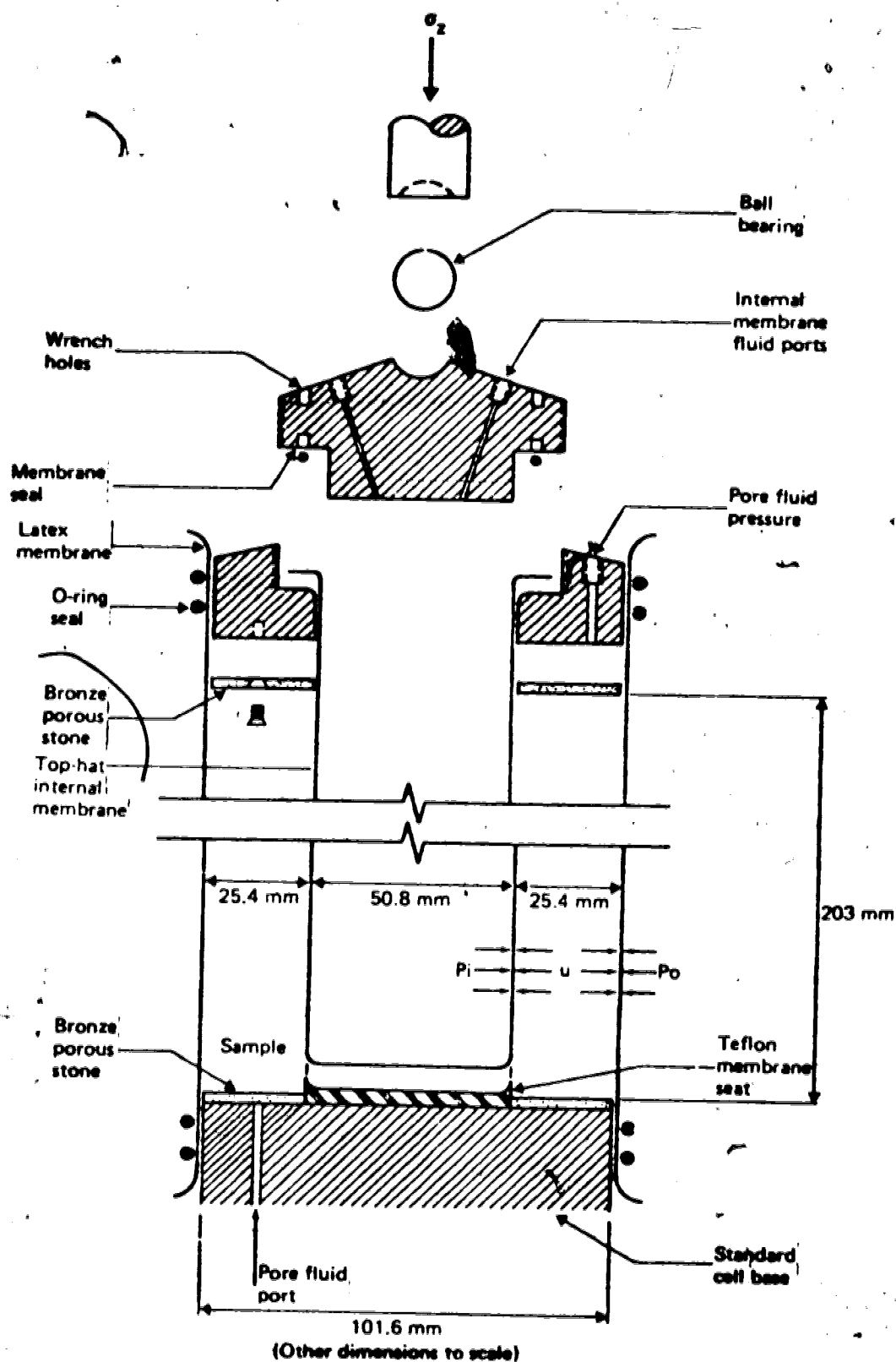
Figure 1. Top-Cap and Top-Hat Membrane for a
Conventional 101.6 mm Triaxial Cell.
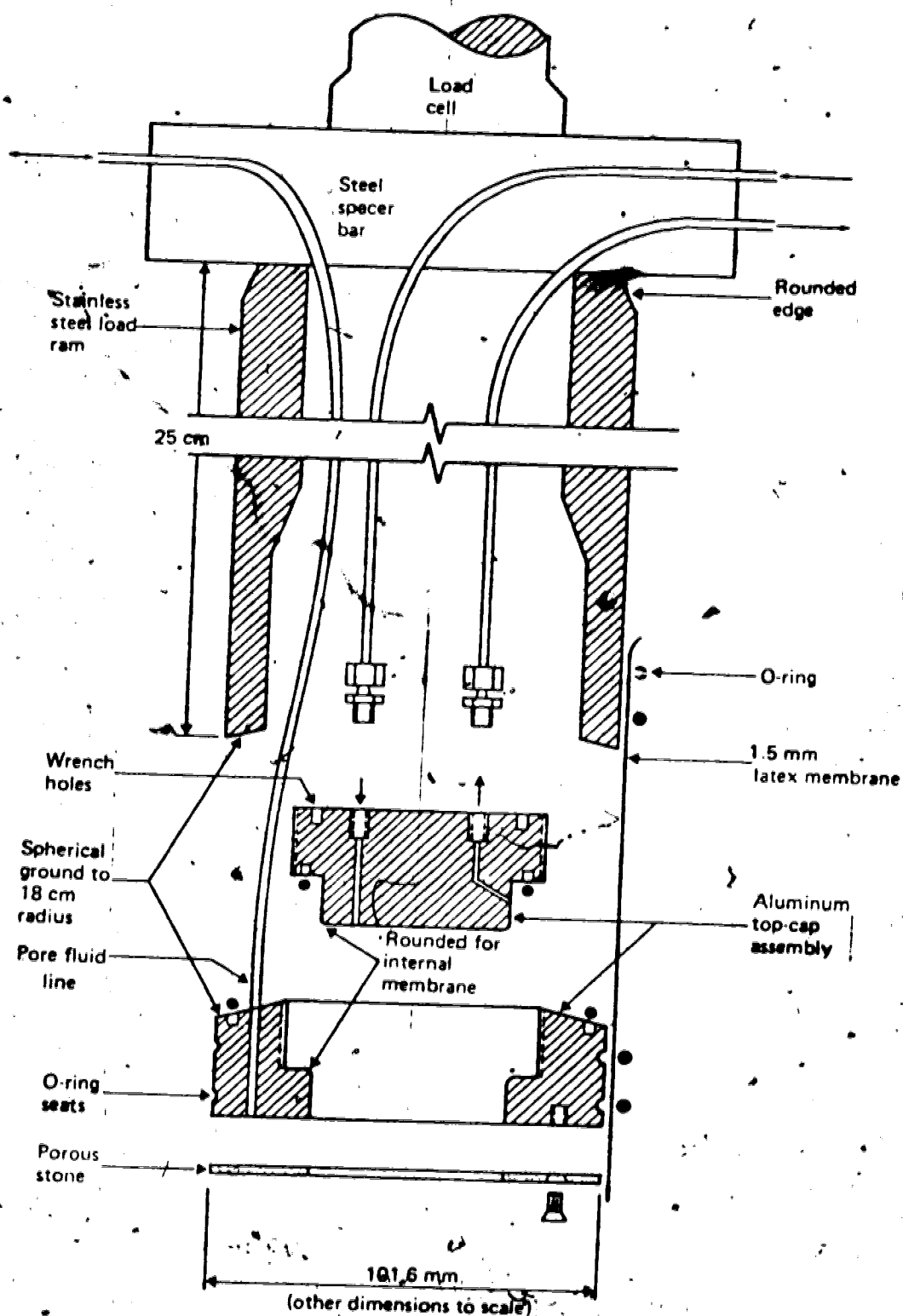
Figure 2. Top-Cap and Ram Assembly for 6.3 MPa Hollow Cylinder Triaxial Apparatus
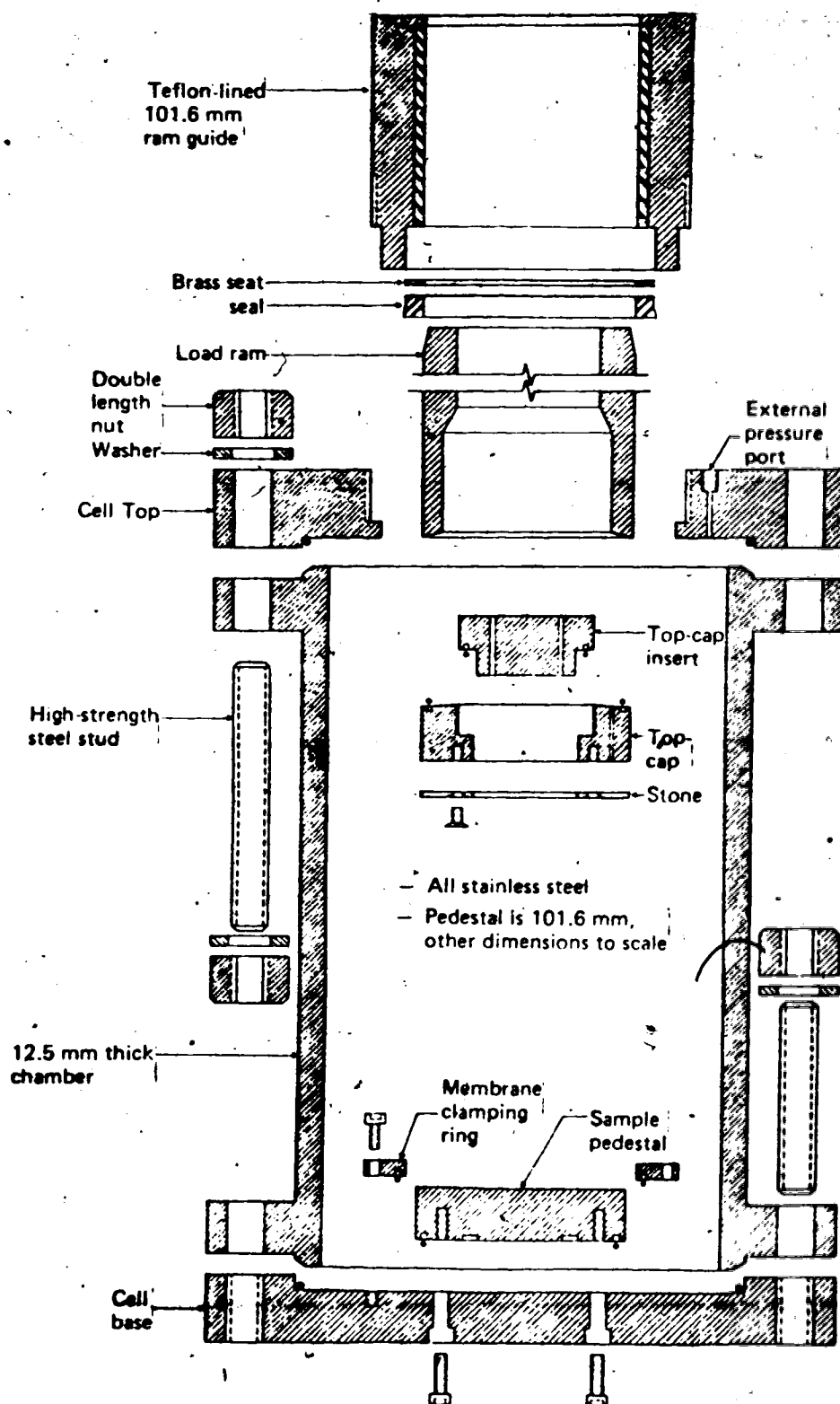
Figure 3. Exploded Sectional View of the High Pressure Triaxial Cell.
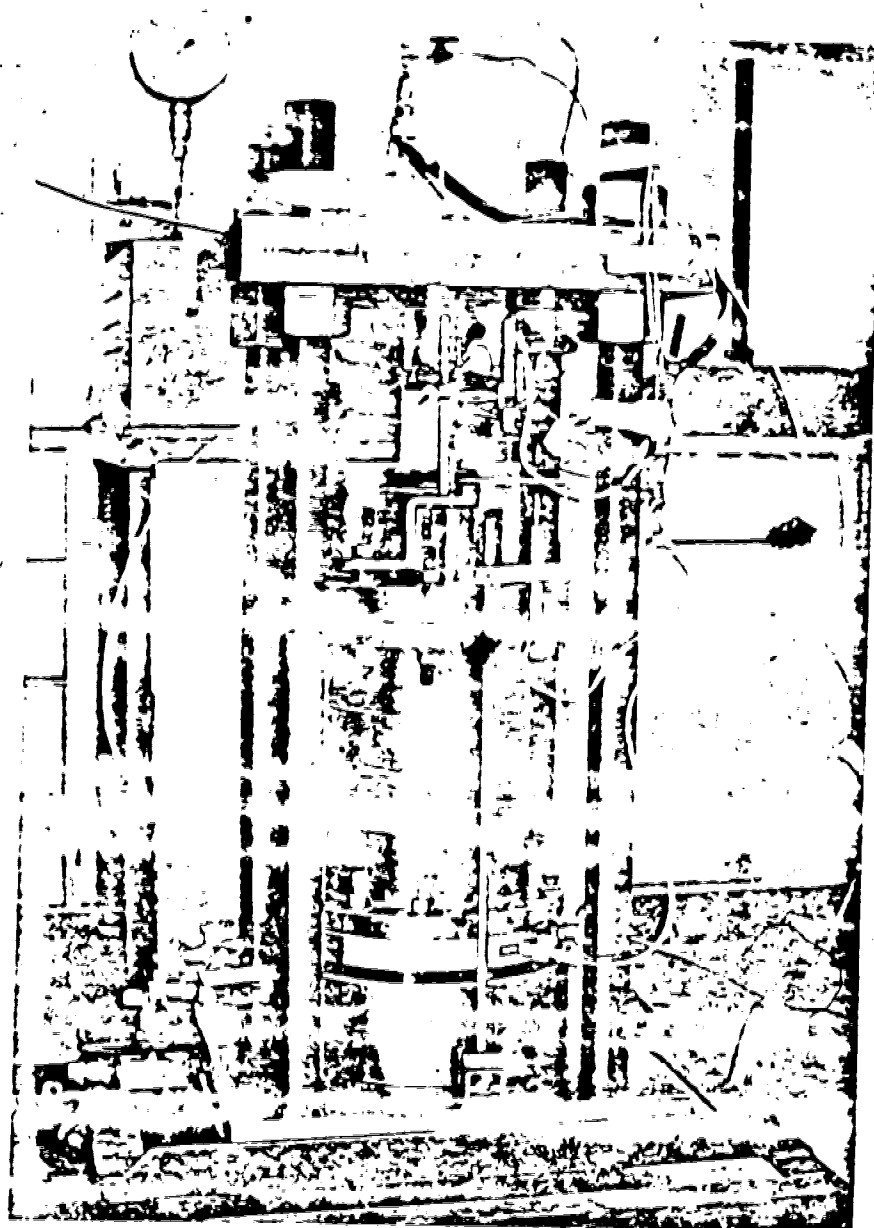
Figure 4:   Hollow Cylinder Triaxial Cell Fully Instrumented
            in a Plane Strain Frame
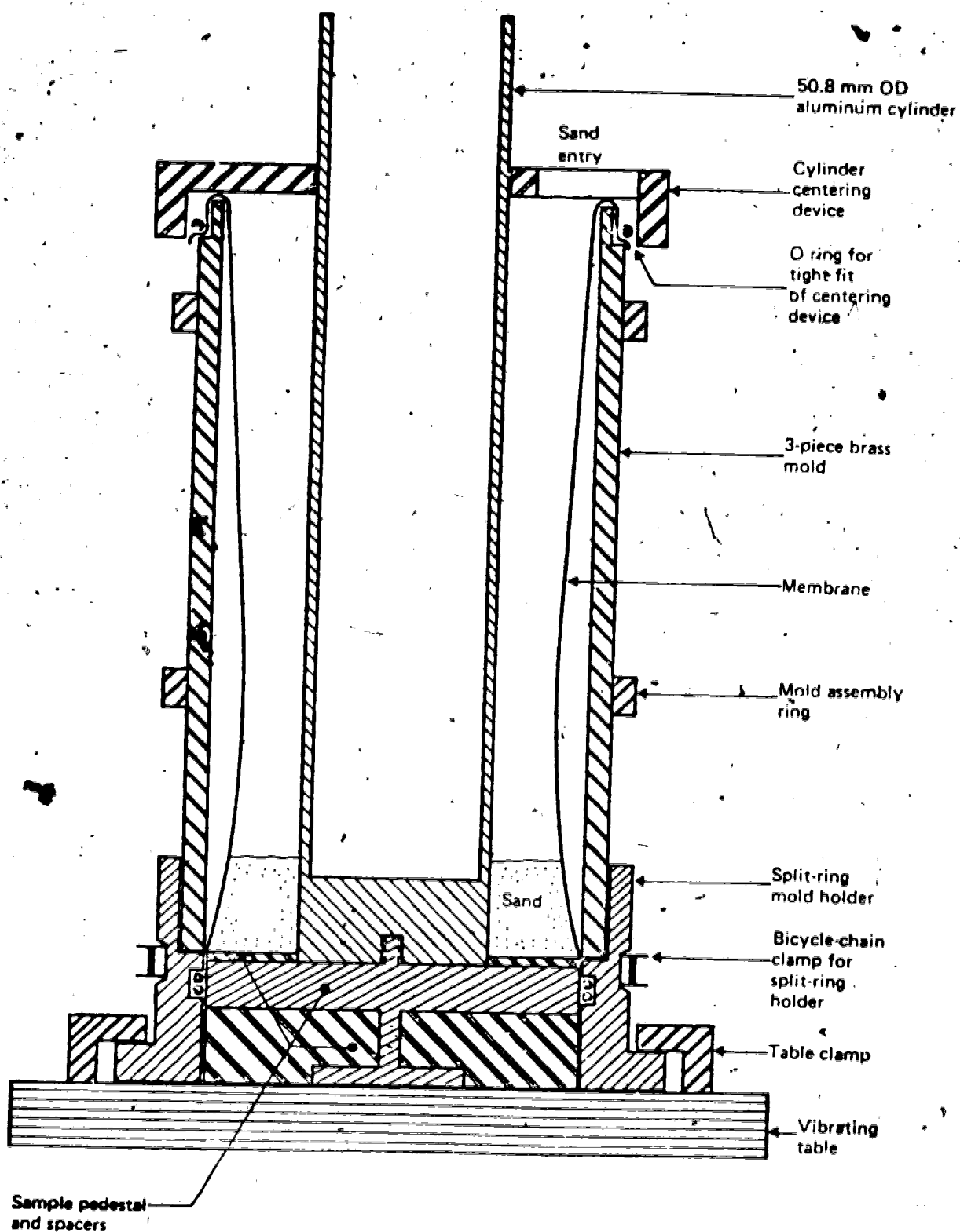
Figure 5. Mold for Hollow Cylinder Sample Assembly

Labels in figure:
- 50.8 mm OD aluminum cylinder
- Sand entry
- Cylinder centering device
- O ring for tight fit of centering device
- 3-piece brass mold
- Membrane
- Mold assembly ring
- Sand
- Split-ring mold holder
- Bicycle-chain clamp for split-ring holder
- Table clamp
- Vibrating table
- Sample pedestal and spacers
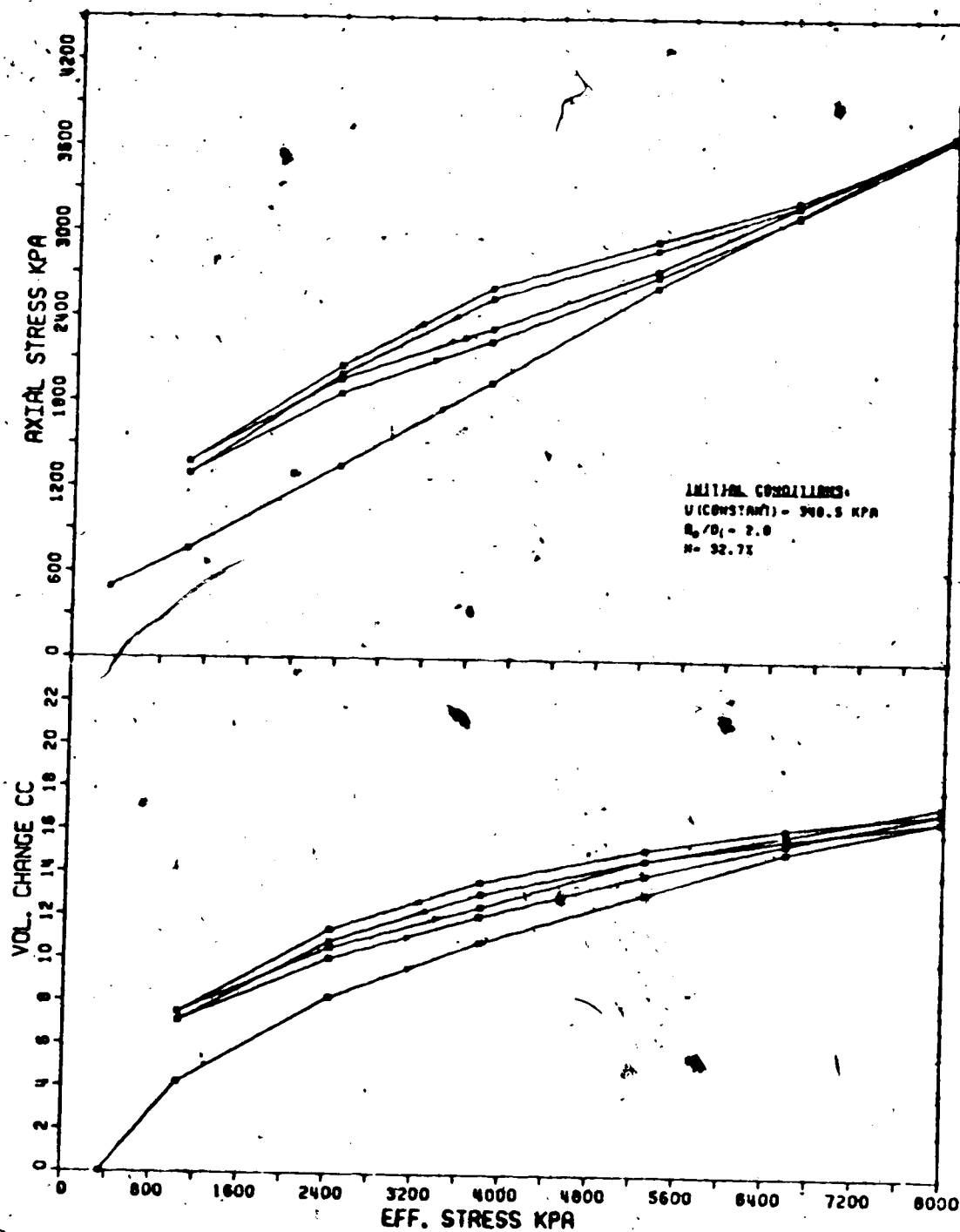
FIGURE6: CYCLIC PLANE AXIAL STRAIN COMPRESSIBILITY DATA (PO=PI)
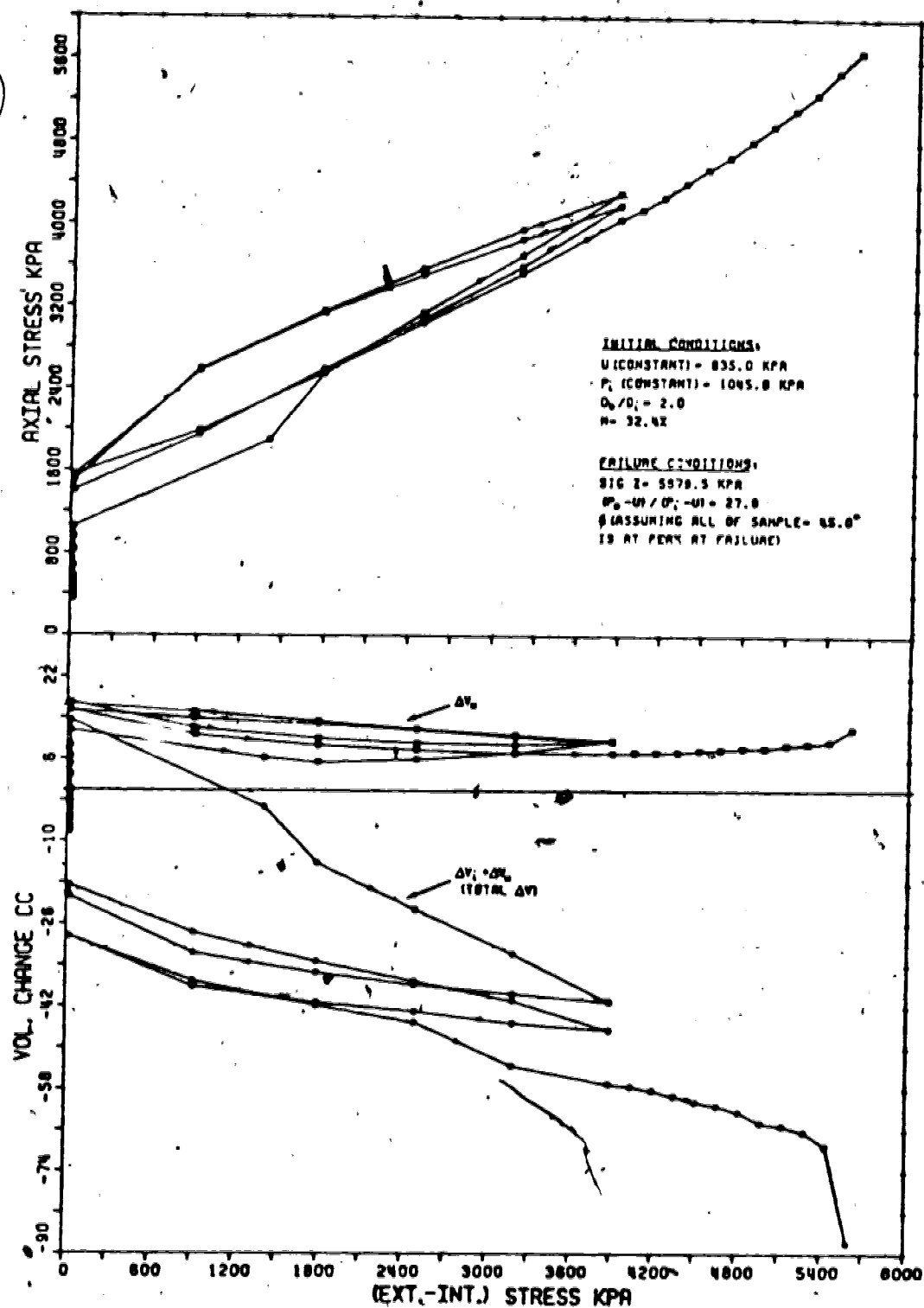
FIGURE7: PLANE STRAIN CYLINDER COLLAPSE BY INCREASE OF EXTERNAL PRESSURE

Computation of the strains in the hollow cylinder test (a copy of pp.42-46 of a thesis by D.C. Procter, 1957)

$\sigma_2 = \sigma_T$ should vary; the size of the variation will be an indication of the size of the distribution error.

b) The size of the distribution error can also be assessed by comparing the peak strength values of tests conducted with $\sigma_2 = \sigma_R$ with equivalent results from tests with $\sigma_2 = \sigma_T$, for the same value of N and the same size of specimen.

c) The overall error in stress analysis for both sizes of cylinder can be estimated by comparing plane strain peak strengths from both $\sigma_2 = \sigma_T$ and $\sigma_2 = \sigma_R$ tests with the equivalent strength obtained in the conventional plane strain apparatus.

Using an approach of this nature it is possible to obtain some indication of the size of the errors which are likely to affect the results.

Finally peak strength results obtained from this mean stress analysis are compared to the same results analysed by the method suggested by Haythornthwaite (1966). This serves as a further check on the accuracy of the analysis, and is discussed in section 3:4:2.

3:3 Mean Principal Strain Computation

It is necessary to compute from measured displacements and volume changes the principal strain increments during an imposed increment in the axial direction. Since the calculated displacements can only be mean values, it is clear that only mean strains can be computed with any accuracy. It is assumed that the principal stress and strain directions are mutually coincident with the axes of specimen symmetry. It is noted that this computation, while being relatively

simple, is nevertheless tedious, and consequently the following analysis is presented in a form which can be easily programmed for a digital computer.

It is required to investigate the mean axial, radial and tangential principal strains ϵ_A, ϵ_R and ϵ_T and also the volumetric strain v, by considering the changes measured in the specimen length L, specimen volume Vs, and the inner bore volume Vb.

For the sake of continuity it is helpful to state a notation convention:

Suffix ( )i — indicates the value of a quantity after the ith increment, i.e. (L)i.

Suffix ( )j — indicates the value of a quantity after the jth increment, i.e. (L)j, and $j = i + 1$.

Suffix ( )o — indicates the initial values of a quantity, i.e. (L)o.

Prefix d — indicates the increment of principal strain occurring during the jth increment, i.e. $d\epsilon_A$.

Prefix D — indicates the total change which has occurred in a quantity after a specified increment, i.e. $(DL)_i$.

Compressive, natural strains are considered positive, and the small strain approximation is assumed to apply:

$$dv = d\epsilon_A + d\epsilon_R + d\epsilon_T \qquad (3:30)$$

The mean radial strain must now be defined. It is, however, more convenient to define the mean strain increment rather than the total

mean strain, whence:

$$d\epsilon_R = \frac{\text{mean change of specimen wall thickness during } i^{th} \text{ increment}}{\text{mean wall thickness during } j^{th} \text{ increment.}}$$

Hence if y is the mean wall thickness:

$$d\epsilon_R = \left[\frac{(y)i - (y)j}{(y)i + (y)j}\right] \times 2 \qquad\qquad (3:31)$$

Clearly $y = b - c$, where b and c are the outer and inner radii of the specimen

$$\text{Similarly } d\epsilon_A = \left[\frac{(L)i - (L)j}{(L)i + (L)j}\right] \times 2 \qquad\qquad (3:32)$$

It now remains to calculate the progressive values of L, b and c. This approach is a convenient one since these values are also required for mean stress calculations (section 3:2).

If the total volume of specimen and bore is V_Z, where $V_Z = Vb + Vs$, it follows that:

$$(L)_i = (L)_0 - (DL)_i \qquad\qquad (3:33)$$

$$(b)_i = \sqrt{\left[\frac{(V_Z)_i}{\pi (L)_i}\right]} \qquad\qquad (3:34)$$

$$(c)_i = \sqrt{\left[\frac{(Vb)_i}{\pi (L)_i}\right]} \qquad\qquad (3:35)$$

and similarly for (L)j, (b)j and (c)j.

Hence from equations 3:32 and 3:33

$$d\epsilon_A = \left[\frac{(DL)j - (DL)i}{2(L)_0 - (DL)j - (DL)i}\right] \times 2 \qquad\qquad (3:36)$$

and from equation 3:31:

$$d\epsilon_R = \left[\frac{\left((b)_i - (b)_j\right) - \left((c)_i - (c)_j\right)}{\left((b)_i + (b)_j\right) - \left((c)_i + (c)_j\right)} \right] \times 2 \qquad (3:37)$$

where, from equation 3:34

$$(b)_i = \sqrt{\left[\frac{(vs)_0 + (vb)_0 - (Dvs)_i - (Dvb)_i}{\pi((L)_0 - (DL)_i)} \right]}$$

$$(b)_j = \sqrt{\left[\frac{(vs)_0 + (vb)_0 - (Dvs)_j - (Dvb)_j}{\pi((L)_0 - (DL)_j)} \right]}$$

and from equation 3:35

$$(c)_i = \sqrt{\left[\frac{(vb)_0 - (Dvb)_i}{\pi((L)_0 - (DL)_i)} \right]}$$

$$(c)_j = \sqrt{\left[\frac{(vb)_0 - (Dvb)_j}{\pi((L)_0 - (DL)_j)} \right]}$$

Also from equation 3:30

$$d\epsilon_T = dv - d\epsilon_A - d\epsilon_R \qquad (3:38)$$

where

$$dv = \left[\frac{(Dvs)_j - (Dvs)_i}{2(vs)_0 - (Dvs)_j - (Dvs)_i} \right] \times 2 \qquad (3:39)$$

Finally total strain calculations can be made on a cumulative basis:

$$(\epsilon_R)_j = \sum_1^j (d\epsilon_R) \qquad (3:40)$$

$$(\epsilon_A)_j = \sum_1^j (d\epsilon_A) \qquad (3:41)$$

$$(\epsilon_T)_j = \sum_1^j (d\epsilon_T) \qquad (3:42)$$

$$(v)_j = \sum_1^j (dv) \qquad (3:43)$$

From equations 3:36 to 3:43 inclusive all strain quantities required

for analysis can be obtained.

3:4 Alternative Failure Criteria for Soil

3:4:1 Conventional Approach

. The philosophy concerning the conception of various failure criteria is well-known, and need only be briefly dealt with.

A general stress state σ_1, σ_2, σ_3 may be represented in 3-dimensional stress space by two vector components, the hydrostatic stress component along the hydrostatic axis ($\sigma_1 = \sigma_2 = \sigma_3$) and the deviatoric stress component, being situated in the octahedral plane perpendicular to the hydrostatic axis and containing the limit of the hydrostatic stress component (Fig. 3c). The locus of all such stress states which are situated in the same octahedral plane and at which failure of a particular soil occurs, is a failure envelope bounding all possible stress states that may occur for that soil in that plane. Since the stress level at yield is dependent on the mean stress applied to the soil, the size of the envelope is directly dependent on the hydrostatic stress component associated with the octahedral plane containing the envelope. Consequently generating lines, meeting at the space origin for the case of cohesionless materials, may be drawn through the envelopes on all octahedral planes to form a conical shaped failure surface. These surfaces are described in general by a governing mathematical equation relating σ_1, σ_2, σ_3 and ϕ, and it is the form of the equation which determines the resulting shape of the surface.

The three failure criteria normally considered in the case of soil are the Mohr-Coulomb, the Extended Tresca and the Extended Von Mises,

APPENDIX E

Calibration of the Hollow Cylinder Triaxial Device

The HCTD has to be calibrated for volume change correction and ram friction. The volume changes that are measured are subjected to three sources of error :   .

1. expansion of the cell and pressure lines
2. compression of the water in the cell, lines and measuring systems
3. air going into solution

The axial load on the sample is measured outside the cell, hence the vertical load acting at the top of the sample has to be corrected for the friction developed between the ram and the cell.

Calibration of the Bore Volume Change Apparatus

The sample used for calibration purposes is a hollow cylinder aluminum one of similar dimensions to that of a test specimen. The sample is assembled in an identical manner as previously described for the soil samples, with the same system of, membranes, O-rings and clamps.

The HCTD was assembled in the plane-strain frame and the bore pressure applied by means of the nitrogen pressure system. The bore pressure was increased in increments of approximately 1.4 MPa and the volume changes recorded. Volume changes due to the deformation of the sample is small and were ignored. The results of the calibration are shown in Figure C.1.

Calibration of the Cell Volume Change Apparatus
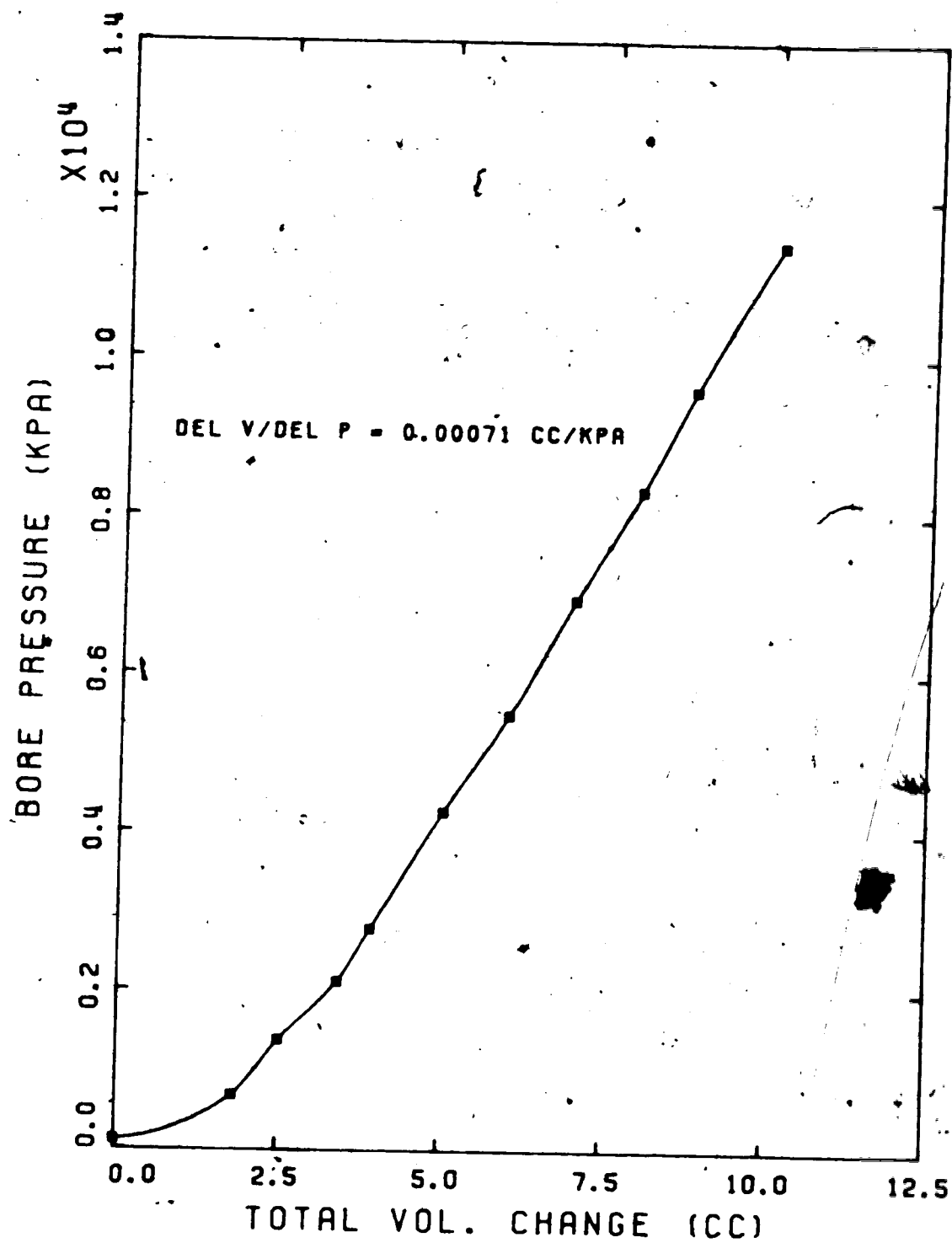
Figure E.1 Bore Volume Change Correction Curve

The cell pressure was applied in a similar procedure as described above. At the end of each increment, the bore pressure was increased to approximately the same pressure in order to minimize the sample deformation. Volume changes due to sample deformation were again ignored. The results of this calibration are shown in Figure C.2.

Calibration for Ram Friction

This calibration provided several difficulties. Two load cells would be required to measure the ram friction, one on top of the sample and the other on the outside of the cell. The load cell inside the cell would have had to be designed to withstand cell pressures of up to 14 MPa and would also have to be specially designed as an annular ring in order to accomodate the internal membrane set up. It was thus decided to find an alternate method of measuring the ram friction.

A machined aluminum plate, 4.05 in. in diameter, was attached to the loading cap and initially supported on an aluminum block sitting on the base of the cell. Upon application of cell pressure, the loading cap and ram would be activated and an external axial load could be measured on the load cell. This method is equivalent to actual test loading conditions but does not allow the investigation of ram friction dependency on cell pressure.

The aluminum plate is attached to the loading cap by clamping a small rubber membrane to the plate and cap and

DEL V/DEL P = 0.00882 CC/KPA
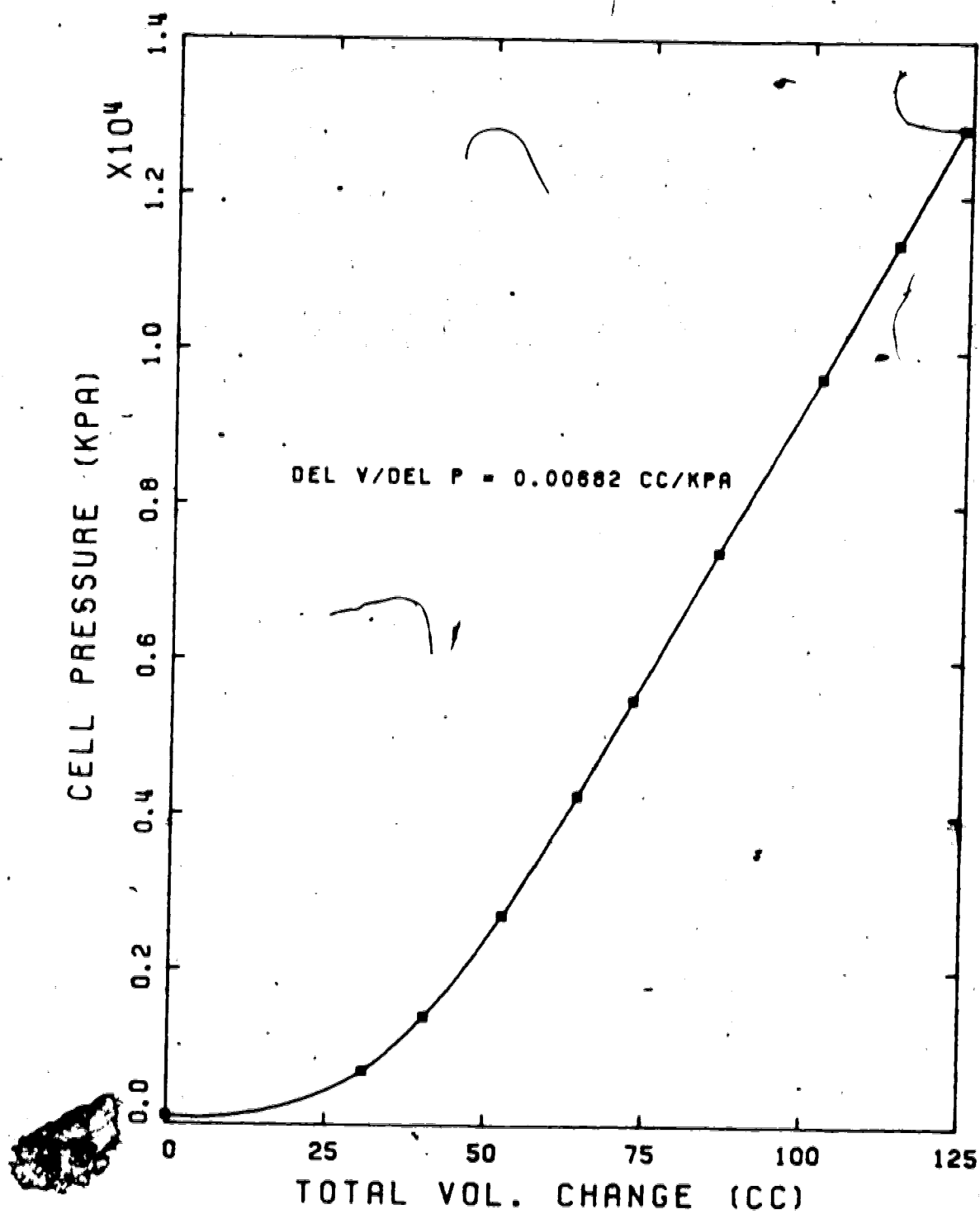
Figure E.2 Cell Volume Change Correction Curve

sealing the membrane at the ram by means of O-rings and clamps. The cell pressure is then applied and measured on a transducer. The load cell is read at each pressure increment. Results of the test are shown in Figure C.3. This calibration curve shows that ram friction is almost independent of cell pressure.

Correction for Membrane Effects

The effect of membrane thickness on the strength of the samples has been ignored. Bishop and Henkel (1976) have shown this effect to be small for 1.5 in. diameter samples. They also show that for undrained tests no hoop tension is induced in the membrane and that the correction is applied to the axial stresses and not the lateral pressure. For 4 in. diameter samples, the correction is strain dependent and hence zero for plane-strain conditions in the vertical direction (as is the case in this testing program).

$$P_i = 1.21 + 1.017P_e \text{ KN}$$
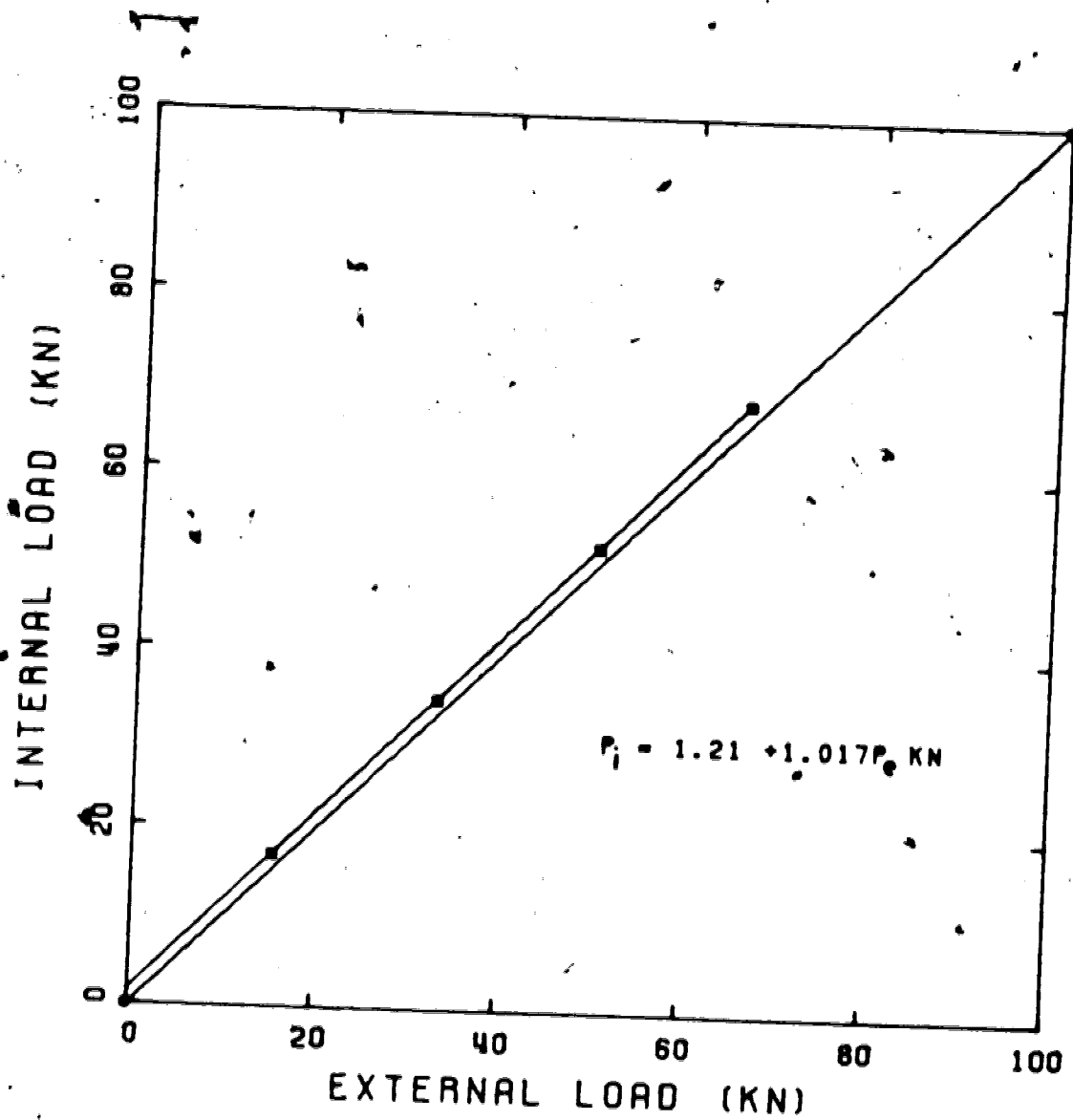
Figure E.3 Ram Friction Calibration Curve

APPENDIX F

Problems encountered with the laboratory equipment

The high pressures used in the laboratory program required consideration to be given to all sources of error resulting from leaks in the apparatus, membranes and lines. Poulos (1964) discusses various sources of leaks and these are summarized below.

Flow of Fluid through Membranes

Flow through membranes can be caused by hydraulic pressure gradients, vapour pressure and mole fraction gradients. The rate of flow of water is directly proportional to the hydraulic pressure difference. Soaking of membranes in silicone oil prior to the test resulted in equal or higher permeabilities than those soaked in water.

This problem of flow through membranes is of more concern in long term tests than short term tests. The duration of tests in this program is less than 5 hours and this source of leaks is of little significance.

Leakage past Bindings

This source of error is again of more importance for long term tests. Smooth pedestals with a single O-ring on each side of the porous disc resulted in leakage of approximately 0.1 ml/day, which is negligible for short term tests.

The membrane clamping system was modified in this program to reduce the number of bindings and O-rings required. The author was concerned more with large leaks

developing (due to puncturing of membranes or poor seals)
than these small leaks observed by Poulos.

Leakage from Valves and Fittings

Poulos showed that Klinger valves are generally
unsuitable for any type of laboratory work. The Klinger
valves that were in use with the pressure systems used by
this author were observed to leak noticeably at relatively
low pressures and were thus replaced by circle seal valves.
These valves showed no visible signs of leakage. The
majority of valves used in the plumbing systems are Swagelok
no-volume change valves and these have also performed
satisfactory.

Leaks through valves and fittings will be critical in
long term tests as small leaks will not be noticeable due to
rapid evaporation of the fluid. However, careful
calibration of the volume change apparatus can accomodate
all these types of leaks. The apparatus in use in this
program showed no measureable volume changes occuring over a
24 hour period.

Rupturing of Membranes

This was the biggest problem faced by the author during
his laboratory program. At pressures exceeding 5.6 MPa, the
internal membrane tends to pinch between the top of the
sample and the load cap or porous stone. A thin Teflon ring
placed over such joints proved partially successful, but it

was found that the membrane developed small holes in the
vicinity of this ring. The teflon ring was replaced by a
Neoprene rubber ring which has performed satisfactory thus
far.

The internal membrane has been the dominating factor in
the many tests that have had to be abandoned due to
development of large leaks. The thickness of the membrane
has been increased but this has not solved the problem
completely. Any imperfections in the membrane will result
in a hole developing due to sand grain penetration at high
pressure. A redesign of this membrane (and probably of the
load cap) will be required if a testing program is to be
conducted successfully on a regular basis.

The external membrane has performed satisfactory. Only
one hole developed and this was probably due to a weakness
along the seam.

Pressure Systems used in the Laboratory

The hydrogen pressure system used for the internal
pressure operated well and maintained pressure to within a
few kPa. The biggest drawback of this system is the size of
its accumulator and reservoir (1100 ml). The total volume
changes occurring during the entire test are large, and most
of this volume is lost from the reservoir if a leak occurs
in the membrane as the pressure system has to be shut down.
The reservoir has no indicator for the oil/water interface
and it is thus possible to pump oil through the system.

It is suggested that a larger accumulator/reservoir system be provided for future testing and that some means of monitoring the oil/water interface be installed.

The other pressure system initially used (Wykeham) proved unsatisfactory as it did not maintain pressure very well. Replacement parts were not available as it is now outdated. This system was finally replaced by a constant pressure pump which has an accumulator built into the system. This pressure system has also operated exceedingly well and has a reservoir which can be filled manually during the test.

APPENDIX G

Grain size distributions and compressibility data
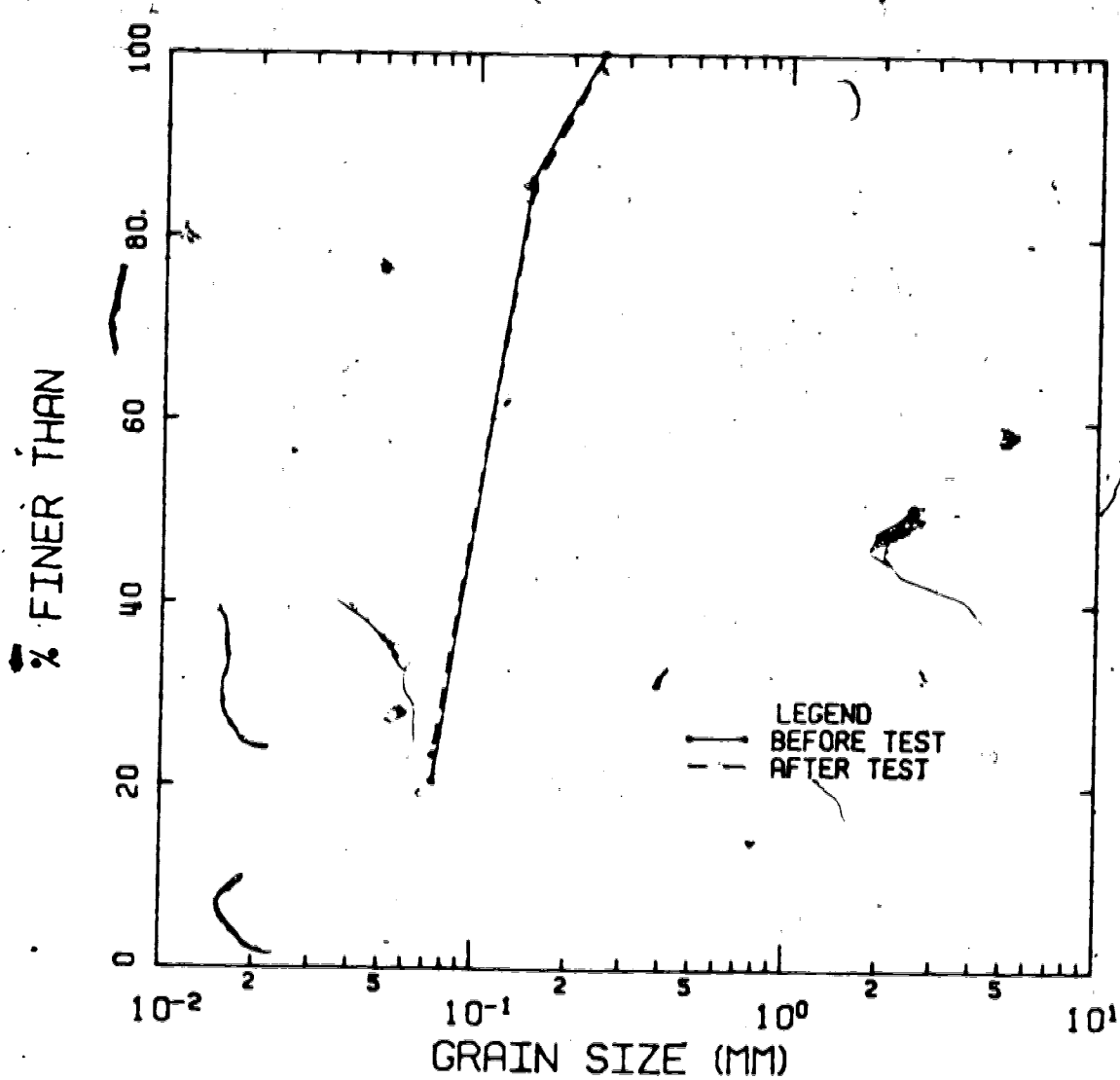
Figure G.1 Grain size distribution for the Oedometer sample
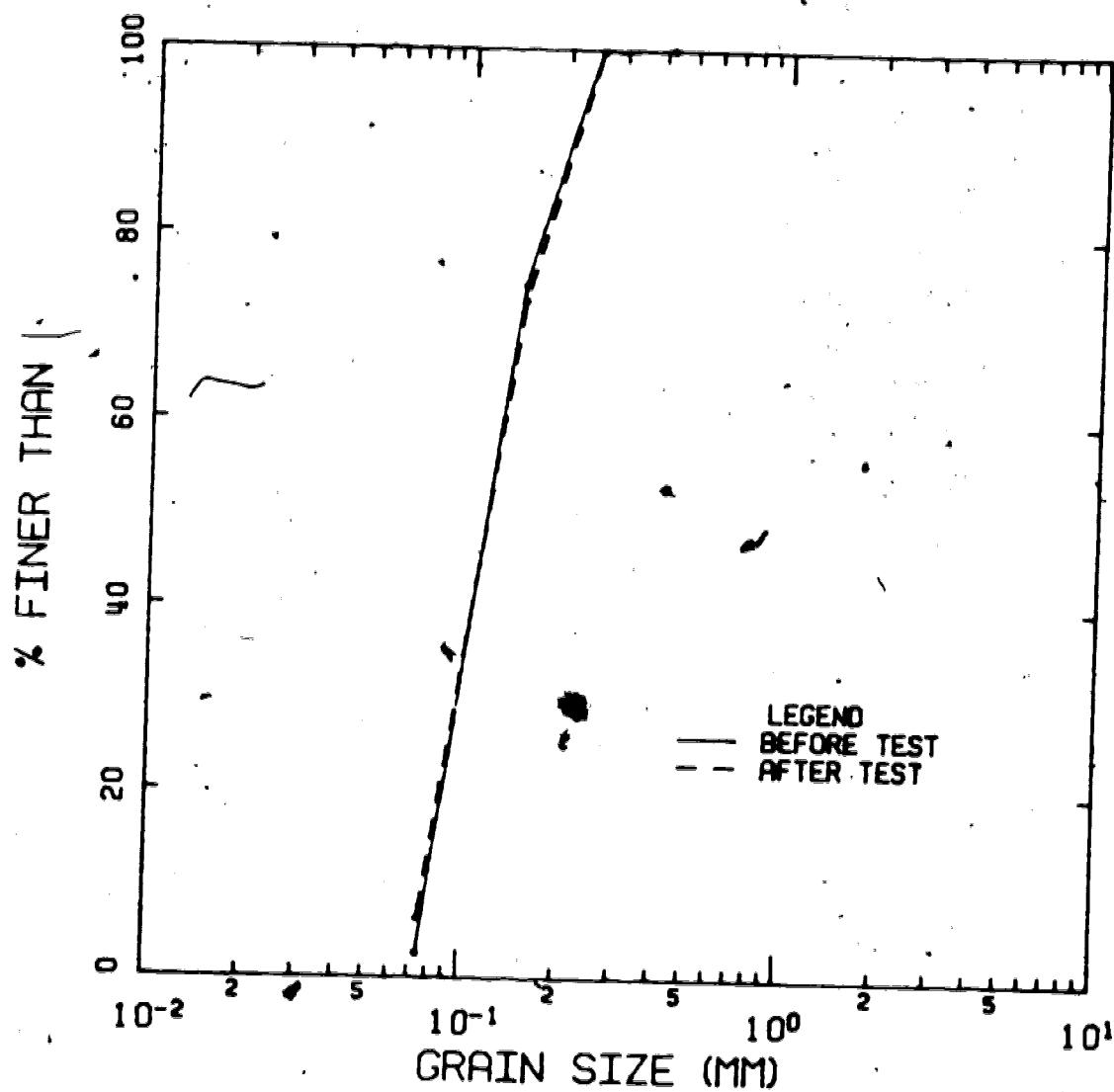
Figure G.2 Grain size distribution for Test #A-1
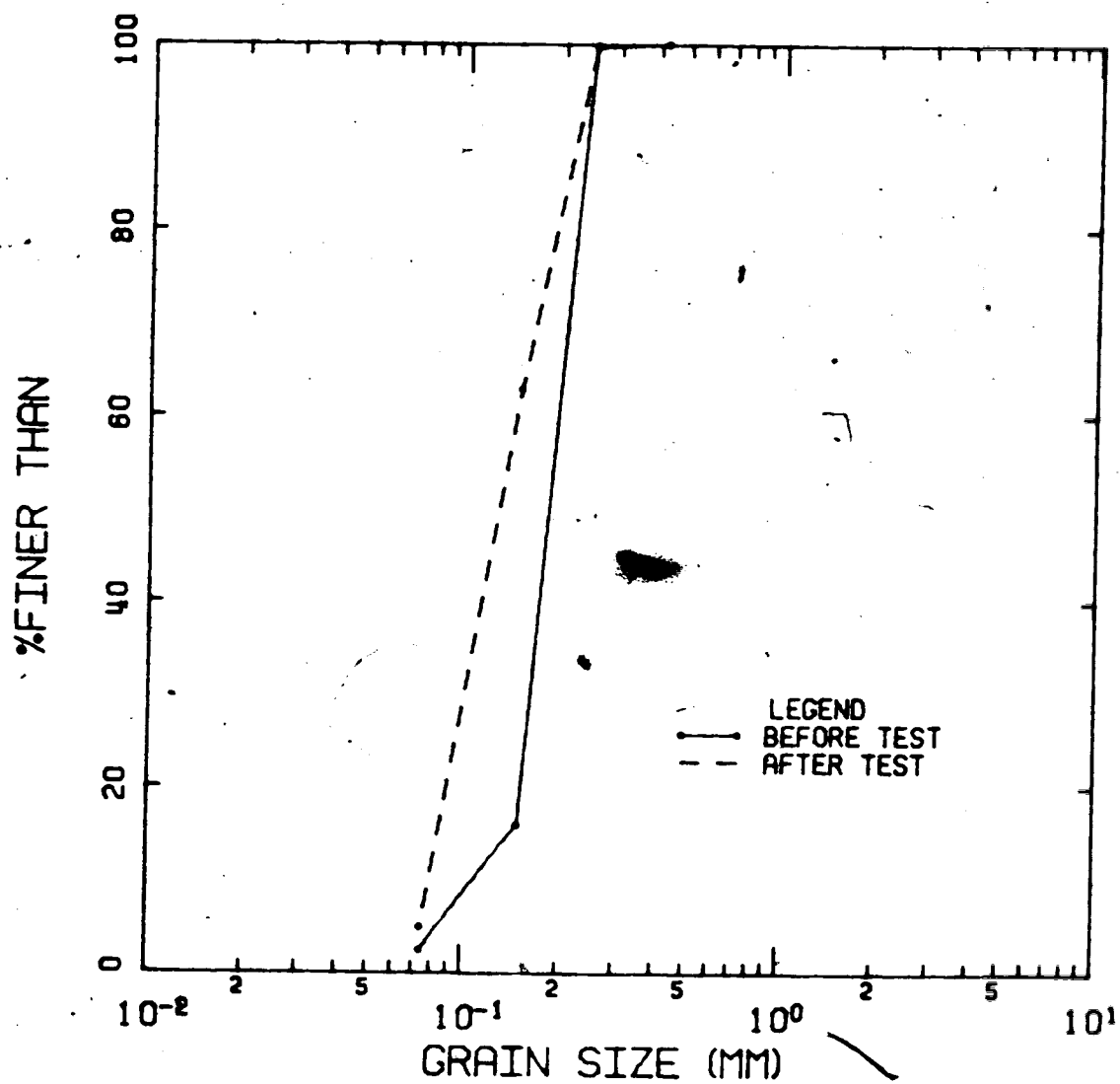
Figure G.3 Grain size distribution for Test #A-2
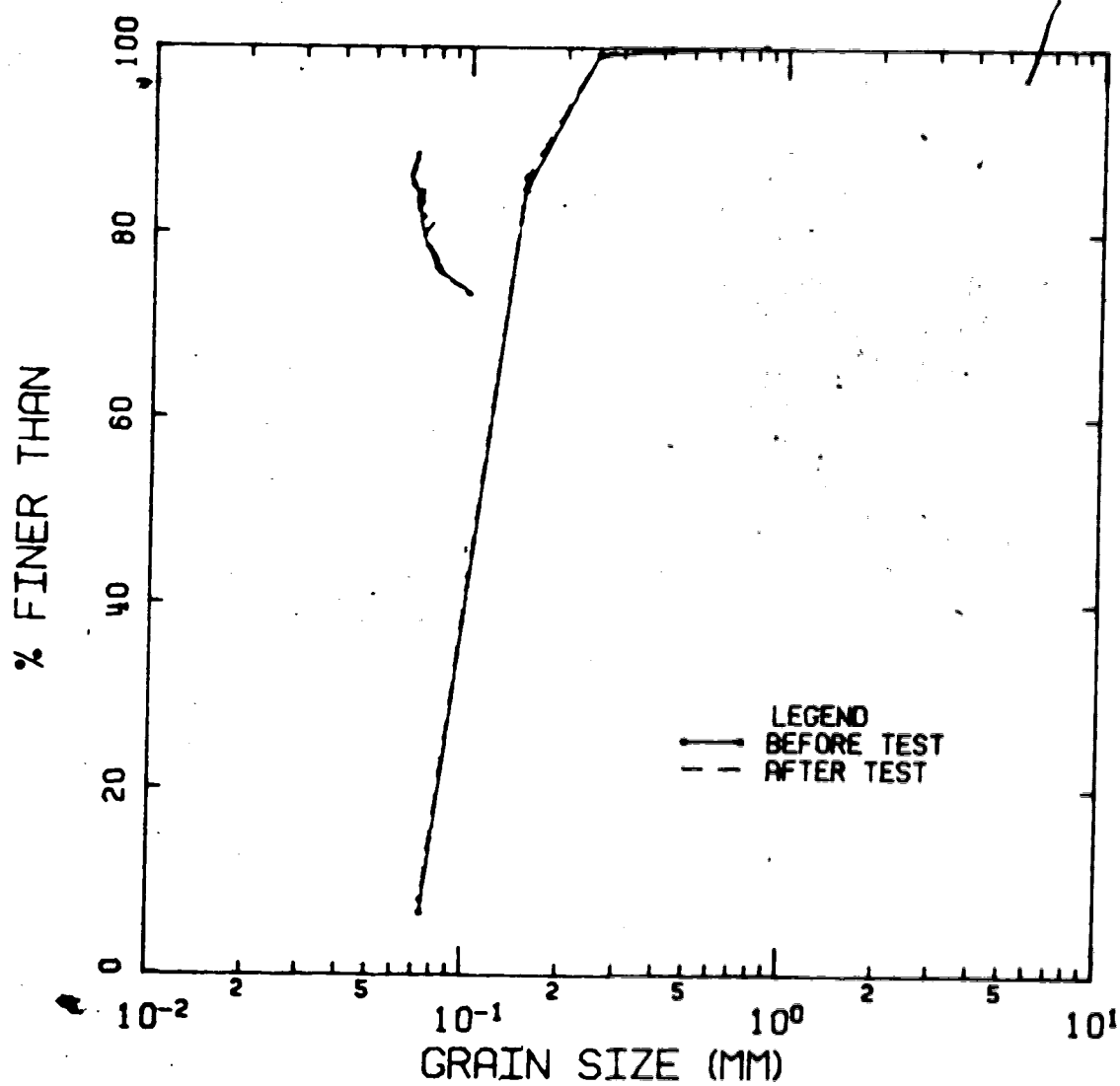
Figure G.4 Grain size distribution for Test #B-1
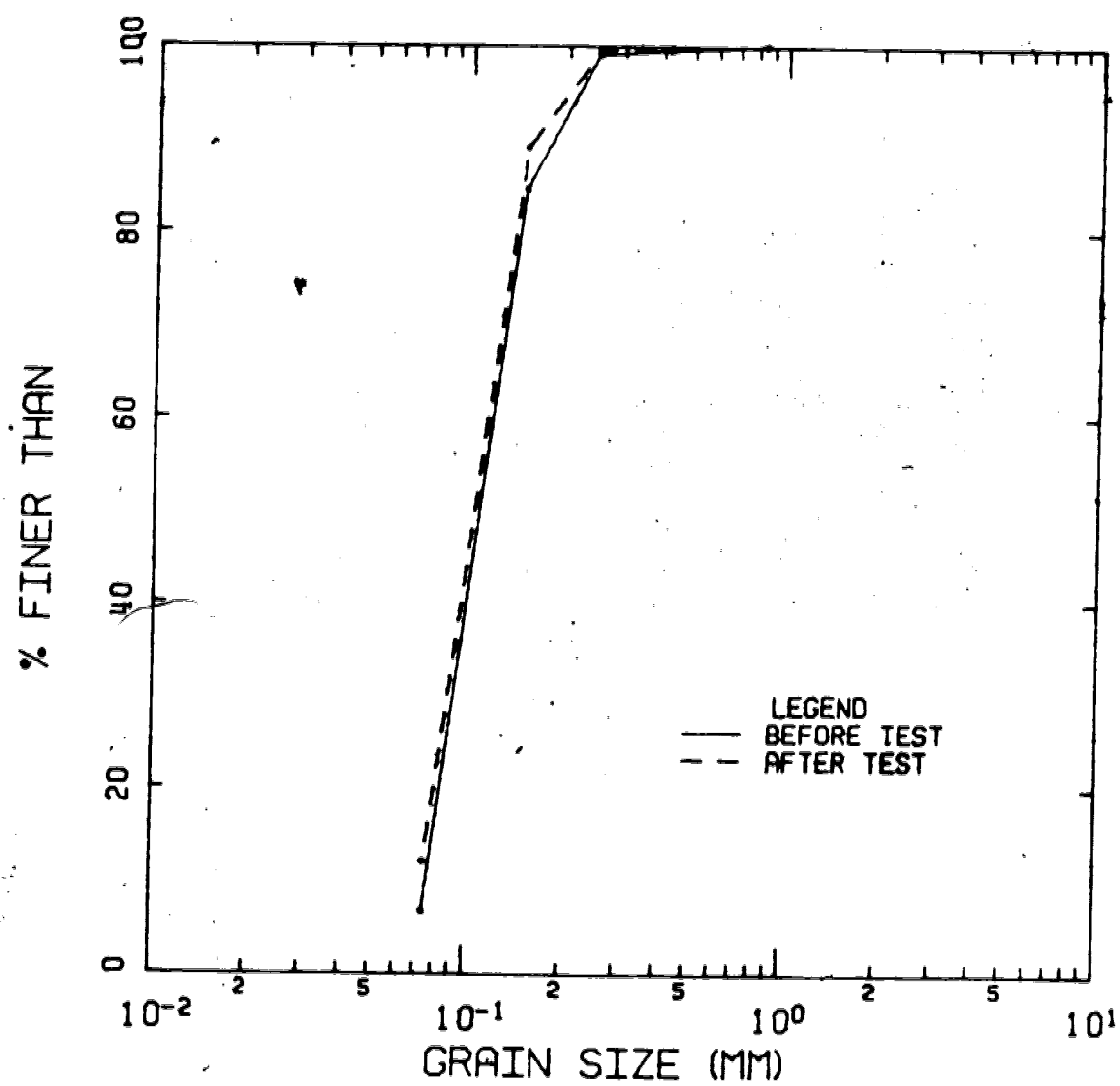
Figure G.5 Grain size distribution for Test #B-2
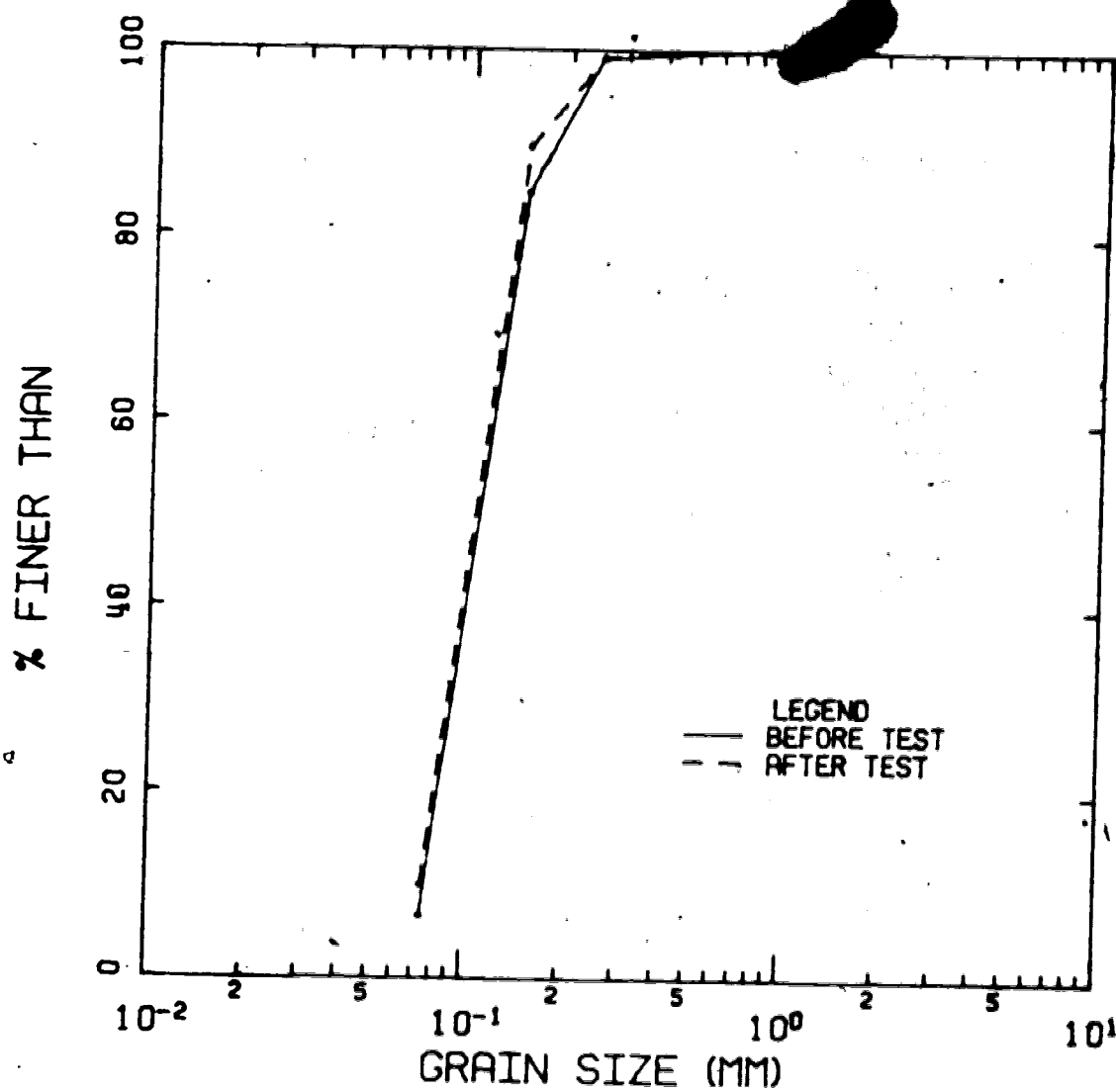
Figure G.6 Grain size distribution for Test #C-1
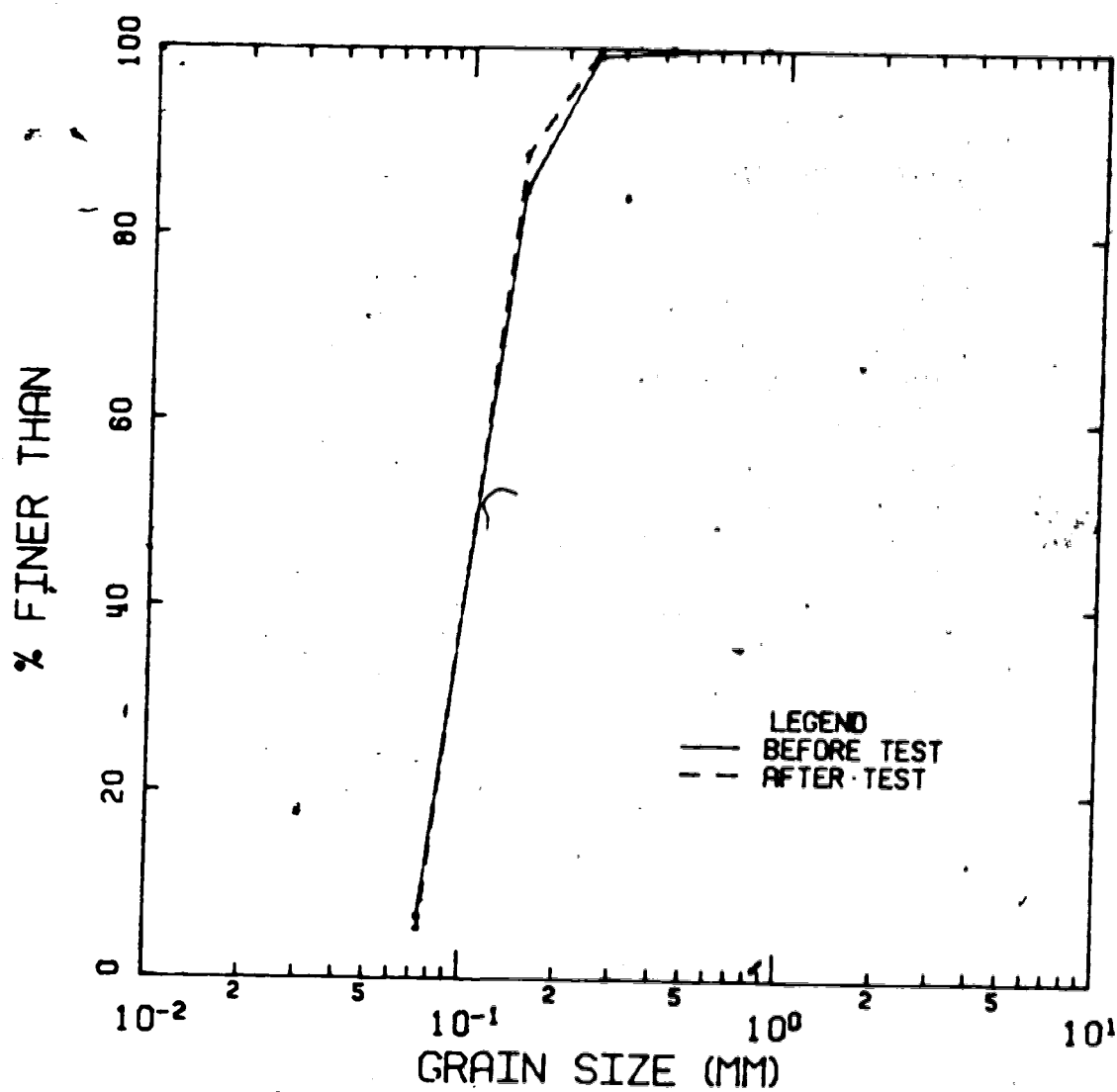
Figure G.7 Grain size distribution for Test #C-2
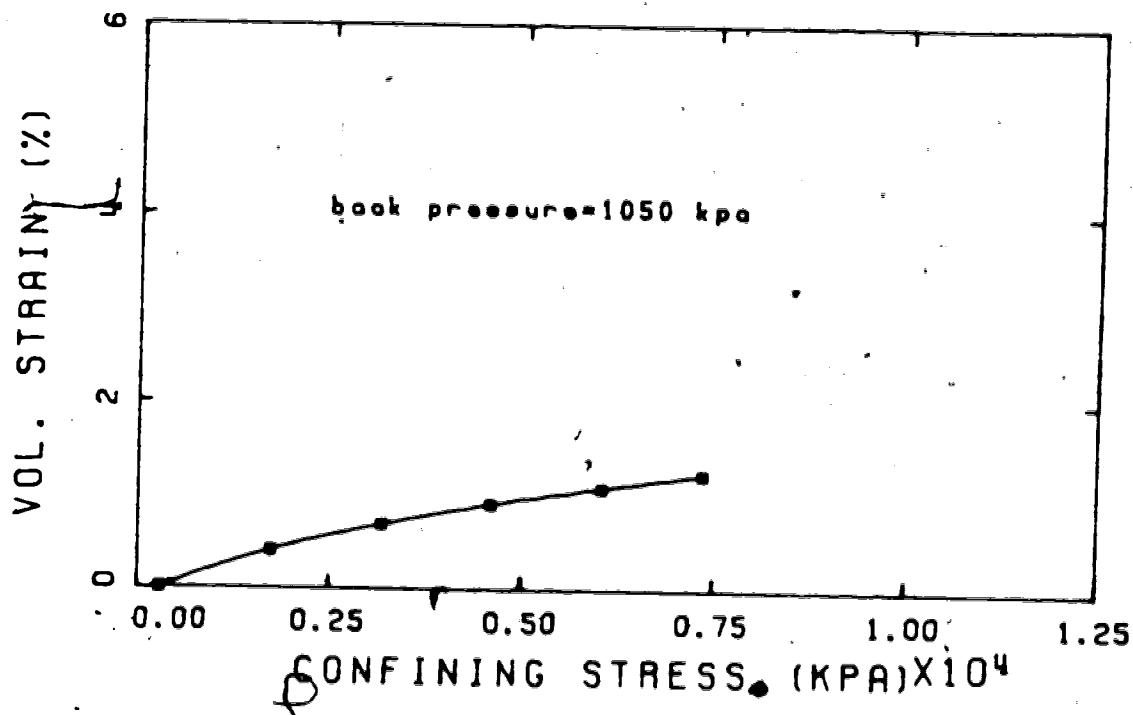
Figure G.8 Compressibility test, Sample #A-1
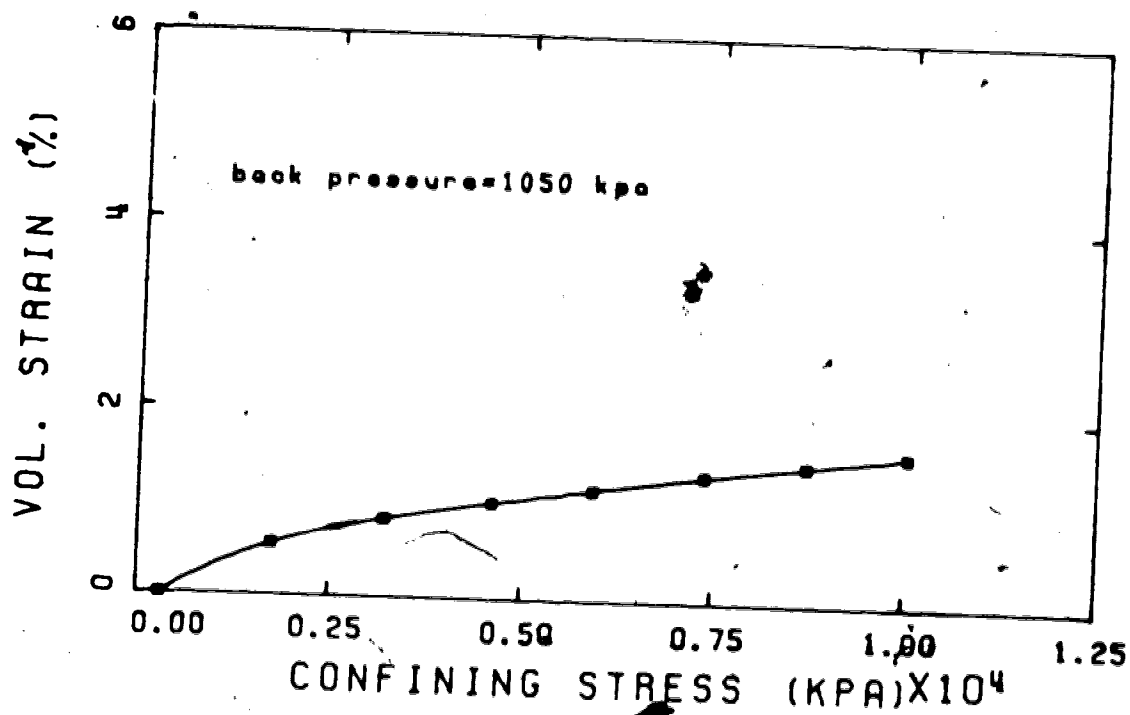
Figure G.9 Compressibility test, Sample #A-2
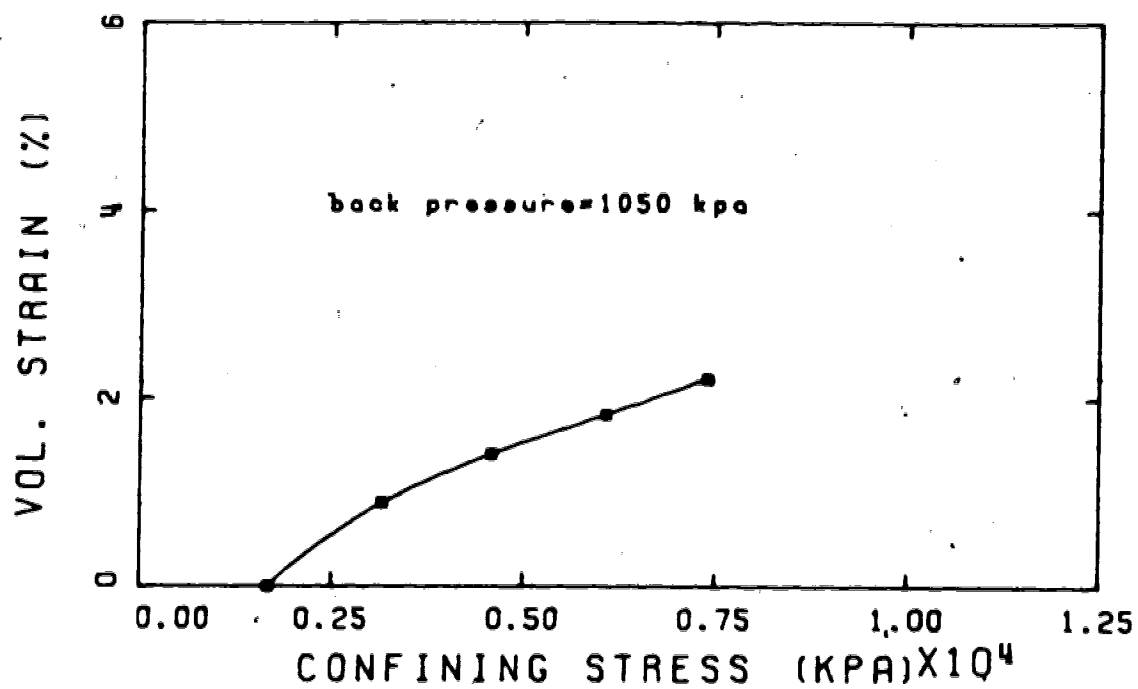
Figure G.10 Compressibility test, Sample #B-1
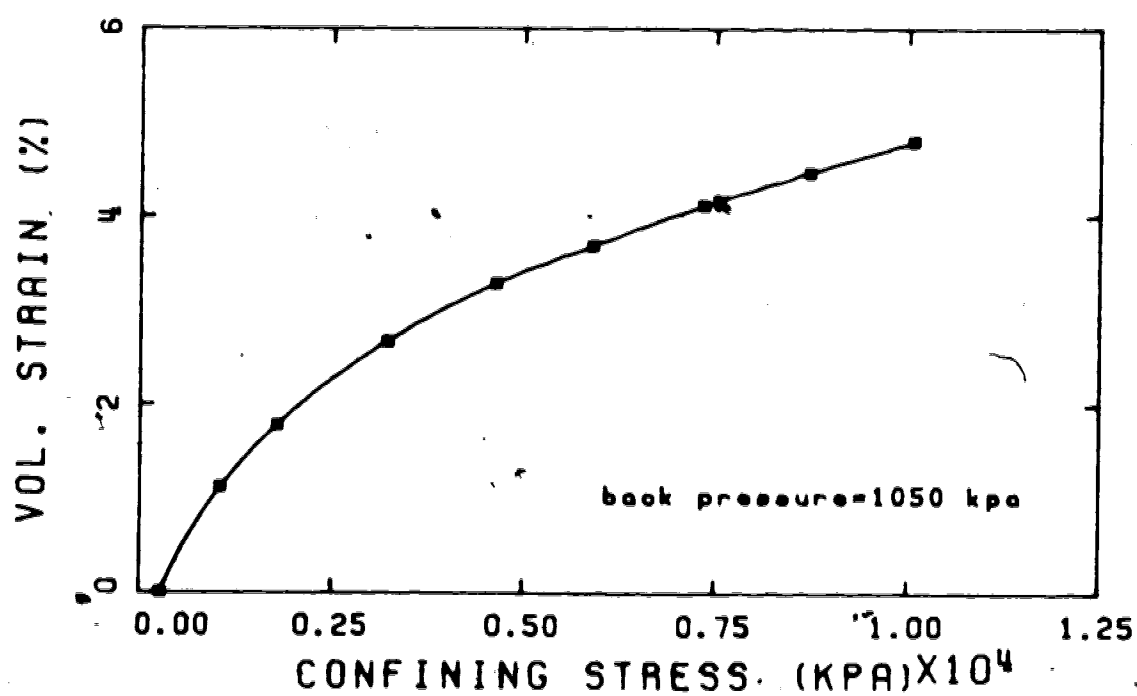
Figure G.11 Compressibility test, Sample #B-2
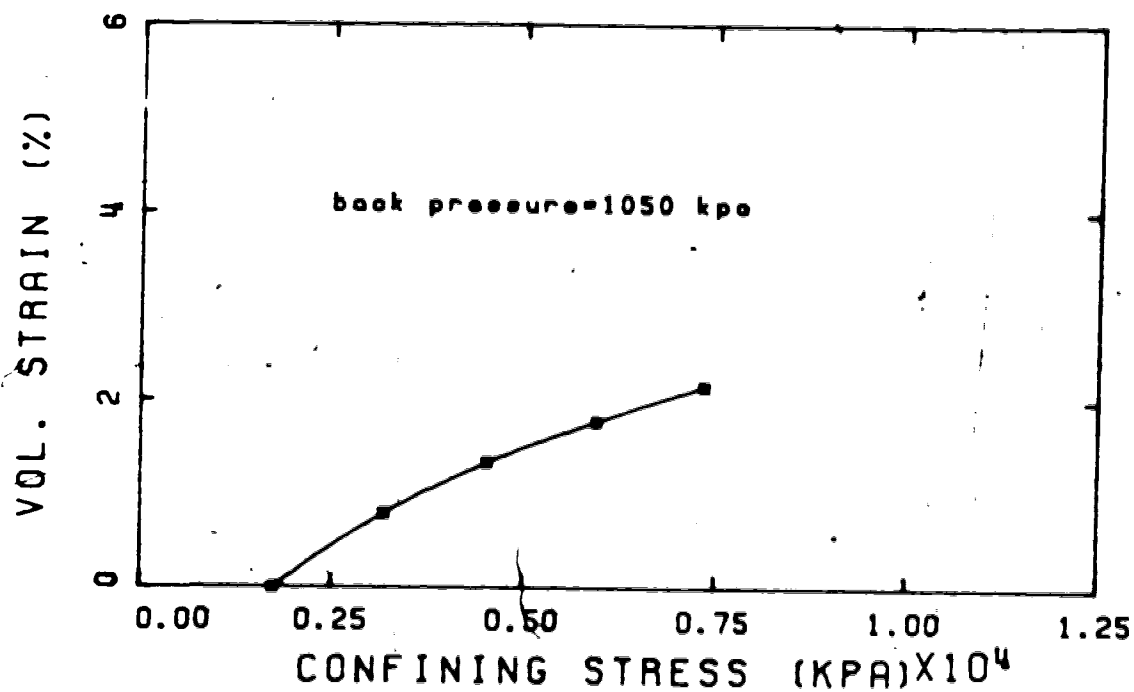
Figure G.12 Compressibility test, Sample #C-1
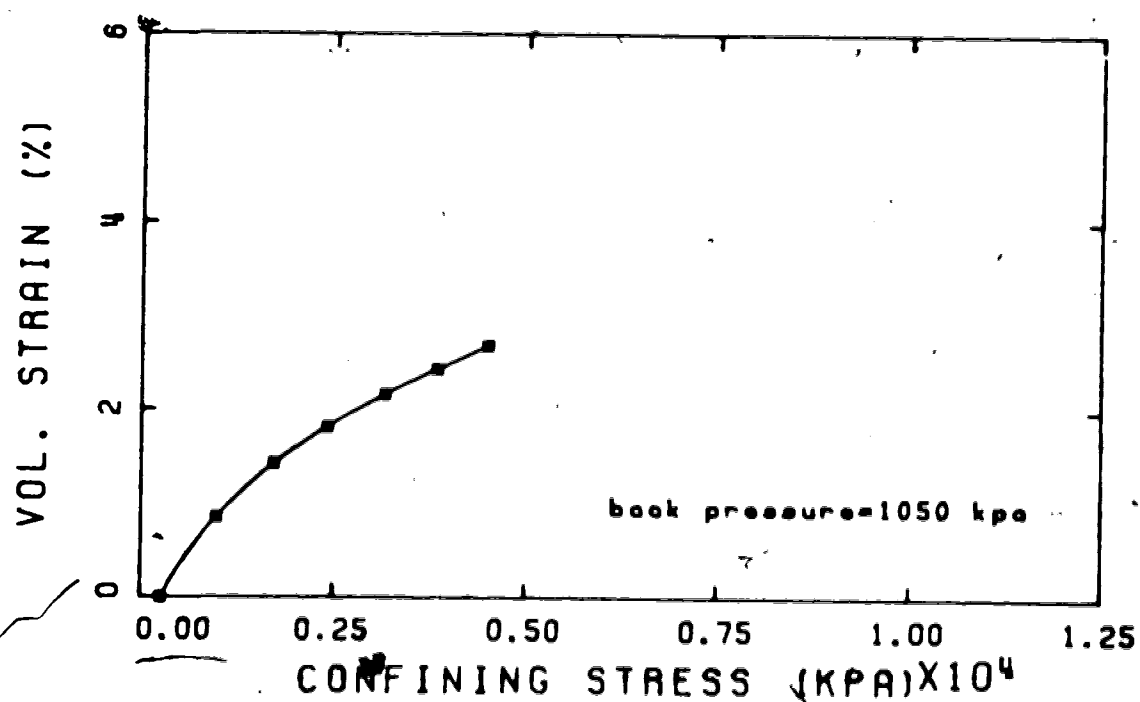
Figure G.13 Compressibility test, Sample #C-2

APPENDIX H

Computer program for the numerical model developed in Chapter 4

```
C   A PROGRAM FOR SOLVING THE STRESS DISTRIBUTION IN A HOLLOW CYLINDER
C   USING A POWER LAW FOR THE FAILURE CRITERION (TAU=A*SIGN**B)
C   THE STRESS-STRAIN LAW MAY BE EITHER PERFECTLY-PLASTIC (OR STRAIN-WEAKENING).
C   STRAIN SOFTENING EFFECTS MAY BE MODELLED BY USING A BI-LINEAR
C   VARIATION OF YOUNGS MODULUS WITH AVERAGE RADIAL STRESS
C
      DIMENSION SIGT(20,100),RAD(20,100),SIGR(20,100),SIGTP(20)
      DIMENSION STRESS(20),RADP(20),SIGRP(20),THEL(20),PE(20),PI(20)
      DIMENSION URA(20),URB(20),EPSP(20),EPSEL1(20),TITLE(20)
      DOUBLE PRECISION SIGR,SIGTH,SIGRE,DELTA,DIFA,DMAX
      COMMON SIGR,SIGT,SIGTH,A,B,JJ
      COMMON E1,E2,MU,DELR,R1,R2,KP,KL,LL,ALPHA,K
      COMMON RAD,PI,PE,URA,URB,EPSP,EPSEL1
      REAL MU,INFL
C
C   R1= INTERNAL RADIUS
C   R2= EXTERNAL RADIUS
C   A,B= FAILURE CRITERION PARAMETERS (FROM CURVE FITTING)
C   JJ= NUMBER OF DATA POINTS
C   NN= NUMBER OF ITERATION POINTS USED IN THE ANALYSIS (USUALLY 40)
C   MU= POISSONS RATIO
C   ALPHA= DILATION PARAMETER
C   DELR= SIZE OF THE ITERATION GRID (APPROX. R2-R1/NN)
C   EA,EB= YOUNGS MODULUS AT SIGR=PE (FROM THE E-SIGR PLOT)
C   SLA,SLB= SLOPES OF THE E-SIGR PLOT
C   SMAX=CUTOFF VALUE (MIN.) FOR E
C   INFL= VALUE OF SIGR AT WHICH THE SLOPEOF THE PLOT CHANGES.
C   MP= 1 FOR CONSTANT EXTERNAL PRESSURE
C      =2 FOR CONSTANT INTERNAL PRESSURE
C   NDATA = 1 FOR COMPLETE DATA OUTPUT
C         = 2 FOR DISPLACEMENT OUTPUT ONLY
C
      READ(5,99) (TITLE(I),I=1,20)
      READ(5,100) R1,R2,A,B,JJ,NN,MP,NDATA
      READ(5,101) MU,ALPHA,DELR
      READ(5,114) EA,EB,SLA,SLB
      READ(5,115) SMAX,INFL
      DO 5 I=1,JJ
      READ(5,102) PE(I),PI(I)
    5 CONTINUE
      WRITE(6,140)(TITLE(I),I=1,20)
      WRITE(6,129)
      WRITE(6,130) EA,EB,SLA,SLB,A,B,MU,ALPHA,R1,R2
C
C   CALC. STRESSES FROM ELASTIC SOLUTION UNTIL FAILURE COMMENCES.
C
      DO 10 I=1,JJ
      SIGR(I,1)=PI(I)
      TOP=(2.0*PE(I)*R2**2.0)-PI(I)*(R1**2.0+R2**2.0)
      BOT=(R2**2.0)-(R1**2.0)
      SIGT(I,1)=TOP/BOT
      SIGD=(PI(I)-PE(I))/2.0
      TAU=(SIGT(I,1)-SIGR(I,1))/2.0
      XX=(SIGT(I,1)+SIGR(I,1))/2.0
      ULT=A*(XX**B)
      IF(TAU GE ULT) K=1
      IF(TAU GE ULT) GO TO 15
      IF(TAU LT ULT) KP=1
```

```
      IF(MP.EQ.2) GO TO 8
      IF(SIGD.GE.INFL) E1=EA-SLA*(PE(I)-SIGD)
      IF(SIGD.LT.INFL) E1=EB-SLB*(PE(I)-SIGD)
      GO TO 9
8     CONTINUE
      IF(SIGD.GT.INFL) E1=EB-SLB*(SIGD-PI(I))
      IF(SIGD.LT.INFL) E1=EA-SLA*(SIGD-PI(I))
9     E2=E1
      LL=1
      CALL PSI(I,J)
10    CONTINUE
      WRITE(6,120)
      GO TO 65
15    CONTINUE
      EF=E1
      KP=2
      J=1
      LC=0
      MC=0
      DO 20 I=K,JJ
      RAD(I,1)=R1
      J=1
      SIGR(1,1)=PI(I)
      CALL SIGMA(I,J)
      SIGT(1,1)=SIGTH
      DO 30 J=2,NN
      L=J-1
      DELTA=((SIGT(I,L)-SIGR(I,L))/RAD(I,L))*DELR
      SIGR(I,J)=SIGR(I,L)+DELTA
      CALL SIGMA(I,J)
      SIGT(I,J)=SIGTH
      RAD(I,J)=RAD(I,L)+DELR
      IF(RAD(I,J).GT.R2) GO TO 60
      AA=(PE(I)*R2**2.0)-SIGR(I,J)*RAD(I,J)**2.0
      CC=(R2**2.0)-(RAD(I,J)**2.0)
      SIGD=AA/CC
      IF(SIGD.LE.0.0) J=2
      IF(SIGD.LE.0.0) GO TO 40
      SIGREL=SIGD-(A*SIGD**B)
      DIFF=(SIGR(I,J)-SIGREL)
      IF(DIFF.GE.0.0) LC=1
      IF(DIFF.LT.0.0) MC=1
      DIFA=ABS(DIFF)
      DMAX=0.01*SIGR(I,J)
      IF(DIFA.LE.DMAX) GO TO 40
      IF(LC.EQ.MC) GO TO 40
30    CONTINUE
40    RADP(I)=RAD(I,J)
      LL=J
      LC=0
      MC=0
      KK=J+1
      KL=J+4
      CHG=(R2-RADP(I))/4.0
      DO 45 J=KK,KL
      LA=J-1
      RAD(I,J)=RAD(I,LA)+CHG
      TX=(PE(I)*R2**2.0)-(SIGR(I,LL)*RAD(I,LL)**2.0)
      TY=(RAD(I,LL)**2.0)*(R2**2.0)*(PE(I)-SIGR(I,LL))
      BX=(R2**2.0)-(RAD(I,LL)**2.0)
```

```
      SIGR(I,J)=(TX/BX)-TY/(BX*RAD(I,J)**2.0)
   45 SIGT(I,J)=(TX/BX)+TY/(BX*RAD(I,J)**2.0)
      SIGO=(PE(I)+SIGR(I,LL))/2.0
      IF(MP.EQ.2) GO TO 46
      IF(SIGO.GE.INFL) E1=EA-SLA*(PE(I)-SIGO)
      IF(SIGO.LT.INFL) E1=EB-SLB*(PE(I)-SIGO)
      GO TO 47
   46 CONTINUE
      IF(SIGO.GE.INFL) E1=EB-SLB*(SIGO-PI(I))
      IF(SIGO.LT.INFL) E1=EA-SLA*(SIGO-PI(I))
   47 E2=E1
      STRESS(I)=SIGREL
      THEL(I)=(2.0*SIGO)-SIGREL
      SIGTP(I)=SIGT(I,LL)
      SIGRP(I)=SIGR(I,LL)
      CALL PSI(I,J)
   20 CONTINUE
      IF(RAD(I,LL).LE.R2) GO TO 65
   60 CONTINUE
      WRITE(6,108)
   65 CONTINUE
      IF(NDATA.EQ.2) GO TO 68
      WRITE(6,106)
      DO 64 I=1,JJ
      WRITE(6,107) (SIGR(I,J),J=1,KL)
   64 CONTINUE
      WRITE(6,109)
      DO 66 I=1,JJ
      WRITE(6,107) (SIGT(I,J),J=1,KL)
   66 CONTINUE
      WRITE(6,110)
      DO 67 I=1,JJ
      WRITE(6,111) (RAD(I,J),J=1,KL)
   67 CONTINUE
      WRITE(6,104)
      WRITE(6,105) (SIGRP(I),STRESS(I),RADP(I),I=1,JJ)
      WRITE(6,121)
      WRITE(6,122) (EPSEL1(I),EPSP(I),I=1,JJ)
   68 CONTINUE
      WRITE(6,112)
      DO 70 I=1,JJ
      WRITE(6,113) (PI(I),URA(I),URB(I))
   70 CONTINUE
   99 FORMAT(20A4)
  100 FORMAT(4F10.0,.413)
  101 FORMAT(3F10.0)
  102 FORMAT(2F10.0)
  104 FORMAT(//,10X,'SIGR-(PL)',10X,'SIGR-(EL)',10X,'PLASTIC RADIUS')
  105 FORMAT(/,10X,F10.2,10X,F10.2,10X,F10.6)
  107 FORMAT(1H ,'VALUES OF THE RADIAL STRESS DURING ITERATIONS')
  107 FORMAT(10X,8F12.3)
  108 FORMAT(10X,'**ERROR** PLASTIC RADIUS EXCEEDS OUTER RADIUS')
  109 FORMAT(///,'VALUES OF THE TANG. STRESS DURING ITERATIONS')
  110 FORMAT(///,'VALUES OF THE RADIUS DURING ITERATIONS')
  111 FORMAT(10X,8F12.8)
  112 FORMAT(///,'SUMMARY OF THE WALL CLOSURES',/,10X,'INT. PRESS.',10X,
     *'INT. DISPL.',10X,'EXT. DISPL.')
  113 FORMAT(/,10X,F10.2,10X,F10.8,10X,F10.8)
  114 FORMAT(4F10.0)
  115 FORMAT(2F10.0)
```

```
120 FORMAT(10X,'SHEAR STRENGTH OF MATERIAL NOT EXCEEDED AT INT. WALL')
121 FORMAT(///,10X,'ELASTIC STRAIN INCR.',10X,'PLASTIC STRAIN INCR')
122 FORMAT(13X,F12.8,13X,F12.8)
129 FORMAT(1H ,10X,'VALUES OF PARAMETERS USED IN THE ANALYSIS.')
130 FORMAT(//,10X,'EA=',F12.2,/,10X,'EB=',F12.2,/,10X,'SLA=',F10.2,/,
    *,10X,'SLB=',F10.2,/,10X,'A=',F7.4,/,10X,'B=',F6.4,/,10X,'MU=',F6.4,
    */,10X,'ALPHA=',F4.2,/,10X,'INT. RAD.=',F10.8,/,10X,'EXT. RAD.=
    *',F10.8)
140 FORMAT(20X,20A4)
    CALL EXIT
    STOP
    END
    SUBROUTINE SIGMA(I,J)

C
C                          SIGMA
C                         *******
C
    DIMENSION SIGR(20,100),SIGT(20,100)
    COMMON SIGR,SIGT,SIGTH,A,B,JJ
    DOUBLE PRECISION SIGR,SIGTH,SIGREL,DELTA,DIFA,DMAX
    REAL M
    M=2.0
10  M=M+1.0
    SIGTH=M*SIGR(I,J)
    RAT3=(SIGTH-SIGR(I,J))/2.0
    RAT4=(((SIGTH+SIGR(I,J))/2.0)**B)*A
    IF(RAT3.LT.RAT4) GO TO 10
    M=M-1.0
20  M=M+0.1
    SIGTH=M*SIGR(I,J)
    RAT3=(SIGTH-SIGR(I,J))/2.0
    RAT4=(((SIGTH+SIGR(I,J))/2.0)**B)*A
    IF(RAT3.LT.RAT4) GO TO 20
    M=M-0.1
30  M=M+0.01
    SIGTH=M*SIGR(I,J)
    RAT3=(SIGTH-SIGR(I,J))/2.0
    RAT4=(((SIGTH+SIGR(I,J))/2.0)**B)*A
    IF(RAT3.LT.RAT4) GO TO 30
    SIGTH=M*SIGR(I,J)
    AAAA=0.0
    RETURN
    END
    SUBROUTINE PSI(I,J)

C
C                          PSI
C                         *****
C
C A PROGRAM WHICH CALCULATES THE PLASTIC STRAIN INCREMENTS (B ELASTIC
C STRAIN INCREMENTS). THE ELASTIC STRAINS IN THE PLASTIC REGION ARE FOUND
C BY ASSUMING THAT THEY ARE EQUIVALENT TO THE STRAINS THAT WOULD DEVELOP
C IF THE CYLINDER RESPONDED IN A PURELY ELASTIC MANNER.
C
    DIMENSION SIGR(20,100),RAD(20,100),SIGTA(20),SIGTB(20)
    DIMENSION EPSP(20),EPSEL1(20),EPST1(20),EPST2(20)
    DIMENSION PI(20),PE(20),URA(20),URB(20),SIGT(20,100)
    DOUBLE PRECISION SIGR,SIGTH
    COMMON SIGR,SIGT,SIGTH,A,B,JJ
    COMMON E1,E2,MU,DELR,R1,R2,KP,KL,LL,ALPHA,K
    COMMON RAD,PI,PE,URA,URB,EPSP,EPSEL1
```

```fortran
      REAL MU
      IF(I.GT.1) GO TO 6
      DO 5 KS=1,JJ
    5 EPSP(KS)=0.0
      URA(1)=0.0
      URB(1)=0.0
      SUM=0.0
    6 KKK=I-1
      FAC1=(1.0-MU**2.0)/E1
      FAC2=(1.0-MU**2.0)/E2
      FAL=MU/(1.0-MU)
      FACM=(1.0+MU)/E1
      IF(KP.EQ.1) GO TO 55
      EPSA=0.0
      CTE=1.0+ALPHA
      FACT=SUM*100.0
   10 EPSA=EPSA+0.02
      EPSE=EPSA
      MMM=LL-1
      DO 50 KJ=1,MMM
      DELE=-(DELR/RAD(1.KJ))*(EPSE*CTE+FACT)
      EPSE=EPSE+DELE
   50 CONTINUE
      IF(EPSE.LT.0.0) GO TO 10
      EPSP(I)=(EPSA/100.0)-EPSP(KKK)
C
C  NOTE: EPSP(I) REPRESENTS THE PLASTIC STRAIN INCREMENTS
C
   55 CONTINUE
      IF(KP.NE.1) GO TO 65
      TOP1=(2.0*PE(I)*R2**2.0)-PI(I)*(R1**2.0*R2**2.0)
      TOP2=(PE(I)*(R1**2.0*R2**2.0))-2.0*PI(I)*R1**2.0
      BOT=(R2**2.0)-(R1**2.0)
      SIGTA(I)=TOP1/BOT
      SIGTB(I)=TOP2/BOT
      IF(I.EQ.1) GO TO 60
      DSIGRB=PE(I)-PE(KKK)
      DSIGRA=PI(I)-PI(KKK)
      DSIGTB=SIGTB(I)-SIGTB(KKK)
      DSIGTA=SIGTA(I)-SIGTA(KKK)
      EPSEL1(I)=FAC1*(DSIGTA-(FAL*DSIGRA))
      EPSEL2(I)=FAC2*(DSIGTB-(FAL*DSIGRB))
      EPST1(I)=EPSP(I)+EPSEL1(I)
      SUM=SUM+FACM*(DSIGTA-DSIGRA)
      IF(KP.EQ.1) GO TO 70
   65 CONTINUE
      TXX=SIGT(1,LL)-TDIF
      TYY=SIGR(1,LL)-RDIF
      EPSEL1(I)=FAC1*(TXX-(FAL*TYY))
      IF(EPSEL1(I).LT.0.0) EPSEL1(I)=0.0
      EPST1(I)=EPSP(I)+EPSEL1(I)
      SUM=SUM+FACM*(TXX-TYY)
      SIGTB(I)=SIGT(1,KL)
      DSIGRB=PE(I)-PE(KKK)
      DSIGTB=SIGTB(I)-SIGTB(KKK)
      EPST2(I)=FAC2*(DSIGTB-(FAL*DSIGRB))+
   70 DELUA=R1*EPST1(I)
      DELUB=R2*EPST2(I)
      URA(I)=URA(KKK)+DELUA
      URB(I)=URB(KKK)+DELUB
```

```
      R1=R1-DELUA
      R2=R2-DELUB
60    CONTINUE
      TDIF=SIQT(I,LL)
      RDIF=SIGR(I,LL)
      RETURN
      END
```

APPENDIX I

Data reduction and plotting programs for the hollow cylinder tests

```
C
C          HOLLOW2
C          *******
C
C     A PROGRAM TO TAKE HOLLOW CYLINDER DATA AND REDUCE IT TO MEASURES
C     WHICH CAN BE PLOTTED IN A MEANINGFUL MANNER.  ALL PERTINENT STRESSES
C     AND STRAINS WILL BE LISTED ON PAPER (FILE DEVICE 6) AND ALSO ON A FILE
C     WHICH CAN BE USED FOR STORING DATA FOR  PROCESSING (FD 1 AND FD 2).
C
      REAL LCO,LCCF,IDTO,IDTCF,MS
      COMMON TITLE(20),PE(150),PI(150),P(150),AX(150),VIM(150),
     *VPF(150),DA(150),STR(150),VEM(150),EPSI(150),EPSE(150),DELI(150),
     *STE(150),SRI(150),SRE(150),STI(150),DELE(150),ADA(150),.
     *SRM(150),STM(150),R1(150),R2(150),EPSV(150),EPSR(150),
     *EPST(150),EAX(150),DELV(150),DELT(150),DELR(150),RAD(150)
      COMMON JJ,H,SAMVOL,MX,MY,MZ,MC,MEL,MCAL,DINT,DEXT,WDRY,PIE
      COMMON ADTO,ADTCF,LCO,LCCF,PPTO,PPTCF,CPTO,CPTCF
      CALL DATA
      CALL REDUC
      CALL STRAIN
      IF(MEL.GT.2) GO TO 10
      CALL STRESS
      IF(MEL.EQ.1) GO TO 20
   10 CONTINUE
      CALL ELPLA
   20 CONTINUE
      CALL EXIT
      STOP
      END
      SUBROUTINE DATA
C
C          DATA
C          ****
C
      REAL LCO,LCCF,IDTO,IDTCF,MS
      COMMON TITLE(20),PE(150),PI(150),P(150),AX(150),VIM(150),
     *VPF(150),DA(150),STR(150),VEM(150),EPSI(150),EPSE(150),DELI(150),
     *STE(150),SRI(150),SRE(150),STI(150),DELE(150),ADA(150),.
     *SRM(150),STM(150),R1(150),R2(150),EPSV(150),EPSR(150),
     *EPST(150),EAX(150),DELV(150),DELT(150),DELR(150),RAD(150)
      COMMON JJ,H,SAMVOL,MX,MY,MZ,MC,MEL,MCAL,DINT,DEXT,WDRY,PIE
      COMMON ADTO,ADTCF,LCO,LCCF,PPTO,PPTCF,CPTO,CPTCF
      READ(5,100) (TITLE(I),I=1,20)
C
      READ(5,101) LCO,LCCF,PPTO,PPTCF,ADTO,ADTCF,CPTO,CPTCF
C
C     THESE ARE THE ELECTRONICS CONTROL FACTORS:   LCO=LOAD CELL ZERO.
C     LCCF=LOAD CELL CALIBRATION FACTOR IN KNEWTS(KN) PER MILLIVOLT(MV).
C     PPTO=PORE PRESSURE TRANSDUCER ZERO. PPTCF=PORE PR. CAL FAC(KPA/MV).
C     ADTO=AXIAL LVDT ZERO. ADTCF=AXIAL LVDT CAL FAC (MM/V).
C     CPTO=CELL PRESSURE TRANSDUCER ZERO. CPTCF=CELL PR. CAL. FAC (KPA/MV)
C
C     READ PROGRAM CONTROL CARDS
C
      READ(5,104) MX,MY,MZ,MC,MEL,MCAL
C
C     MX=1  FOR ZERO EXT  VOL  CHANGE READINGS
C       =2 FOR ZERO INT. VOL. CHANGE READINGS
```

```
C    -3 IF BOTH INT. AND EXT. VOL. CHANGE RECORDED
C
C    MY=1 FOR CONSTANT EXT. PRESSURE
C      =2 FOR CONSTANT INT. PRESSURE
C      =3 FOR CHANGING EXT. & INT.PRESSURE
C    MZ=1 FOR TOTAL STRESS ANALYSIS
C      =2 FOR EFFECTIVE STRESS ANALYSIS
C    MC=NO. OF DATA POINTS FOR CONSOLIDATION PHASE OF TEST.
C
C    READ THE INITIAL SAMPLE DATA
C
      READ(5,102) H,DINT,DEXT,WDRY
C
C    H=SAMPLE HEIGHT IN CENTIMETRES. DINT= SAMPLE INTERNAL DIAMETER IN CMS.
C    DEXT = EXTERNAL DIAMETER IN CENTIMETRES. WDRY= DRY WEIGHT OF SAMPLE IN GMS.
C
C    READ IN INDIVIDUAL DATA POINTS
C
      DO 99 N=1,150,1
      READ(5,103) PE(N),PI(N),P(N),AX(N),VIM(N),VPF(N),DA(N)
      IF(PE(N).EQ.999.) GO TO 98
      JJ=N
   99 CONTINUE
C
C    NOTE THAT THE LAST DATA CARD MUST BE 999
C
C    PE() IS EXTERNAL STRESS READING IN MV, PI()= INT STR RDG IN MV. P=
C    PORE PRES. IN MV. AX()=AXIAL LOAD IN MV. VIM= VOL CHG OF INTERNAL
C    MEMBRANE IN CC. VPF=VOL CHG OF PORE FLUID IN CC. DA()= AXIAL
C    DEFLECTION IN VOLTS
C
C    ALL DATA IS NOW READ IN: INITIAL SAMPLE CHARACS ARE NOW COMPUTED
C
C    FORMAT STATEMENTS FOR TEST DATA INITIALIZATION
C
  100 FORMAT(20A4)
  101 FORMAT(8F8.3)
  102 FORMAT(4F10.6)
  103 FORMAT(8F8.5)
  104 FORMAT(6I2)
   98 CONTINUE
      RETURN
      END
      SUBROUTINE REDUC
C
C    REDUC
C    ******
C
      REAL LCD,LCCF,IDTO,IDTCF,MS
      COMMON TITLE(20),PE(150),PI(150),P(150),AX(150),VIM(150),
     *VPF(150),DA(150),STR(150),VEM(150),EPSI(150),EPSE(150),DELI(150),
     *STE(150),SRI(150),SRE(150),STI(150),DELE(150),ADA(150),
     *SRM(150),STM(150),R1(150),R2(150),EPSV(150),EPSR(150),
     *EPST(150),EAX(150),DELV(150),DELT(150),DELR(150),RAD(150)
      COMMON JJ,H,SAMVOL,MX,MY,MZ,MC,MEL,MCAL,DINT,DEXT,WDRY,PIE
      COMMON ADTO,ADTCF,LCD,LCCF,PPTO,PPTCF,CPTO,CPTCF
   98 ARI=3.14159*DINT**2* .0001/4
```

```
      ARE=3 14159*DEXT**2* 0001/4
      VOLIN=ARI*H* 01
      SAMA=ARE-ARI
      SAMVOL=SAMA*H*0 01
      DRYDEN=(WDRY/SAMVOL)/1000000
      POR=(2.65-DRYDEN)/2 65
      WATVOL=POR*SAMVOL
      SATDEN=DRYDEN+POR
      PUR=POR*100
      HM=H*0 01
C
C     WRITE OUT SAMPLE INITIAL CONDITIONS
C
      WRITE(6,200) (TITLE(I),I=1,20)
      CALL STARS
      WRITE(6,201)
      CALL STARS
      WRITE(6,202) M,DEXT,DINT,WDRY,VOLIN,SAMA,SAMVOL,DRYDEN,SATDEN,PUR
      CALL STARS
      WRITE(1,215) JJ,SAMVOL,POR,VOLIN,H,DEXT,DINT,MX,MY,MZ,MC,MEL
C
C     WRITE OUT CALIBRATION FACTORS AND ZEROS
C
      WRITE(6,203)
      CALL STARS
      WRITE(6,204) LCO,LCCF,PPTD,PPTCF,ADTO,ADTCF,CPTO,CPTCF
      CALL STARS
C
C     WRITE OUT RAW ELECTRONICS DATA IN A CLOSELY SPACED LIST
C
      WRITE(6,205)JJ
      CALL STARS
      WRITE(6,206)
      CALL STARS
      WRITE(6,207) (PE(N),PI(N),P(N),AX(N),VIM(N),VPF(N),DA(N),
     *N,N=1,JJ)
      CALL STARS
C
  215 FORMAT(I5,F10.9,F10.3,F10.8,3F10.3,5I5)
  200 FORMAT(1H1,////,1X,20A4)
  201 FORMAT(////,20X,'SAMPLE CHARACTERISTICS BEFORE TEST BEGINNING')
  202 FORMAT(//,
     *20X,'SAMPLE HEIGHT         = ',F10.3,' CENTIMETRES',/,
     *20X,'EXTERIOR DIAMETER     = ',F10.3,' CENTIMETRES',/,
     *20X,'INTERIOR DIAMETER     = ',F10.3,' CENTIMETRES',/,
     *20X,'TOTAL DRY WEIGHT      = ',F10.3,' GRAMS      ',/,
     *20X,'INTERIOR VOLUME       = ',F10.8,' CUBIC METRES',/,
     *20X,'SAMPLE X-SEC AREA     = ',F10.9,' SQUARE METRES',/,
     *20X,'SAMPLE VOLUME         = ',F10.9,' CUBIC METRES',/,
     *20X,'DRY DENSITY           = ',F10.3,' MEGAGRAMS/ CU M',/,
     *20X,'SATURATED DENSITY     = ',F10.3,' MEGAGRAMS/ CU M',//,
     *20X,'POROSITY              = ',F10.3,' %',///)
  203 FORMAT(///,20X,'CALIBRATION FACTORS AND ELECTRONICS ZEROS')
  204 FORMAT(//,
     *20X,'AXIAL LOAD CELL ZERO VALUE              = ',F10.3,' MV',/,
     *20X,'LOAD CELL CALIBRATION FACTOR            = ',F10.3,' KN/MV',/,
     *20X,'PORE PRESSURE TRANSDUCER ZERO VALUE     = ',F10.3,' MV',/,
     *20X,'PORE PRES. TRANS. CALIBRATION FACTOR    = ',F10.3,' KPA/MV',/,
     *20X,'AXIAL DISPLACEMENT TRANSDUCER ZERO      = ',F10.3,' VOLTS',/,
```

```fortran
     *20X,'AXIAL LVDT CALIBRATION FACTOR         = ',F10.3,' MM/VOLT',/,
     *20X,'CELL PRESSURE TRANSDUCER ZERO VALUE   = ',F10.3,' MV',/,
     *20X,'CELL PRES. TRANS. CALIBRATION FACTOR  = ',F10.3,' KPA/MV',/)
205 FORMAT(///,20X,'THE TOTAL NUMBER OF INPUT DATA POINTS IS',I5)
206 FORMAT(1H1,///,20X,'OUTPUT OF THE RAW TEST DATA (AN ECHO-CHECK)',///,
     *1X, EXTER  INTER   PORE    AXIAL   DEL VOL DEL VOL AXIAL  DIAMET
     *ER',/,1X,'PRESS. PRESS.  PRESS.  LOAD    INTERIOR PORE FL DISPL
     *DISPL ',//,1X,'MV    - MV      MV      MV      CU CMS  CU CMS   VD
     *LTS  VOLTS',/ )
207 FORMAT(7(1X,F7.3),I5)
C
C       CALCULATION OF MASSAGED DATA
C
C
       PIE=3.141592654
       DA(1)=0.0
       DO 91 N=2,JJ,1
       DA(N)=(ABS(DA(N)-ADTO)*ADTCF)
91     CONTINUE
       DO 96 N=1,JJ,1
       PI(N)=(ABS(PI(N)-PPTO)*PPTCF)
       PE(N)=(ABS(PE(N)-PPTO)*PPTCF)
       P(N)=(ABS(P(N)-PPTO)*PPTCF)
       IF(MCAL.NE.1) GO TO 96
       VIM(N)=VIM(N)-API(1)-PI(N))*0.0007252
96     CONTINUE
       RETURN
       END
       SUBROUTINE STRAIN

C                                                STRAIN
C                                                ******
C
C
       REAL LCO,LCCF,IDTO,IDTCF,MS
       COMMON TITLE(20),PE(150),PI(150),P(150),AX(150),VIM(150),
     *VPF(150),DA(150),STR(150),VEM(150),EPSI(150),EPSE(150),DELI(150),
     *STE(150),SRI(150),SRE(150),STI(150),DELE(150),ADA(150),
     *SRM(150),STM(150),R1(150),R2(150),EPSV(150),EPSR(150),
     *EPST(150),EAX(150),DELV(150),DELT(150),DELR(150),RAD(150)
       COMMON JJ,H,SARVOL,MX,MY,MZ,MC,MEL,MCAL,DINT,QEXT,WDRY,PIB
       COMMON ADTO,ADTCF,LCO,LCCF,PPTO,PPTCF,CPTO,CPTCF
C
C
C       CALCULATE AXIAL STRAINS
C
       ADA(1)=0.0
       DO 30 I=1,JJ
       J=I+1
       X=(DA(J)-DA(I))*2.0
       Y=(2.*H*10.)-DA(J)-DA(I)
       EAX(I)=X/Y
       ADA(J)=ADA(I)-EAX(I)*100.0
30     CONTINUE
C
C       CALCULATE MEAN RADIAL STRAIN
C
       EPSR(1)=0.0
       R1(1)=DINT/2.0
       R2(1)=DEXT/2.0
       A=DINT/2.0
```

```
      B=DEXT/2.0
      DO 35 N=2,JJ,1
      CHG2=(VIM(N)+VPF(N))/(PIE*H)
      CHG1=VIM(N)/(PIE*H)
      R1(N)=SQRT(A**2.-CHG1)
      R2(N)=SQRT(B**2.-CHG2)
   35 CONTINUE
      DO 40 I=1,JJ
      J=I+1
      X=(R2(I)-R2(J)-R1(I)+R1(J))*2.0
      Y=R2(I)+R2(J)-R1(I)-R1(J)
      DELR(I)=X/Y
      EPSR(J)=EPSR(I)+DELR(I)*100.0
      IF(J.EQ.JJ)GO TO 45
   40 CONTINUE
   45 CONTINUE
C
C
C     CALCULATION OF MEAN VOLUMETRIC STRAIN
      EPSV(1)=0.0
      DO 50 I=1,JJ
      J=I+1
      X=(VPF(J)-VPF(I))*2.0
      Y=(2.*SAMVOL*1000000.0)-VPF(J)-VPF(I)
      DELV(I)=X/Y
      EPSV(J)=EPSV(I)+DELV(I)*100.0
      IF(J.EQ.JJ)GO TO 55
   50 CONTINUE
   55 CONTINUE
C
C
C     CALCULATION OF MEAN TANGENTIAL STRAIN
      EPST(1)=0.0
      DO 60 I=1,JJ
      J=I+1
      DELT(I)=DELV(I)-DELR(I)
      EPST(J)=EPST(I)+DELT(I)*100.0
      IF(J.EQ.JJ)GO TO 65
   60 CONTINUE
   65 CONTINUE
   90 CONTINUE
C
C
C     CALCULATION OF CHANGE IN INTERNAL DIAMETER
      DO 100 N=1,JJ
      DELI(N)=(A-R1(N))*2.0
  100 DELE(N)=(B-R2(N))*2.0
      WRITE(6,211)
      CALL STARS
      WRITE(6,212)
      CALL STARS
      WRITE(6,213) (PE(N),PI(N),P(N),VIM(N),VPF(N),ADA(N),
     *N,N=1,JJ)
      CALL STARS
  211 FORMAT(1H1,20X,'TRUE VALUES OF THE RAW DATA')
  212 FORMAT(//,11X,'EXTER  INTER  PORE     PORE    PORE   AXIAL   DAT
     *A',/,11X,'PRESS. PRESS. PRESS.  VOL CHG VOL CHG STRAIN POINT',
     */,11X,'*KPA*  *KPA*  *KPA*   *CC*    *CC*     (%)      ')
  213 FORMAT(10X,2F8.1,2X,F6.1,2X,F5.1,3X,F5.1,2X,F8.5,2X,I3)
      WRITE(6,200) (TITLE(I),I=1,20)
```

```
      CALL STARS
      WRITE(6,220)
      CALL STARS
      WRITE(6,221)
      CALL STARS
      WRITE(6,222)(EPSV(N),EPST(N),EPSR(N),DELI(N),ADA(N),N=1,JJ)
      CALL STARS
  220 FORMAT(////,20X,'PROCESSED DATA')
  221 FORMAT(//,10X,
     *'MEAN VOL.  MEAN TANG.  MEAN RADIAL    DIAM    MEAN AXIAL',
     */,10X,    STRAIN     STRAIN      STRAIN    CHANGE     STRAIN',
     */,10X,     (%)         (%)         (%)       (CM)        (%)',/,
     *)
  222 FORMAT(/,10X,F7.4,6X,F7.4,6X,F7.4,6X,F7.4)
      WRITE(2,350) (EPSV(N),EPSR(N),EPST(N),DELI(N),DELE(N),N=1,JJ)
  350 FORMAT(3(F7.3,2X),2(F7.4,2X))
  223 FORMAT(4X,2(4,3F12.8)
  200 FORMAT(1H1,////,1X,20A4)
      WRITE(6,197)
      CALL STARS
      WRITE(6,198)
      WRITE(6,199) (R1(N),R2(N),N=1,JJ)
  197 FORMAT(1H1,//,3X,'VALUES OF RADII DURING TESTING')
  198 FORMAT(//,2X,'INT  RADIUS(CM)        EXT. RADIUS(CM)',/)
  199 FORMAT(2X,F10.6,15X,F10.6)
      RETURN
      END
      SUBROUTINE STRESS
C
C                              STRESS
C                              ******
C
C
C
      REAL LCO,LCCF,IDTO,IDTCF,MS
      COMMON TITLE(20),PE(150),PI(150),P(150),AX(150),VIM(150),
     *VPF(150),DA(150),STR(150),VEM(150),EPSI(150),EPSE(150),DELI(150),
     *STE(150),SRI(150),SRE(150),STI(150),DELE(150),ADA(150),
     *SRM(150),STM(150),R1(150),R2(150),EPSV(150),EPSR(150),
     *EPST(150),EAX(150),DELV(150),DELT(150),DELR(150),RAD(150),
      COMMON JJ,H,SAMVOL,MX,MY,MZ,MC,MEL,MCAL,DINT,DEXT,WDRY,PIE
      COMMON ADTO,ADTCF,LCO,LCCF,PPTO,PPTCF,CPTO,CPTCF
C
C     CALCULATE RADIAL AND TANGENTIAL STRESSES
C
      DO 89 N=1,JJ,1
      A=R1(N)
      B=R2(N)
      SA=((2.*PE(N)*B**2.)-PI(N)*(A**2.+B**2.))/10000.0
      SB=(PE(N)*(A**2.+B**2.)-(2.*PI(N)*A**2.))/10000.0
      STI(N)=(SA/(B**2.-A**2.))*10000.0
      STE(N)=(SB/(B**2.-A**2.))*10000.0
      SRI(N)=PI(N)
      SRE(N)=PE(N)
C
C     CALC. MEAN STRESSES
C
      SRM(N)=(PI(N)+PE(N))/2.0
      STM(N)=(PE(N)*B-PI(N)*A)/(B-A)
C
C     CALCULATE AXIAL STRESSES
C
```

```
C
      FA=(ABS(AX(N)-LCO)*LCCF)
      IF(MCAL NE 1) GO TO 70
      FA=(FA*1 017)+1 21
70    FB=(PI(N)*PIE*R1(N)**2.0)/10000 0
      FC=(PE(N)*PIE*(B**2 0-R2(N)**2.0))/10000 0
      IF(FC.LE.0 0) FC=0 0
      F=FA-FB-FC
      AX(N)=(F/(PIE*(R2(N)**2 0-R1(N)**2.0)))*10000.0
89    CONTINUE
C
C     SUBTRACT THE PORE PRESSURE TO REDUCE THE STRESSES TO EFFECTIVE STRESSES
C
C
      IF(MZ EQ.1)GO TO 88
      DO 87 N=1,JJ,1
      STI(N)=STI(N)-P(N)
      STE(N)=STE(N)-P(N)
      SRI(N)=SRI(N)-P(N)
      SRE(N)=SRE(N)-P(N)
      SRM(N)=SRM(N)-P(N)
      STM(N)=STM(N)-P(N)
      AX(N)=AX(N)-P(N)
87    CONTINUE
88    CONTINUE
      WRITE(6.211) (TITLE(I),I=1,20)
      CALL STARS
      WRITE(6.212)
      CALL STARS
      WRITE(6.213)
      CALL STARS
      WRITE(6.215) (SRI(I),STI(I),SRE(I),STE(I),AX(I),SRM(I),STM(I),
     *I=1,JJ)
C
C     WRITE THE DATA ON A FILE DEVICE WHOSE CALL NUMBER IS 1
C
      WRITE(1.214)(STI(N),STE(N),SRI(N),SRE(N),PI(N),PE(N),AX(N),N=1,JJ)
      WRITE(1.250) (SRM(N),STM(N),N=1,JJ)
211   FORMAT(1H1,////,1X,20A4)
212   FORMAT(////,'LINEAR ELASTIC ANALYSIS OF  THE TEST DATA')
213   FORMAT(////.5X,'SIG R1        SIG TH1      SIG R2',
     *9X,'SIG TH2       SIG Z        SIG RM',
     *9X,'SIG THM')
215   FORMAT(/,2X,F10.2,3X,F10 2,4X,F10.2,4X,F10.2,4X,F10.2,4X,F10.2,
     *4X,F10.2)
214   FORMAT(7F15.6)
250   FORMAT(2F15.6)
      RETURN
      END
      SUBROUTINE STARS
C
C                                                   STARS
C                                                   ******
C
      WRITE(6.1)
1     FORMAT(1X,'************************************************
     *******************')
      RETURN
      END
      SUBROUTINE ELPLA
```

```
C     ELPLA
C     ......
C
C     AN ELASTIC -PERFECTLY PLASTIC ANALYSIS OF THE TEST DATA
C     :::::::::::::::::::::::::::::::::::::::::::::::::::::::::::
C
      REAL LCO,LCCF,L,IDTCF,MS,N,K,L,NTHI
      COMMON TITLE(20),PE(150),PI(150),P(150),AX(150),VIM(150),
     *VPF(150),DA(150),STR(150),VEM(150),EPSI(150),EPSE(150),DELI(150),
     *STE(150),SRI(150),SRE(150),STI(150),DELE(150),ADA(150),
     *SRM(150),STM(150),R1(150),R2(150),EPSV(150),EPSR(150),
     *EPST(150),EAX(150),DELV(150),DELT(150),DELR(150),RAD(150)
      COMMON JJ,H,SAMVOL,MX,MY,MZ,MC,MEL,MCAL,DINT,DEXT,WDRY,PIE
      COMMON ADTO,ADTCF,LCO,LCCF,PPTO,PPTCF,CPTO,CPTCF
C
C     CALC. STRENGTH PARAMETER      N = (1+SIN THI)/(1-SIN THI)
C     :::::::::::::::::::::::::::::::::::::::::::::::::::::::::::::::
C
C     NOTE : AT COLLAPSE, R = B
C
      DO 5 I=1,JJ
      PE(I)=PE(I)-P(I)
      PI(I)=PI(I)-P(I)
    5 CONTINUE
      AA=(PE(JJ)*R2(JJ)**2.0)-(PI(JJ)*R1(JJ)**2.0)
      BB=R2(JJ)**2.0-R1(JJ)**2.0
      SIGO=2.0*AA/BB
      RAT1=R2(JJ)/R1(JJ)
      RAT2=SIGO/PI(JJ)
      N=1.0
   10 N=N+1.0
      K=N-1.0
      L=N+1.0
      RAT3=RAT1**K
      RAT4=RAT2/L
      IF(RAT3.LT.RAT4) GO TO 10
      N=N-1.0
   20 N=N+0.1
      K=N-1.0
      L=N+1.0
      RAT3=RAT1**K,
      RAT4=RAT2/L
      IF(RAT3.LT.RAT4) GO TO 20
      N=N-0.1
   30 N=N+0.01
      K=N-1.0
      L=N+1.0
      RAT3=RAT1**K
      RAT4=RAT2/L
      IF(RAT3.LT.RAT4) GO TO 30
      NTHI=N
      THI=ASIN((NTHI-1.0)/(NTHI+1.0))
      THI=(THI*180.0)/PIE
      WRITE(6,99)
      CALL STARS
      WRITE(6,100)
      CALL STARS
      WRITE(6,120) NTHI,THI
   99 FORMAT(1H1,////,5X,'ELASTIC-PERFECTLY PLASTIC ANALYSIS OF TEST DAT
```

```
      '*A')
  100 FORMAT(////,10X,'N',5X,'THI')
  120 FORMAT(8X,F5.2,5X,F5.1)
C
C     CALCULATE THE RADIUS OF THE PLASTIC ZONE
C     -----------------------------------------
C
C     NOTE : FAILURE COMMENCES ON THE INSIDE SURFACE WHEN R = A
C
      EXP=1.0/(NTHI-1.0)
      DO 40 I=1,JJ
      AA=(PE(I)*R2(I)**2.0)-(PI(I)*R1(I)**2.0)
      BB=R2(I)**2.0-R1(I)**2.0
      SIGO=2.0*AA/BB
      FAIL=PI(I)*(NTHI+1.0)
      IF(SIGO.LT.FAIL) RAD(I)=R1(I)
      IF(SIGO.LT.FAIL) GO TO 40
      CC=SIGO/FAIL
      RAD(I)=(CC**EXP)*R1(I)
   40 CONTINUE
      WRITE(6,200)
      CALL STARS
      WRITE(6,220) (I,R1(I),RAD(I),I=1,JJ)
  200 FORMAT(////,20X,'DEVELOPMENT OF THE PLASTIC ZONE',//,8X,'DATA POIN
     *T',12X,'INT. RAD.',10X,'PLASTIC RADIUS')
  220 FORMAT(/,12X,I2,18X,F10.6,15X,F10.6)
C
C     CALC. STRESSES ON INSIDE SURFACE OF SAMPLE.
C     --------------------------------------------
C
C     NOTE : ELASTIC SOLUTION USED UNTIL FAILURE OCCURS.
C
      THN=NTHI-1.0
      DO 80 I=1,JJ
      RATIN=((R1(I)/R2(I))**2.0)+((R2(I)**2.0-R1(I)**2.0)/(2.0*R2(I)**2.
     *0))*(NTHI+1.0)
      RATIO=PE(I)/PI(I)
      IF(RATIO.GE.RATIN) GO TO 50
      SRI(I)=PI(I)
      D=(2.0*PE(I)*R2(I)**2.0)-PI(I)*(R1(I)**2.0+R2(I)**2.0)
      E=(R2(I)**2.0)-(R1(I)**2.0)
      STI(I)=D/E
      GO TO 60
   50 CONTINUE
      SRI(I)=PI(I)
      STI(I)=NTHI*SRI(I)
   60 CONTINUE
C
C     CALC. STRESSES ON EXTERNAL SURFACE OF SAMPLE.
C     ----------------------------------------------
C
      IF(RATIO.GE.RATIN) GO TO 70
      SRE(I)=PE(I)
      F=PE(I)*(R2(I)**2.0+R1(I)**2.0)-2.0*PI(I)*R1(I)**2.0
      STE(I)=F/E
      GO TO 72
   70 CONTINUE
      SIGO=(PE(I)*R2(I)**2.0-PI(I)*R1(I)**2.0)/E
      SIGRR=2.0*SIGO/(NTHI+1.0)
      SRE(I)=PE(I)
```

```
      G=PE(I)*(R2(I)**2.0+RAD(I)**2.0)-2.0*SIGRR*RAD(I)**2.0
      H=R2(I)**2.0-RAD(I)**2.0
      STE(I)=G/H
C
C     CALC. MEAN RADIAL STRESSIN SAMPLE
C     ------------------------------------------------------
C
   72 CONTINUE
      IF(RAD(I).GE.R1(I)) GO TO 75
      SRM(I)=(PI(I)*R1(I)+PE(I)*R2(I))/(R1(I)+R2(I))
      GO TO 80
   75 F1=(RAD(I)**NTHI)/(NTHI*R1(I)**THN)
      F2=(R2(I)-RAD(I))/(R2(I)+RAD(I))
      FR=(F1-R1(I)/NTHI+(F2*RAD(I)**NTHI/(R1(I)**THN)))*PI(I)
      SRM(I)=(FR+(PE(I)*R2(I)*F2))/(R2(I)-R1(I))
   80 CONTINUE
      WRITE(6,300)
      CALL STARS
      WRITE(6,320) (SRI(I),STI(I),SRE(I),STE(I),SRM(I),I=1,JJ)
      WRITE(1,330) (STI(I),STE(I),SRI(I),SRE(I),SRM(I),I=1,JJ)
  300 FORMAT(1H1,////,'RADIAL & TANGENTIAL STRESSES ON SURFACES OF SAMPLE',//,
     A'E',//,5X,'SIG R1',5X,'SIG TH1',5X,'SIG R2',5X,'SIG TH2',
     *5X,'SIG RM')
  320 FORMAT(/,2X,F10.2,3X,F10.2,4X,F10.2,4X,F10.2,4X,F10.2)
  330 FORMAT(5F15.6)
      RETURN
      END
```

```
C       PLOTTING PROGRAM FOR HOLLOW CYLINDER TESTS
C       ########################################
C   THIS PROGRAM PLOTS A NUMBER OF DIAGRAMS RESULTING FROM HOLLOW
C   CYLINDER TESTS IN A TRIAXIAL APPARATUS. PLANE STRAIN.
C   A NUMBER OF FILE DEVICES ARE TO BE SPECIFIED IN THE COMMAND STATEMENTS
C   FD 1 : FIRST LINE - SAMPLE CHARACTERIZATION DATA
C            'N' LINES - 8 COLUMNS OF TEST DATA
C   FD 2 : 'N' LINES OF 7 COLUMNS OF TEST DATA
C   FD 3 : FORMAT 20A4: TITLES FOR PLOTS
C   FD 6 : PROGRAM OUTPUT FILE
C   FD 9 : FILE TO STORE PLOT DATA
C
        DIMENSION A(99,30),B(99,20),C1(99),C2(99),C3(99),C4(99),C5(99),
       *C6(99),C7(99),C8(99),C9(99),C10(99),C11(99),C12(99),C13(99),
       *C14(99),C15(99),C16(99),C17(99),C18(99),C19(99),C20(99),C21(99),
       *C22(99),C23(99),C24(99),T15(20),T1(20),T2(20),T3(20),T4(20),
       *T5(20),T6(20),T7(20),C25(99),C26(99),IOP(10)
        REAL*8 TITLE(5)
        READ(1,10)N,SAMVOL,POR,WOLIN,H,DEXT,DINT,MX,MY,MZ,MC,MEL
        READ(1,11)((A(J,K),K=1,7),J=1,N)
        READ(1,14)((A(J,K),K=8,9),J=1,N)
        READ(1,16) ((A(J,K),K=10,14),J=1,N)
        READ(2,12)((B(J,K),K=1,5),J=1,N)
        READ(3,13)((T(J,K),K=1,20),J=1,8)
        READ(4,22) (TITLE(I),I=1,8)
        NN=N-1
        NOP=7
        IOP(1)=0
        IOP(2)=1
        IOP(3)=0
        IOP(4)=999
        IOP(5)=1
        IOP(6)=0
        IOP(7)=0
        XMARG=3.0
        YMARG=1.5
C
C   C1=EXT. TANG. STRESS
C   C2=INT. TANG. STRESS
C   C4=INT. RADIAL STRESS
C   C5=AXIAL STRESS
C   C6=EXT. TANG. STRAIN
C   C7=INT. TANG. STRAIN
C   C8=INTERNAL PRESSURE
C   C9=EXTERNAL PRESSURE
C   C10=INT. DIAMETER CHANGE
C   C11=EXT. DIAMETER CHANGE
C   C12=INT. DEV. STRESS
C   C14=MEAN TANG. STRESS
C   C15=MEAN RADIAL STRESS (LINEAR ASS.)
C   C16=MEAN DEV. STRESS (LINEAR ASS.)
C   C17=MEAN DEV. STRESS (EL.-PL. ANALYSIS)
C   C18=MEAN RADIAL STRESS (EL.-PL. ANALYSIS)
C   C19=MEAN TANG. STRAIN
C   C24=VOLUMETRIC STRAIN
C   C24=MEAN RADIAL STRESS+MEAN TANG. STRESS
C   C25=MAX. STRESS TO BE PLOTTED
C   C26=MAX. STRAIN TO BE PLOTTED
        DO 40 J=1,N,1
        C1(J)=(A(J,11))
```

```
      C2(J)=(A(J,10))
      C3(J)=0.0
      C4(J)=(A(J,12))
      C5(J)=(A(J,7))
      C6(J)=(B(J,5)/DEXT)*100.0
      C7(J)=(B(J,4)/DINT)*100.0
      C8(J)=(A(J,5))
      C9(J)=(A(J,6))
      C10(J)=B(J,4)
      C11(J)=B(J,5)
      C12(J)=C2(J)-C4(J)
      C13(J)=0.0
      C14(J)=A(J,9)
      C15(J)=A(J,8)
      C16(J)=C14(J)-C15(J)
      C18(J)=A(J,14)
      C17(J)=C14(J)-C18(J)
      C19(J)=B(J,3)
      C20(J)=0.0
      C21(J)=-(B(J,1))
      C22(J)=0.0
      C23(J)=0.0
      C24(J)=C15(J)+C14(J)
   40 CONTINUE
      AMAX=0.0
      BMAX=0.0
      CMAX=0.0
C
C CALC. MAX. STRESS TO BE PLOTTED
C
      IF(MY.EQ.1) GO TO 18
      AA=C16(N)-C2(N)
      IF(AA.LT.0.0) AMAX=C2(N)
      IF(AA.GT.0.0) AMAX=C16(N)
   18 CONTINUE
      IF(MY.EQ.2) GO TO 17
      AA=C16(N)-C1(N)
      IF(AA.LT.0.0) BMAX=C1(N)
      IF(AA.GT.0.0) BMAX=C16(N)
      BB=BMAX-C12(N)
      IF(BB.LT.0.0) BMAX=C12(N)
      IF(BB.GT.0.0) BMAX=BMAX
   17 CONTINUE
C
C CALC. MAX. STRAIN TO BE PLOTTED
C
      C=C6(N)-C7(N)
      IF(C.LT.0.0) CMAX=C7(N)
      IF(C.GT.0.0) CMAX=C6(N)
      DO 20 I=1,5,1
      C25(I)=0.0
      C26(I)=0.0
   20 CONTINUE
      IF(AMAX.EQ.0.0) C25(5)=BMAX
      IF(BMAX.EQ.0.0) C25(5)=AMAX
      C26(5)=CMAX
      DO 39 K=1,20
      T1(K)=T(1,K)
      T2(K)=T(2,K)
      T3(K)=T(3,K)
```

```
      T4(K)=T(4,K)
      T5(K)=T(5,K)
      T6(K)=T(6,K)
   39 T7(K)=T(7,K)
C
   10 FORMAT(I5,F10.8,F10.3,F10.8,3F10.3,5I5))
   11 FORMAT(7F15.6)
   12 FORMAT(3(F7.3,2X),2(F7.4,2X))
   13 FORMAT(20A4)
   14 FORMAT(2F15.6)
   15 FORMAT(4(F7.3,2X))
   16 FORMAT(5F15.6)
   22 FORMAT(20A8)
C
C   PLOTTING CALLS TO CGPL2
C
C   PLOT 1 : MEAN DEV. STRESS VS. MEAN TANG. STRAIN
C           ----------------------------------------
C
      C16(1)=0.0
      CALL CGPEP1(XMARG,YMARG)
      CALL CGPEP2(NDP,IOP)
      CALL CGPL(C19,C16,C16,N,129,1,1,3,1,0.0,1.0,4,0.0,0.0,2500,0,7,0,
     *T1,7)
      CALL CGPEP5(-2.5,-4.7,TITLE(3),8.0,08,0.1)
      CALL SYMBOL(2.0,1.5,0.08,'SAMPLE #',0.0,8)
C
C   PLOT 2 : MEAN VOL. STRAIN VS. MEAN TANG. STRAIN
C           ----------------------------------------
C
      CALL CGPL(C19,C21,C19,N,129,1,1,3,1,0.0,1.0,4,0.0,-0.4,-9.9,9,4,0,
     *T2,7)
C
C   PLOT 3 : INTERNAL PRESSURE VS. WALL MOVEMENT
C           ------------------------------------
C
      CALL CGPL(C10,C8,C8,N,1,1,1,3,1,0.0,-9.9,9,3,0,0.0,-9.9,5,0,
     *T3,7)
      CALL CGPEP5(-1.7,0.6,TITLE(1),8.0,08,0.3)
      CALL CGPEP5(-1.95,-2.0,TITLE(3),8.0,08,0.1)
      CALL SYMBOL(1.5,2.0,0.08,'SAMPLE #',0.0,8)
      CALL CGPL(C11,C8,C8,N,132,1,1,3,1,0.0,-9.9,9,3,0,0.0,-9.9,5,0,
     *T3,7)
      CALL CGPEP5(-1.7,0.6,TITLE(2),8.0,08,0.3)
C
C   PLOT 4 : AXIAL STRESS VS. RADIAL+TANG. STRESS(MEAN)
C           ------------------------------------------
C
      CALL CGPL(C24,C5,C5,N,129,1,1,3,1,0.0,-9.9,5,0,0.0,-9.9,3,0,
     *T4,7)
      CALL CGPEP5(-4.5,0.35,TITLE(3),8.0,08,0.1)
      CALL SYMBOL(1.0,2.5,0.08,'SAMPLE #',0.0,8)
      IF(MEL.EQ.1) GO TO 50
C
C   PLOT 5 : EXT. TANG. STRESS VS. EXT. TANG. STRAIN
C           -----------------------------------------
C
      CALL CGPL(C6,C1,C1,NN,129,1,1,3,1,0.0,-9.8,4,0,0.0,-9.9,7,0,
     *T5,7)
      CALL CGPEP5(-3.95,-0.15,TITLE(3),8.0,08,0.1)
```

```
C     CALL SYMBOL(0.5,6.0,0.08,'SAMPLE #',0.0,8)
C
C   PLOT 6 : INT. DEV. STRESS VS. INT. TANG. STRAIN
C     ----------------------------------------------
C
      C12(1)=0.0
      CALL CGPL(C7,C12,C12,N,129,1,1,3,1,0.0,-9.9,4.0,0.0,2500.0,7.0,
     *T6,7)
      CALL CGPEP5(-2.0,-0.15,TITLE(3),8.0,08,0.1)
      CALL SYMBOL(2.5,6.0,0.08,'SAMPLE #',0.0,8)
C
C   PLOT 7 : COMPARISON OF MEAN STRESS-STRAIN CURVES USING DIFF.SIG RM ASS.
C     ---------------------------------------------------------------------
C
      CALL CGPL(C18,C17,C17,N,1,1,1,3,1,0.0,0.10.4,0.0,0.2500.0,7.0,
     *T7,7)
      CALL CGPEP5(-2.0,-3.0,TITLE(5),8.0.08,0.3)
      CALL CGPL(C18,C16,C16,N,132,1,1,3,1,0.0,-9.9,4.0,0.0,-9.9,7.0,
     *T7,7)
      CALL CGPEP5(-2.0,-3.0,TITLE(4),8.0.08,0.3)
      CALL CGPEP5(-2.5,-4.4,TITLE(3),8.0.08,0.1)
      CALL SYMBOL(2.0,1.5,0.08,'SAMPLE #',0.0,8)
C
C   PLOT 8 : VARIATION OF AVERAGE STRESSES WITH PRESSURE.
C     ---------------------------------------------------
C
      CALL CGPL(C8,C14,C14,N,1,1,1,3,1,0.0,-9.9,7,0.0,0.-9.9,4.0,
     *T8,7)
      CALL CGPEP5(-2.0,-0.5,TITLE(6),8.0.08,0.3)
      CALL CGPL(C8,C15,C15,N,132,1,1,3,1,0.0,-9.9,7,0.0,0.-9.9,
     *4.0,T8,7)
      CALL CGPEP5(-2.0,-0.5,TITLE(7),8.0.08,0.3)
      CALL CGPL(C8,C5,C5,N,133,1,1,3,1,0.0,-9.9,7,0.0,0.-9.9,4.0,
     *T6,7)
      CALL CGPEP5(-2.0,-0.5,TITLE(8),8.0.08,0.3)
      CALL CGPL(C1,C1,C1,N,0,1,1,3,1,0.0,-9.9,4.0,0.0,-9.9,7.0,
     *T1,7)
   50 CONTINUE
      STOP
      END
```